DISSERTATION

RANDOM DECREMENT BASED METHOD FOR PARAMETER IDENTIFICATION OF WIND-EXCITED BUILDING MODELS USING ACCELERATION RESPONSES

Submitted by
Chiu Jen Ku
Department of Civil Engineering

In partial fulfill of the requirements
For the Degree of Doctor of Philosophy
Colorado State University
Fort Collins, Colorado
Summer 2004

COLORADO STATE UNIVERSITY

June 7, 2004

WE HEREBY RECOMMEND THAT THE DISSERTATION PREPARED UNDER OUR SUPERVISION BY CHIU JEN KU ENTITLED RANDOM DECREMENT BASED METHOD FOR PARAMETER IDENTIFICATION OF WIND-EXCITED BUILDING MODELS USING ACCELERATION RESPONSES BE ACCEPTED AS FULLFILLING IN PART REQUIREMENTS FOR THE DEGREE OF DOCTOR OF PHILOSOPHY.

Committee on Graduate Work

C. Byron Winn

Co-Advisor

Robert N. Meroney

Advisor

Jack E. Cermak

Co-Advisor

Sandra Woods

Department Head

ABSTRACT OF DISSERTATION

RANDOM DECREMENT BASED METHOD FOR PARAMETER IDENTIFICATION OF WIND-EXCITED BUILDING MODELS USING ACCELERATION RESPONSES

This research addresses the parameter identification problem of a linear dynamic system from forced acceleration responses without any knowledge of input forces. Such a problem is attributed to the added effect of an applied force in its impulse acceleration response function. When using the random decrement technique for such acceleration responses, the random decrement signature of the acceleration response has the added effect resulting from the random decrement signature of the applied force. This result has greatly restricted the practical value and applicability of such a random decrement acceleration signature in the time domain identification.

The random decrement based method has been proposed in this study to provide a solution to the identification problem. The random decrement based method elaborates response data in the time domain and, then, frequency domain by combining the random decrement technique with the fast Fourier transform based algorithms. The theoretical derivation of the random decrement based method initially develops a new frequency response function approach for the acceleration responses, by means of a small modification of the traditional approach. The adoption of the modified frequency response function establishes a theoretical basis defined for the frequency response functions of the random decrement signatures, if the dominant vibration modes are significantly excited, well separated, and lightly damped.

Numerical and experimental simulations have been implemented to identify the modal parameters of building models from forced acceleration responses using the random decrement based method. The numerical simulation is based on various dynamic systems subjected separately to white noise excitations and fluctuating wind forces. The experimental simulation employs a five-story aeroelastic building model tested in a wind tunnel. These simulations are particularly critical to manifest the characteristics of the random decrement acceleration signatures when using the random decrement based method. The applicability of the random decrement based method has been verified by both numerical and experimental results. The performance, limitations, and difficulties encountered by the proposed random decrement based method are also discussed.

Chiu Jen Ku
Department of Civil Engineering
Colorado State University
Fort Collins, CO 80523
Summer 2004

ACKNOWLEDGMENTS

My mentors, Dr. F.Y. Cheng and Dr. W.W. Yu of University of Missouri – Rolla, have my continued gratitude for their guidance and inspiration in the field of structural engineering.

My sincerest thanks go to my advisor, Dr. J.E. Cermak, and the academic committee members, Dr. D.W. Boggs, Dr. R.N. Meroney, Dr. J.A. Peterka, Dr. C.B. Winn, for their meticulous reviews of the manuscript. Their comments and suggestions have been of great value to the completion of this research study.

The assistance and contribution in this research study from the following people are gratefully acknowledged: Dr. G.C. Huang, D. Li, Dr. G.C. Woo, Dr. Y.C. Wu, Dr. I.D. Yan, Dr. J.S. Yang, Ms. M. Chang, Ms. L.M. Liang, Ms. M.F. Lin, Ms. H. Yang, Mr. S.M. Dodge, Mr. C.S. Hsiao, Mr. S.M. Liou, Mr. C.H. Shao, and staff in engineering research center of Colorado State University.

I highly appreciate my American family, Dr. Porter Woods and Mrs. Gail Woods, for their encouragement and invaluable help during my study in Colorado State University. Last, but not least, everlasting thanks go to my parents Chung Yen Ku and Hei Mei Chen, sister Ching Hsin, brother Chiu Yu, and my friend Li-Shu Chou, for their love and support.

Dedicated to my Parents

TABLE OF CONTENTS

NOMENCLATURE

Abbreviations

ANSDF	Averaged normalized spectral density function
AR	Autoregressive
ARMA	Autoregressive moving average
COMAC	Coordinate modal assurance criterion
DOF	Degree of freedom
ERA	Eigen-system realization algorithms
FFT	Fast Fourier transform
FRF	Frequency response function
MA	Moving average
MAC	Mode assurance criterion
MDOF	Multi-degree of freedom
N/A	Not available
RD	Random decrement
RDS_1F	Random decrement signatures formed by single forcing function
RESP_2F	Responses resulting from two forcing functions
SDF	Spectral density function
SDOF	Single degree of freedom

Greek

α	Exponent of wind velocity profile
Γ	Correlation matrix
γ_{ij}^2	Ordinary coherence function, *Coh*
$\Delta_{XX}(f)$	Random decrement signatures in frequency domain
Δt	Time interval
δ	Dirac delta function
δ_{XX}	Auto random decrement signatures
δ_{XY}	Cross random decrement signatures
$\delta^R_{\ddot{X}\ddot{X}}$	Random decrement signatures of non-forced acceleration responses
$\delta^L_{\ddot{X}\ddot{X}}$	Random decrement signatures of applied forces
ε	White noise processes
ξ	Relative error of modal ratios
ζ	Damping ratio
ζ_1	Fundamental damping ratio
θ_{ij}	Phase angle
κ	von Karman constant
Λ, λ	Eigen-value matrix
λ_i	The i^{th} eigen-value vector
μ	Mean value
ξ	Relative error

Π	Toeplitz matrix of correlation matrices
ρ	Air density
σ	Standard derivation
τ_d	Time shift
Φ	Modal matrix
φ_i	The i^{th} mode shape
$\overline{\varphi}_i$	The i^{th} mass normalized mode shape
ϕ_{ij}	Modal components of the j^{th} mode shape
$\lvert\chi^2\rvert$	Aerodynamic admittance
$\psi_{ij}(f_k)$	Mode shape component (i,j) at the k^{th} mode shape
$\overline{\Psi}$	Mass normalized modal matrix
Ω	Circular frequency matrix
ω	Circular frequency, rad/sec
ω_d	Damped circular frequency
ω_1	Fundamental circular frequency

Roman

A	Parameter matrix
A_i	The i^{th} AR parametric matrix
A_s	Projected area normal to wind
a	Acceleration
B_i	The i^{th} MA
C	Damping matrix
c	Damping coefficient
C_d	Drag coefficient
Co	Coincident spectral density function
Coh	Coherence function
d	Displacement
$F(t), f(t)$	Force vector
$F'(t)$	Fluctuating force
f	Frequency
f_{Nq}	Nyquist frequency
f_s	Shedding frequency
G	$\phi^{\mathrm{T}}M^{-1}$
$G_{X_iX_i}(f)$	Auto-spectral density function of responses
$G_{X_iX_j}(f)$	Cross-spectral density function of responses
$G_{\Delta\Delta}^{RD}(f)$	Spectral density function of random decrement signatures
H	Height of a building
$H(t)$	diagonal matrix of $e^{\lambda t}$
$H_k(f)$	Frequency response function vector
$H_{ij}(f)$	Frequency response function between the responses at i and j points
$H^{(I)}\ H^{(II)}\ H^{(III)}$	Frequency response function estimator
$h(t)$	Impulse response function

$h^a(t)$	Impulse acceleration response function
I	Identity matrix
I_t	Turbulence intensity
Im{ }	Imaginary component of a complex function
K, k	Stiffness matrix
i, j, k	Index number
k_ζ, k_ζ'	Constants of correlation in the vertical direction
M	Mass matrix
m	Mass
n	Normalized frequency
$PH(f)$	Phase function
p	Probability density function
$Q(t)$	Modal coordinate
Qu	Quadrature spectral density function
$q(t)$	Modal response
q_0	Modal initial condition
R	Correlation function matrix
Re{ }	Real component of a complex function
R_{XX}	Auto-correlation function/matrix
R_{XY}	Cross-correlation function/matrix
S_{DF}	Spectral density function of alongwind force
S_{LF}	Spectral density function of crosswind force
$S_{u_{ii}}, S_u$	Auto-spectral density function of longitudinal wind velocity
$S_{u_{ij}}$	Cross-spectral density function of fluctuating wind velocities
S	Strouhal number
s	Variable
s^2	Sample variance
$sign[\ ]$	Sign function
T	Time length
$T_{X(t)}, T_{Y(t)}$	Triggering condition
t, τ	Time variable
U	Longitudinal wind velocity
$u*$	Surface friction velocity
u, u'	Fluctuating wind velocity
V	Reference wind speed
v	Velocity
Var	Variance
W	Width of a building
X, Y	Stochastic vector process
x_d	Initial displacement
x_v	Initial velocity
x_0	Initial condition
z_0	Aerodynamic roughness length
z_1	Reference height
z	Height
Δz	Distance of height

$z(t)$	State vector

Notation

$E[\ ]$	Expectation operator
$\dot{x}$, x'	dx/dt
$\ddot{x}$, x''	d^2x/dt^2
$\dddot{x}$, x'''	d^3x/dt^3
$\hat{(\ )}$	Estimate
$\bar{(\ )}$	Mean value
$\underline{(\ )}$	Vector
$\tilde{(\ )}$	Specially defined value
$\square^{-1}$	Inverse of a matrix
$\square^{T}$	Transpose of a matrix
$\square^{*}$	Complex conjugate of a matrix
$\lvert\ \rvert$	Absolute value
$\cap$	Intersection
ln	Natural logarithm
Σ	Summation
∞	Infinite value
$\angle$	Angle

Chapter 1

INTRODUCTION

1.1 Background and Motivation

The present trend of constructing structures, which are slenderer and lighter, has made them susceptible to vibrations under a strong wind environment. The issues of serviceability and occupant comfort in tall and flexible buildings have become practical concerns in design criteria to structural engineers. As a matter of fact, such issues are mainly associated with the control of excessive acceleration of wind-induced motion experienced by the occupants of the top floors of a building. Problems of this type can be solved by the design of intelligent structures that can mitigate such undesired vibrations by incorporating control systems in the buildings. The control systems, such as passive, semi-active, and active control schemes, have gradually become an integral part of the structures in the last three decades. The performance of these control systems depends on better understanding the dynamic properties of the installed structure through analytical, numerical or experimental methods, or a combination of them.

The use of analytical finite element models consisting of mass, damping, and stiffness matrices for structures has been proven to be very beneficial in evaluating such control performance. However, theoretical modeling alone cannot describe the dynamic behavior of real structures with complete confidence, because certain structural properties in an analytical model must be assumed or determined empirically. Experimental testing of a structure can furnish valuable information to complement the theoretical modeling

with the experimental determination of the structural properties. In order to construct the accurate finite element model of a tested structure from its experimental information, the application of an identification procedure lying in a theoretical framework of modeling plays a crucial role.

Modal parameter identification is a special area of system identification, in which the mathematical structure of a model representing a dynamic system is known to be in a form of modal parameters [Ghanem and Shinozuka, 1995; Hjelmstad, 1996; Allemang and Brown, 1998; Petsounis and Fassois, 2001]. Different approaches to identify the modal parameters of linear dynamic systems have been addressed in the literature. Comprehensive surveys of the literature can be found in the following papers of authors: [Astrom and Eykhoff, 1971; Hart and Yao, 1977; Ibanez, 1979; Strejc, 1981; Berman, 1984; Kozin and Natke, 1986; Juang and Pappa, 1988; Natke, 1989, 1990; Mottershead and Friswell, 1993].

Generally, the approaches for modal parameter identification can be categorized into frequency domain techniques and time domain techniques. Most of the frequency domain identification techniques are based on the fast Fourier transform (FFT) algorithm invented by Cooley and Tukey [1965] in the late 1960s. The use of the FFT can rapidly evaluate frequency response functions of a dynamic system from the measured external excitations and resultant responses of the system in the frequency domain. In the course of developing the frequency domain techniques, the time domain techniques have been used as alternative approaches. One of the popular approaches is the random decrement (RD) technique, presented by Cole [Cole, 1968]. To realize the information about the modal parameters of a dynamic system, the RD technique is intended to transform

random responses to free vibration responses that certain identification techniques strongly depend upon in the absence of known external excitations.

The theoretical background of the RD technique in a statistical description has been established in the 1980s [Vandiver, 1982; Bedewi, 1986]. It was shown that the RD signatures of displacement and velocity responses are equivalent to the corresponding free vibration responses, when the dynamic system is subjected to Gaussian white noise excitations. However, Huang, et al. [1998] noted that the RD signatures of acceleration responses are never equivalent to the free vibration responses, because of the existence of the Dirac delta function resulting from the white noise excitations in such RD signatures. The emergence of the Dirac delta function calls into question the use of such acceleration responses in the identification approaches, when acceleration measurement is of crucial importance to wind-excited structures. This result motivates the research reported in the dissertation, in which the topic is random decrement based method for parameter identification of wind-excited building models using acceleration responses.

1.2 Objectives and Scope

The objective of this research is to develop and demonstrate an identification procedure that can be applied to process the acceleration responses of a linear dynamic system for estimating the modal parameters of the dynamic system. In order to meet the objective of the research, attention is mainly placed on theoretical derivation, numerical verification, and experimental verification with respect to applicability of the random decrement based method to various types of acceleration responses.

To start, the mathematical model used to describe the vibration of dynamic systems throughout this research study is hypothesized to be a second-order linear ordinary differential equation with lumped coefficient matrices: a lumped mass model. The proposed identification procedure should have the same content of applicability as that of the above mathematical model. In addition, the external excitations acting on a dynamic system are Gaussian and can be modeled using white noise excitations and real wind forces.

The utility of the Gaussian white noise excitations makes it more tractable to theoretically derive the correlation functions of dynamic responses, which are important to interpret the characteristics of the RD signatures. The real wind forces are simulated by a multivariate autoregressive moving average model with the practical consideration of the temporal and spatial correlations in the different degrees of freedom of a structure.

The following task is to exploit the concept of the RD technique to further explore the properties of the RD signatures of responses in the time and frequency domains. The outcome of this task is expected to establish the relations between the RD signatures of the responses and the corresponding free vibration responses of the dynamic system and thus pave the way to develop the RD based method.

The development of the RD based method is another task that combines the RD technique with the FFT based algorithms to provide a solution for the RD acceleration signatures, which do not resemble the free vibration responses. The applicability of the RD based method for extracting the modal parameters that determine the modal model of a dynamic system is investigated by analyzing simulated and experimental acceleration data. In addition to resolving this problem, this method is also expected to be applicable

to practical issues, such as: (1) measurement noise; (2) lack of input measurement; and (3) limited number of sensors.

1.3 Research Outline

This dissertation is organized in seven chapters. Following the brief statement above in this chapter, the contents of the subsequent chapters are introduced:

Chapter 2 presents an efficient procedure to simulate fluctuating wind forces using a multivariate autoregressive moving average model with the consideration of temporal and spatial correlations in different degrees of freedom of a structure. The detailed derivation of a two-stage least squares algorithm is introduced to determine the parameter matrices of the multivariate autoregressive moving average model. The application of the procedure is demonstrated in the simulations of Gaussian fluctuating alongwind and crosswind forces when acting on a two-degrees-of-freedom example building. The results of the simulations based on the given spectral models reveal the considerable potential of the simulation procedure. The generated wind forces can then be used to implement the dynamic response analysis of the building.

Chapter 3 proposes a new procedure by adapting the concept behind the random decrement (RD) technique to define the initial conditions of an analytical free vibration response from the synchronous RD displacement and velocity signatures. The analytical free vibration response is then compared with the specified RD signature to further examine the properties within the RD signatures. To illuminate the proposed procedure, the theoretical background of the RD technique in conjunction with a general triggering condition is introduced. The validity of the procedure with two individual triggering

conditions is confirmed through a single-degree-of-freedom dynamic system driven by a white noise excitation and a simulated wind force, separately. Comparisons between the RD signatures and the corresponding free vibration responses reveal that the RD acceleration signature contains the added effect of the RD signature of the applied force. The RD signature is not equivalent to the free vibration response when the dynamic system is subjected to the simulated wind force.

Chapter 4 demonstrates a generalized relationship between the RD acceleration signatures and the RD force signatures, since the influence of the RD force signatures on the RD acceleration signatures has been found. To access more information about the RD signatures in relation to free vibration responses, the theoretical foundation of the RD signatures is further developed. Numerical simulations are undertaken through a 2DOF linear dynamic system loaded by Gaussian white noise excitations and fluctuating wind forces to complement the theoretical basis. The free vibration responses of the dynamic system are determined from the procedure that selects the initial conditions from the formed RD displacement and velocity signatures. The resulting free vibration responses are then compared with the associated RD signatures. Comparison of the results reveals that each RD acceleration signature consists of two portions contributed respectively by the non-forced acceleration response and the applied force.

Chapter 5 proposes a random decrement based method to identify the modal parameters of a linear dynamic system, when only forced acceleration responses are available to use. The RD based method elaborates response data in the time and, then, frequency domains by correlating the RD technique with fast Fourier transform based algorithms. However, the added effect of the RD force signatures in the RD acceleration

signatures should be addressed. In response to this, a novel frequency response function (FRF) approach for the acceleration responses, with a modification of the traditional one, is verified in advance. Then, the derivation of the RD based method follows the concept of the verified FRF approach to achieve the theoretical basis of the FRFs defined for the RD signatures. Numerical simulations of various DOF linear dynamic systems loaded individually by white noise excitations and simulated wind forces foster the applicability of the RD based method. In the course of these numerical simulations, an innovation of the RD technique to effectively avoid the added effect of the RD force signatures in the RD acceleration signatures was discovered. In addition, the identification accuracy of the mode shapes can be further enhanced, when a proper time length is extracted from the formed RD signatures in order to evaluate their FRFs.

Chapter 6 focuses on verifying the applicability of the proposed RD based method by identifying natural frequencies and mode shapes of a five-story aeroelastic building model using acceleration responses measured from wind tunnel tests. Owing to a limited number of sensors, the acceleration responses are measured group by group and the modal parameters of each mode are, therefore, identified group by group. The FRF approach using the FFT based algorithms to evaluate the modal parameters is also used for the purpose of a cross validation. The results reveal that the natural frequencies and mode shapes identified from the RD based method give an excellent match with those from the FRF approach. The satisfaction of the orthogonality condition of the identified mode shapes to a lumped mass model further validates the applicability of the proposed RD based method in practical applications of acceleration measurement.

Chapter 7 summarizes the conclusions of the present study and recommends future tasks.

References

Cermak, J. E. (1974), "Applications Of Fluid Mechanics To Wind Engineering", A Freeman Scholar Lecture, presented in The Winter Annual Meeting of ASME.

ASCE Aerospace Division Task Committee (1996), "Wind-Tunnel Studies Of Buildings And Structures", Journal of Aerospace Engineering, Vol. 9, No. 1, pp. 19-36.

Allemang, R. J. and Brown, D. L. (1998), "A Unified Matrix Polynomial Approach To Modal Identification", Journal of Sound and Vibration, Vol. 211, No. 3, pp. 301-322.

Astrom, K. J. and Eykhoff, P. (1971), "System Identification – A Survey", Automatica, Vol. 7, pp. 123-162.

Bedewi, N. E. (1986), The Mathematical Foundation of the Auto and Cross-Random Decrement Techniques and the Development of a System Identification Technique for the Detection of Structural Deterioration, Ph.D. Dissertation, Department of Mechanical Engineering, University of Maryland.

Berman, A. (1984), "System Identification Of Structural Dynamic Models – Theoretical And Practical Bounds", AIAA/ASME/ASCE/ASH Structures, Structural Dynamics and Materials Conference, pp.123-129.

Cole, H. A. (1968), "On-The-Line Analysis Of Random Vibration", AIAA/ASME 9th Structures, Structural Dynamics and Materials Conference, AIAA Paper No. 68-288.

Cooley, J. W. and Tukey, J. W. (1965), "An Algorithm For The Machine Calculation Of Complex Fourier Series", Mathematics and Computations, Vol. 19, No. 90, pp. 297-301.

Ghanem, R. and Shinozuka, M. (1995), "Structural-System Identification. I: Theory", Journal of Engineering Mechanics, Vol. 121, No. 2, pp. 255-264.

Hart, G. C. and Yao, J. T. P. (1977), "System Identification In Structural Dynamics", Journal of the Engineering Mechanics Division, Vol. 103, No. EM6, pp. 1089-1104.

Hjelmstad, K. D. (1996), "On The Uniqueness Of Modal Parameter Estimation", Journal of Sound and Vibration, Vol. 192, No. 2, pp. 581-598.

Huang, C. S., Yeh, C. H., and Tsai, I. C. (1998), "Random Decrement Technique For Ambient Vibration Test In Time-domain System Identification", Journal of the Chinese Institute of Civil and Hydraulic Engineering, Vol. 10, No. 3, pp. 537-547. (In Chinese)

Ibanez, P. (1979), "Review Of Analytical And Experimental Techniques For Improving Structural Dynamic Models", Welding Research Council, Bulletin 249.

Juang, J. N. and Pappa, R. S. (1988), "A Comparative Overview Of Modal Testing And System Identification For Control Of Structures", The Shock and Vibration Digest, Vol. 20, No. 6, pp. 4-15.

Kozin, F. and Natke, H. G. (1986), "System Identification Techniques", Structural Safety, Vol. 3, pp. 269-316.

Mottershead, J. E. and Friswell, M. I. (1993), "Model Updating In Structural Dynamics: A Survey", Journal of Sound and Vibration, Vol. 167, No. 2, pp. 347-375.

Natke, H. G. (1989), "Survey On The Identification Of Mechanical Systems", Road Vehicle Systems and Related Mathematics, Edited by Neunzert, H., pp. 69-116.

Natke, H. G. (1990), "Recent Trends In System Identification", Proceedings of the European Conference on Structural Dynamics, Edited by Kratzig, et al., pp. 283-289.

Petsounis, K. A. and Fassois, S. D. (2001), "Parametric Time-Domain Methods For The Identification Of Vibrating Structures – A Critical Comparison And Assessment", Mechanical Systems and Signal Processing, Vol. 15, No. 6, pp. 1031-1060.

Strejc, V. (1981), "Trends In Identification", Automatica, Vol. 17, pp. 7-21.

Vandiver, J. K., Dunwoody, A. B., Campbell, R. B., and Cook, M. F. (1982), "A Mathematical Basis For The Random Decrement Vibration Signature Analysis Technique", ASME Journal of Mechanical Design, Vol. 104, pp. 307-313.

Chapter 2

SIMULATIONS OF MULTIVARIATE FLUCTUATING WIND FORCES

2.1 Introduction

In structural dynamics applications, a dynamic response analysis in the frequency domain is often performed for computational convenience. However, when considering structural non-linearities or structure-excitation interactions, a dynamic response analysis in the frequency domain may not be appropriate. Instead, a dynamic response analysis in the time domain may provide an alternative to analyze such problems of linear or nonlinear structures. The time domain analysis of structural responses, when subjected to stochastic wind forces, requires simulation of the discrete time series of wind forces. Therefore, it is important to evaluate the veracity of a stochastic wind force simulation before one performs successfully temporal and spatial domain analysis of wind-induced structural responses.

Actually, many researchers have used simulations of a stochastic process based on a specified spectral density function or correlation function. One of the traditional approaches to generate time series of multivariate and multi-dimensional stationary stochastic processes is based on a superposition of trigonometric functions with statistically independent phase angles [Shinozuka, 1971, 1987; Shinozuka and Jan, 1972; Shinozuka et al., 1990]. Such a simulation approach was also employed as a basic tool for the Monte Carlo solution of various problems in stochastic structural dynamics

including linear and nonlinear problems [Shinozuka, 1972]. However, this approach has the disadvantage of computational inefficiency, since the summation of a large set of trigonometric functions is involved in the simulation procedure. Although the use of the fast Fourier transform (FFT) algorithm can overcome such computational inefficiency [Shinozuka and Deodatis, 1991], it also requires the expense of increased demand on computer storage, when dealing with long period simulated data.

In contrast with the Shinozuka method, the autoregressive moving average (ARMA) models and the autoregressive (AR) models offer more efficient algorithms for simulating time series of multivariate and multi-dimensional stochastic processes, in accordance with a target spectral density function matrix or correlation function matrix. In these models, a simple recursive numerical operation is employed to generate the multivariate and multi-dimensional time series, once the parameter coefficient matrices of these models are estimated. The advantage of such parametric time series models is that they significantly reduce computational effort. These models also do not require considerable computer storage. In addition, such time series models can reproduce the prescribed correlation matrix and spectral matrix to a close approximation.

The AR model has been widely applied for wind simulations by several authors. Iwatani [1982] used the AR method proposed by Akaike [1969, 1971, 1988] to simulate one-dimensional and multivariate fluctuating wind velocities in accordance with specified power spectra and cross spectra. Iannuzzi and Spinelli [1987] investigated three different simulation methods, including Goto and Toki method [1969], Shinozuka method [1971], and Iwatani method [1982], for single and multiple time series of wind velocities. Such simulated wind velocities were then transformed into the fluctuations of

wind forces when applied to the field of structural aerodynamics. It was shown that the dynamic response of a structure is substantially affected by the characteristics of the simulated fluctuating forces, including the degree of correlation between the fluctuating components. Tsukagoshi et al. [1993] took advantage of the simulation procedure proposed by Tamura et al. [1988] to simulate the fluctuating alongwind and crosswind forces to carry out the time domain dynamic response analysis of a high-rise building with a tuned mass damper.

This chapter presents a procedure to simulate wind forces by integrating the multivariate ARMA model with the consideration of temporal and spatial correlations in the different degrees of freedom of a structure. The derivation of a two-stage least squares algorithm for determining the parameter coefficient matrices of the multivariate ARMA model is introduced in detail. The feasibility of the procedure is demonstrated in simulations of alongwind and crosswind fluctuating forces for the subject building shown in Figure 2.3.1. Comparisons of the respective spectral density functions and correlation functions calculated from the simulated aerodynamic forces with the target functions show considerable agreement.

2.2 Time Series Models

2.2.1 AR, MA and ARMA Models

A M-variate autoregressive (AR) model of order P is given by:

$$Y(n\Delta t) = -\sum_{j=1}^{P} A_j Y[(n-j)\Delta t] + B_0 \varepsilon(n\Delta t) \tag{2.2.1}$$

where A_j is the j^{th} autoregressive $M\times M$ parameter matrix, B_0 is the zeroth moving average $M\times M$ parameter matrix, and $\varepsilon(n\Delta t)$ is a $M\times 1$ vector of uncorrelated white noise processes

with zero mean vector and covariance matrix. The structure of the covariance matrix is defined by:

$$E\left\{\varepsilon(n\Delta t)\varepsilon[(n+k)\Delta t]^T\right\} = \begin{cases}\Sigma, & k=0\\ 0, & k\neq 0\end{cases} \tag{2.2.2}$$

where Σ is a $M\times M$ symmetric positive definite matrix. Thus, the M-variate vector of stochastic processes $Y(n\Delta t)$ at time $n\Delta t$ is a linear combination of its previous time histories and a vector of white noise processes.

A M-variate moving average (MA) model of order Q is given by:

$$Y(n\Delta t) = \sum_{j=0}^{Q} B_j \varepsilon[(n-j)\Delta t] \tag{2.2.3}$$

where B_j is the j^{th} moving average $M\times M$ parameter matrix. The M-variate vector $Y(n\Delta t)$ at time $n\Delta t$ is expressed by the previous and present vectors of white noise processes.

A M-variate autoregressive moving average (ARMA) model of orders P and Q, denoted ARMA(P,Q), is obtained by combining both autoregressive and moving average terms in the model:

$$Y(n\Delta t) + \sum_{j=1}^{P} A_j Y[(n-j)\Delta t] = \sum_{j=0}^{Q} B_j \varepsilon[(n-j)\Delta t] \tag{2.2.4}$$

[Wei, 1990]

2.2.2 AR Model and Yule-Walker Method

In this section, the Yule-Walker method is introduced for estimating the AR parameter matrix that is typically related to the correlation function matrix in a linear relation [Yule, 1927; Walker, 1931]. By post-multiplying both sides of Equation (2.2.1) with $Y^T[(n\text{-}k)\Delta t]$ and then taking the expectation, the following result is obtained:

$$\sum_{j=1}^{P} A_j R_{YY}[(j-k)\Delta t] = -R_{YY}[k\Delta t] \qquad k = 1,2,\ldots,P \tag{2.2.5}$$

$$\sum_{j=0}^{P} A_j R_{YY}(j\Delta t) = B_0 R_{\varepsilon Y}(0) \qquad k = 0 \tag{2.2.6}$$

in which $R_{YY}(k\Delta t)$ denotes the $M\times M\times(P+1)$ correlation function matrix of the stochastic processes Y, and A_0 is assumed to be a $M\times M$ identity matrix, I_M. The above Equations (2.2.5) and (2.2.6) are known as the Yule-Walker equations.

Similarly, by post-multiplication of both sides of Equation (2.2.1) by $\varepsilon^T[n\Delta t]$, $\varepsilon^T[(n\text{-}1)\Delta t]$, …, $\varepsilon^T[(n\text{-}k)\Delta t]$, …, $\varepsilon^T[(n\text{-}P)\Delta t]$, individually, and then taking the expectation to obtain the correlation function matrix $R_{Y\varepsilon}$ between $Y(n\Delta t)$ and $\varepsilon[(n\text{-}j)\Delta t]$ leads to the following equations:

$$R_{Y\varepsilon}(0) = B_0 \qquad k = 0 \tag{2.2.7}$$

$$R_{Y\varepsilon}(-k\Delta t) + \sum_{j=1}^{k} A_j R_{Y\varepsilon}[(j-k)\Delta t] = 0 \qquad k = 1,2,\ldots,P \tag{2.2.8}$$

$$R_{Y\varepsilon}(k\Delta t) = 0 \qquad k > 0 \tag{2.2.9}$$

$$E\left\{Y(n\Delta t)\varepsilon\left[(n+k)\Delta t\right]\right\} = R_{Y\varepsilon}(k\Delta t) = R_{\varepsilon Y}^T(-k\Delta t) \tag{2.2.10}$$

Subsequently, by virtue of substitution of Equation (2.2.7) into Equation (2.2.6) and use of Equation (2.2.10), one obtains:

$$B_0 B_0^T = \sum_{j=0}^{P} A_j R_{YY}(j\Delta t) \qquad k = 0 \tag{2.2.11}$$

The Yule-Walker equations can also be expressed in a matrix form as follows:

$$\left[A_1 \quad A_2 \quad \ldots \quad A_P\right]\Pi = -\left[R_{YY}^T(\Delta t) \quad R_{YY}^T(2\Delta t) \quad \ldots \quad R_{YY}^T(P\Delta t)\right] \tag{2.2.12}$$

in which the Toeplitz matrix, Π, contains $P\times P$ sub-matrices,

$$\Pi = \begin{bmatrix} R_{YY}(0) & R_{YY}^T(\Delta t) & \cdots & R_{YY}^T[(P-1)\Delta t] \\ R_{YY}(\Delta t) & R_{YY}(0) & \cdots & R_{YY}^T[(P-2)\Delta t] \\ \cdots & \cdots & \cdots & \cdots \\ R_{YY}[(P-1)\Delta t] & R_{YY}[(P-2)\Delta t] & \cdots & R_{YY}(0) \end{bmatrix} \tag{2.2.13}$$

From Equation (2.2.12), the parameter matrix $A_j, j = 1, 2, \ldots, P$, for the AR model can be determined from the specified target correlation function matrix $R_{YY}(k\Delta t)$. Since $B_0 B_0^T$ is a positive definite matrix, it follows that the right hand side of Equation (2.2.11) is also a positive definite matrix. Therefore, B_0 can be solved, for example, by the Cholesky decomposition. Once the parameter matrices are obtained, Equation (2.2.1) can be used to generate the simulated multivariate time series, driven by a white noise vector.

2.2.3 ARMA Model and Two-Stage Matching Method

Gersch et al. [1970, 1976, 1977] extended the earlier theoretical works [Thiel, 1950; Durbin, 1960] by using a two-stage least-squares method to realize parameters of a multivariate ARMA model, as well as a scalar ARMA model, from a given stationary covariance matrix. They then applied the ARMA model for the synthesis and identification of random vibration systems in mechanical and structural engineering problems. Spanos et al. [1985, 1986] further presented a two-stage order-of-magnitude matching method to determine the parameters of a scalar ARMA model based on a prior higher-order AR model in accordance with a target turbulence spectrum. Such an ARMA model could simulate a stochastic process without synthesizing the response of a dynamic system. Subsequently, Samaras et al. [1985] and Spanos and Schultz [1986] made further use of the two-stage least squares method so that a multivariate ARMA model with the same orders of AR and MA could be established by a prescribed correlation function

matrix or spectral density function matrix. Mignolet and Spanos [1987a and b, 1989, 1990] continued a series of studies on various optimal procedures by the minimization of frequency domain errors to estimate the parameter matrix of a multivariate ARMA model with different AR and MA orders. Similarly, it was found that the two-stage ARMA algorithm could be extensively used in a multi-dimensional and multivariate stochastic process [Naganuma et al. 1987; Mignolet and Spanos, 1992a and b]. Furthermore, Li and Kareem [1990a and b] studied a three-stage matching method by combining the two-stage least squares ARMA algorithm with digital interpolation filters to simulate wind forces at the prescribed time increments.

In this study, the two-stage least squares method to estimate the requisite parameter matrix of a multivariate ARMA model has been selected and used as follows. In the first stage, a target process is required to be well approximated in terms of an AR process. In this regard, a prior AR model of higher order P' is readily obtained from Equations (2.2.5) and (2.2.6) in the preceding section. In the second stage, the ARMA model may be derived by the correlation function matrices, R_{YY} and $R_{Y\varepsilon}$. The correlation function matrix $R_{Y\varepsilon}$ is solved from the prior AR model, according to Equations (2.2.7) and (2.2.8). Hence, if both sides of Equation (2.2.4) are post-multiplied by $Y[(n\text{-}m_p)\Delta t]$ and $\varepsilon[(n\text{-}m_q)\Delta t]$, respectively, and then processed by the expectation, the following relations can be given:

$$B_{m_q} - \sum_{j=1}^{P} A_j R_{Y\varepsilon}[(j-m_q)\Delta t] = R_{Y\varepsilon}(-m_q \Delta t) \tag{2.2.14}$$

$$-\sum_{j=1}^{Q} B_j R_{Y\varepsilon}^{T}[(m_p-j)\Delta t] + \sum_{j=1}^{P} A_j R_{YY}[(j-m_p)\Delta t] = -R_{YY}(-m_p \Delta t) \tag{2.2.15}$$

in which m_p = 1, 2, ..., P and m_q = 1, 2, ..., Q. The matrix expression of these two equations is:

$$\begin{aligned}&\left[B_1 \quad \cdots \quad B_Q \quad A_1 \quad \cdots \quad A_P\right]D = \\ &\left[R_{Y\varepsilon}(-\Delta t) \quad \cdots \quad R_{Y\varepsilon}(-Q\Delta t) \quad -R_{YY}(\Delta t) \quad \cdots \quad -R_{YY}(P\Delta t)\right]\end{aligned} \tag{2.2.16}$$

The matrix, D, in Equation (2.2.16) is a $M(P+Q)\times M(P+Q)$ matrix and consists of four sub-matrices:

$$D = \begin{bmatrix} I & \Gamma^T \\ \Gamma & \Pi \end{bmatrix} = \begin{bmatrix} I_m & \cdots & 0 & -R_{Y\varepsilon}^T(0) & \cdots & 0 \\ \vdots & \ddots & \vdots & \vdots & \ddots & \vdots \\ 0 & \cdots & I_m & -R_{Y\varepsilon}^T[(1-P)\Delta t] & \cdots & -R_{Y\varepsilon}^T(0) \\ -R_{Y\varepsilon}(0) & \cdots & -R_{Y\varepsilon}[(1-Q)\Delta t] & R_{YY}(0) & \cdots & R_{YY}^T[(P-1)\Delta t] \\ \vdots & \ddots & \vdots & \vdots & \ddots & \vdots \\ 0 & \cdots & -R_{Y\varepsilon}(0) & R_{YY}[(P-1)\Delta t] & \cdots & R_{YY}(0) \end{bmatrix} \tag{2.2.17}$$

in which Π is the $P\times P$ Toeplitz matrix as well as Equation (2.2.13) and Γ contains $P\times Q$ sub-matrices in which the $(m,n)^{th}$ is represented by:

$$\begin{aligned}\Gamma_{mn} &= -R_{Y\varepsilon}[(m-n)\Delta t] \qquad m \le n \\ &= 0 \qquad\qquad\qquad\qquad \text{otherwise}\end{aligned} \tag{2.2.18}$$

Once the AR and MA parameter matrices A_i, i = 1, 2, ... , P, and B_i, i = 0, 1, 2, ... , Q, are obtained, the time series can be generated recursively by the aid of Equation (2.2.4).

2.3 Simulation Procedure of Fluctuating Wind Forces

A multi-dimensional and multivariate Gaussian stochastic process is the common characterization of the wind velocity field in the atmospheric boundary layer. In this

respect, a simulation procedure should be applicable not only to scalar processes, but also to multi-dimensional and/or multivariate processes. Often, simulation of the wind velocity field when applied in structural design for line-like structures can be simplified to a one-dimensional stochastic process – the longitudinal component of the wind vector. It is also required to consider the temporal and spatial correlations of wind-induced longitudinal forces associated with different degrees of freedom of a large structure. As a result, the simulation of fluctuating wind forces in this study is represented as a one-dimensional (longitudinal) and multivariate (multiple discrete heights) Gaussian stochastic process.

The simulation procedure adopts the concept presented by Tamura [1988] to consider the temporal and spatial correlations in the different degrees of freedom of a structure. The procedure can typically be undertaken in three steps: 1. Target spectra of aerodynamic loads; 2. Fourier transform between spectra and correlation functions; 3. Generation of fluctuating wind forces. A detailed description for the procedure is introduced in the following subsections to simulate two cases of one-dimensional and multivariate turbulent wind forces.

2.3.1 Target Spectra of Aerodynamic Loads

The appropriate choice of stationary power spectra is a starting point to simulate the time series of the alongwind and crosswind forces acting on structures. The spectral description of the fluctuating alongwind force at a height z and a frequency f is given by:

$$S_{DF}(z,f) = \left[\rho C_D A_s \overline{U}(z)\right]^2 \left|\chi(z,f)\right|^2 S_u(z,f) \qquad (2.3.1)$$

in which ρ, A_s, and C_D are air density, sectional area, and drag coefficient, respectively. Equation (2.3.1) is formulated on the basis of the strip and the quasi-steady theories for the fluctuating alongwind force. The power law in Equation (2.3.2) describes the longitudinal mean velocity $\overline{U}(z)$ in the atmospheric boundary layer under neutral thermal conditions.

$$\frac{\overline{U}(z)}{\overline{V}_1(z_1)} = \left(\frac{z}{z_1}\right)^{\alpha} \tag{2.3.2}$$

in which $\overline{V}_1(z_1)$ is a reference mean velocity at a height z_1 from the ground and α is an exponent of the mean wind velocity profile. Both $\overline{V}_1$ and α can be determined from actual measurement of wind. The auto-spectral density function of the longitudinal fluctuating velocity, $S_u(z, f)$, is multiplied by the aerodynamic admittance, $|\chi(z, f)|^2$, for the correlation of the fluctuating velocity. The spectral density function of the fluctuating wind velocity proposed by Kaimal et al. [1972] and the aerodynamic admittance proposed by Vickery [1968] are formulated, respectively, as:

$$\frac{fS_u(z,f)}{u_*^2} = \frac{200n}{(1+50n)^{5/3}}, \quad 0 < f < \infty \tag{2.3.3}$$

$$|\chi(z,f)|^2 = \left[1+\left(\frac{2f\sqrt{A_s}}{\overline{U}(z)}\right)^{4/3}\right]^{-2} \tag{2.3.4}$$

in which u_* is a surface friction velocity and $n = \frac{fz}{\overline{U}(z)}$.

The correlation between wind velocities, corresponding to different degrees of freedom in a building, may be considered only at the center of each height. In addition, such a correlation at one face of the building may be assumed as the same as the opposite

face. Therefore, the simulation procedure of the fluctuating forces is a one-dimensional and multivariate stochastic process. The cross-spectral density function of the fluctuating wind velocities $S_{u_{ij}}(\Delta z, f)$ for any two points is represented in complex polar pattern as:

$$\begin{aligned} S_{u_{ij}}(\Delta z, f) &= \left|S_{u_{ij}}(\Delta z, f)\right| e^{-i\theta_{ij}(\Delta z, f)} \\ &= Co_{u_i u_j}(\Delta z, f) - iQu_{u_i u_j}(\Delta z, f) \end{aligned} \tag{2.3.5}$$

in which $i = \sqrt{-1}$ and

$$\begin{aligned} \left|S_{u_{ij}}(\Delta z, f)\right| &= \sqrt{Co^2_{u_i u_j}(\Delta z, f) + Qu^2_{u_i u_j}(\Delta z, f)} \\ &= \sqrt{S_{u_i}(z_i, f) S_{u_j}(z_j, f)}\, Coh(\Delta z, f) \end{aligned} \tag{2.3.6}$$

The real and imaginary components in Equation (2.3.5) are known as the coincident spectral density function (co-spectrum) and quadrature spectral density function (quad-spectrum), respectively. The co-spectrum and quad-spectrum of the wind velocities are expressed as [Bendat and Piersol, 2000]:

$$Co_{u_i u_j}(\Delta z, f) = \sqrt{S_{u_i}(z_i, f) S_{u_j}(z_j, f)}\, Coh(\Delta z, f) \cos\theta_{ij}(\Delta z, f) \tag{2.3.7}$$

$$Qu_{u_i u_j}(\Delta z, f) = \sqrt{S_{u_i}(z_i, f) S_{u_j}(z_j, f)}\, Coh(\Delta z, f) \sin\theta_{ij}(\Delta z, f) \tag{2.3.8}$$

in which

$$Coh(\Delta z, f) = \sqrt{\frac{Co^2_{u_i u_j}(\Delta z, f) + Qu^2_{u_i u_j}(\Delta z, f)}{S_{u_i}(f) S_{u_j}(f)}} \tag{2.3.9}$$

$$\theta_{ij}(\Delta z, f) = \tan^{-1} \frac{Qu_{u_i u_j}(\Delta z, f)}{Co_{u_i u_j}(\Delta z, f)} \tag{2.3.10}$$

$Coh(\Delta z, f)$ and $\theta_{ij}(\Delta z, f)$, defined by Equations (2.3.9) and (2.3.10), are the square root of the coherence function and the phase angle, respectively, and may be given from published wind tunnel or field measurements.

In the atmosphere, the foregoing two expressions are approximated through the application of the following equations for the vertical direction [Davenport, 1961, 1968; Panofsky et al., 1974; Shiotani and Iwatani, 1979]:

$$Coh(\Delta z, f) = e^{-\frac{k_\varsigma f \Delta z}{\overline{U}_a}} \tag{2.3.11}$$

$$\theta_{ij}(\Delta z, f) = \frac{k_\varsigma' f \Delta z}{\overline{U}_a} \tag{2.3.12}$$

in which k_ς, a decay constant of the correlation in the vertical direction, is assumed to be 8 and k_ς' is constant to be 9 for the simulation of the alongwind forces in this study. $\overline{U}_a$ is the average mean velocities at two different points, separated in height by distance Δz.

For the crosswind motion, a conversion between the longitudinal velocity and the pressure on the side faces of a building may not be available. The reason is because the interaction between the separated shear layer and the side faces of a building significantly affects the aerodynamic pressures acting over the side faces of the building. In addition, the crosswind motion is partially the result of buffeting by lateral component of turbulence in the approaching wind. Therefore, the application of the mentioned theories and formulas for the alongwind motion on the crosswind motion remains rather doubtful [Kareem, 1982]. On the other hand, the wind tunnel measurements may provide a direct approach to determine the crosswind forces.

To demonstrate, a similar model for the spectral density function of the crosswind force $S_{LF}(z, f)$ proposed by Kareem [1984], as follows, is used in this study.

$$\frac{fS_{LF}(z,f)}{\sigma_{LF}^2} = a \times b \times \left(\frac{f}{f_s}\right)^{0.9} \qquad f \le f_s$$
$$= a \times b \times \left(\frac{f}{f_s}\right)^{3.0} \qquad f \ge f_s \tag{2.3.13}$$

$$a = \frac{B}{\left[1-\left(\frac{f}{f_s}\right)^2\right]^2 + \left[2B\left(\frac{f}{f_s}\right)\right]^2} \tag{2.3.14}$$

$$b = 1.32\left[\left(\frac{1}{3\alpha}\right)^{0.5} + 0.154\left(1-\frac{z}{H}\right)^{3.5}\right] \tag{2.3.15}$$

in which H and W are the height and the width of a building, respectively; $f_s = \frac{S\overline{U}(z)}{W}$ is shedding frequency; $\sigma_{LF}{}^2$ is the mean square value of the crosswind force; S is the Strouhal number; $B = 2^{\frac{1}{2}} I_t(z)$ is the bandwidth coefficient; and $I_t(z)$ is the turbulence of intensity at a height z. The spatial correlation for the simulation of the crosswind forces in this study is considered by assuming k_ζ, and k_ζ' to be 3 and 0, correspondingly, in Equations (2.3.11) and (2.3.12).

2.3.2 Fourier Transform between Spectra and Correlation Functions

Once the appropriate spectral density functions of fluctuating forces have been obtained, their correlation functions can be transformed by making use of the Wiener-Khinchine relationship [Bendat and Piersol, 2000] as follows:

$$R_{F_iF_j}(\tau) = \int_{-\infty}^{\infty} S_{F_iF_j}(\Delta z, f) e^{i2\pi f\tau} df$$
$$= \int_{\frac{-1}{2\Delta t}}^{\frac{1}{2\Delta t}} S_{F_iF_j}(\Delta z, f; \Delta t) e^{i2\pi f\tau} df \tag{2.3.16}$$

in which

$$S_{F_iF_j}(\Delta z, f; \Delta t) = \sum_{k=-\infty}^{\infty} S_{F_iF_j}\left(\Delta z, f + \frac{k}{\Delta t}\right) \tag{2.3.17}$$

$$-\frac{1}{2\Delta t} \le f \le \frac{1}{2\Delta t}$$

The auto-correlation function in Equation (2.3.16) is further simplified to:

$$R_{F_iF_i}(\tau) = 2\int_0^{\frac{1}{2\Delta t}} S_{F_iF_i}(\Delta z, f; \Delta t)\cos(2\pi f\tau)df \tag{2.3.18}$$

From the definition of Equation (2.3.5), it follows that the cross-spectral density function of the fluctuating forces is given by:

$$S_{F_iF_j}(\Delta z, f; \Delta t) = Co_{F_iF_j}(\Delta z, f; \Delta t) - iQu_{F_iF_j}(\Delta z, f; \Delta t) \tag{2.3.19}$$

Substituting Equation (2.3.19) into Equation (2.3.16), in turn, the cross-correlation function can be obtained in terms of $Co_{FiFj}(\Delta z, f; \Delta t)$ and $Qu_{FiFj}(\Delta z, f; \Delta t)$ as:

$$R_{F_iF_j}(\tau) = 2\int_0^{\frac{1}{2\Delta t}} \left[Co_{F_iF_j}(\Delta z, f; \Delta t)\cos 2\pi f\tau + Qu_{F_iF_j}(\Delta z, f; \Delta t)\sin 2\pi f\tau\right]df \tag{2.3.20}$$

$f_{Nq} = \frac{1}{2\Delta t}$ is the Nyquist frequency of the sampling procedure with sampling interval, Δt. Therefore, the sampling frequency must be at least twice the significant frequency components in a signal to prevent aliasing.

2.3.3 Generation of Fluctuating Wind Forces

After the target correlation functions are obtained from the target spectra, the parameter matrices of the multivariate ARMA model in Equation (2.2.4) can be determined from Equations (2.2.12) and (2.2.16). The multivariate ARMA model, driven

by the white noise processes, is assumed as Gaussian stochastic processes for generating stationary time histories of wind forces in this study. Such an assumption is believed to be valid for aerodynamic loads that involve integral effects of the random pressure field over large areas.

Fluctuating alongwind and crosswind forces were generated at two points for an example building. The specifications and parameters illustrated in Figure 2.3.1 and Table 2.3.1 were used for this example. The selected orders of the ARMA(P, Q) model, defined in Equation (2.2.4), for the alongwind force were ARMA(85,77) with a prior order P' of 460, while the simulation of the crosswind force made use of ARMA(75,75) with a prior order P' of 450. The time interval Δt was set as 0.2 second. To fulfill the prescribed probabilistic characteristics for the wind forces, each set of Gaussian random numbers was individually generated as inputs in the multivariate ARMA model. Within the time histories of the wind forces, the initial 500 seconds were generated in advance to maintain the subsequent simulated data stationary. Following the initial period, an additional 8000 seconds was generated, which was adopted for the evaluation of the spectral density functions and correlation functions in each case of the simulated forces.

Table 2.3.1 Parameters for Simulation Examples

Air Density, ρ	1.225 kg/m^3
Drag Coefficient, C_D	1.3
Reference Height, z_1	10 m
Exponent of Wind Profile, α	1/7
Strouhal Number S	0.216
The Intensity of Turbulence $I_t(z)$	0.15
Reference Mean Velocity, $\overline{V}_1(z_1)$	40 m/sec

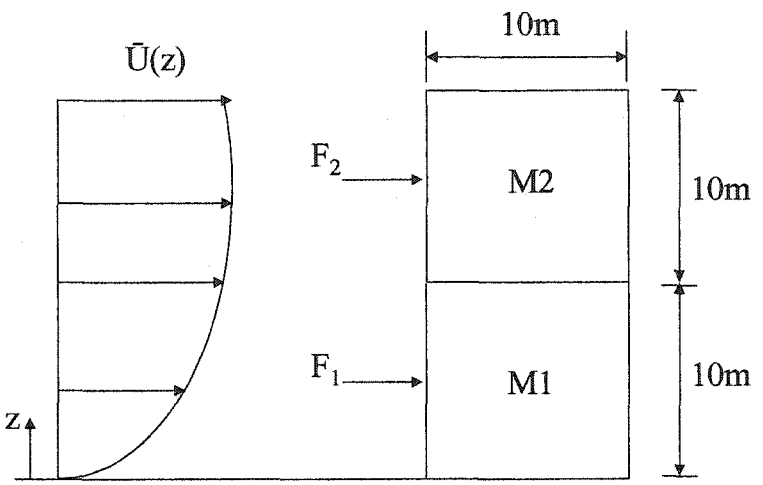

Figure 2.3.1 Specifications of the Example Building

Figures 2.3.2 and 2.3.3 illustrate the normalized auto-spectral density functions of the target and the simulation for the alongwind and crosswind forces, respectively. The spectral density functions of the simulated wind forces were determined by the average of nine FFT based computations. Each FFT based computation was based on the data length of 1600 seconds and 50 % overlap from the whole simulated data of 8000 seconds. The auto- and cross- correlation functions for the target and the simulation of the alongwind and crosswind forces are illustrated in Figures 2.3.4 and 2.3.5, respectively. The simulation of the fluctuating alongwind forces essentially stresses the property of a time delay in the spatial correlation between the two simulated forces as displayed in Figure 2.3.4. On the other hand, the simulation of the fluctuating crosswind forces only

focuses on the spatial correlation without a time delay between two simulated forces as illustrated in Figure 2.3.5. These results show that the characteristics of the simulated fluctuating wind forces agree fairly well with those of the target ones.

2.4 Concluding Remarks

The use of the multivariate ARMA model including the temporal and spatial correlations in the different degrees of freedom of a structure provides an efficient simulation procedure for wind forces. The results show that the simulation procedure is useful for the simulations of the fluctuating wind forces along the height of the building.

Whenever the wind forcing functions are generated by means of the parametric time series model, *e.g.*, ARMA or AR model, the time-domain dynamic response analysis of the building can be implemented immediately by solving numerically the equations of motion.

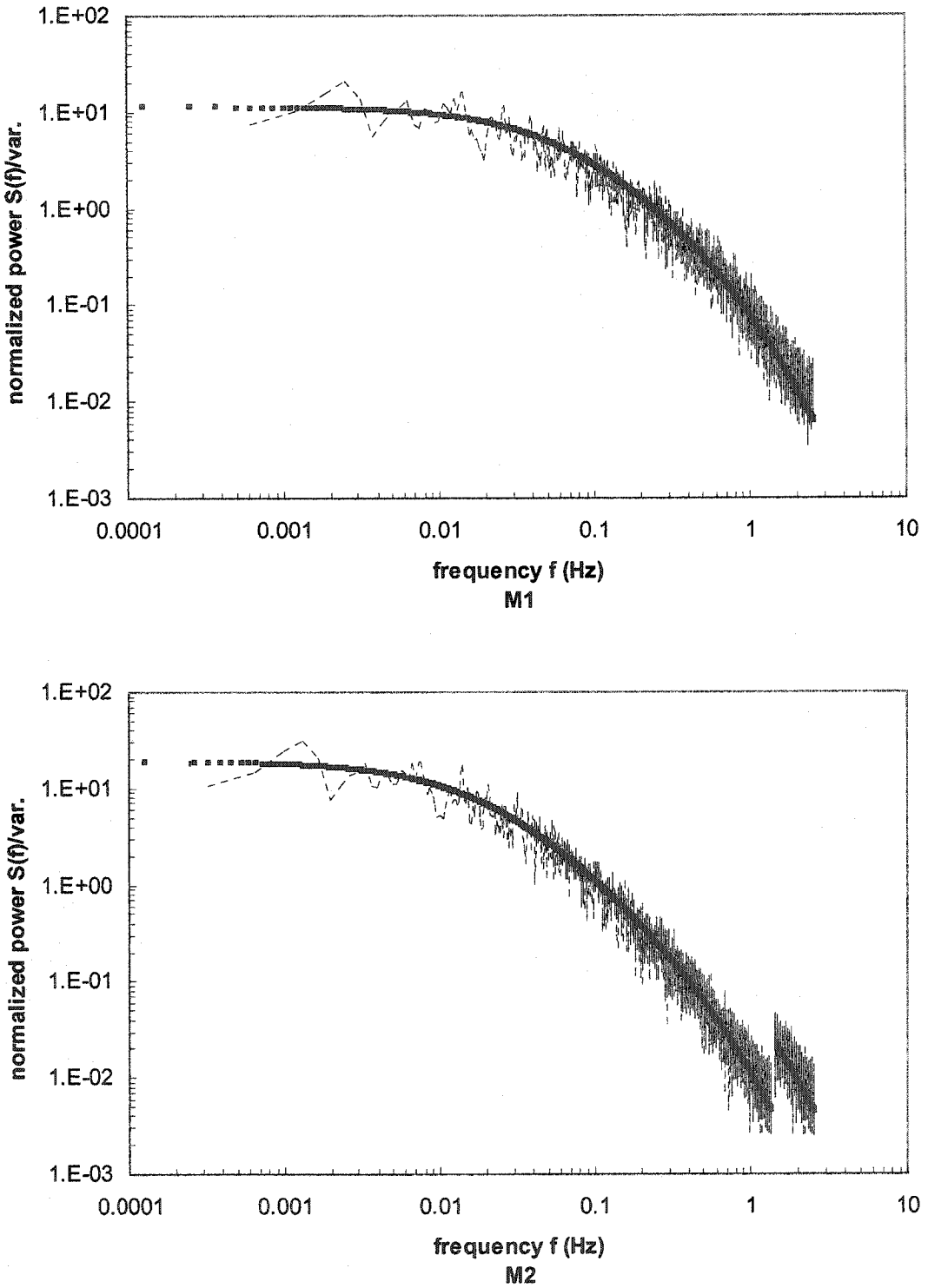

Figure 2.3.2 Comparison of Power Spectral Density Function for Alongwind Forces

The Target ■■■■■; The ARMA(85,77) Simulation -----

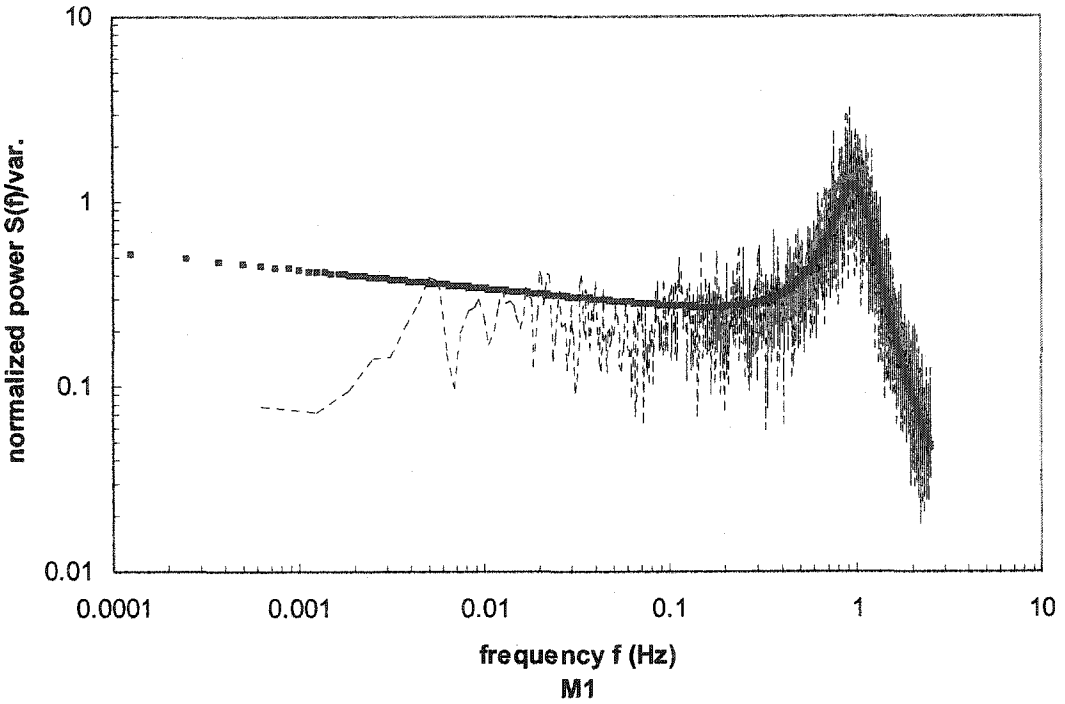

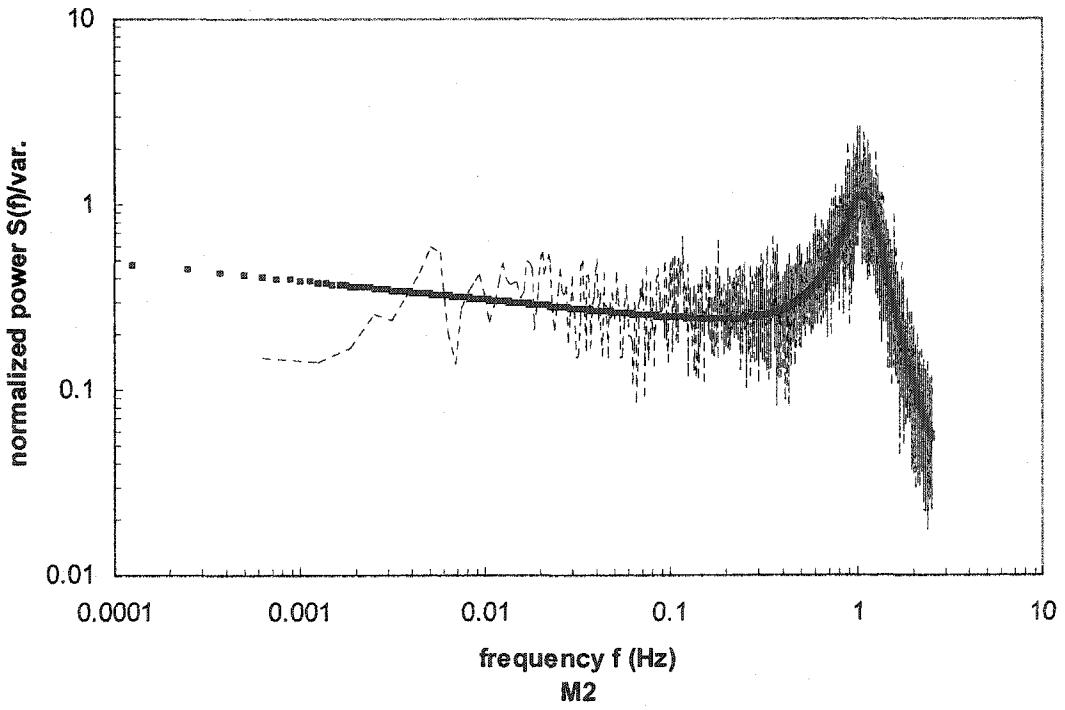

Figure 2.3.3 Comparison of Power Spectral Density Function for Crosswind Forces

The Target ■■■■■; The ARMA(75,75) Simulation -----

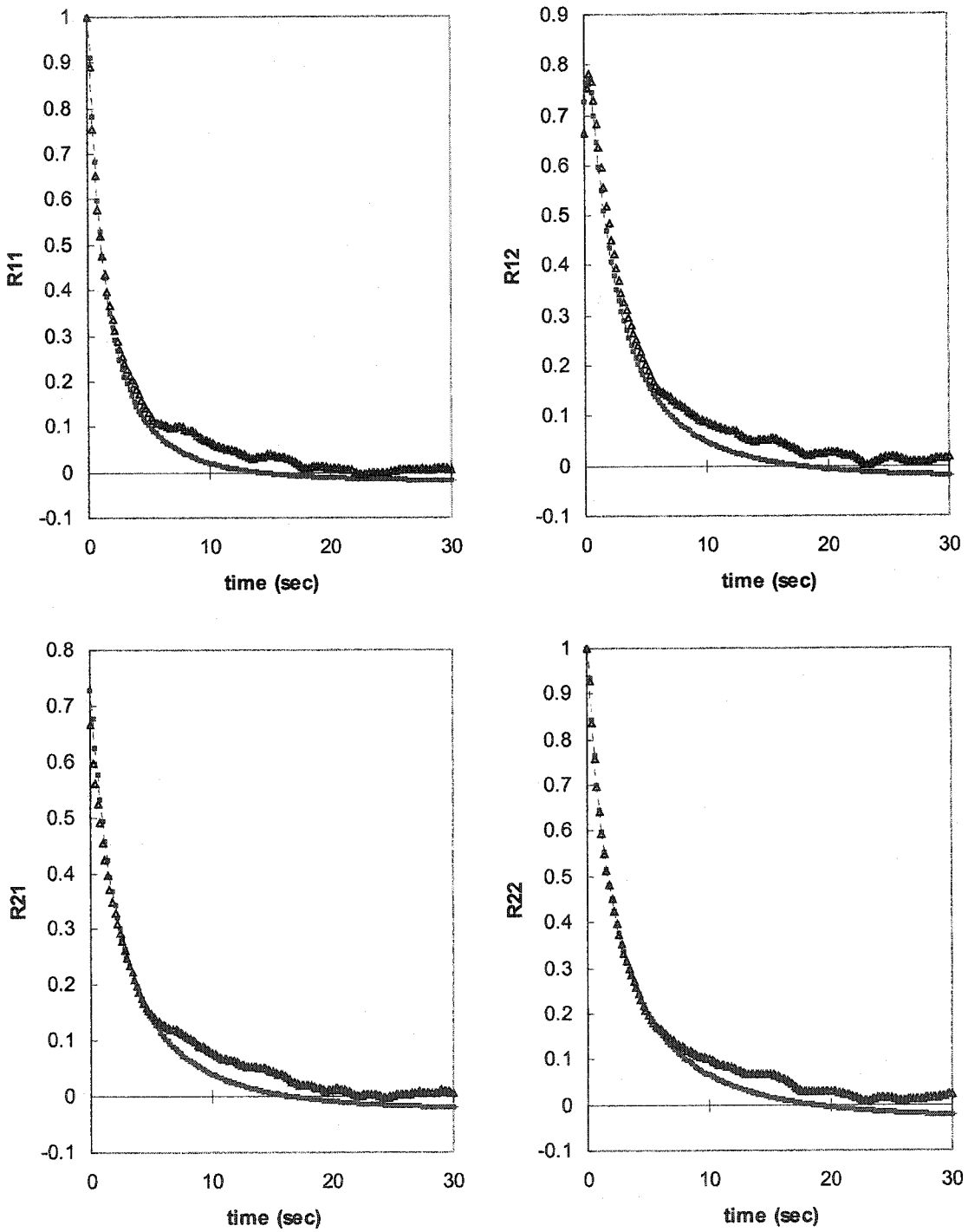

Figure 2.3.4 Comparison of Correlation Functions for Alongwind Forces

The Target ■--■--■; The ARMA(85,77) Simulation ΔΔΔΔΔ

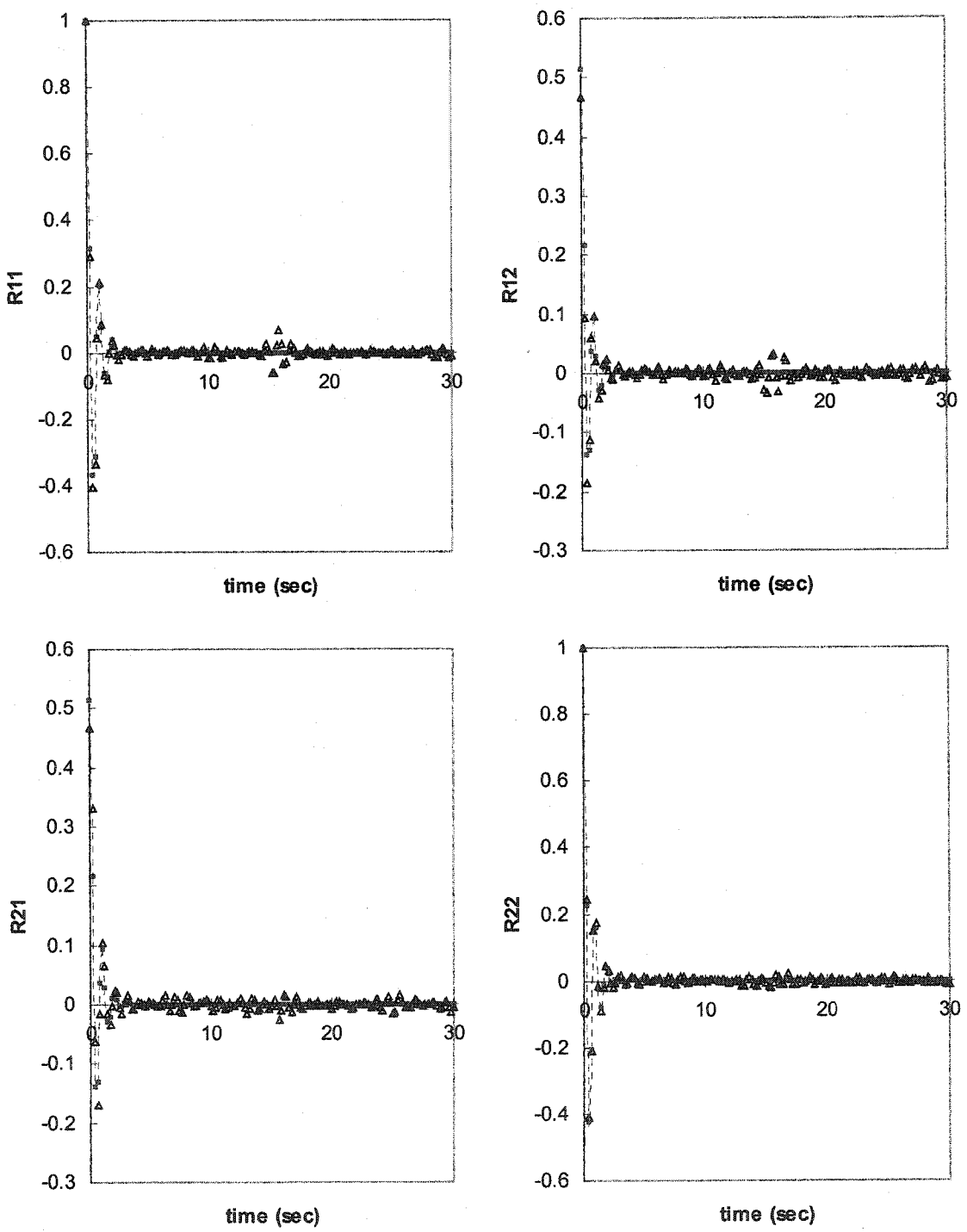

Figure 2.3.5 Comparison of Correlation Functions for Crosswind Forces

The Target ■--■--■; The ARMA(75,75) Simulation ΔΔΔΔΔ

References

Akaike, H. (1969), "Fitting Autoregressive Models For Prediction", Annuals of the Institute of Statistical Mathematics, Vol. 21, No. 2, pp. 243-247.

Akaike, H. (1971), "Autoregressive Model Fitting For Control", Annuals of the Institute of Statistical Mathematics, Vol. 23, No. 2, pp. 163-180.

Akaike, H. and Nakagawa, T. (1988), Statistical Analysis and Control of Dynamic Systems, 1st Edition, Kluwer Academic.

Bendat, J. S. and Piersol, A. G. (2000), Random Data: Analysis and Measurement Procedures, 3rd Edition, John Wiley & Sons, pp. 128-147.

Davenport, A. G. (1961), "The Spectrum Of Horizontal Gustiness Near The Ground In High Winds", Royal Meteorological Society, pp. 194-211.

Davenport, A. G. (1968), "The Dependence Of Wind Loads On Meteorological Parameters", Proceedings of the International Research Seminar on Wind Effects on Buildings and Structures, Vol. 1, pp. 19-82.

Durbin, J. (1960), "The Fitting Of Time-Series Models", Econometrica: Journal of the Econometric Society, Vol. 28, No. 3, pp. 703.

Gersch, W. and Luo, S. (1970), "Discrete Time Series Synthesis Of Randomly Excited Structural System Response", The Journal of the Acoustical Society of America, Vol. 51, pp. 402-408.

Gersch, W. and Liu, R. S. Z. (1976) "Time Series Methods For The Synthesis Of Random Vibration Systems", Journal of Applied Mechanics, ASME, Vol. 98, pp. 159-165.

Gersch, W. and Yonemoto, J. (1977) "Synthesis Of Multivariate Random Vibration Systems: A Two-Stage Least Squares ARMA Model Approach", Journal of Sound and Vibration, Vol. 52, No. 4, pp. 553-565.

Goto, H. and Toki, K. (1969), "Structural Response To Nonstationary Random Excitation", Proceeding of the 4th World Conference on Earthquake Engineering, pp. 130-144.

Iannuzzi, A. and Spinelli, P. (1987), "Artificial Wind Generation And Structural Response", Journal of Structural Engineering, Vol. 113, No. 12, pp. 2382-2398.

Iwatani, Y. (1982), "Simulation Of Multidimensional Wind Fluctuations Having Any Arbitrary Power Spectra And Cross Spectra", Journal of Wind Engineering, Japan Association for Wind Engineering, No. 11, pp. 5-18.

Kaimal, J. C., Wyngaard, J. C., Izumi, Y., and Coté, O. R. (1972), "Spectral Characteristics Of Surface Layer Turbulence", Journal of Royal Meteorological Society, Vol. 98, pp. 563-589.

Kareem, A. (1984), "Model For Predicting The Acrosswind Response Of Buildings", Engineering Structures, Vol. 6, pp. 136-141.

Kareem, A. (1982), "Acrosswind Response Of Buildings", Journal of the Structural Division, ASCE, Vol. 108, No. ST4, pp. 869-887.

Li, Y. S. and Kareem, A. (1990a), "ARMA Representation Of Wind Field", Journal of Wind Engineering and Industrial Aerodynamics, Vol. 36, pp. 415-427.

Li, Y. S. and Kareem, A. (1990b), "ARMA Systems In Wind Engineering", Probabilistic Engineering Mechanics, Vol. 5, No. 2, pp. 50-59.

Mignolet, M. P. and Spanos, P. D. (1987a), "Recursive Simulation Of Stationary Multivariate Random Processes – Part I", Journal of Applied Mechanics, ASME, Vol. 54, pp. 674-680.

Mignolet, M. P. and Spanos, P. D. (1990), "MA To ARMA Modeling Of Wind", Journal of Wind Engineering and Industrial Aerodynamics, Vol. 36, pp. 429-438.

Mignolet, M. P. and Spanos, P. D. (1992a), "Simulation Of Homogeneous Two-Dimensional Random Field: Part I – AR And ARMA Models", Journal of Applied Mechanics, ASME, Vol. 59, pp. S260-S269.

Naganuma, T., Deodatis, G., and Shinozuka, M. (1987), "ARMA Model For Two Dimensional Processes", Journal of Engineering Mechanics, Vol. 113, No. 2, pp. 234-251.

Panofsky, H. A., Thomson, D. W., Sullivan, D. A., and Moravek, D. E. (1974), "Two-Point Velocity Statistics Over Lake Ontario", Boundary Layer Meteorology, Vol. 7, pp. 309-321.

Samaras, E., Shinozuka, M., and Tsurui, A. (1985), "ARMA Representation Of Random Processes", Journal of Engineering Mechanics, Vol. 111, No. 3, pp. 449-461.

Shinozuka, M. (1971), "Simulation Of Multivariate And Multidimensional Random Processes", The Journal of the Acoustical Society of America, Vol. 49, No. 1, pp.357-368.

Shinozuka, M. (1972), "Monte Carlo Solution Of Structural Dynamics", Computers & Structures, Vol. 2, pp. 855-874.

Shinozuka, M. (1987), "Stochastic Fields And Their Digital Simulation", Stochastic Methods in Structural Dynamics, edited by Schuëller, G. I. And Shinozuka, M., Martinus Nijhoff Publishers, pp. 93-133.

Shinozuka, M. and Deodatis, G. (1991), "Simulation Of Stochastic Processes By Spectral Representation", Applied Mechanics Review, ASME, Vol. 44, No. 4, pp. 191-203.

Shinozuka, M. and Jan, C. M. (1972), "Digital Simulation Of Random Processes And Its Applications", Journal of Sound and Vibration, Vol. 25, No. 1, pp. 111-128.

Shinozuka, M., Yun, C. B., and Seya, H. (1990), "Stochastic Methods In Wind Engineering", Journal of Wind Engineering and Industrial Aerodynamics, Vol. 36, pp. 829-843.

Shiotani, M. and Iwatani, Y. (1979), "Gust Structures Over Flat Terrains And Their Modification By A Barrier", Proceedings of the 5th International Conference, Vol. 1, pp. 203-214.

Spanos, P. D. and Mignolet, M. P. (1992b), "Simulation Of Homogeneous Two-Dimensional Random Fields: Part II – MA And ARMA Models", Journal of Applied Mechanics, ASME, Vol. 59, pp. S270-S277.

Spanos, P. D. and Mignolet, M. P. (1989), "ARMA Monte Carlo Simulation In Probabilistic Structural Analysis", The Shock and Vibration Digest, Vol. 21, No. 11, pp. 3-14.

Spanos, P. D. and Mignolet, M. P. (1987b), "Recursive Simulation Of Stationary Multivariate Random Processes - Part II", Journal of Applied Mechanics, ASME, Vol. 54, pp. 681-687.

Spanos, P. D. and Mignolet, M. P. (1986), "Z-Transform Modeling Of P-M Wave Spectrum", Journal of Engineering Mechanics, Vol. 112, No. 8, pp. 745-759.

Spanos, P. D. and Schultz, K. P. (1985), "Two-Stage Order-Of-Magnitude Matching For The Von Karman Turbulence Spectrum", The 4th International Conference on Structural Safety and Reliability, pp. I211-I216.

Spanos, P. D. and Schultz, K. P. (1986), "Numerical Synthesis Of Trivariate Velocity Realizations Of Turbulence", International Journal of Nonlinear Mechanics, Vol. 21, No. 4, pp. 269-277.

Tamura, Y., Wada, A., Ohkoshi, T., and Kawamura, M. (1988), "Simulation Of Wind-Induced Vibrations Of Tall Buildings", Summaries of Technical Papers of Annual Meeting, Architectural Institute of Japan, PP. 143-144 (in Japanese).

Thiel, H. (1950), Economic Forecast and Policy, North Holland Publishing Company, Amsterdam.

Tsukagoshi, H., Tamura, Y., Sasaki, A., and Kanai, H. (1993), "Response Analyses On Along-wind And Across-wind Vibrations of Tall Buildings In Time Domain", Journal of Wind Engineering and Industrial Aerodynamics, Vol. 46 & 47, pp. 497-506.

Vickery, B. J. (1968), "Load Fluctuations In Turbulent Flow", Journal of the Engineering Mechanics Division, ASCE, Vol. 94, No. EM1, pp. 31-46.

Walker, G. (1931), "On Periodicity In Series Of Related Terms", Proceedings of the Royal Society of London, Vol. 131, pp. 518-532.

Wei, W. S. (1990), Time Series Analysis – Univariate and Multivariate Methods, 1st Edition, Addison-Wesley, pp. 332-337.

Yule, G. U. (1927), "On A Method Of Investigating Periodicities In Disturbed Series, With Special Reference To Wolfer's Sunspot Numbers", Philosophical Transactions of the Royal Society of London, Vol. 226, pp. 267-298.

Chapter 3

RANDOM DECREMENT TECHNIQUE

3.1 Introduction

The random decrement (RD) technique was explored initially and developed heuristically by Cole [1968, 1971], while investigating the application of correlation functions for the measurement of on-line damping ratio and natural period in aircraft model tests at NASA. The RD technique provided a simple and direct method, instead of the FFT based approach, to implement data analysis of vibration systems excited by random forces. Since the RD technique was introduced, practical applications have widely appeared, such as identification of modal parameters and on-line monitoring of damages in structural and mechanical systems [Houbolt, 1975; Yang et al., 1976, 1978, 1981; Caldwell, 1978; Jerry, 1981, 1986, 1992; Tamura et al., 1993, 1994, 1996]. In addition, the RD technique provided the principal basis for the Ibrahim time domain algorithm [Ibrahim, 1977; Ibrahim and Mikulcik, 1977] that requires a set of free vibration responses to simultaneously identify all parameters of the dominant modes in a system. To further explain the concept of the RD technique, the mathematical descriptions were developed from an intuitive standpoint [Chang, 1975; Yang, 1976; Caldwell, 1978; Huan, 1983]. However, such an intuitively developed RD technique has been criticized for its lack of a rigorous mathematical proof.

A strict theoretical proof for the RD technique was not proposed until 1982 by Vandiver et al., who established the general relationship between the auto-correlation

function and the auto RD signature for a linear and time-invariant dynamic system: one excited by a Gaussian stochastic process with a zero mean. Bedewi [1986] expanded the work of Vandiver to theoretically develop the multiple-signal RD technique for a linear multiple-degree-of-freedom (MDOF) dynamic system. It was also indicated by Bedewi that the auto and cross RD displacement signatures are identical to the corresponding free vibration responses of a dynamic system, when input forces are Gaussian white noise processes. Brincker et al. [1990, 1992] proposed the generalized formulae of the RD signatures in terms of correlation functions for different triggering conditions, and he also pointed out the introduction of the bias because of finite-size trig windows. Spanos and Zeldin [1998] showed that the RD signature is not a system free vibration response if the input excitation is not white noise, since the RD signature associated with a linear dynamic system is influenced by the parameters of the excitation.

Up to this point, the relation between the RD signature and the free vibration response was typically derived for displacement response. In other words, the characteristics of the RD signature for other responses still needed more attentions at that time. Therefore, Huang et al. [1996, 1998, 1999] focused on expanding the mathematical derivation of the relations between the RD signatures and the corresponding free vibration responses from displacement response to velocity response and acceleration response. It was satisfactorily shown that the RD displacement and velocity signatures are equivalent to the corresponding free vibration responses. However, it was indicated that the RD acceleration signatures are never equivalent to the corresponding free vibration responses because singular behavior exists in such RD signatures. This singular behavior mainly resulted from the statistical property of white noise excitation that is the

input force to a dynamic system. This consequence motivates investigations regarding whether the RD technique is still useful in extracting the free vibration response from an acceleration response, in spite of the existence of the singularity.

The new challenge, an analytical free vibration acceleration response, is difficult to achieve without knowledge of the initial displacement and velocity conditions. In this study, a new procedure is proposed to determine the required initial conditions from the synchronous RD signatures of displacement and velocity responses in a numerical simulation. Given such initial conditions, the analytical free vibration responses can be obtained and then compared with the corresponding RD signatures.

To accomplish a better understanding of the proposed procedure, the theoretical background of the RD technique associated with the general triggering condition is first introduced as a prerequisite. Following the introduction of the RD technique, the variances of the estimated RD signatures with the general triggering condition are further derived. The generalized relevance of the auto RD signatures and the analytical free vibration responses is established when the input excitation to a SDOF dynamic system is a Gaussian white noise process. In addition to the theoretical development of the RD technique, the supplement of numerical simulation is presented by taking advantage of a single-degree-of-freedom (SDOF) dynamic system loaded by a white noise excitation. The application of the proposed procedure with two different triggering conditions is made to gain a better understanding of the properties within the RD signatures. The practical application of the RD technique to wind-induced responses is then contrasted to results of the theoretical derivations under the assumption of a Gaussian white noise.

3.2 Development of Random Decrement Technique

The basic concept of the RD technique proposed by Cole is illustrated in Figure 3.2.1. As shown, an ensemble average signature is formed to represent a free vibration response of a system by processing pre-selected segments from measured data. In Figure 3.2.2, there are three parts due to initial displacement $x_d(t)$, initial velocity $x_v(t)$, and forcing function $x_F(t)$, which constitute the total response. The starting time, t_0, of each sampling segment is selected so that each sampling segment of time length τ begins at the same displacement x_d and the slope of the initial displacement alternates between the positive and negative. Eventually, the formation of the RD signature $\delta_{XX}(\tau)$ is carried out by averaging N sampling segments. This preceding description is expected to use a mathematical expression as following:

$$\delta_{XX}(\tau) = \frac{1}{N}\sum_{n=1}^{N} X_n(t_0+\tau)\Big| X_n(t_0) = x_d \tag{3.2.1}$$

in which

$$\begin{aligned} X_n(t_0) &= x_d \qquad && n = 1,2,3,\ldots \\ \dot{X}_n(t_0) &\geq 0 \qquad && n = 1,3,5,\ldots \\ \dot{X}_n(t_0) &\leq 0 \qquad && n = 2,4,6,\ldots \end{aligned}$$

Furthermore, it is seen from Figure 3.2.2 that the averaging part due to the initial velocity is cancelled out, because the slopes of the initial velocity responses are expected to change sign randomly. Correspondingly, as the number of the averaged segments increases, the part due to the forcing function is also averaged to vanish because of its random characteristic. In the end, only the part due to the initial displacement x_d remains and their average is a free decay curve of the system.

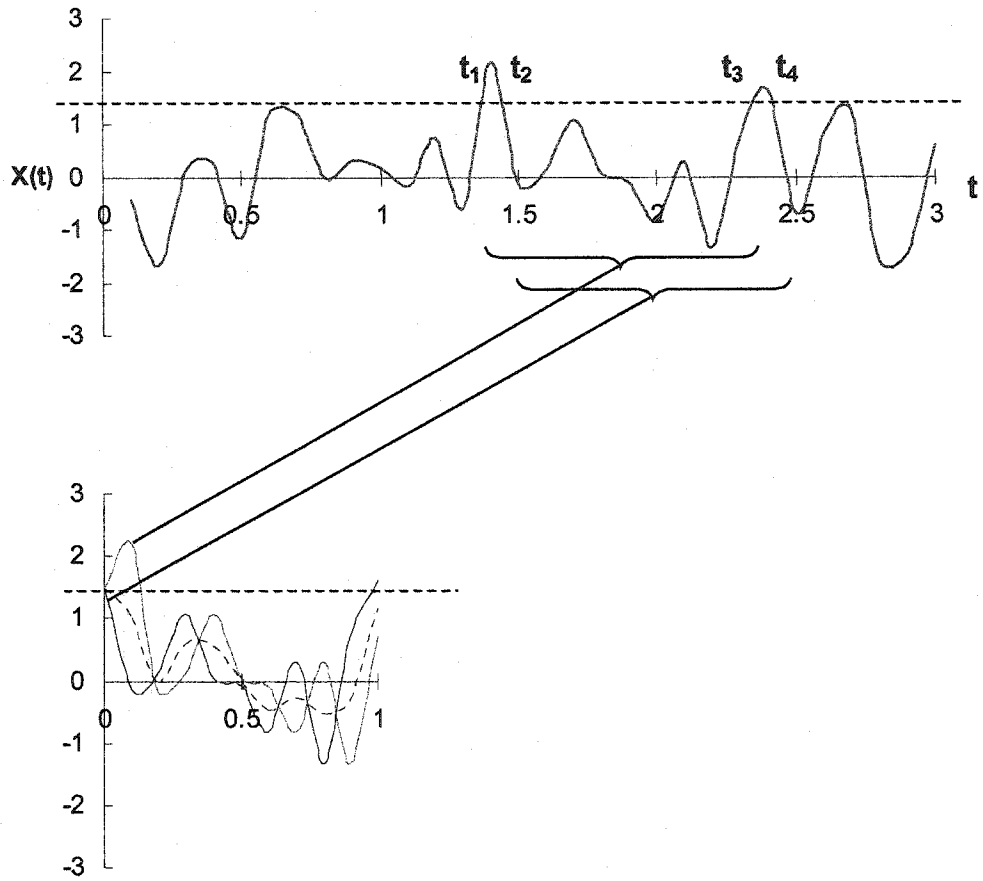

Figure 3.2.1 Extraction of Random Decrement Signature

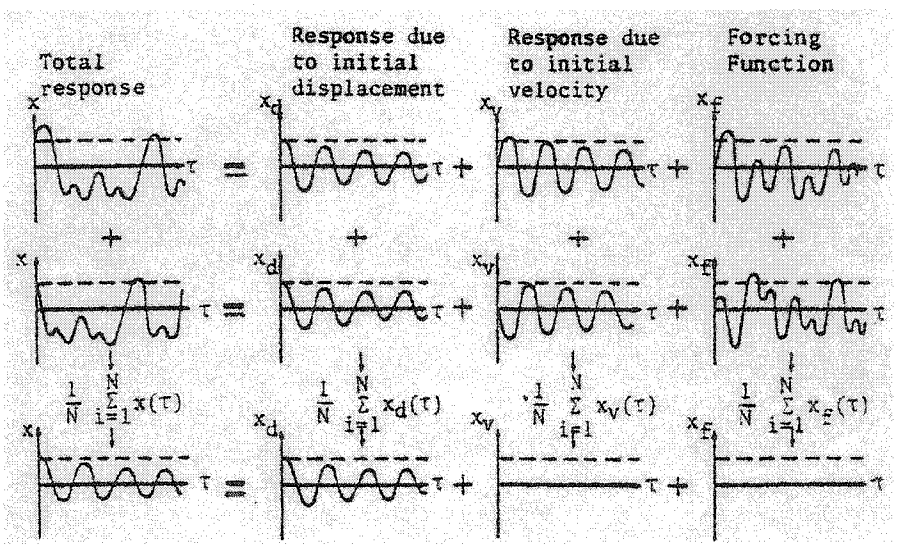

Figure 3.2.2 Principles of Random Decrement Technique [Yang et al., 1981]

3.3 Definition of Random Decrement Signatures

In general, the theoretical definition of the auto RD signatures, $\delta_{XX}(\tau)$ and $\delta_{YY}(\tau)$, and cross RD signatures, $\delta_{XY}(\tau)$ and $\delta_{YX}(\tau)$, for stationary stochastic processes, $X(t)$ and $Y(t)$, can be expressed as:

$$\delta_{XX}(\tau) = E[X(t+\tau)|T_{X(t)}] \tag{3.3.1}$$

$$\delta_{YY}(\tau) = E[Y(t+\tau)|T_{Y(t)}] \tag{3.3.2}$$

$$\delta_{XY}(\tau) = E[X(t+\tau)|T_{Y(t)}] \tag{3.3.3}$$

$$\delta_{YX}(\tau) = E[Y(t+\tau)|T_{X(t)}] \tag{3.3.4}$$

in which $T_{X(t)}$ and $T_{Y(t)}$ denote as triggering conditions at a time of t and $E[|]$ represents the conditional expectation operator [Stark and Woods, 1994]. It is assumed that the triggering condition is not null. Otherwise, the following derivations are invalid.

3.4 Relation between Correlation Functions and RD Signatures

Vandiver et al. [1982] and Bedewi [1986] theoretically presented the proportional relation between the auto and cross RD signatures and the correlation functions, which is defined by using the level crossing triggering condition. To fulfill the application of any particular triggering condition, Brincker et al. [1992] and Asmussen [1997] further proposed the formulation of the general triggering condition. On the basis of the general triggering condition, a versatile relation between the RD signatures and their correlation functions was established.

In the ensuing subsections, the formulations of three various triggering conditions are applied to demonstrate the versatility of the RD signatures. Moreover, the variances

of the estimated RD signatures, based on the general triggering condition, are derived in this study following the introduction of the statistical properties for the RD signatures.

3.4.1 General Triggering Condition

As described, establishing the generalized formula of the RD signatures is a starting point for all various triggering conditions. In this respect, a mathematical tool based on the minimum mean square error estimator is applied in the following derivation. To begin, it is assumed that random vector $\underline{X} = (X_1, X_2, ..., X_n)$ and random variable Y are jointly Gaussian distributed with zero means. The conditional mean and the conditional variance are derived, respectively, as [Papoulis and Pillai, 2002]:

$$\mu_{Y|\underline{X}} = E[Y|\underline{X}] = \underline{A}\underline{X}^T = \sum_{i=1}^{n} a_i X_i \tag{3.4.1}$$

$$\sigma^2_{Y|\underline{X}} = Var[Y|\underline{X}] = E[YY^T] - E[\underline{A}\underline{X}^T Y] = R_{YY} - \underline{A}R^T_{\underline{X}Y} \tag{3.4.2}$$

in which $\underline{A} = [a_1, a_2, ..., a_n]$ is a constant vector and R denotes a correlation function matrix. Since $(Y - \underline{A}\underline{X}^T)$ is independent of x_i, it follows that $E[\underline{X}(Y - \underline{A}\underline{X}^T)] = \underline{0}$. As a result, $\underline{A}$ can be explicitly determined by:

$$\underline{A} = R_{\underline{X}Y} R^{-1}_{\underline{X}\underline{X}} \tag{3.4.3}$$

in which

$$R_{\underline{X}\underline{X}} = \begin{bmatrix} R_{X_1X_1} & R_{X_1X_2} & \cdots & R_{X_1X_n} \\ & R_{X_2X_2} & \cdots & R_{X_2X_n} \\ & & \ddots & \vdots \\ sym. & & & R_{X_nX_n} \end{bmatrix} \tag{3.4.4}$$

$$R_{\underline{X}Y} = \begin{bmatrix} R_{X_1Y} & R_{X_2Y} & \cdots & R_{X_nY} \end{bmatrix} \tag{3.4.5}$$

Corresponding to the conditional mean in Equation (3.4.1), the general formulae of the RD signatures in connection with the correlation functions and the triggering condition $T_{X(t)} = \{X(0) = x_0, \dot{X}(0) = \dot{x}_0\}$ are established as follows [Brincker, 1992]:

$$\begin{aligned}\delta_{XX}(\tau) &= E[X(\tau)|X(0) = x_0, \dot{X}(0) = \dot{x}_0] \\ &= \begin{bmatrix} R_{XX}(\tau) & R_{\dot{X}X}(\tau) \end{bmatrix} \begin{bmatrix} \sigma_X^2 & R_{X\dot{X}}(0) \\ R_{\dot{X}X}(0) & \sigma_{\dot{X}}^2 \end{bmatrix}^{-1} \begin{bmatrix} x_0 \\ \dot{x}_0 \end{bmatrix} \\ &= \frac{R_{XX}(\tau)}{\sigma_X^2} x_0 - \frac{R'_{XX}(\tau)}{\sigma_{\dot{X}}^2} \dot{x}_0 \end{aligned} \tag{3.4.6}$$

$$\begin{aligned}\delta_{YX}(\tau) &= E[Y(\tau)|X(0) = x_0, \dot{X}(0) = \dot{x}_0] \\ &= \begin{bmatrix} R_{XY}(\tau) & R_{\dot{X}Y}(\tau) \end{bmatrix} \begin{bmatrix} \sigma_X^2 & R_{X\dot{X}}(0) \\ R_{\dot{X}X}(0) & \sigma_{\dot{X}}^2 \end{bmatrix}^{-1} \begin{bmatrix} x_0 \\ \dot{x}_0 \end{bmatrix} \\ &= \frac{R_{XY}(\tau)}{\sigma_X^2} x_0 - \frac{R'_{XY}(\tau)}{\sigma_{\dot{X}}^2} \dot{x}_0 \end{aligned} \tag{3.4.7}$$

It should be noted that the first derivative of the auto-correlation function occurring at the zero time delay, $\tau = 0$, is zero [Bendat and Piersol, 2000], *i.e.*

$$R'_{XX}(0) = \left. \frac{dE[X(t)X(t+\tau)]}{d\tau} \right|_{\tau=0} = E[X(t)\dot{X}(t)] = -E[\dot{X}(t)X(t)] = 0$$

Subsequently, the conditional variances of the RD signatures, as follows, can also be calculated by relating to Equation (3.4.2).

$$\begin{aligned} Var[X(\tau)|X(0) = x_0, \dot{X}(0) = \dot{x}_0] &= R_{XX}(0) - \frac{R_{XX}^2(\tau)}{R_{XX}(0)} - \frac{R_{\dot{X}X}^2(\tau)}{R_{\dot{X}\dot{X}}(0)} \\ &= R_{XX}(0) - \frac{R_{XX}^2(\tau)}{\sigma_X^2} - \frac{R_{XX}'^2(\tau)}{\sigma_{\dot{X}}^2} \end{aligned} \tag{3.4.8}$$

$$\begin{aligned} Var[Y(\tau)|X(0) = x_0, \dot{X}(0) = \dot{x}_0] &= R_{YY}(0) - \frac{R_{XY}^2(\tau)}{R_{XX}(0)} - \frac{R_{\dot{X}Y}^2(\tau)}{R_{\dot{X}\dot{X}}(0)} \\ &= R_{YY}(0) - \frac{R_{XY}^2(\tau)}{\sigma_X^2} - \frac{R_{XY}'^2(\tau)}{\sigma_{\dot{X}}^2} \end{aligned} \tag{3.4.9}$$

However, the RD signatures are estimated in practice from a finite number of samples because of a finite length record. Therefore, it is important to realize in essence whether the estimates of the auto and cross RD signatures are unbiased or not. If the stochastic processes are strictly assumed to be ergodic, the estimates of the auto and cross RD signatures for a finite number of samples can be expressed by:

$$\hat{\delta}_{XX}(\tau) = \frac{1}{N}\sum_{i=1}^{N} X_i(\tau) | X_i(0) = x_0, \dot{X}_i(0) = \dot{x}_0 \tag{3.4.10}$$

$$\hat{\delta}_{YX}(\tau) = \frac{1}{N}\sum_{i=1}^{N} Y_i(\tau) | X_i(0) = x_0, \dot{X}_i(0) = \dot{x}_0 \tag{3.4.11}$$

in which the hat ^ over $\delta(\tau)$ indicates the estimate of the true $\delta(\tau)$. As is well known, the sample mean and the sample variance of N random variables x_i are defined, respectively, by:

$$\bar{x} = \frac{1}{N}\sum_{i=1}^{N} x_i \tag{3.4.12}$$

$$s^2 = \frac{1}{N-1}\sum_{i=1}^{N} (x_i - \bar{x})^2 \tag{3.4.13}$$

It can be shown that if the random variables are uncorrelated with the same mean μ and variance σ^2, the expectation and the variance of the sample mean are given, respectively, as follows [Bendat and Piersol, 2000]:

$$E[\bar{x}] = \mu \tag{3.4.14}$$

$$Var[\bar{x}] = \frac{\sigma_x^2}{N} \tag{3.4.15}$$

Therefore, the means and variances of the estimated RD signatures in Equations (3.4.10) and (3.4.11) are derived in terms of Equations (3.4.6-9) and (3.4.14-15) as follows:

$$E[\hat{\delta}_{XX}(\tau)] = \frac{R_{XX}(\tau)}{\sigma_X^2} x_0 - \frac{R'_{XX}}{\sigma_{\dot{X}}^2} \dot{x}_0 = \delta_{XX} \tag{3.4.16}$$

$$E[\hat{\delta}_{YX}(\tau)] = \frac{R_{XY}(\tau)}{\sigma_X^2} x_0 - \frac{R'_{XY}}{\sigma_{\dot{X}}^2} \dot{x}_0 = \delta_{YX} \tag{3.4.17}$$

and

$$Var[\hat{\delta}_{XX}(\tau)] = \frac{1}{N}\left(R_{XX}(0) - \frac{R_{XX}^2(\tau)}{\sigma_X^2} - \frac{R_{XX}'^2(\tau)}{\sigma_{\dot{X}}^2} \right) \tag{3.4.18}$$

$$Var[\hat{\delta}_{YX}(\tau)] = \frac{1}{N}\left(R_{YY}(0) - \frac{R_{XY}^2(\tau)}{\sigma_X^2} - \frac{R_{XY}'^2(\tau)}{\sigma_{\dot{X}}^2} \right) \tag{3.4.19}$$

From Equations (3.4.16-19), it follows that the means of the estimated RD signatures are unbiased and the variances of the estimated RD signatures decrease when the number of the superimposed samples increases. Generally, the variance of the estimated RD signatures increases with the increase of the time lags from its initial position. Besides, it can be concluded that the variances of the estimated RD signatures are independent of the triggering conditions.

3.4.2 Level Crossing Triggering Condition

The level crossing triggering condition, as illustrated in Figure 3.4.1, is frequently used in data processing. When $X(t)$ and $Y(t)$ are Gaussian stochastic processes, Equations (3.4.6) and (3.4.7) yield functions of time delay τ and a chosen triggering level x_0 for the triggering condition $T_{X(t)} = \{X(t) = x_0\}$ as follows:

$$\delta_{XX}(\tau) = E[X(\tau) | X(0) = x_0] = \frac{R_{XX}(\tau)}{R_{XX}(0)} x_0 \tag{3.4.20}$$

$$\delta_{YX}(\tau) = E[Y(\tau)|X(0) = x_0] = \frac{R_{XY}(\tau)}{R_{XX}(0)} x_0 \tag{3.4.21}$$

, respectively, in which $R_{XX}(\tau)$ is the auto-correlation function of the stochastic process, $X(t)$, and $R_{XY}(\tau)$ is the cross-correlation function between the stochastic processes, $X(t)$ and $Y(t)$.

The conditional variances of the RD signatures for such a triggering condition can be derived directly from Equations (3.4.8) and (3.4.9).

$$Var[X(\tau)|X(0) = x_0] = R_{XX}(0) - \frac{R_{XX}^2(\tau)}{R_{XX}(0)} \tag{3.4.22}$$

$$Var[Y(\tau)|X(0) = x_0] = R_{YY}(0) - \frac{R_{XY}^2(\tau)}{R_{XX}(0)} \tag{3.4.23}$$

If the stochastic processes are assumed to be ergodic, the estimates of the conditional means and the conditional variances are directly obtained from Equations (3.4.16-17) and (3.4.18-19) as:

$$E[\hat{\delta}_{XX}(\tau)] = \frac{R_{XX}(\tau)}{\sigma_X^2} x_0 = \delta_{XX} \tag{3.4.24}$$

$$E[\hat{\delta}_{YX}(\tau)] = \frac{R_{XY}(\tau)}{\sigma_X^2} x_0 = \delta_{YX} \tag{3.4.25}$$

and

$$Var[\hat{\delta}_{XX}(\tau)] = \frac{1}{N}\left(R_{XX}(0) - \frac{R_{XX}^2(\tau)}{\sigma_X^2} \right) \tag{3.4.26}$$

$$Var[\hat{\delta}_{YX}(\tau)] = \frac{1}{N}\left(R_{YY}(0) - \frac{R_{XY}^2(\tau)}{\sigma_X^2} \right) \tag{3.4.27}$$

Equations (3.4.20-27) are the same expressions as the results of Vandiver and Bedewi whose derivations used the concept of the normal probability distribution instead.

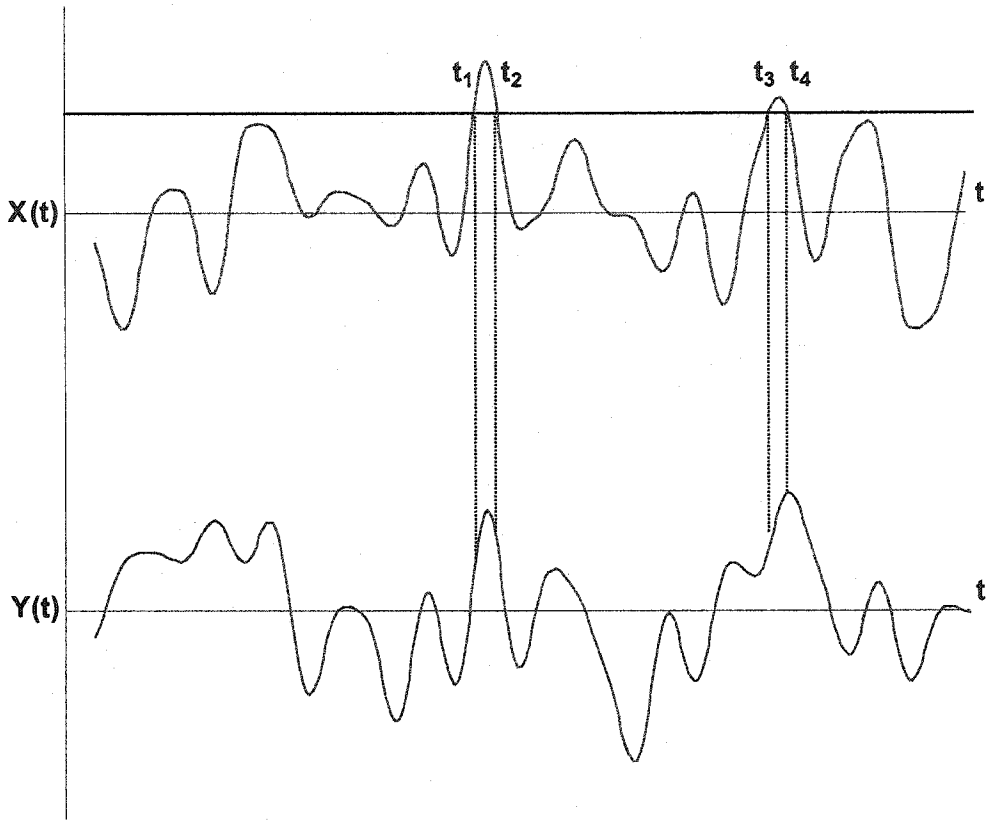

Figure 3.4.1 Multi-Signal RD Technique and Level-Crossing Triggering Condition

3.4.3 Constant Slope Triggering Condition

The triggering condition can be based on a constant slope, $T_{X(t)} = \{\dot{X}(t) = \dot{x}_0\}$. Such a triggering condition implies that the final position of the amplitude $X(t)$ is zero as well as the zero slope, $\dot{X}(t) = 0$, for the level crossing triggering condition. It is because the contributions from the positive and negative components of the stochastic process $X(t)$ detected at the instant of $\dot{X}(t) = \dot{x}_0$ are averaged out. With the introduction of the above triggering condition, Equations (3.3.1) and (3.3.4) are therefore rewritten as:

$$\delta_{XX}(\tau) = E[X(t+\tau)|\dot{X}(t) = \dot{x}_0] \tag{3.4.28}$$

$$\delta_{YX}(\tau) = E[Y(t+\tau)|\dot{X}(t) = \dot{x}_0] \tag{3.4.29}$$

From Equations (3.4.6) and (3.4.7), it follows that the auto and cross RD signatures for such a triggering condition can be given straightforwardly as:

$$\delta_{XX}(\tau) = -\frac{R'_{XX}(\tau)}{\sigma^2_{\dot{X}}}\dot{x}_0 \tag{3.4.30}$$

$$\delta_{YX}(\tau) = -\frac{R'_{XY}(\tau)}{\sigma^2_{\dot{X}}}\dot{x}_0 \tag{3.4.31}$$

In addition, the derivation of Equations (3.4.30) and (3.4.31) relating to the concept of the normal probability density function is well shown here. As mentioned, if $X(t)$ and $Y(t)$ and their first derivatives, $\dot{X}(t)$ and $\dot{Y}(t)$, are assumed as the Gaussian stochastic processes with zero means, it is known that the marginal and joint probability density functions of these stochastic processes are respectively defined as:

$$p_{X(t)}(X) = \frac{1}{\sqrt{2\pi}\sigma_X}\exp\left(\frac{-X^2}{2\sigma^2_X}\right) \tag{3.4.32}$$

$$p_{\dot{X}(t)}(\dot{X}) = \frac{1}{\sqrt{2\pi}\sigma_{\dot{X}}}\exp\left(\frac{-\dot{X}^2}{2\sigma^2_{\dot{X}}}\right) \tag{3.4.33}$$

and

$$p_{\dot{X}(t)X(t+\tau)}(\dot{X},X) = \frac{1}{2\pi\sigma_{\dot{X}}\sigma_X\sqrt{1-\rho^2_{\dot{X}X}}}\cdot \exp\left\{\frac{-1}{2(1-\rho^2_{\dot{X}X})}\left[\left(\frac{\dot{X}}{\sigma_{\dot{X}}}\right)^2 - 2\rho_{\dot{X}X}\left(\frac{\dot{X}}{\sigma_{\dot{X}}}\right)\left(\frac{X}{\sigma_X}\right)+\left(\frac{X}{\sigma_X}\right)^2\right]\right\} \tag{3.4.34}$$

$$p_{\dot{X}(t)Y(t+\tau)}(\dot{X},Y) = \frac{1}{2\pi\sigma_{\dot{X}}\sigma_Y\sqrt{1-\rho^2_{\dot{X}Y}}}\cdot \exp\left\{\frac{-1}{2(1-\rho^2_{\dot{X}Y})}\left[\left(\frac{\dot{X}}{\sigma_{\dot{X}}}\right)^2 - 2\rho_{\dot{X}X}\left(\frac{\dot{X}}{\sigma_{\dot{X}}}\right)\left(\frac{Y}{\sigma_Y}\right)+\left(\frac{Y}{\sigma_Y}\right)^2\right]\right\} \tag{3.4.35}$$

in which

$$\begin{aligned}\sigma_X^2 &= R_{XX}(0)\\ \sigma_Y^2 &= R_{YY}(0)\\ \rho_{\dot{X}X}(\tau) &= \frac{R_{\dot{X}X}(\tau)}{\sigma_{\dot{X}}\sigma_X}\\ \rho_{\dot{X}Y}(\tau) &= \frac{R_{\dot{X}Y}(\tau)}{\sigma_{\dot{X}}\sigma_Y}\end{aligned} \tag{3.4.36}$$

Based on the definition of the conditional probability density function,

$$p_{Y|X}(y|x) = \frac{p_{XY}(x,y)}{p_X(x)} \tag{3.4.37}$$

the following results are obtained:

$$p_{X(t+\tau)|\dot{X}(t)}(X|\dot{X}=\dot{x}_0) = \frac{1}{\sqrt{2\pi}\sigma_a}\exp\left[\frac{-1}{2\sigma_a^2}\left(X - \frac{R_{\dot{X}X}(\tau)}{\sigma_{\dot{X}}^2}\dot{x}_0\right)^2\right] \tag{3.4.38}$$

$$p_{Y(t+\tau)|\dot{X}(t)}(Y|\dot{X}=\dot{x}_0) = \frac{1}{\sqrt{2\pi}\sigma_b}\exp\left[\frac{-1}{2\sigma_b^2}\left(Y - \frac{R_{\dot{X}Y}(\tau)}{\sigma_{\dot{X}}^2}\dot{x}_0\right)^2\right] \tag{3.4.39}$$

in which

$$\begin{aligned}\sigma_a &= \sigma_X\sqrt{1-\rho_{\dot{X}X}^2}\\ \sigma_b &= \sigma_Y\sqrt{1-\rho_{\dot{X}Y}^2}\end{aligned} \tag{3.4.40}$$

The expectations of Equations (3.4.38) and (3.4.39) are simply the definitions of the auto and cross RD signatures in Equations (3.4.28) and (3.4.29). Therefore, the auto and cross RD signatures are:

$$\delta_{XX}(\tau) = \frac{R_{\dot{X}X}(\tau)}{\sigma_{\dot{X}}^2}\dot{x}_0 = \frac{-R'_{XX}(\tau)}{\sigma_{\dot{X}}^2}\dot{x}_0 \tag{3.4.41}$$

$$\delta_{YX}(\tau) = \frac{R_{\dot{X}Y}(\tau)}{\sigma_{\dot{X}}^2}\dot{x}_0 = \frac{-R'_{XY}(\tau)}{\sigma_{\dot{X}}^2}\dot{x}_0 \tag{3.4.42}$$

which are the same expressions as Equations (3.4.30) and (3.4.31).

Similarly, the means and variances of the estimated RD signatures for Equations (3.4.41) and (3.4.42) can be determined as:

$$E[\hat{\delta}_{XX}(\tau)] = -\frac{R'_{XY}}{\sigma^2_{\dot{X}}}\dot{x}_0 = \delta_{XX} \tag{3.4.43}$$

$$E[\hat{\delta}_{YX}(\tau)] = -\frac{R'_{XY}}{\sigma^2_{\dot{X}}}\dot{x}_0 = \delta_{YX} \tag{3.4.44}$$

and

$$Var[\hat{\delta}_{XX}(\tau)] = \frac{1}{N}\left(R_{XX}(0) - \frac{R'^2_{XX}(\tau)}{\sigma^2_{\dot{X}}}\right) \tag{3.4.45}$$

$$Var[\hat{\delta}_{YX}(\tau)] = \frac{1}{N}\left(R_{YY}(0) - \frac{R'^2_{XY}(\tau)}{\sigma^2_{\dot{X}}}\right) \tag{3.4.46}$$

3.4.4 Positive Peak Triggering Condition

When the positive peak triggering condition $T_{X(t)} = \{0 \le X(t) < \infty, \dot{X}(t) = 0\}$ is specified, Equations (3.3.1) and (3.3.4) are reformulated as [Asmussen, 1997]:

$$\delta_{XX}(\tau) = E[X(t+\tau) | 0 \le X(t) < \infty, \dot{X}(t) = 0] \tag{3.4.47}$$

$$\delta_{YX}(\tau) = E[Y(t+\tau) | 0 \le X(t) < \infty, \dot{X}(t) = 0] \tag{3.4.48}$$

The results of the auto and cross RD signatures for the positive peak triggering condition are given as:

$$\delta_{XX}(\tau) = \frac{R_{XX}(\tau)}{R_{XX}(0)}\tilde{x}_0 \tag{3.4.49}$$

$$\delta_{XY}(\tau) = \frac{R_{XY}(\tau)}{R_{XX}(0)}\tilde{x}_0 \tag{3.4.50}$$

in which $\tilde{x}_0 = \frac{\int_0^\infty x p_X(x)dx}{\int_0^\infty p_X(x)dx} = \sqrt{\frac{2}{\pi}}\sigma_X$ is defined as the triggering level.

3.5 Auto RD Signatures and Free Vibration Responses for a SDOF System

For a linear under-damped SDOF system, the governing equation of motion can be described by:

$$m\ddot{x}(t) + c\dot{x}(t) + kx(t) = \tilde{f}(t) \tag{3.5.1}$$

or

$$\ddot{q}(t) + 2\zeta_1\omega_1\dot{q}(t) + \omega_1^2 q(t) = f(t) \tag{3.5.2}$$

in which

$$\omega_1 = \sqrt{\frac{k}{m}} \tag{3.5.3}$$

$$\zeta_1 = \frac{c}{2\sqrt{km}} \tag{3.5.4}$$

$$f(t) = \frac{\tilde{f}(t)}{\sqrt{m}} \tag{3.5.5}$$

$$x(t) = \frac{q(t)}{\sqrt{m}} \tag{3.5.6}$$

The modal displacement response, $q(t)$, resulting from the effect of an arbitrary forcing function $f(t)$ and zero initial conditions, can be solved by Duhamel convolution integral as [Crandall and Mark, 1963]:

$$\begin{aligned} q(t) &= \int_0^t f(s)h(t-s)ds \\ &= \int_{-\infty}^t f(s)h(t-s)ds \end{aligned} \tag{3.5.7}$$

in which $h(t)$ is an impulse response function of the system for the modal displacement response $q(t)$ and ω_d is the damped natural frequency:

$$\begin{aligned} h(t) &= \frac{1}{\omega_d} e^{-\zeta_1 \omega_1 t} \sin(\omega_d t) \qquad t \geq 0 \\ &= 0 \qquad\qquad\qquad\qquad\quad t < 0 \end{aligned} \tag{3.5.8}$$

$$\omega_d = \sqrt{(1-\zeta_1^2)}\omega_1 \tag{3.5.9}$$

The subsequent derivatives of Equation (3.5.7) with respect to t are given by:

$$\dot{q}(t) = \int_{-\infty}^{t} f(s)\dot{h}(t-s)ds + h(0)f(t) \tag{3.5.10}$$

$$\ddot{q}(t) = \int_{-\infty}^{t} f(s)\ddot{h}(t-s)ds + \dot{h}(0)f(t) + h(0)\dot{f}(t) \tag{3.5.11}$$

$$\dddot{q}(t) = \int_{-\infty}^{t} f(s)\dddot{h}(t-s)ds + \ddot{h}(0)f(t) + \dot{h}(0)\dot{f}(t) + h(0)\ddot{f}(t) \tag{3.5.12}$$

It is noted that the lower limit of integration in Equation (3.5.7) is expanded to minus infinity, since $f(t) = 0$ for $t < 0$. It means that the modal response $q(t)$ and its derivatives are zero when time t is less than zero for a linear causal system.

Since $h(0) = 0$, $\dot{h}(0) = 1$ and $\ddot{h}(0) = -2\zeta_1\omega_1$, it follows that the expressions of Equations (3.5.7) and (3.5.10-12) can be further simplified as:

$$q(t) = \int_{-\infty}^{t} f(s)h(t-s)ds \tag{3.5.13}$$

$$\dot{q}(t) = \int_{-\infty}^{t} f(s)\dot{h}(t-s)ds \tag{3.5.14}$$

$$\ddot{q}(t) = \int_{-\infty}^{t} f(s)\ddot{h}(t-s)ds + f(t) \tag{3.5.15}$$

$$\ddot{q}(t) = \int_{-\infty}^{t} f(s)\ddot{h}(t-s)ds - 2\zeta_1\omega_1 f(t) + \dot{f}(t) \tag{3.5.16}$$

Moreover, on the basis of the assumption that $\tilde{f}(t)$ is a stationary random forcing function with a zero mean, the responses are also stationary stochastic processes with zero means. Hence, from the definition of correlation functions for the stationary modal responses,

$$R_{qq}(\tau) = E[q(t)q(t+\tau)] \tag{3.5.17}$$

the following mathematical expressions are obtained upon substitution of Equations (3.5.13-16) into Equation (3.5.17) and transformation of variables $\tau = t - s$.

$$\begin{aligned} R_{qq}(\tau) &= E\left[\int_0^\infty\int_0^\infty f(t-\tau_1)f(t+\tau-\tau_2)h(\tau_1)h(\tau_2)d\tau_1 d\tau_2\right] \\ &= \int_0^\infty\int_0^\infty R_{ff}(\tau+\tau_1-\tau_2)h(\tau_1)h(\tau_2)d\tau_1 d\tau_2 \end{aligned} \tag{3.5.18}$$

$$R_{\dot{q}q}(\tau) = \int_0^\infty\int_0^\infty R_{ff}(\tau+\tau_1-\tau_2)\dot{h}(\tau_1)h(\tau_2)d\tau_1 d\tau_2 \tag{3.5.19}$$

$$R_{\dot{q}\dot{q}}(\tau) = \int_0^\infty\int_0^\infty R_{ff}(\tau+\tau_1-\tau_2)\dot{h}(\tau_1)\dot{h}(\tau_2)d\tau_1 d\tau_2 \tag{3.5.20}$$

$$R_{\ddot{q}\dot{q}}(\tau) = \int_0^\infty\int_0^\infty R_{ff}(\tau+\tau_1-\tau_2)\ddot{h}(\tau_1)\dot{h}(\tau_2)d\tau_1 d\tau_2 + \int_0^\infty R_{ff}(\tau-\tau_2)\dot{h}(\tau_2)d\tau_2 \tag{3.5.21}$$

$$\begin{aligned} R_{\ddot{q}\ddot{q}}(\tau) &= \int_0^\infty\int_0^\infty R_{ff}(\tau+\tau_1-\tau_2)\ddot{h}(\tau_1)\ddot{h}(\tau_2)d\tau_1 d\tau_2 \\ &+ \int_0^\infty R_{ff}(\tau-\tau_2)\ddot{h}(\tau_2)d\tau_2 + \int_0^\infty R_{ff}(\tau+\tau_1)\ddot{h}(\tau_1)d\tau_1 + R_{ff}(\tau) \end{aligned} \tag{3.5.22}$$

$$R_{\dot{q}\dot{q}}(\tau)=\int_0^\infty\int_0^\infty R_{ff}(\tau+\tau_1-\tau_2)\dot{\tilde{h}}(\tau_1)\dot{\tilde{h}}(\tau_2)d\tau_1 d\tau_2+\int_0^\infty R_{ff}(\tau+\tau_1)\ddot{\tilde{h}}(\tau_1)d\tau_1$$
$$+\int_0^\infty R_{\dot{f}\dot{f}}(\tau-\tau_2)\ddot{\tilde{h}}(\tau_2)d\tau_2-2\zeta_1\omega_1\int_0^\infty R_{ff}(\tau-\tau_2)\ddot{\tilde{h}}(\tau_2)d\tau_2 \qquad (3.5.23)$$
$$-2\zeta_1\omega_1 R_{ff}(\tau)+R_{\dot{f}\dot{f}}(\tau)$$

$$R_{\ddot{q}\ddot{q}}(\tau)=\int_0^\infty\int_0^\infty R_{ff}(\tau+\tau_1-\tau_2)\ddot{\tilde{h}}(\tau_1)\ddot{\tilde{h}}(\tau_2)d\tau_1 d\tau_2+\int_0^\infty R_{\dot{f}\dot{f}}(\tau-\tau_2)\ddot{\tilde{h}}(\tau_2)d\tau_2$$
$$-2\zeta_1\omega_1\int_0^\infty R_{ff}(\tau-\tau_2)\ddot{\tilde{h}}(\tau_2)d\tau_2-2\zeta_1\omega_1\int_0^\infty R_{ff}(\tau+\tau_1)\dddot{\tilde{h}}(\tau_1)d\tau_1 \qquad (3.5.24)$$
$$+\int_0^\infty R_{\dot{f}\dot{f}}(\tau+\tau_1)\dddot{\tilde{h}}(\tau_1)d\tau_1+4\zeta_1^2\omega_1^2 R_{ff}(\tau)-2\zeta_1\omega_1 R_{\dot{f}\dot{f}}(\tau)$$
$$-2\zeta_1\omega_1 R_{\dot{f}\dot{f}}(\tau)+R_{\ddot{f}\ddot{f}}(\tau)$$

in which $\tau_1=t-s_1\geq 0$ and $\tau_2=t+\tau-s_2\geq 0$.

Taking a Gaussian white noise stochastic process with uniform spectral density function S_0 into account, the following formula can be established for the auto-correlation function of $\tilde{f}(t)$.

$$R_{\tilde{f}\tilde{f}}(\tau+\tau_1-\tau_2)=E\left[\tilde{f}(t-\tau_1)\tilde{f}(t+\tau-\tau_2)\right]=2\pi S_0\delta(\tau+\tau_1-\tau_2) \qquad (3.5.25)$$

in which δ is represented as the Dirac delta function. The Dirac delta function and its derivatives have the following properties [Bracewell, 1999]:

$$\delta(x)=0 \quad \text{for} \quad x\neq 0 \qquad (3.5.26)$$

$$\int_{-\infty}^{\infty}\delta(x)dx=1 \qquad (3.5.27)$$

$$\int_{-\infty}^{\infty}f(x)\delta(x-a)dx=f(a) \qquad (3.5.28)$$

$$\int_{-\infty}^{\infty}f(x)\delta^{(n)}(x)dx=(-1)^n\int_{-\infty}^{\infty}\frac{\partial^n f(x)}{\partial x^n}\delta(x)dx \qquad (3.5.29)$$

$$\int_{-\infty}^{\infty} f(x)\delta'(x-a)dx = -f'(a) = -\int_{-\infty}^{\infty} f(x)\delta'(a-x)dx \tag{3.5.30}$$

Based on the relationship of Equation (3.5.5), the auto-correlation function of $f(t)$ is solved by:

$$\begin{aligned} R_{ff}(\tau+\tau_1-\tau) &= E\left[f(t-\tau_1)f(t+\tau-\tau_2)\right] \\ &= \frac{1}{m}E\left[\tilde{f}(t-\tau_1)\tilde{f}(t+\tau-\tau_2)\right] \\ &= \frac{2\pi S_0\delta(\tau+\tau_1-\tau_2)}{m} \end{aligned} \tag{3.5.31}$$

After substituting Equation (3.5.8) and its derivatives, Equation (3.5.31) with the assumption of the Gaussian white noise process, and the properties of the Dirac delta function into Equations (3.5.18-24), the correlation functions of the modal responses are given by:

$$\begin{aligned} R_{qq}(\tau) &= \frac{2\pi S_0}{m\omega_d^2}\int_0^{\infty}\left[\int_0^{\infty} e^{-\zeta_1\omega_1\tau_2}\sin(\omega_d\tau_2)\delta(\tau+\tau_1-\tau_2)d\tau_2\right]e^{-\zeta_1\omega_1\tau_1}\sin(\omega_d\tau_1)d\tau_1 \\ &= \frac{2\pi S_0}{m\omega_d^2}\int_0^{\infty} e^{-\zeta_1\omega_1(\tau_1+\tau)}\sin[\omega_d(\tau_1+\tau)]e^{-\zeta_1\omega_1\tau_1}\sin(\omega_d\tau_1)d\tau_1 \\ &= \frac{\pi S_0 e^{-\zeta_1\omega_1\tau}}{2m\zeta_1\omega_1^3}\left[\cos(\omega_d\tau)+\frac{\zeta_1}{\sqrt{1-\zeta_1^2}}\sin(\omega_d\tau)\right] \end{aligned} \tag{3.5.32}$$

$$R_{\dot{q}q}(\tau) = -R'_{qq}(\tau) = \frac{\pi S_0 e^{-\zeta_1\omega_1\tau}}{2m\zeta_1\omega_1^2}\frac{1}{\sqrt{1-\zeta_1^2}}\sin(\omega_d\tau) \tag{3.5.33}$$

$$R_{\dot{q}\dot{q}}(\tau) = -R''_{qq}(\tau) = \frac{\pi S_0 e^{-\zeta_1\omega_1\tau}}{2m\zeta_1\omega_1}\left[\cos(\omega_d\tau)-\frac{\zeta_1}{\sqrt{1-\zeta_1^2}}\sin(\omega_d\tau)\right] \tag{3.5.34}$$

$$R_{\ddot{q}\dot{q}}(\tau) = -R'_{\dot{q}\dot{q}}(\tau) = \frac{2\pi S_0 e^{-\zeta_1\omega_1\tau}}{m}\left[\frac{1-2\zeta_1^2}{4\zeta_1\sqrt{1-\zeta_1^2}}\sin(\omega_d\tau)+\frac{1}{2}\cos(\omega_d\tau)\right] \tag{3.5.35}$$

$$R_{\ddot{q}\ddot{q}}(\tau) = -R''_{\dot{q}\dot{q}}(\tau) + \frac{2\pi S_0 \delta(\tau)}{m}$$
$$= \frac{\pi S_0 \omega_1 e^{-\zeta_1 \omega_1 \tau}}{2m}\left[\left(\frac{1}{\zeta_1} - 4\zeta_1\right)\cos(\omega_d \tau) + \frac{(4\zeta_1^2 - 3)}{\sqrt{1-\zeta_1^2}}\sin(\omega_d \tau)\right] \quad (3.5.36)$$
$$+ \frac{2\pi S_0 \delta(\tau)}{m}$$

$$R_{\dot{q}\ddot{q}}(\tau) = -R'''_{\dot{q}\dot{q}}(\tau) - \frac{2\pi S_0\left[2\zeta_1 \omega_1 \delta(\tau) + \delta'(\tau)\right]}{m}$$
$$= \frac{2\pi S_0 \omega_1^2 e^{-\zeta_1 \omega_1 \tau}}{m}\left[\frac{(8\zeta_1^4 - 8\zeta_1^2 + 1)}{4\zeta_1\sqrt{1-\zeta_1^2}}\sin(\omega_d \tau) + (-2\zeta_1^2 + 1)\cos(\omega_d \tau)\right] \quad (3.5.37)$$
$$- \frac{2\pi S_0\left[2\zeta_1 \omega_1 \delta(\tau) + \delta'(\tau)\right]}{m}$$

$$R_{\ddot{q}\dot{q}}(\tau) = -R'''_{\dot{q}\dot{q}}(\tau) + \frac{2\pi S_0\left[4\zeta_1^2 \omega_1^2 \delta(\tau) - \delta''(\tau)\right]}{m}$$
$$= \frac{2\pi S_0 \omega_1^3 e^{-\zeta_1 \omega_1 \tau}}{m}\left[\frac{20\zeta_1^2 - 16\zeta_1^4 - 5}{4\sqrt{1-\zeta_1^2}}\sin(\omega_d \tau) - \frac{16\zeta_1^6 - 28\zeta_1^4 + 13\zeta_1^2 - 1}{4\zeta_1(1-\zeta_1^2)}\cos(\omega_d \tau)\right]$$
$$+ \frac{2\pi S_0\left[4\zeta_1^2 \omega_1^2 \delta(\tau) - \delta''(\tau)\right]}{m} \quad (3.5.38)$$

$$\tau \geq 0.$$

It should be noted that

$$R_{\ddot{q}\ddot{q}}(\tau) \neq \frac{\partial^4}{\partial \tau^4} R_{qq}(\tau) \quad (3.5.39)$$

$$R_{\dot{q}\ddot{q}}(\tau) \neq -\frac{\partial^5}{\partial \tau^5} R_{qq}(\tau) \quad (3.5.40)$$

$$R_{\dot{q}\dot{q}}(\tau) \neq -\frac{\partial^6}{\partial \tau^6} R_{qq}(\tau) \quad (3.5.41)$$

because of the existence of the Dirac delta function in the calculation process.

By making use of Equation (3.5.6), the correlation functions of the dynamic responses are then obtained as:

$$R_{xx}(\tau) = \frac{1}{\sqrt{m}} R_{qq}(\tau) \frac{1}{\sqrt{m}}$$
$$= \frac{\pi S_0 e^{-\zeta_1 \omega_1 \tau}}{2m^2 \zeta_1 \omega_1^3} \left[\cos(\omega_d \tau) + \frac{\zeta_1}{\sqrt{1-\zeta_1^2}} \sin(\omega_d \tau) \right] \tag{3.5.42}$$

$$R_{\dot{x}x}(\tau) = \frac{1}{\sqrt{m}} R_{\dot{q}q}(\tau) \frac{1}{\sqrt{m}}$$
$$= \frac{\pi S_0 e^{-\zeta_1 \omega_1 \tau}}{2m^2 \zeta_1 \omega_1^2} \frac{1}{\sqrt{1-\zeta_1^2}} \sin(\omega_d \tau) \tag{3.5.43}$$

$$R_{\dot{x}\dot{x}}(\tau) = \frac{1}{\sqrt{m}} R_{\dot{q}\dot{q}}(\tau) \frac{1}{\sqrt{m}}$$
$$= \frac{\pi S_0 e^{-\zeta_1 \omega_1 \tau}}{2m^2 \zeta_1 \omega_1} \left[\cos(\omega_d \tau) - \frac{\zeta_1}{\sqrt{1-\zeta_1^2}} \sin(\omega_d \tau) \right] \tag{3.5.44}$$

$$R_{\ddot{x}\dot{x}}(\tau) = \frac{1}{\sqrt{m}} R_{\ddot{q}\dot{q}}(\tau) \frac{1}{\sqrt{m}}$$
$$= \frac{2\pi S_0 e^{-\zeta_1 \omega_1 \tau}}{m^2} \left[\frac{1-2\zeta_1^2}{4\zeta_1 \sqrt{1-\zeta_1^2}} \sin(\omega_d \tau) + \frac{1}{2} \cos(\omega_d \tau) \right] \tag{3.5.45}$$

$$R_{\ddot{x}\ddot{x}}(\tau) = \frac{1}{\sqrt{m}} R_{\ddot{q}\ddot{q}}(\tau) \frac{1}{\sqrt{m}}$$
$$= \frac{\pi S_0 \omega_1 e^{-\zeta_1 \omega_1 \tau}}{2m^2} \left[\left(\frac{1}{\zeta_1} - 4\zeta_1 \right) \cos(\omega_d \tau) + \frac{\left(4\zeta_1^2 - 3\right)}{\sqrt{1-\zeta_1^2}} \sin(\omega_d \tau) \right] \tag{3.5.46}$$
$$+ \frac{2\pi S_0 \delta(\tau)}{m^2}$$

$$R_{\dot{x}\dot{x}}(\tau)=\frac{1}{\sqrt{m}}R_{\dot{q}\dot{q}}(\tau)\frac{1}{\sqrt{m}}$$
$$=\frac{2\pi S_0\omega_1^2 e^{-\zeta_1\omega_1\tau}}{m^2}\left[\frac{(8\zeta_1^4-8\zeta_1^2+1)}{4\zeta_1\sqrt{1-\zeta_1^2}}\sin(\omega_d\tau)+(-2\zeta_1^2+1)\cos(\omega_d\tau)\right] \quad (3.5.47)$$
$$-\frac{2\pi S_0[2\zeta_1\omega_1\delta(\tau)+\delta'(\tau)]}{m^2}$$

$$R_{\ddot{x}\ddot{x}}(\tau)=\frac{1}{\sqrt{m}}R_{\dot{q}\dot{q}}(\tau)\frac{1}{\sqrt{m}}$$
$$=\frac{2\pi S_0\omega_1^3 e^{-\zeta_1\omega_1\tau}}{m^2}\left[\frac{-16\zeta_1^4+20\zeta_1^2-5}{4\sqrt{1-\zeta_1^2}}\sin(\omega_d\tau)+\right. \quad (3.5.48)$$
$$\left.\frac{-16\zeta_1^6+28\zeta_1^4-13\zeta_1^2+1}{4\zeta_1(1-\zeta_1^2)}\cos(\omega_d\tau)\right]+\frac{2\pi S_0[4\zeta_1^2\omega_1^2\delta(\tau)-\delta''(\tau)]}{m^2}$$

The results of Equations (3.5.42-48) motivate the pursuing interest in obtaining the auto RD signatures under the requirement of the general triggering conditions. With such a requirement, the auto RD signatures of displacement, velocity and acceleration responses, based on Equations (3.4.6-7) and (3.5.42-48), become:

$$\delta_{XX}(\tau)=\frac{R_{XX}(\tau)}{R_{XX}(0)}x_0-\frac{R'_{XX}(\tau)}{R_{\dot{X}\dot{X}}(0)}\dot{x}_0$$
$$=x_0e^{-\zeta_1\omega_1\tau}\left[\cos(\omega_d\tau)+\frac{\zeta_1}{\sqrt{1-\zeta_1^2}}\sin(\omega_d\tau)\right]+\dot{x}_0e^{-\zeta_1\omega_1\tau}\frac{\sin(\omega_d\tau)}{\omega_1\sqrt{1-\zeta_1^2}} \quad (3.5.49)$$
$$=e^{-\zeta_1\omega_1\tau}\left[x_0\cos(\omega_d\tau)+\left(\frac{\zeta_1}{\sqrt{1-\zeta_1^2}}x_0+\frac{1}{\omega_1\sqrt{1-\zeta_1^2}}\dot{x}_0\right)\sin(\omega_d\tau)\right]$$

$$\delta_{\dot{X}\dot{X}}(\tau)=\frac{R_{\dot{X}\dot{X}}(\tau)}{R_{\dot{X}\dot{X}}(0)}\dot{x}_0+\frac{R_{\ddot{X}\dot{X}}(\tau)}{R_{\ddot{X}\dot{X}}(0)}\ddot{x}_0$$
$$=\dot{x}_0e^{-\zeta_1\omega_1\tau}\left[\cos(\omega_d\tau)-\frac{\zeta_1}{\sqrt{1-\zeta_1^2}}\sin(\omega_d\tau)\right]+ \quad (3.5.50)$$
$$\frac{\ddot{x}_0e^{-\zeta_1\omega_1\tau}}{\omega_1(\frac{1}{\zeta_1}-4\zeta_1)+4\delta(0)}\left[\frac{1-2\zeta_1^2}{\zeta_1\sqrt{1-\zeta_1^2}}\sin(\omega_d\tau)+2\cos(\omega_d\tau)\right]$$

$$\delta_{\ddot{x}\ddot{x}}(\tau)=\frac{R_{\ddot{x}\ddot{x}}(\tau)}{R_{\ddot{x}\ddot{x}}(0)}\ddot{x}_0+\frac{R_{\dot{\ddot{x}}\ddot{x}}(\tau)}{R_{\dot{\ddot{x}}\dot{\ddot{x}}}(0)}\dot{\ddot{x}}_0$$

$$=\ddot{x}_0\frac{\omega_1 e^{-\zeta_1\omega_1\tau}\left[\left(\frac{1}{\zeta_1}-4\zeta_1\right)\cos(\omega_d\tau)+\frac{4\zeta_1^2-3}{\sqrt{1-\zeta_1^2}}\sin(\omega_d\tau)\right]+4\delta(\tau)}{\omega_1(\frac{1}{\zeta_1}-4\zeta_1)+4\delta(0)}+$$

$$\dot{\ddot{x}}_0\frac{\omega_1^2 e^{-\zeta_1\omega_1\tau}\left[\frac{8\zeta_1^4-8\zeta_1^2+1}{4\zeta_1\sqrt{1-\zeta_1^2}}\sin(\omega_d\tau)+(1-2\zeta_1^2)\cos(\omega_d\tau)\right]-2\zeta_1\omega_1\delta(\tau)-\delta'(\tau)}{\omega_1^3\frac{-16\zeta_1^6+28\zeta_1^4-13\zeta_1^2+1}{4\zeta_1(1-\zeta_1^2)}+4\zeta_1^2\omega_1^2\delta(0)-\delta''(0)} \tag{3.5.51}$$

For the purpose of comparison, the analytical free vibration responses of the SDOF dynamic system are given as follows:

$$x(t)=e^{-\zeta_1\omega_1 t}\left\{x(0)\cos(\omega_d t)+\frac{1}{\omega_d}\left[\zeta_1\omega_1 x(0)+\dot{x}(0)\right]\sin(\omega_d t)\right\} \tag{3.5.52}$$

$$\dot{x}(t)=e^{-\zeta_1\omega_1 t}\left\{\dot{x}(0)\cos(\omega_d t)+\frac{1}{\omega_d}\left[-\omega_1^2 x(0)-\zeta_1\omega_1\dot{x}(0)\right]\sin(\omega_d t)\right\} \tag{3.5.53}$$

$$\ddot{x}(t)=e^{-\zeta_1\omega_1 t}\left\{\left[-2\zeta_1\omega_1\dot{x}(0)-\omega_1^2 x(0)\right]\cos(\omega_d t)+\left[\left(\frac{\zeta_1\omega_1}{\omega_d}\right)x(0)+\frac{(2\zeta_1^2-1)}{\omega_d}\omega_1\dot{x}(0)\right]\sin(\omega_d t)\right\} \tag{3.5.54}$$

Apparently, the RD displacement signature in Equation (3.5.49) is equivalent to the free vibration displacement response in Equation (3.5.52), when the initial displacement and velocity conditions are given as $x(0)=x_0, \dot{x}(0)=\dot{x}_0$, respectively. Nevertheless, the RD velocity and acceleration signatures are not thought to be of the same forms as the corresponding free vibration responses in Equations (3.5.53) and (3.5.54), since the Dirac delta function $\delta(t)$ and its derivatives are present in Equations

(3.5.50) and (3.5.51). Such results raise the important question whether equivalent relations between the auto RD signatures and the corresponding free vibration responses under certain initial conditions are indeed guaranteed to hold.

To clarify this point, a comparison between the auto RD signatures of responses and the corresponding free vibration responses is considered where the initial amplitude is chosen exclusive of the slope as the triggering point. As a result, Equations (3.5.49-51) become:

$$\begin{aligned}\delta_{XX}(\tau) &= \frac{R_{XX}(\tau)}{R_{XX}(0)}x_0 \\ &= x_0 e^{-\zeta_1\omega_1\tau}\left[\cos(\omega_d\tau)+\frac{\zeta_1}{\sqrt{1-\zeta_1^2}}\sin(\omega_d\tau)\right]\end{aligned} \tag{3.5.55}$$

$$\begin{aligned}\delta_{\dot{X}\dot{X}}(\tau) &= \frac{R_{\dot{X}\dot{X}}(\tau)}{R_{\dot{X}\dot{X}}(0)}\dot{x}_0 \\ &= \dot{x}_0 e^{-\zeta_1\omega_1\tau}\left[\cos(\omega_d\tau)-\frac{\zeta_1}{\sqrt{1-\zeta_1^2}}\sin(\omega_d\tau)\right]\end{aligned} \tag{3.5.56}$$

$$\begin{aligned}\delta_{\ddot{X}\ddot{X}}(\tau) &= \frac{R_{\ddot{X}\ddot{X}}(\tau)}{R_{\ddot{X}\ddot{X}}(0)}\ddot{x}_0 \\ &= \frac{\ddot{x}_0\left\{e^{-\zeta_1\omega_1\tau}\omega_1\left[\left(\frac{1}{4\zeta_1}-\zeta_1\right)\cos(\omega_d\tau)+\frac{4\zeta_1^2-3}{\sqrt{1-\zeta_1^2}}\sin(\omega_d\tau)\right]+\delta(\tau)\right\}}{\omega_1\left(\frac{1}{4\zeta_1}-\zeta_1\right)+\delta(0)}\end{aligned} \tag{3.5.57}$$

When the initial displacement is equal to x_0 and zero initial velocity, *i.e.* $x(0)=x_0$ and $\dot{x}(0)=0$, respectively, the RD displacement signature of Equation (3.5.55) is equivalent to the corresponding free vibration response of Equation (3.5.52) [Vandiver et al., 1982; Bedewi, 1986]. Similarly, under the initial conditions, $x(0) = 0$ and $\dot{x}(0)=\dot{x}_0$, the RD velocity signature of Equation (3.5.56) is also equivalent to the free vibration

velocity responses of Equation (3.5.53) [Huang et al., 1996, 1999]. However, the free vibration acceleration response is not equivalent to the RD acceleration signature, because the Dirac delta function still remains in the second term of Equation (3.5.57) [Huang et al., 1999]. The emphasis of this result is that the Dirac delta function existing in the correlation functions affects the representations of the RD signatures to be the free vibration responses, even if the adjustment of the initial conditions is made by the specified triggering condition. It is interesting to ask next whether or not the auto RD signature of this acceleration response can adequately stand for the free vibration acceleration response. Hence, numerical simulations with the aid of the developed RD technique are implemented to gain the complete understanding of such RD signatures.

3.6 Numerical Simulations of a Linear SDOF System

The demonstration of numerical simulations was dedicated to enhancing the understanding of the RD technique. A SDOF linear dynamic system was considered in the following numerical simulation. The natural frequency and the damping ratio of the SDOF system were set as 1 Hz and 2 %, respectively. A Gaussian white noise with a zero mean and one variance and a fluctuating wind force were applied to drive the SDOF dynamic system. Both of the simulated forces generated dynamic responses with the total number of 400000 points at a time interval of 0.01 second. The dynamic responses including displacement, velocity and acceleration were numerically analyzed by using the Newmark-β method with the assumption of linear acceleration [Cheng, 2001]. The resulting response time series between 30 seconds and 4000 seconds were used to evaluate their RD signatures.

Two different triggering conditions were chosen for the RD signatures in this study. One of them was the traditional level crossing triggering condition [Cole, 1971; Yang and Caldwell, 1976] in which one standard deviation of a specified response was selected as the triggering level for each sample segment. However, for the discrete time data, it is impossible to obtain the precise discrete time t_i in practice such that a sampling point $x(t_i)$ crosses through the specified triggering level σ_x. In this regard, the triggering condition was modified in order that the closest point to the triggering level might be treated as a starting point for each sample segment. The modified triggering condition is:

$$\left\{\left[\left|x(t_i)-\sigma_x\right| \le 0.08\sigma_x\right] \cap \left[\left|x(t_i)-\sigma_x\right| \le \left|x(t_{i-1})-\sigma_x\right|\right] \cap \left[\left|x(t_i)-\sigma_x\right| \le \left|x(t_{i+1})-\sigma_x\right|\right]\right\} \quad (3.6.1)$$

in which $|\bullet|$ and $\cap$ denote the absolute value and the intersection, respectively. If the difference between the starting point and the selected triggering level is reasonably small and the number of the superimposed sections is sufficiently large, the triggering bias may be negligible.

The other triggering condition presented in this study focused on the selection of a positive peak as a starting point for each sample segment [Tamura et al., 1995]. The positive peak triggering condition is expected as:

$$\begin{gathered}\left\{\left[x(t_i) \ge 0\right] \cap \left[x(t_{i-1}) \le x(t_i)\right] \cap \left[x(t_{i+1}) \le x(t_i)\right]\right\} \\ \text{or} \\ \left\{\left[x(t_i) \ge 0\right] \cap \left[\dot{x}(t_i) = 0\right]\right\}\end{gathered} \quad (3.6.2)$$

The primary advantage of this condition is that the time derivative of $x(t_i)$ as a peak value is demanded to be zero. Because the selection of very small peaks might give rise to a deformed RD signature, the starting point of each sample segment was restricted to the maximum peak of every three sequential peaks from the specified response. In addition,

these three selected peaks were also restricted above 0.5 standard deviation of the specified response.

Common to both triggering conditions above is that each sample segment has a time length of 10.5 seconds and possible overlapping of sample segments is allowed. Nevertheless, it should be noted that the assumption of the uncorrelated sample segments is not valid for such an overlapping condition to estimate the variance of the RD signature [Vandiver et al., 1982]. Therefore, the behavior of the RD signature for the non-overlapped condition was further investigated by the use of the same positive peak triggering condition. To increase properly the number of the superimposed segments, only a short period of 2.3 seconds was considered to perform the RD signatures.

To compare the RD signatures with the analytical free vibration responses, the initial conditions of such free vibration responses should be determined in advance. However, the analytical free vibration acceleration response of a second order differential dynamic system cannot be determined only from the initial acceleration without the knowledge of the initial displacement and velocity conditions. This can be explicitly explained with reference to Equation (3.5.54) where one sees that the formation of the analytical free vibration responses normally requires the initial displacement and velocity conditions. In addition, the initial conditions for the positive peak triggering condition are not easily determined in practice. That is because the final amplitude of the superimposed sample segments for such a condition may not be predictable, though the slope is given as zero. The demand for a practical method to identify the initial conditions for these foregoing cases is apparent.

In this study, the main issue is therefore to use the concept behind the multiple-signal RD technique [Ibrahim, 1977] to determine the initial conditions from the synchronous RD signatures of displacement and velocity responses. The theoretical derivations of the multiple-signal RD technique have been carried out using a simple 2DOF dynamic system as illustrated in Figure 3.4.1 [Bedewi, 1986; Huang, et al., 1998, 1999]. The basic concept of the multiple-signal RD technique was developed to obtain the free vibration responses of a MDOF dynamic system without changing the time correlation between the synchronous response signals. Similarly, it is likely that such a RD technique can simultaneously extract the RD displacement, velocity and acceleration signatures from the corresponding responses of a dynamic system in a numerical simulation. For instance, when any of these responses is specified as a leading response in one of the used triggering conditions, the resulting RD displacement and velocity signatures correspond to their free vibration responses. From this respect, it follows that the initial conditions of the specified analytical free vibration response can be collected directly from such RD displacement and velocity signatures at $t = 0$.

3.6.1 Application of White Noise Excitation

The white noise excitation used in the numerical simulation was implemented to demonstrate the theoretical development of the RD technique concerned in Section 3.5. Based on the application of the white noise excitation, Tables 3.6.1-3 show the initial conditions of the analytical free vibration responses resulting from the level crossing triggering condition and the positive peak triggering condition. The parenthesized values

in the columns of the displacement and velocity responses of the tables denote the theoretical triggering conditions to compare the resulting initial conditions.

For the level crossing triggering condition, the initial conditions are well satisfied with the specified triggering levels. The feature of the zero initial velocity resulting from the level crossing triggering condition in Table 3.6.1 can be further explained in a statistical sense. That is, when the amplitude of the crossing level is selected, the slopes of the selected points crossing the triggering level may be eventually averaged out, as described in Section 3.2. In addition, comparing the initial conditions with the theoretical triggering level obviously validates the assumption of neglecting the triggering window error, as though the number of the superimposed segments is sufficient. For the positive peak triggering condition, the initial values in Table 3.6.2-3 that are satisfactorily close to zero are consistent with the characteristics of the peak value.

Table 3.6.1 Initial Conditions of a Free Vibration Response from RD Signatures with Level Crossing Triggering Condition

Leading Response	Displacement Response	Velocity Response	Acceleration Response
Initial Displacement	0.02223 (0.0223)	0.00003 (0)	-0.01419
Initial Velocity	-0.00047 (0)	0.13964 (0.1399)	-0.00080

Note: 1. The values in parentheses denote the specified triggering level

Table 3.6.2 Initial Conditions of a Free Vibration Response from RD Signatures with Positive Peak Triggering Condition and Overlapped Condition

Leading Response	Displacement Response	Velocity Response	Acceleration Response
Initial Displacement	0.02510	0.00008 (0)	-0.00684
Initial Velocity	-0.00005 (0)	0.11824	-0.00002

Table 3.6.3 Initial Conditions of a Free Vibration Response from RD Signatures with Positive Peak Triggering Condition and Non-overlapped Condition

Leading Response	Displacement Response	Velocity Response	Acceleration Response
Initial Displacement	0.03486	-0.00204 (0)	-0.00899
Initial Velocity	-0.00029 (0)	0.19222	-0.02343

Making reference to the resulting initial conditions, the analytical free vibration responses were produced to compare with the corresponding RD signatures. Figures 3.6.1-3 present the RD signatures with the overlapped condition, while Figures 3.6.4-5 focus on the RD signatures with respect to the non-overlapped condition. As expected from Equations (3.5.55) and (3.5.56), the comparisons between the RD displacement and velocity signatures and the corresponding analytical free vibration responses are approved in the excellent agreement shown in Figures 3.6.1 and 3.6.2. Notably, the RD velocity signature based on the positive peak triggering method shows a uniformly harmonic type of bias, resulting primarily from the errors of the numerical processing and the finite-size trig windows. Inherently, such a numerical error causes the overestimation of the first two points, as shown in Figure 3.6.2 (a), so that the delicate deviation of the free vibration responses from the corresponding RD signatures occurs. When the third points in the RD signatures are purposely collected as the initial conditions instead of the first points, the overall free vibration responses are adapted simultaneously to the associated RD signatures. Hence, this kind of numerical error may be neglected without further adjustment in the current investigation.

The RD acceleration signatures in Figures 3.6.3 are compared to their analytical free vibration responses. Such a comparison is a major intention in this investigation to assess whether the RD acceleration signature is relevant to the analytical free vibration

response. The RD residuals, defined by the difference between the RD signature and its analytical free vibration response, are used as an indication of relevance. The initial two points of the RD acceleration signature and its residuals in Figure 3.6.3 are marked by square and triangle, respectively, in order to distinguish their differences from the other data. Likewise, the initial two points of the RD force signature and the RD acceleration residuals are marked by square and triangle, respectively. These figures also illustrate the other formations of the RD displacement and velocity signatures corresponding to their RD acceleration signatures. The starting points of the formed RD displacement and velocity signatures are assigned as the initial conditions in Equations (3.5.52-54) to yield the analytical free vibration responses and then compare their RD signatures.

The results reveal with interest that the RD acceleration signature resembles the free vibration acceleration response, in spite of the appearance of the singularity at the first point as indicated by Huang and Yeh [1996]. In fact, the singularity reflects the influence of the Dirac delta function pertaining to the property of the correlation function for the white noise excitation. It is verified that the first point of the residuals between the RD acceleration signature and the corresponding free vibration response is identical to the first point of the RD force signature for both of the triggering conditions, as shown in Figure 3.6.3 (iii). Such a peculiar feature is consistent with Equation (3.5.22), which contains essentially the correlation function of the forcing function term. In addition to the time domain data, the frequency domain data in Figure 3.6.3 (iii), based on the FFT-based algorithms, further exhibit the influence of the RD force signatures on the RD acceleration signatures. The appearance of the "jump" around 1 Hz in the frequency

domain data of the RD acceleration residuals supports the preceding interpretation for the harmonic type of bias.

As concerns the non-overlapped condition, the RD signatures given in Figure 3.6.4 appear larger discrepancy than the RD signatures for the overlapped condition, along with the increase of the time delay. The reason is that the number of superimposed sample segments is not sufficient to form the accurate estimates of the RD signatures. The number of superimposed sample segments becomes an important factor to properly enhance the required accuracy of the estimated RD signatures. Despite this, the effect of the RD force signature in the RD acceleration signature can be observed in Figure 3.6.5.

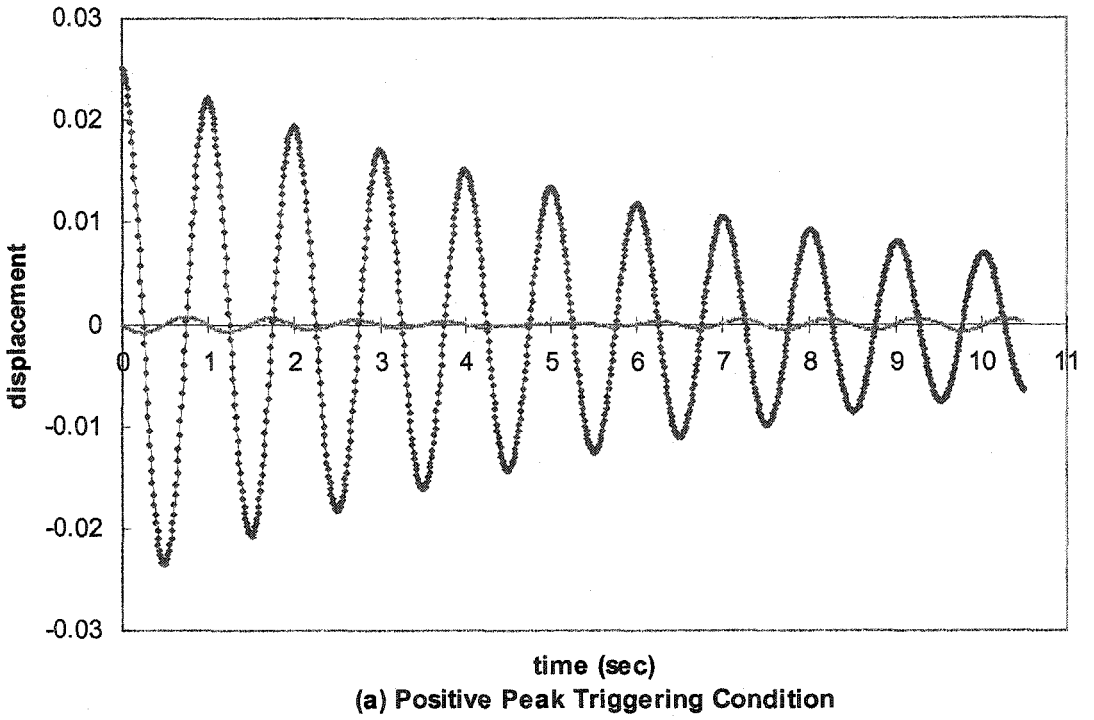

(a) Positive Peak Triggering Condition

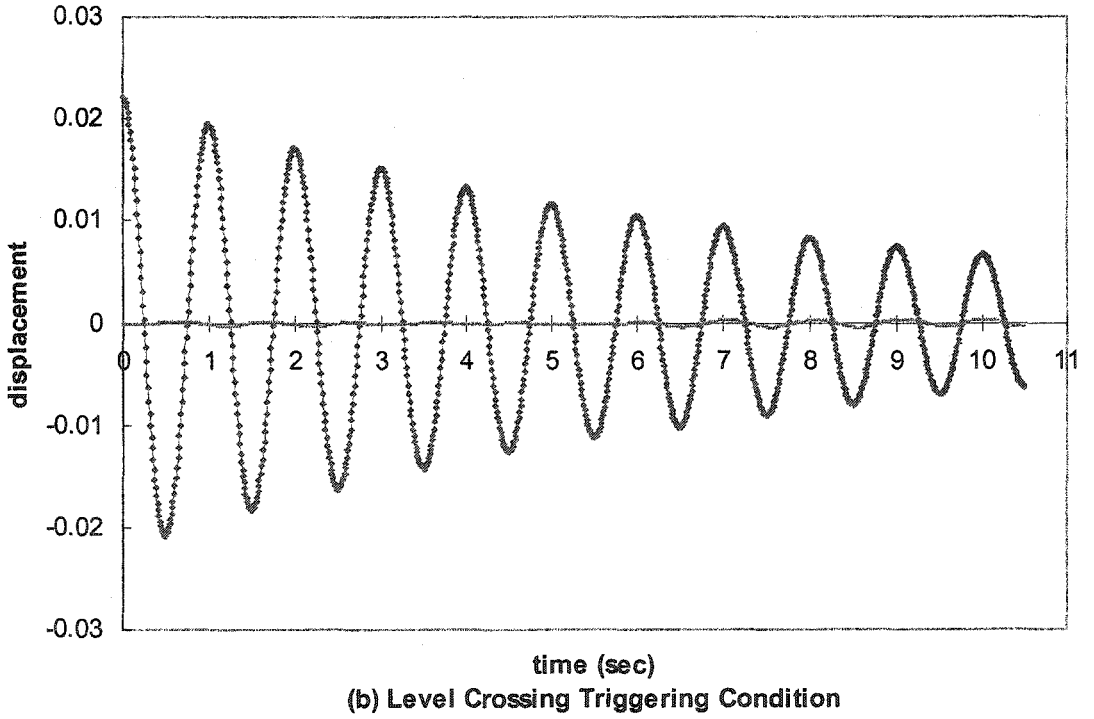

(b) Level Crossing Triggering Condition

Figure 3.6.1 RD Displacement Signatures

——, Free Vibration Response; ♦♦♦♦♦, RD signature; ▲▲▲▲▲, Residuals

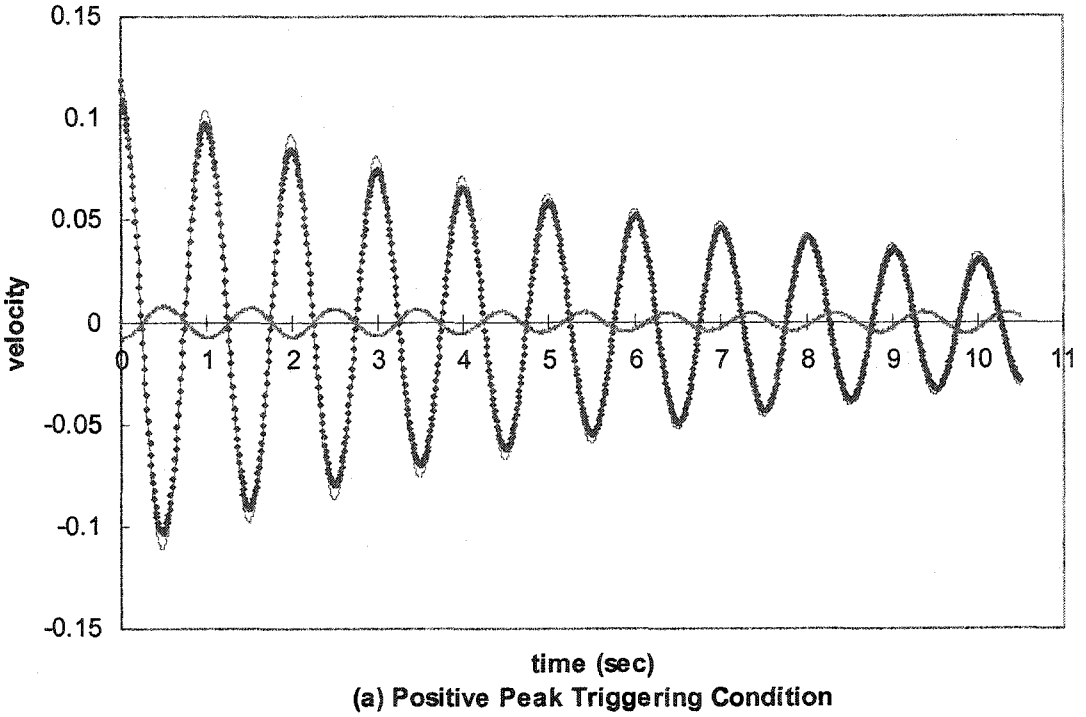

(a) Positive Peak Triggering Condition

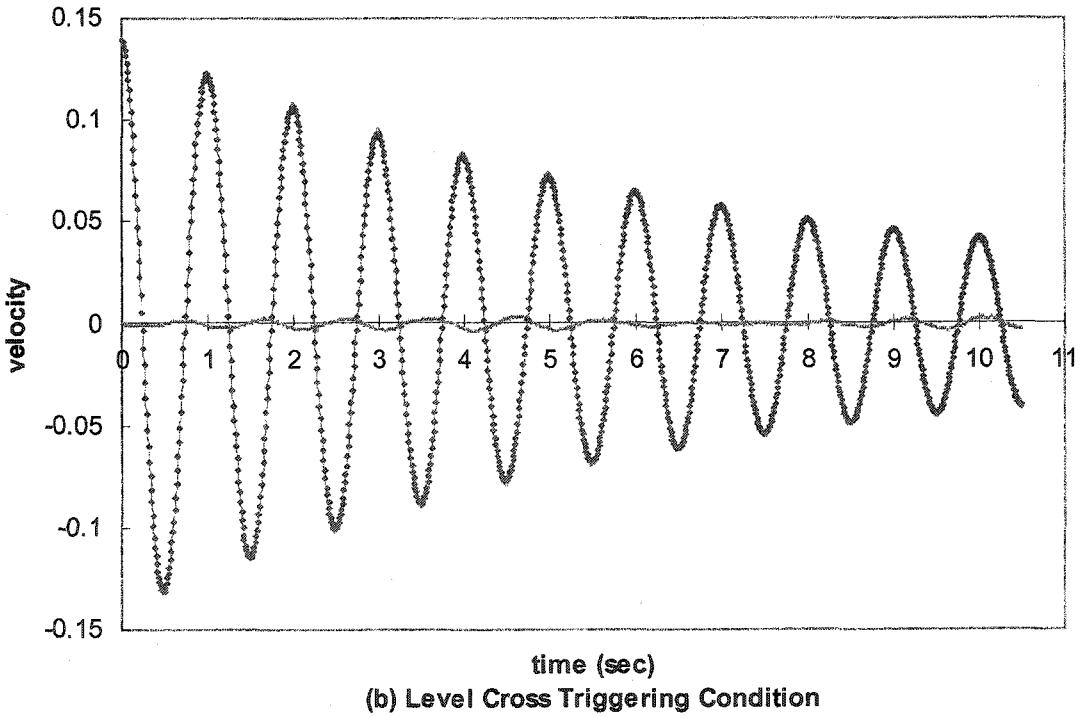

(b) Level Cross Triggering Condition

Figure 3.6.2 RD Velocity Signatures

——, Free Vibration Response; ♦♦♦♦♦, RD Signature; ▲▲▲▲▲, Residuals

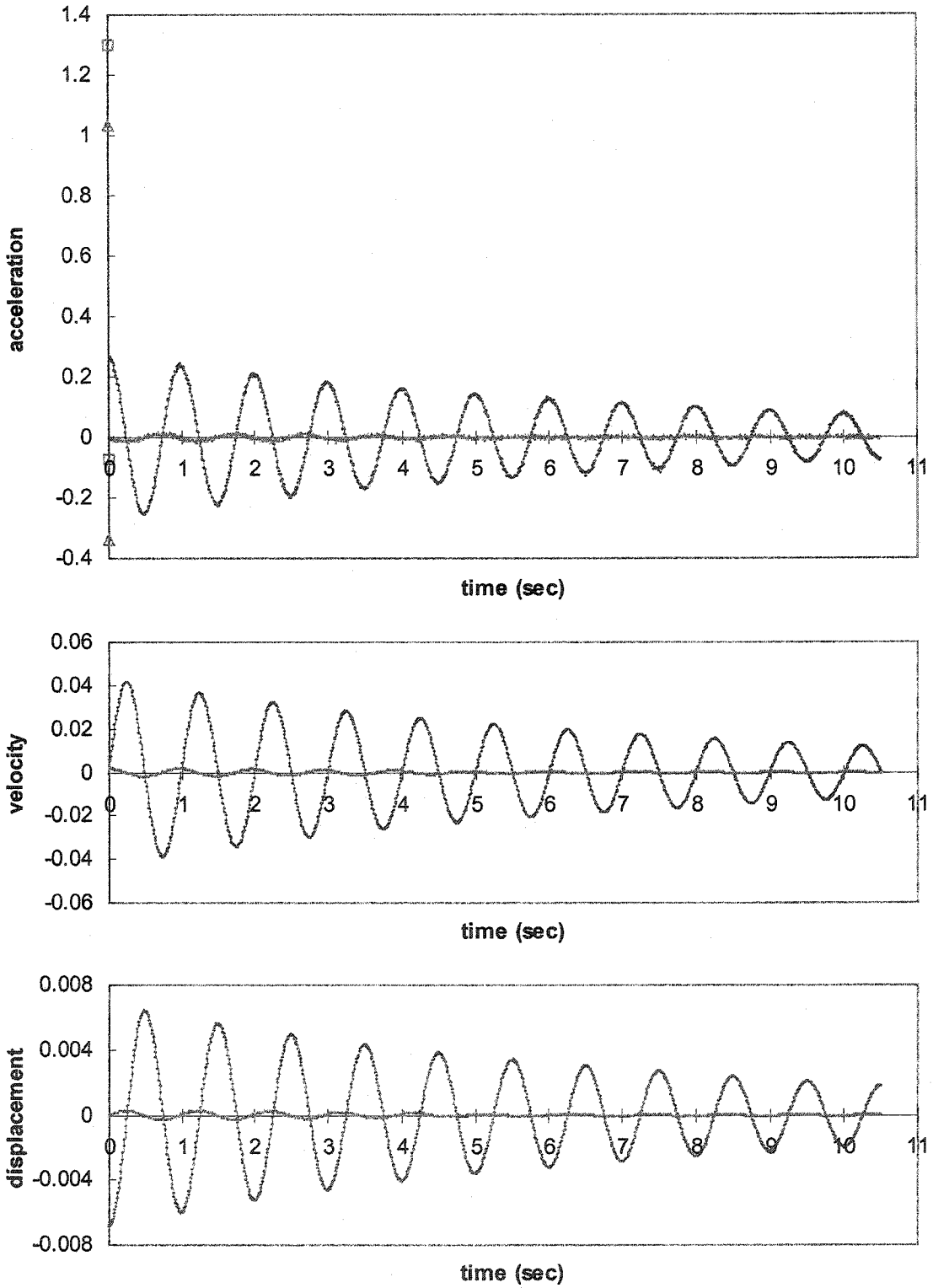

Figure 3.6.3 (i) RD Acceleration Signature with Positive Peak Triggering Condition

——, Free Vibration Response; ♦♦♦♦♦, RD Signature; ▲▲▲▲▲, Residuals

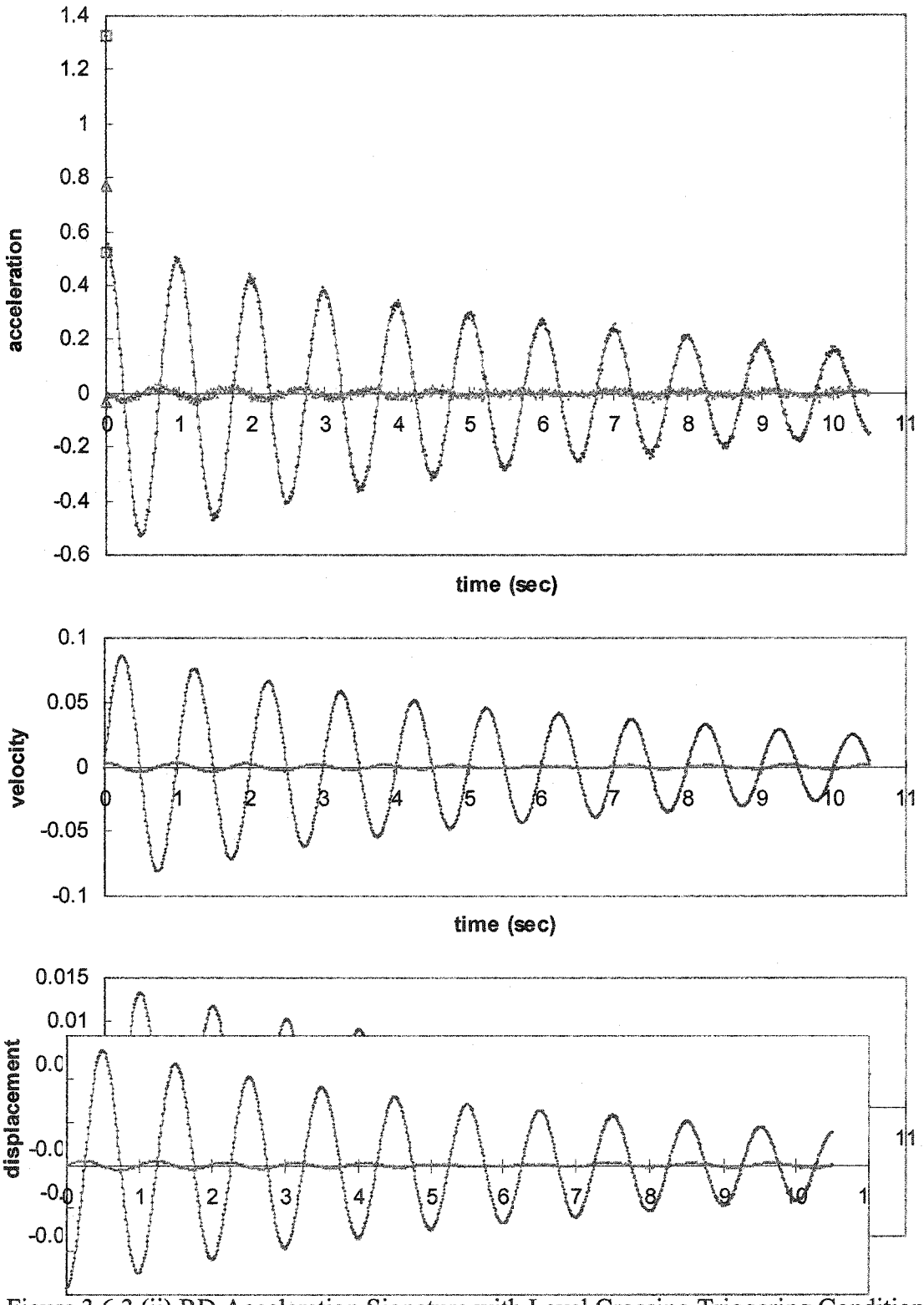

Figure 3.6.3 (ii) RD Acceleration Signature with Level Crossing Triggering Condition

——, Free Vibration Response; ♦♦♦♦♦, RD Signature; ▲▲▲▲▲, Residuals

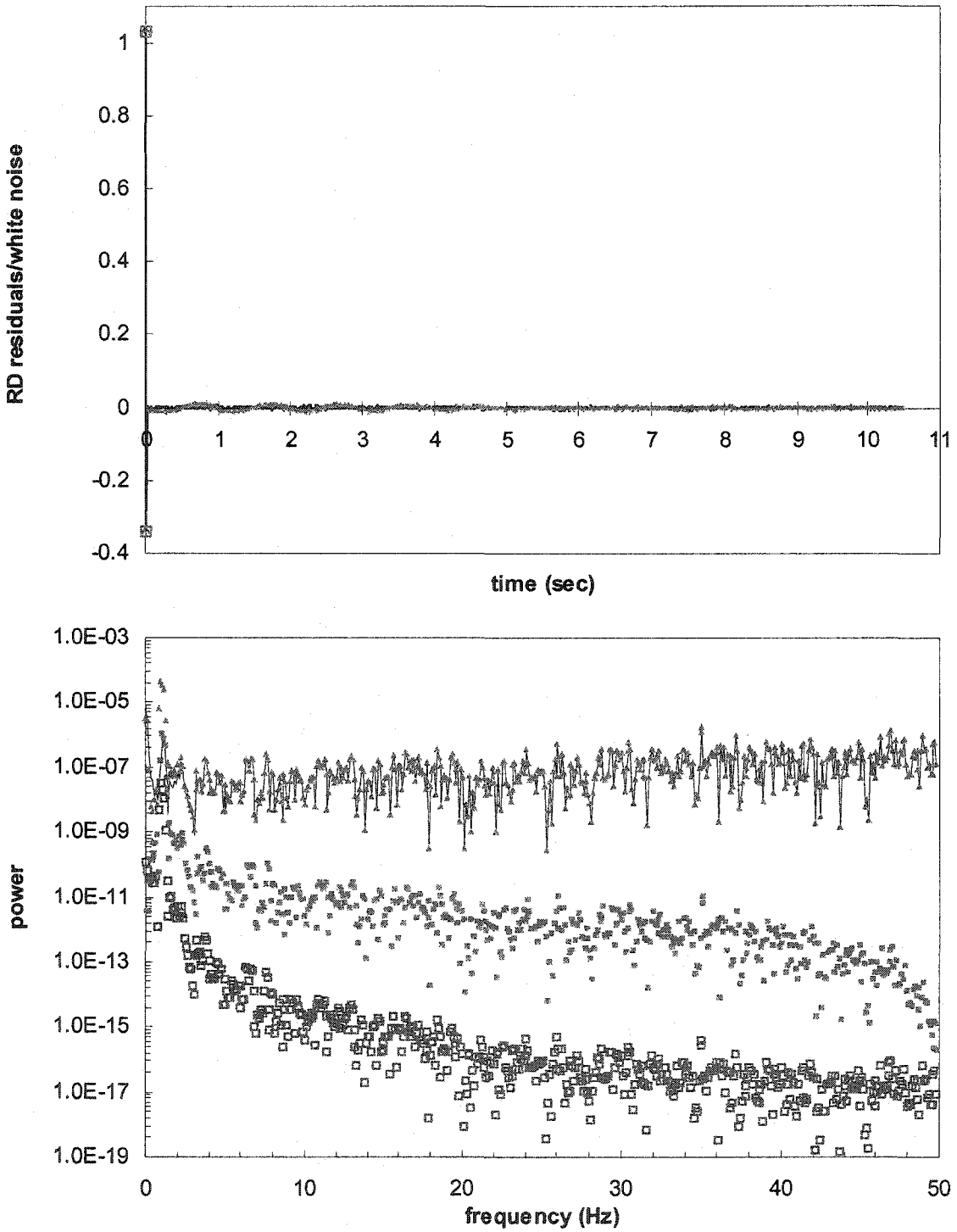

(a) Positive Peak Triggering Condition

Figure 3.6.3 (iii) Relation of RD Acceleration Residuals and White Noises

——, RD White Noise Signature; ▲▲▲▲▲, RD Acceleration Residuals; ■■■■■, RD Velocity Residuals; □□□□□, RD Displacement Residuals

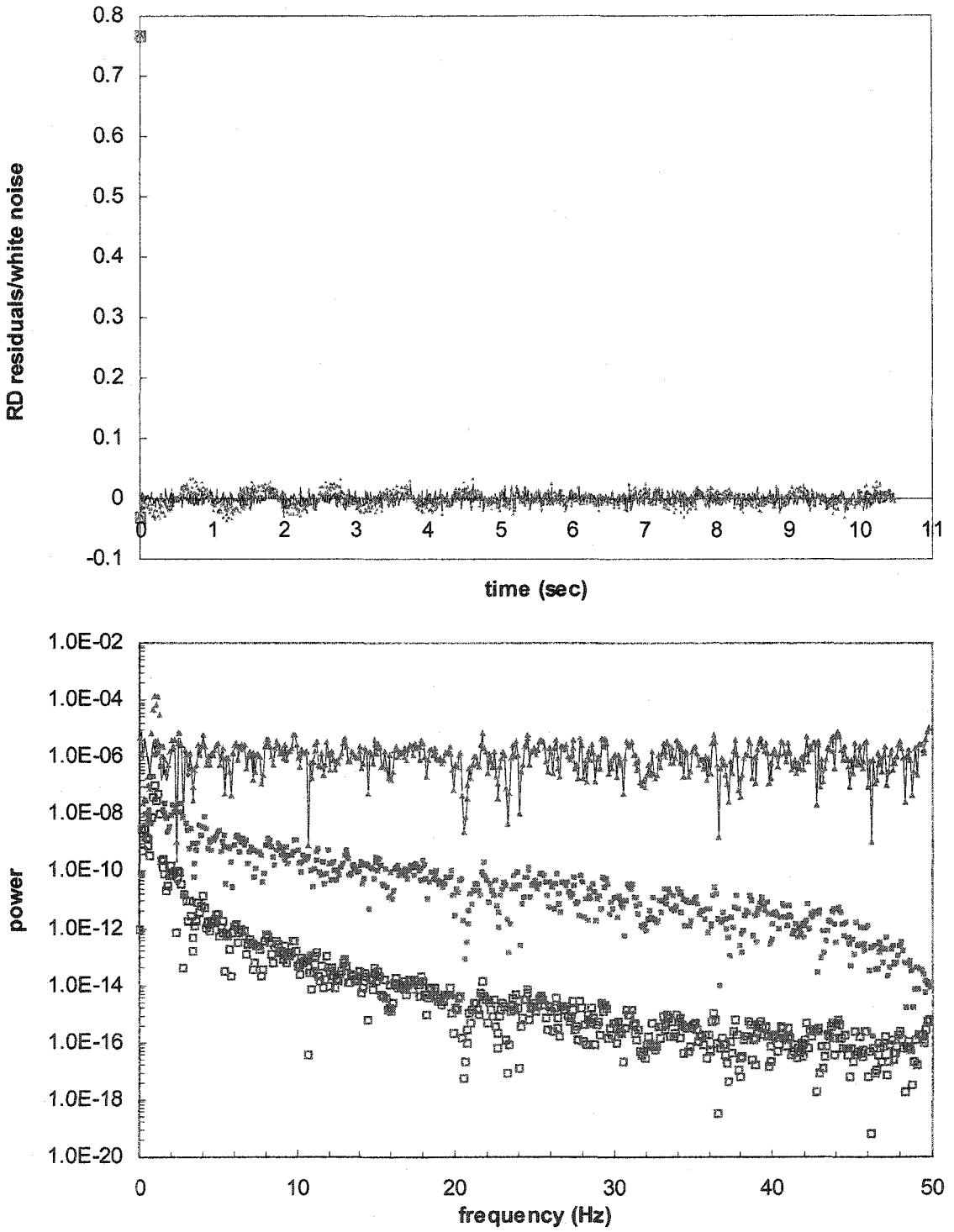

(b) Level Crossing Triggering Condition

Figure 3.6.3 (iii) Relation of RD Acceleration Residuals and White Noises

——, RD White Noise Signature; ▲▲▲▲▲, RD Acceleration Residuals; ■■■■■, RD Velocity Residuals; □□□□□, RD Displacement Residuals

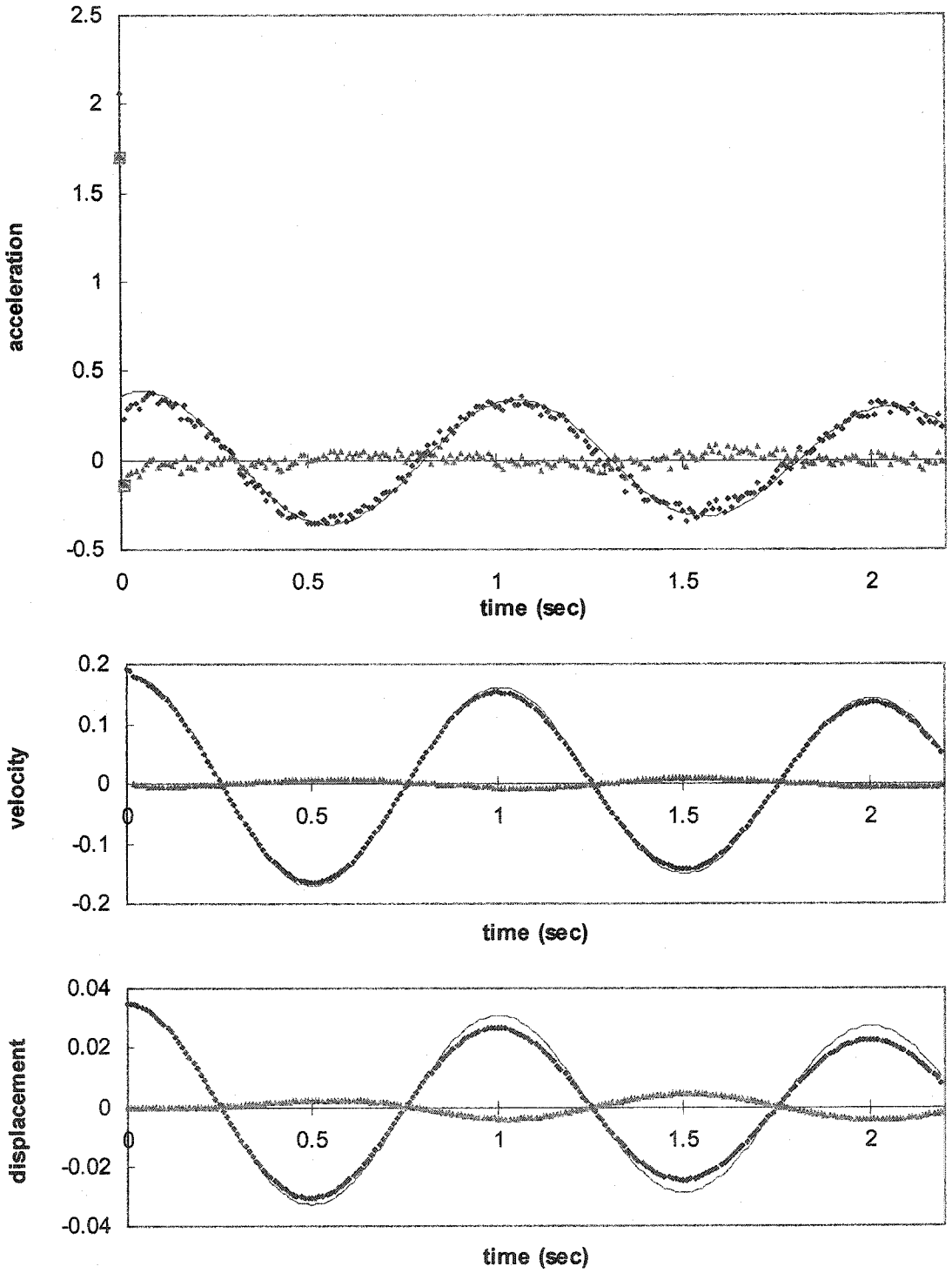

Figure 3.6.4

RD Signatures with Positive Peak Triggering Condition and Non-overlapped Condition

——, Free Vibration Response; ♦♦♦♦♦, RD Signature; ▲▲▲▲▲, Residuals

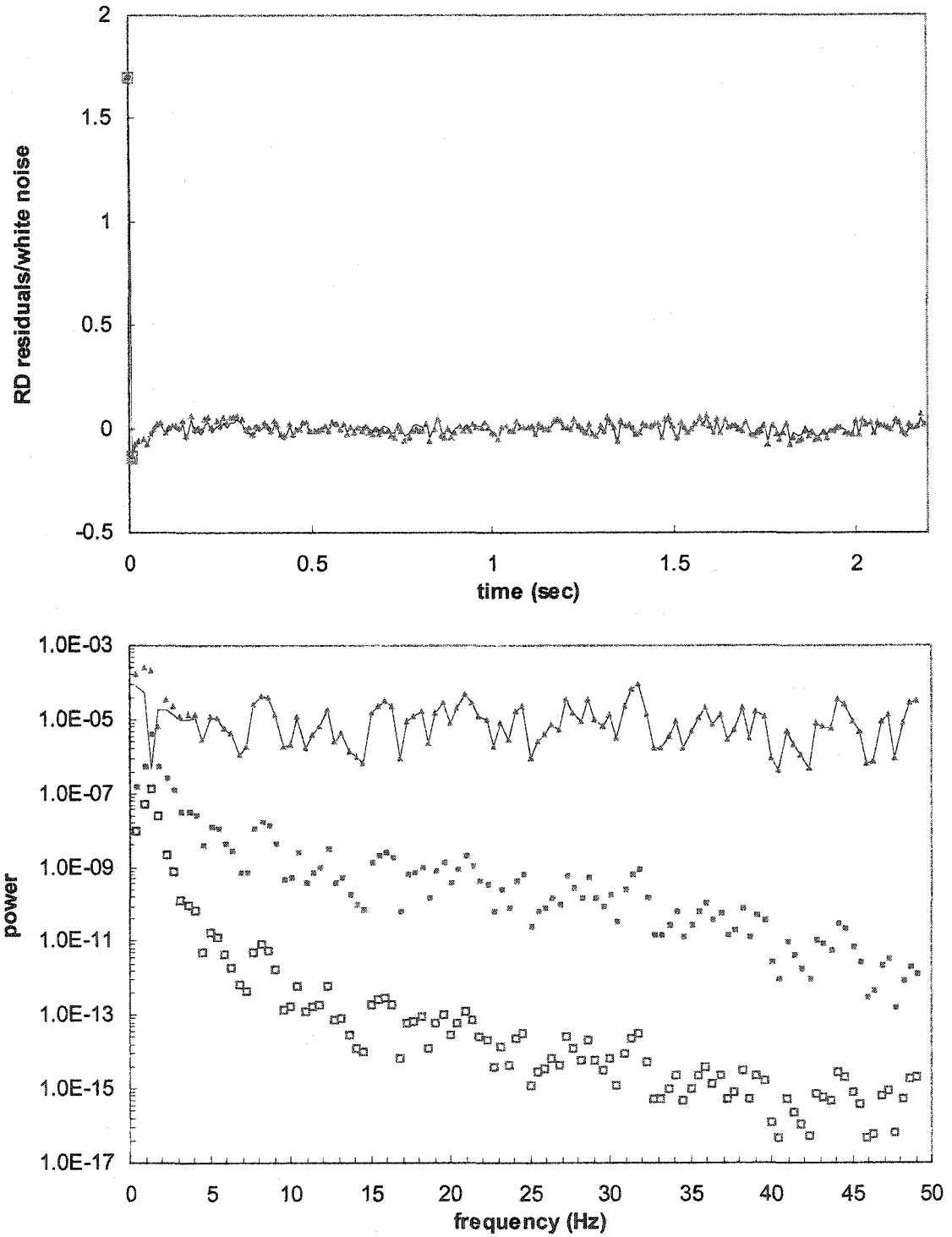

Figure 3.6.5 Relations of RD Acceleration Residuals and White Noise with Positive Peak Triggering Condition and Non-overlapped Condition

——, RD White Noise Signature; ▲▲▲▲▲, RD Acceleration Residuals; ■■■■■, RD Velocity Residuals; □□□□□, RD Displacement Residuals

3.6.2 Application of Simulated Wind Forces

The simulation of wind forces is demanded in order to realize the feasible application of the RD technique to the wind-induced response of a dynamic system. The simulation of the wind force is therefore required to make it as realistic as possible.

A procedure for wind force simulation in this investigation only considers the alongwind motion. The alongwind force on a single point may be expressed in terms of longitudinal velocity as:

$$F(t) = \frac{1}{2}\rho A_s C_D [U(t) - \dot{x}(t)]^2 \tag{3.6.3}$$

in which ρ, A_s, and C_D represent air density, sectional area, and drag coefficient, respectively. $U(t)$ is longitudinal wind velocity which is expected as the sum of a mean, $\overline{U}$, and a fluctuation component, $u'(t)$; and $\dot{x}(t)$ denotes as the structural velocity at the single point. Only the fluctuating force is considered by assuming that the quadratic and structural velocity terms in the bracket of Equation (3.6.3) are negligible [Kareem, 1987; Kareem et al., 1998]. Consequently, it turns out that the fluctuating alongwind force is formulated as:

$$F'(t) = \rho A_s C_D \overline{U} u'(t) \tag{3.6.4}$$

in which ρ = 1.225 kg/m^3, A_s = 0.5 m^2, C_D = 0.8, and $\overline{U} = 15$ m/sec are assigned in advance. Apparently, as long as the simulation of the fluctuating alongwind velocity is carried out, the fluctuating alongwind force can be obtained immediately by means of Equation (3.6.4).

The simulation of a stationary fluctuating wind velocity makes use of the autoregressive moving average model (ARMA) with orders of p and q, which is defined as:

$$Y(n\Delta t)+\sum_{j=1}^{p} A_j Y[(n-j)\Delta t]=\sum_{j=0}^{q} B_j \varepsilon[(n-j)\Delta t] \tag{3.6.5}$$

in which A_j and B_j are parameters of the ARMA model and ε stands for a white noise with zero mean and variance one [Brockwell and Davis, 1996].

In order to determine the parameters of the ARMA model, the two-stage least squares algorithm is utilized in accordance with a target velocity spectrum of Kaimal model [Simiu and Scanlan, 1996] as follows:

$$\frac{fS_u(z,f)}{u_*^2}=\frac{200n}{(1+50n)^{\frac{5}{3}}},\quad 0<f<\infty \tag{3.6.6}$$

in which $n=\dfrac{fz}{\overline{U}(z)}$ and $u_*^2=\dfrac{\overline{u'^2}}{6}$. The orders p and q of the ARMA model were selected as 25 for both, such that the power spectrum and the correlation function of the simulated data are close to those of the target. Once the parameters, A_j and B_j, of the ARMA model are determined, it follows that the time history of the fluctuating alongwind velocity is generated recursively with the aid of Equation (3.6.5).

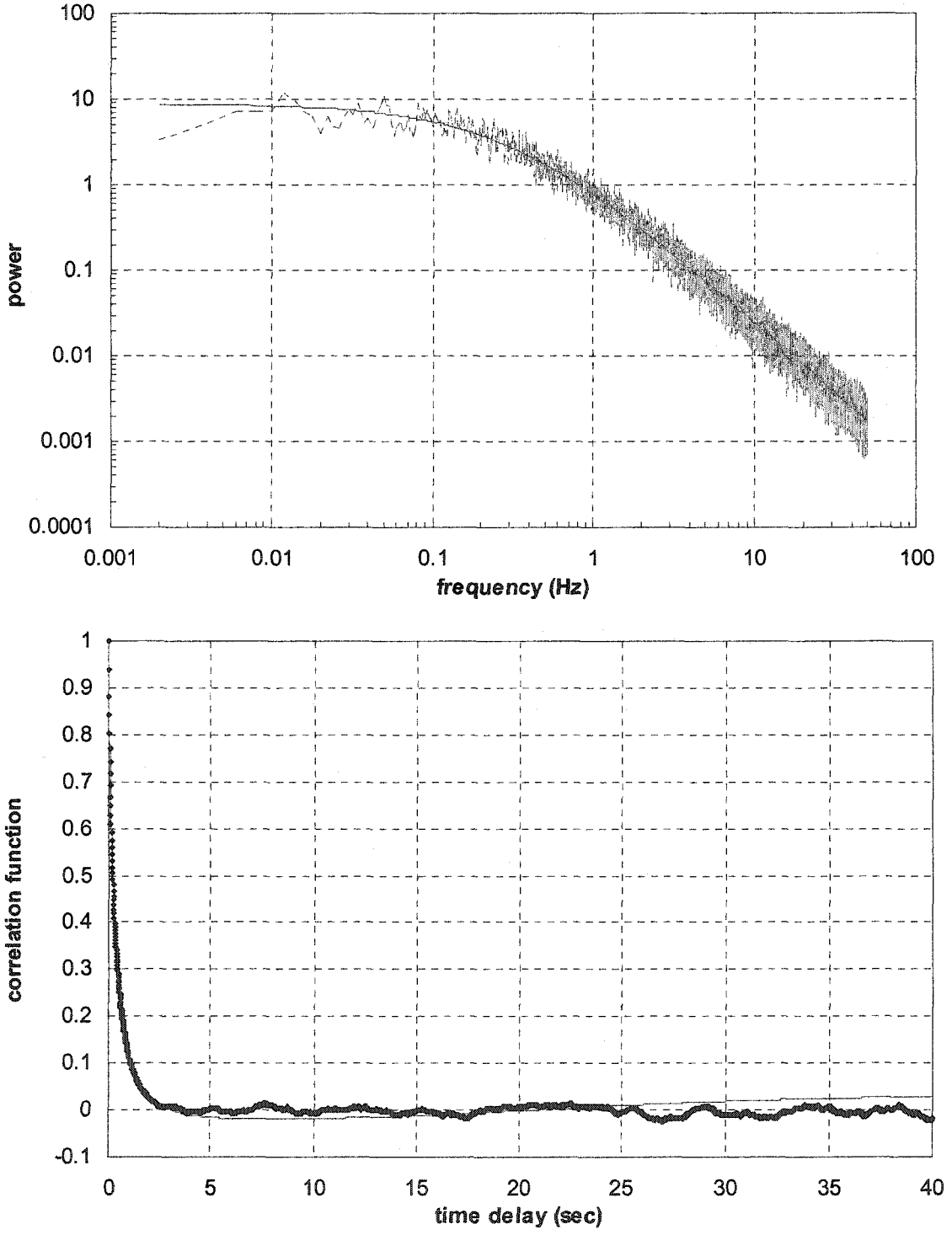

Figure 3.6.6 Comparisons of Wind Velocity

(a) Spectral Density Function —— The Target, ----- The Simulation
(b) Correlation Function —— The Target, ••••• The Simulation

The total time history of the fluctuating velocity was generated up to 405000 points with a time interval of 0.01 second. The total data length of 400000 points was adopted in effect after the initial 5000 points were removed to maintain the simulated data stationary. Figure 3.6.6 illustrates the comparisons of the spectral density function and the correlation function between the simulation and the target. The spectral density function of the simulated wind velocity was calculated through the FFT based approach with a preprocessing of 50 percent overlapping and the Hanning window tapering for each data length of 50000 points. Therefore, the total 15 sets of the spectral density function were available to calculate their ensemble average. The evaluation of the correlation function typically counted on the whole data length of 4000 seconds, but only 40 seconds are displayed in Figure 3.6.6 (b).

In Tables 3.6.4-6, the initial conditions selected from the synchronous RD signatures, corresponding to the resulting responses excited by the simulated alongwind force, were used to perform the analytical free vibration responses. Nonetheless, it is interesting to know whether such RD signatures can still provide the proper initial conditions without deviation. In response to this, the initial point of the auto RD signature in Equation (3.4.6) associated with the general triggering condition was first examined. It turns out that such an initial point is independent of the correlation functions, since the first-term correlation functions on the denominator and numerator are cancelled out and the second-term correlation function on the numerator is zero at the initial point. In other words, the selection of the initial conditions from the starting points of the auto RD signatures under consideration is not affected by the correlation functions. Therefore, the procedure using the RD technique to select the initial conditions from the

synchronous RD signatures of the displacement and velocity responses is considered feasible.

Table 3.6.4 Initial Conditions of a Free Vibration Response from RD Signatures with Level Crossing Triggering Condition and Overlapped Condition

Leading Response	Displacement Response	Velocity Response	Acceleration Response
Initial Displacement	1.06471 (1.06495)	0.00310 (0)	-0.99581
Initial Velocity	0.00861 (0)	6.41416 (6.41100)	0.13185

Note: 1. The Parenthesized Values Denote The Theoretical Initial Conditions

Table 3.6.4 Initial Conditions of a Free Vibration Response from RD Signatures with Positive Peak Triggering Condition and Overlapped Condition

Leading Response	Displacement Response	Velocity Response	Acceleration Response
Initial Displacement	1.30467	-0.00369 (0)	-0.74641
Initial Velocity	-0.00194 (0)	6.73019	-0.02882

Table 3.6.5 Initial Conditions of a Free Vibration Response from RD Signatures with Positive Peak Triggering Condition and Non-Overlapped Condition

Leading Response	Displacement Response	Velocity Response	Acceleration Response
Initial Displacement	1.98516	-0.00216 (0)	-1.37123
Initial Velocity	-0.02159 (0)	11.77498	-1.60907

Corresponding to the specified initial conditions above, the comparisons between the RD signatures and the free vibration responses are demonstrated in Figures 3.6.7-10. The results in Figures 3.6.7-9 reveal that the deviation of the RD signatures from the corresponding free vibration responses gradually increases with the increase of the time delay, in contrast with the results of the white noise excitation. As a result, it follows that

the RD signatures may not be equivalent to the free vibration responses when the external excitation is not a white noise.

Examining carefully the RD acceleration signatures, one can also find deviations of the first few points exhibited in Figure 3.6.9. Among these points, the initial two points of the signatures are marked by square and their residuals are marked by triangle. Further inspection of the time domain and frequency domain analyses of the RD residuals shown in Figure 3.6.10 reflects the significant interference of the RD forcing signatures, as well as the conclusion in Figures 3.6.3 and 3.6.5 for the white noise excitation. It can also be concluded that the estimated RD acceleration signatures indeed depend on the forcing functions under consideration no matter what kind of excitation it is.

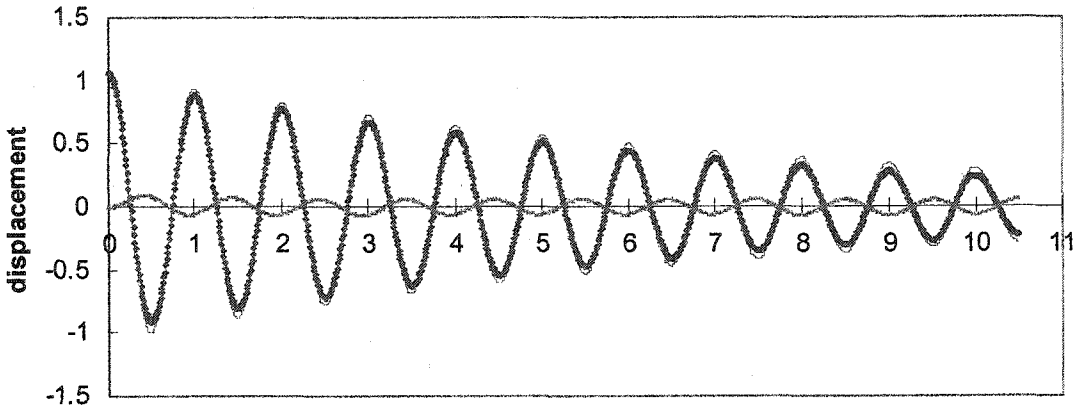

(a) Level Crossing Triggering Condition

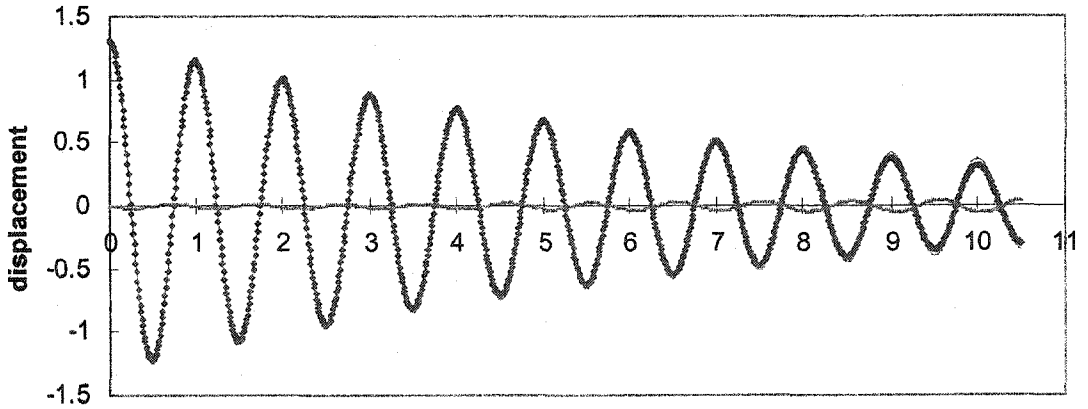

(b) Positive Peak Triggering Condition for Overlapped Condition

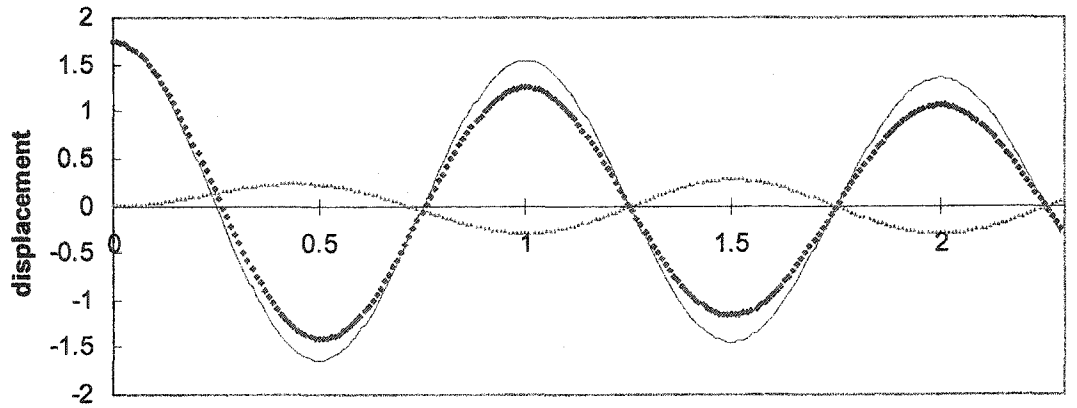

(c) Positive Peak Triggering Condition for Non-overlapped Condition

Figure 3.6.7 RD Displacement Signatures

——, Free Vibration Response; ♦♦♦♦♦, RD Signature; ▲▲▲▲▲, Residuals

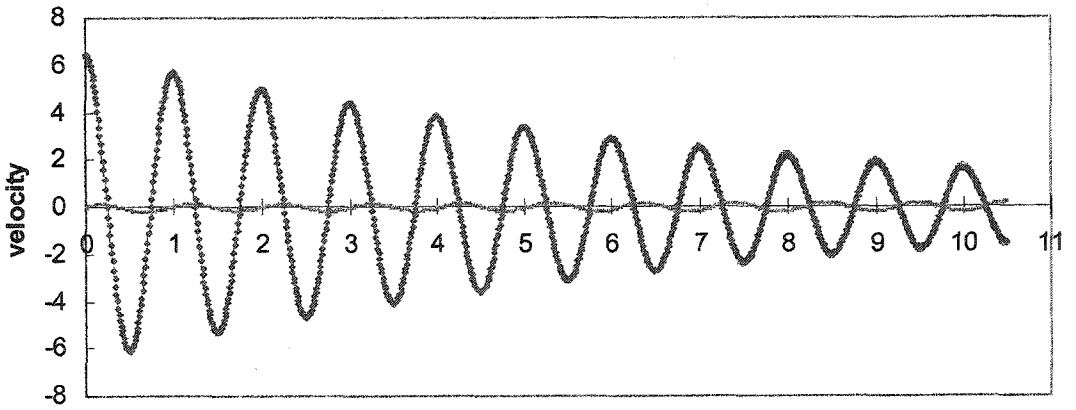

(a) Level Crossing Triggering Condition

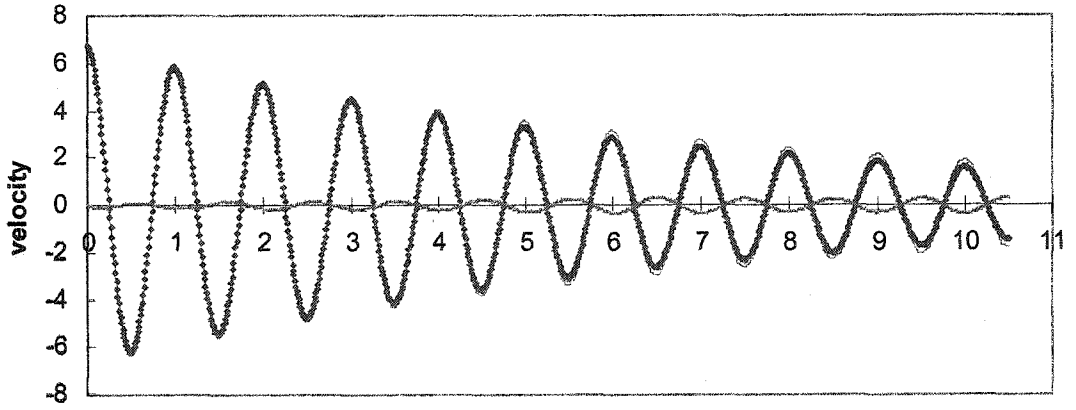

(b) Positive Peak Triggering Condition for Overlapped Condition

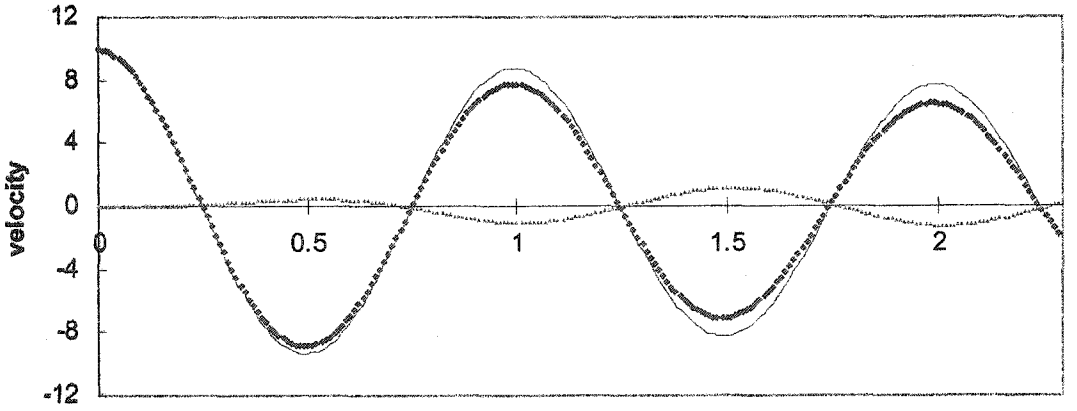

(c) Positive Peak Triggering Condition for Non-overlapped Condition

Figure 3.6.8 RD Velocity Signatures

——, Free Vibration Response; ♦♦♦♦♦, RD Signature; ▲▲▲▲▲, Residuals

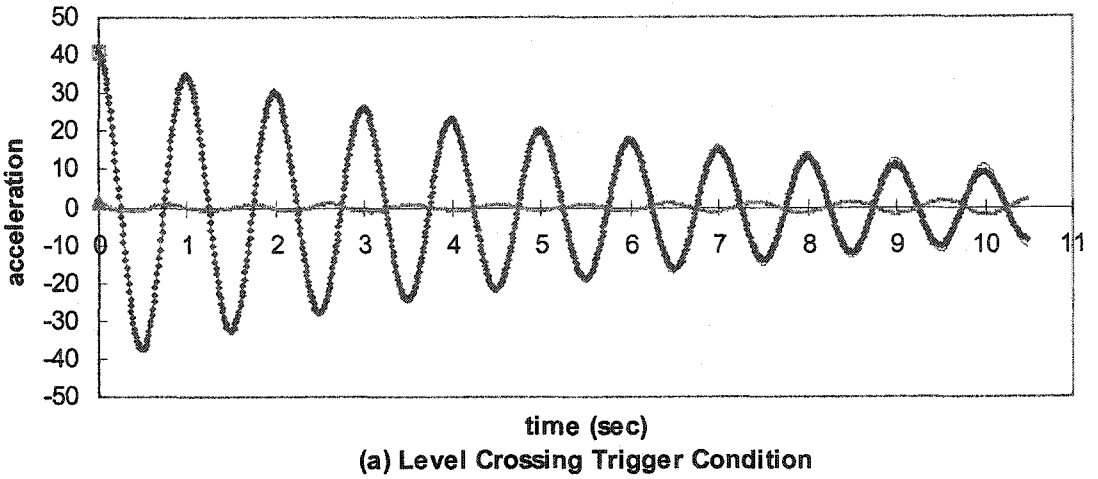

(a) Level Crossing Trigger Condition

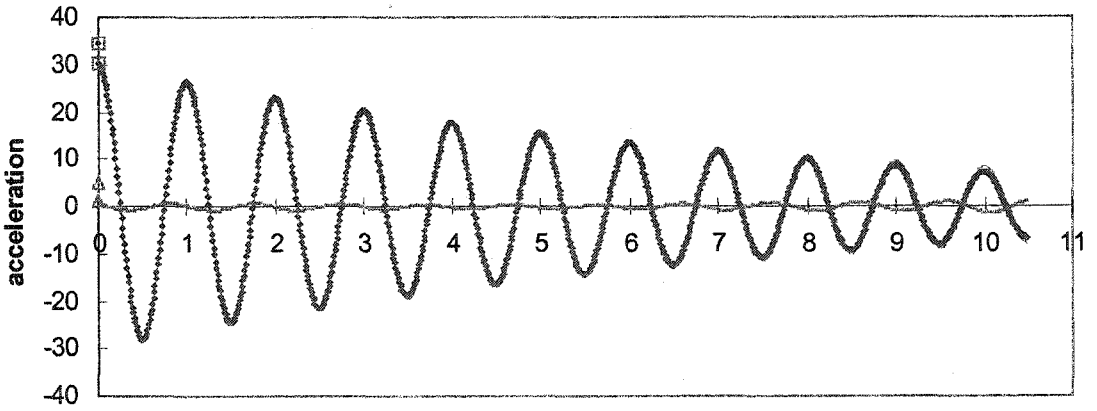

(b) Positive Peak Triggering Condition for Overlapped Condition

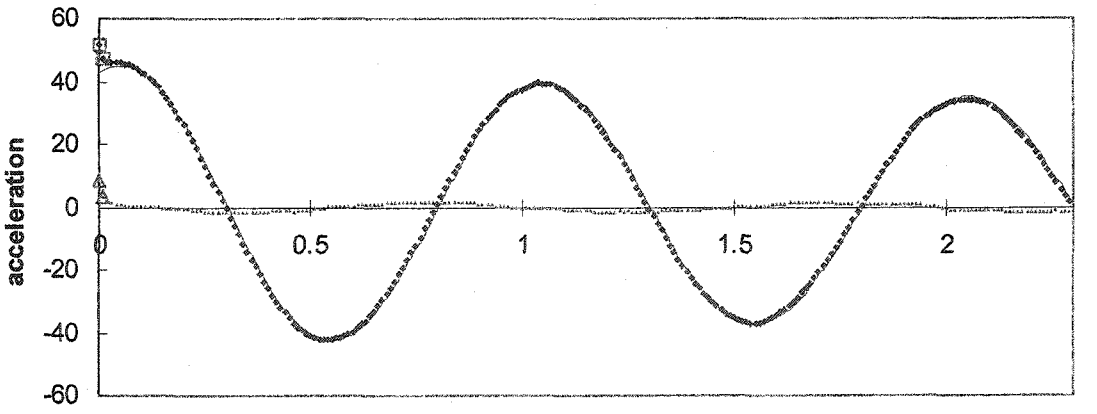

(c) Positive Peak Triggering Condition for Non-overlapped Condition

Figure 3.6.9 RD Acceleration Signatures

——, Free Vibration Response; ♦♦♦♦♦, RD Signature; ▲▲▲▲▲, Residuals

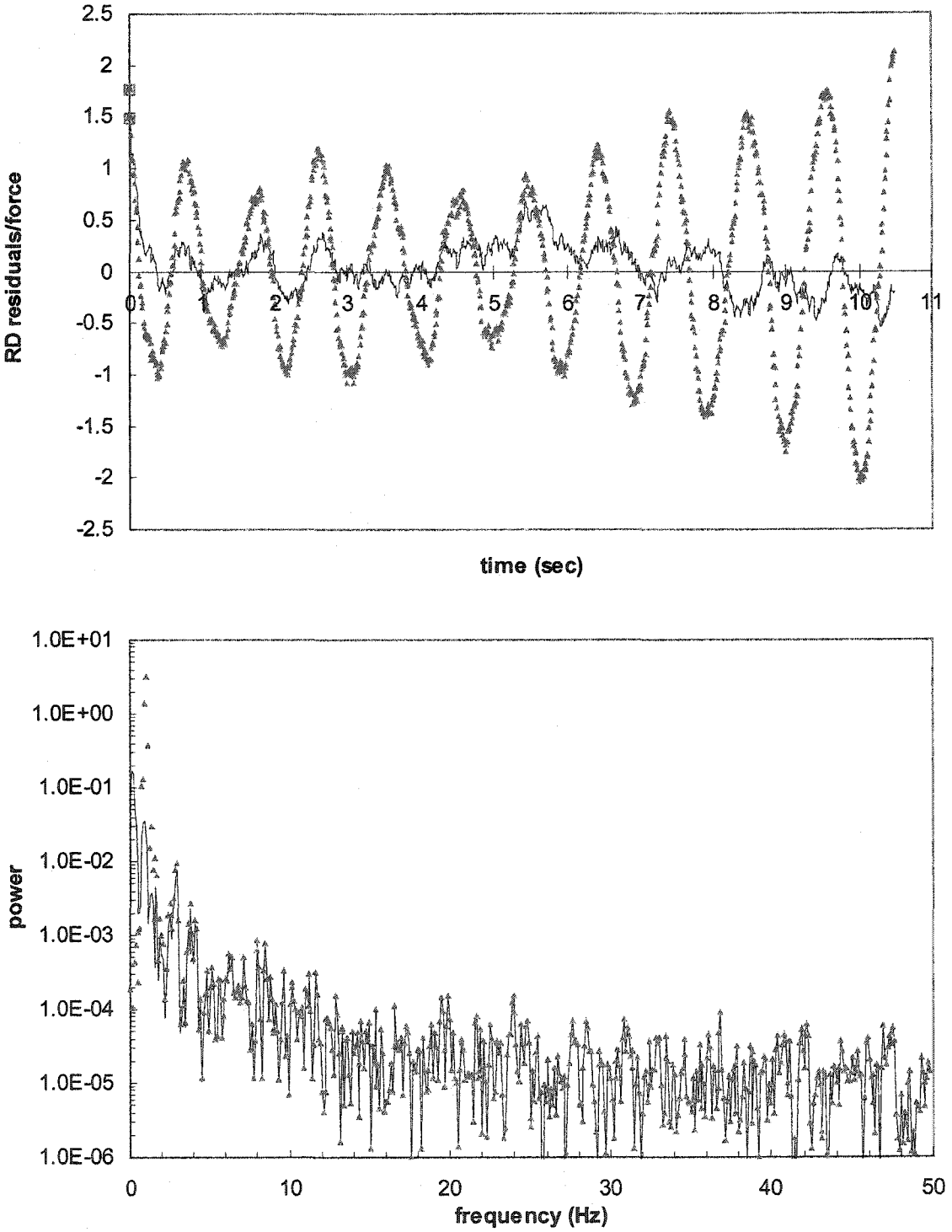

Figure 3.6.10 Relations of RD Acceleration Residuals and Simulated Wind Force

(a) Level Crossing Triggering Condition

——, RD Force Signature; ▲▲▲▲▲, RD Acceleration Residuals

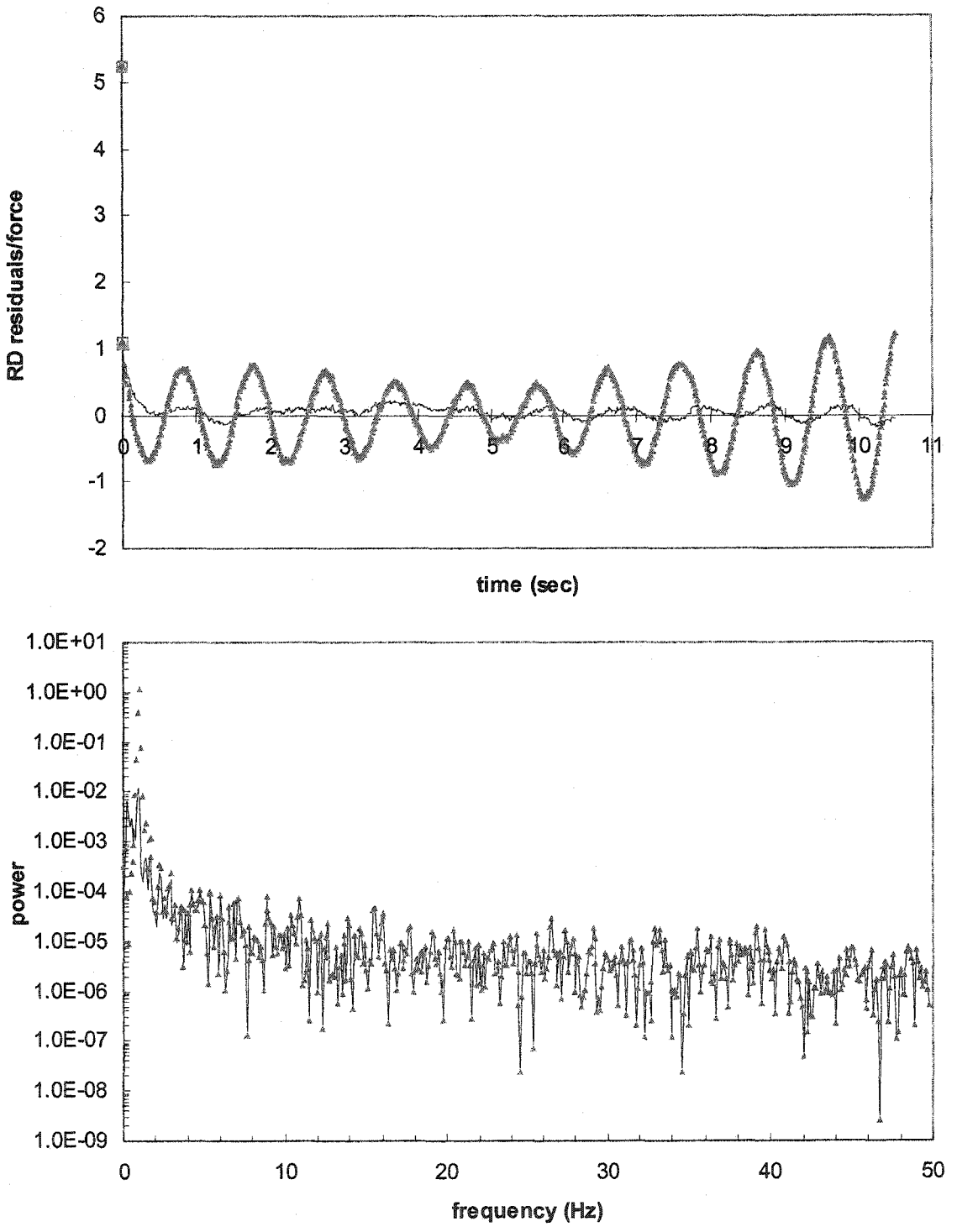

Figure 3.6.10 Relations of RD Acceleration Residuals and Simulated Wind Force

(b) Positive Peak Triggering Condition and Overlapped Condition

——, RD Force Signature; ▲▲▲▲▲, RD Acceleration Residuals

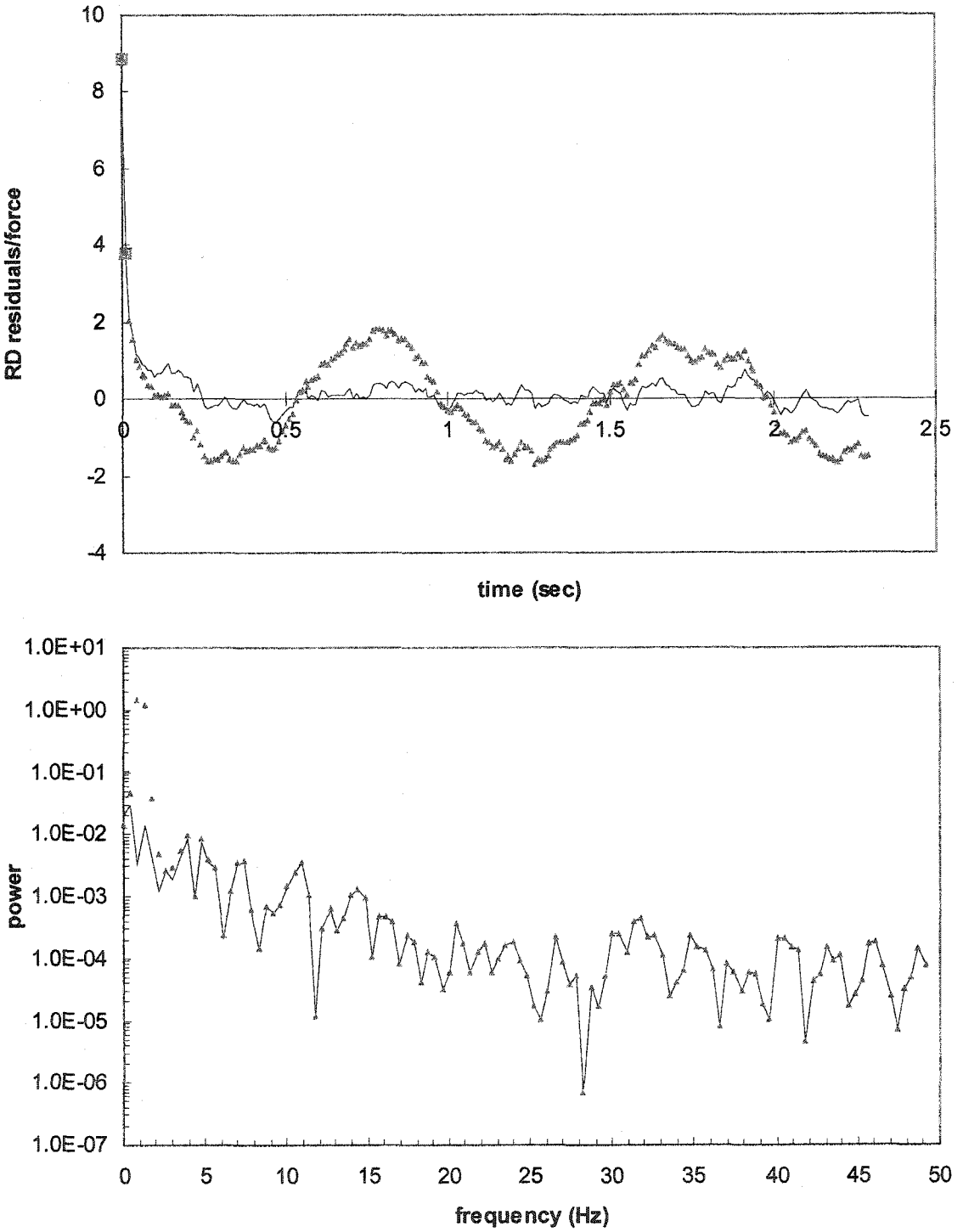

Figure 3.6.10 Relations of RD Acceleration Residuals and Simulated Wind Force

(c) Positive Peak Triggering Condition and Non-overlapped Condition

——, RD Force Signature; ▲▲▲▲▲, RD Acceleration Residuals

3.7 Concluding Remarks

This study emphasized the use of the RD technique to overcome the difficulties of defining the initial conditions, such that the free vibration responses can be obtained and then compared with the corresponding RD signatures. Following the strict theoretical derivation of the RD technique, the numerical simulations were implemented by taking advantage of a SDOF linear time-invariant dynamic system subjected to a white noise excitation and a simulated wind force, separately. Through the theoretical derivation and the numerical simulations, the relevance of the RD signatures and the analytical free vibration responses for the dynamic system was further examined under two various triggering conditions. The significant conclusions with regard to the statistical properties of the RD signatures are summarized in the following:

1. When the SDOF dynamic system is subjected to the white noise excitation, the equivalence relation between the RD acceleration signature with the free vibration acceleration response, except for the initial point at $t = 0$, can be established, while the RD displacement and velocity signatures are expected to be equivalent to the corresponding free vibration responses with certain initial conditions.
2. When the excitation applied to the SDOF dynamic system is simulated for the real wind force, the deviations of the RD signatures from the associated free vibration responses gradually increase along with the increase of the time delay. This means that the RD signatures of the responses are not equivalent to their free vibration responses of the dynamic system under consideration. With this result in mind, the treatment of the RD signatures as free vibration responses under practical circumstances should be prudently followed.

3. Figures 3.6.3(iii), 3.6.5 and 3.6.10 reveal that the RD acceleration signature indeed depends on the RD signature of the forcing function, regardless of what kind of input force it is. Such a fact is consistent with Equation (3.5.22) in which the correlation function of the forcing function is substantially included. In this respect, it is recommended that a force measurement should be undertaken to accompany any acceleration measurement to obtain a better estimate of the RD acceleration signature.

References

Asmussen, J. C. (1997), Modal Analysis based on the Random Decrement Technique – Application to Civil Engineering Structures, Ph.D. Dissertation, Department of Building Technology and Structural Engineering, University of Aalborg, Denmark.

Bedewi, N. E. (1986), The Mathematical Foundation of the Auto and Cross-Random Decrement Techniques and the Development of a System Identification Technique for the Detection of Structural Deterioration, Ph.D. Dissertation, Department of Mechanical Engineering, University of Maryland.

Bendat, J. S. and Piersol, A. G. (2000), Random Data Analysis and Measurement Procedures, 3rd Edition, John Wiley & Sons, pp. 87-89 and pp. 165-170.

Bracewell, R. (1999), "The Impulse Symbol", Chapter 5 in The Fourier Transform and Its Applications, 3rd Edition, McGraw-Hill.

Brincker, R., Jensen, J. L., and Krenk, S. (1990), "Spectral Estimation By The Random Dec Technique", The 9th International Conference on Experimental Mechanics, pp. 2049-2058.

Brincker, R., Krenk, S., Kirkegaard, P. H., and Rytter, A. (1992), "Identification Of Dynamical Properties From Correlation Function Estimates", Bygningsstatiske Meddelllser, Vol. 63, No. 1, pp. 1-38.

Brockwell, P. J. and Davis, R. A. (1996), Introduction to Time Series and Forecasting, First Edition, Springer, pp. 81-106.

Caldwell, D. W. (1978), The Measurement of Damping and the Detection of Damage in Linear and Nonlinear Systems by the Random Decrement Technique, Ph.D. Dissertation, University of Maryland.

Chang, C. S. (1975), "Study Of Dynamic Characteristics Of Aeroelastic Systems Utilizing Randomdec Signatures", NASA CR-132563.

Cheng, F. Y. (2001), Matrix Analysis of Structural Dynamics: Applications and Earthquake Engineering, 1st Edition, Marcel Dekker, pp. 329-331.

Cole, H. A. (1968), "On-The-Line Analysis Of Random Vibrations", AIAA/ASME 9th Structures, Structural Dynamics and Materials Conference, AIAA Paper No. 68-288.

Cole, H. A. (1971), "Method And Apparatus For Measuring The Damping Characteristic Of A Structure", United State Patent No. 3,620,069.

Crandall, S. H. and Mark, W. D. (1963), Random Vibration in Mechanical Systems, 2nd Edition, Academic Press, pp. 58-64.

Houbolt, J. C. (1975), "On Identifying Frequencies And Damping In Subcritical Flutter Testing", The Proceedings of the Flutter Testing Techniques, pp. 1-41.

Huan, S. L., Mcinnis, B. C., and Denman, E. D. (1983), "Analysis Of The Random Decrement Method", International Journal of Systems Science, Vol. 14, No. 4, pp. 417-423.

Huang, C. S. and Yeh, C. H. (1999), "Some Properties Of Randomdec Signatures", Mechanical Systems and Signal Processing, Vol. 13, No. 3, pp. 491-507.

Huang, C. S., Yeh, C. H., and Tsai, I. C. (1998), "Random Decrement Technique For Ambient Vibration Test In Time-domain System Identification", Journal of the Chinese Institute of Civil and Hydraulic Engineering, Vol. 10, No. 3, pp. 537-547. (In Chinese)

Huang, C. S., Yeh, C. H., Lin, S. C., and Yeh, K. T. (1996), The Application of Random Decrement Technique to Ambient Vibration Measurement – A Proportional Damping System, Report of National Center for Research on Earthquake Engineering, Taiwan, NCREE-96-013.

Ibrahim, S. R. (1977), "Random Decrement Technique For Modal Identification Of Structures", Journal of Spacecraft, AIAA, Vol. 14, No. 11, pp. 696-700.

Ibrahim, S. R. and Mikulcik, E. C. (1977), "A Method For The Direct Identification Of Vibration Parameters From The Free Response", The Shock and Vibration Bulletin, 47, Part 4 Structural Dynamics, System Identification, Computer Applications, pp. 183-198.

Jerry, A. P. (1981), The Dynamic Behavior of Tall Buildings, Ph.D. Dissertation, University College London, UK.

Jerry, A. P. (1986), "Damping In Tall Building – A Mechanism And A Predictor", Earthquake Engineering and Structural Dynamics, Vol. 14, pp. 733-750.

Jerry, A. P. (1992), "Establishing Non-linear Damping Characteristics Of Structures From Non-stationary Response Time-histories", The Structural Engineer, Vol. 70, No. 4, pp. 61-66.

Kareem, A. (1987), "Wind Effects On Structures: A Probabilistic Viewpoint", Probabilistic Engineering Mechanics, Vol. 2, No. 4, pp. 166-200.

Kareem, A., Tognarelli, M. A., and Gurley, K. R. (1998), "Modeling And Analysis Of Quadratic Term In The Wind Effects On Structures", Journal of Wind Engineering and Industrial Aerodynamics, Vol. 74-76, pp. 1101-1110.

Papoulis, A. and Pillai, S. U. (2002), Probability, Random Variables, and Stochastic Processes, 4th Edition, McGraw Hill, pp. 269.

Simiu, E. and Scanlan, R. H. (1996), Wind Effects on Structures – Fundamental and Applications to Design, 3rd Edition, John Wiley & Sons, pp. 59.

Spanos, P. D. and Zeldin, B. A. (1998), "Generalized Random Decrement Method For Analysis Of Vibration Data", Vol. 120, pp. 806-813.

Stark, H. and Woods, J. W. (1994), Probability, Random Processes, and Estimation Theory for Engineers, 2nd Edition, Prentice Hall, pp. 170-171.

Tamura, Y., Shimada, K., and Hibi, K. (1993), "Wind Response Of A Tower (Typhoon Observation At The Nagasaki Huis Ten Bosch Domtoren)", Journal of Wind Engineering and Industrial Aerodynamics, Vol. 50, pp. 309-318.

Tamura, Y., Yamada, M., and Yokota, H. (1994) "Estimation Of Structural Damping Of Buildings", Structures Congress XII, Vol. 2, pp. 1012-1017.

Tamura, Y., Shimada, K., Sasaki, A., Kohsaka, R., and Fujii, K. (1995), "Variation Of Structural Damping Ratios And Natural Frequencies Of Tall Buildings During Strong Winds", The 9th International Conference on Wind Engineering, pp.1396-1407.

Tamura, Y., Kohsaka, R., Nakamura, O., Miyashita, K., and Modi, V. J. (1996), "Wind-Induced Responses Of An Airport Tower – Efficiency Of Tuned Liquid Damper", Journal of Wind Engineering and Industrial Aerodynamics, Vol. 65, pp. 121-131.

Vandiver, J. K., Dunwoody, A. B., Campbell, R. B., and Cook, M. F. (1982), "A Mathematical Basis For The Random Decrement Vibration Signature Analysis Technique", ASME Journal of Mechanical Design, Vol. 104, pp. 307-313.

Yang, J. C. S. and Caldwell, D. W. (1976), "The Measurement Of Damping And The Detection Of Damages In Structures By The Random Decrement Technique", the 46th Shock and Vibration Bulletin, pp. 129-136.

Yang, J. C. S. and Caldwell, D. W. (1978), "A Method For Detecting Structural Deterioration In Piping Systems", ASME Probabilistic Analysis and Design of Nuclear Power Plant Structures Manual, PVP-PB-030, pp. 97-117.

Yang, J. C. S., Aggour, M. S., Dagalakis, N., and Miller, F. (1981), "Damping Of Offshore Platform Model By Randomdec Method", Proceedings, the 2nd Specialty Conference on Dynamic Response of Structures, pp. 819-832.

Chapter 4

MULTI-SIGNAL RANDOM DECREMENT TECHNIQUE

4.1 Introduction

The identification of modal parameters is a process to determine the constitutive properties of a complicated dynamic system in the forms of natural frequencies, damping ratios, and corresponding mode shapes. The identified modal parameters can typically formulate a mathematical model, which portrays a physical insight of the dynamic system. The importance of building an accurate and reliable mathematical model for a real dynamic system is its capability to simulate and to predict the dynamic behavior of the system. Additionally, a number of practical applications, such as structural modal updating, structural control, and structural damage assessment, can be successfully performed in the future.

Over the past three decades, many researchers have endeavored to develop system identification techniques in order to determine the modal parameters of dynamic systems. Especially, the remarkable progress in computer technology further enhances the ability of system identification techniques for civil engineering applications. Most system identification techniques require full measurements of external dynamic excitation and its corresponding dynamic response. However, the external excitation on a real structure is difficult, if not impossible, to well define and accurately measure. In this regard, special attention is given to system identification techniques, which may not have to rely on knowing the external excitation. One of such special techniques without *a priori*

knowledge of the external excitation is random decrement technique, or RD technique, in short, which is applied to convert vibration responses into free vibration responses.

The RD technique was originally proposed by Cole [1971] to obtain a single mode RD signature of one single measurement. Following the proposed RD technique, Ibrahim [1977] extensively introduced the concept of multiple-signal RD technique for a multiple degrees-of-freedom (MDOF) dynamical system. Similar to the traditional single-signal RD technique, it reduces multiple-mode stationary random responses of a multiple-measurement to their free vibration responses. These free vibration responses can further be used to identify the modal parameters of the MDOF dynamic system under tests by means of the so-called Ibrahim time domain system identification.

To establish the theoretical foundation for the application of the multiple-signal RD technique, Bedewi [1986] and Huang et al. [1996, 1998, 1999] presented strict mathematical derivations on the basis of a linear 2DOF dynamic system when subjected to stationary white noise excitations. Bedewi pointed out that the auto and cross RD displacement signatures are identical to the free vibration displacement responses of a dynamic system with proportional damping. The additional efforts of Huang et al. [1999] focused on deriving the equivalent relations between the RD signatures of velocity and acceleration and their free vibration responses, using complex modal superposition. Huang, et al. showed that, under certain circumstances, the RD displacement and velocity signatures are equal to the corresponding free vibration responses of a dynamic system with non-proportional damping. However, once a white noise process with a time-delay correlation is taken into account, the RD displacement and velocity signatures are not

equal to their free vibration responses in the time-delay region. This study will show that this conclusion should be corrected from a different perspective.

In addition, Huang et al. also indicated that the RD acceleration signatures are never equivalent to the free vibration behavior of the dynamic system, because the singularities from the correlation functions of the white noise excitations appear in such RD acceleration signatures. The appearance of the singularity in the RD acceleration signatures is appreciated since a fascinating question comes out as to whether the underlined RD technique is still useful to extract the free vibration response from the acceleration response of a measurement? The main purpose of this study is to properly answer this question and further establish the generalized relationship between the RD acceleration signatures and the RD force signatures. The theoretical derivations of the RD technique start the state space formulation to lead to a compact and distinct representation of the RD signatures, which can be well compared with the free vibration responses. The theoretical derivations are supplemented with numerical simulations to illuminate better understanding of the RD technique.

In the numerical simulations, two simulated wind forces were also applied to generate the wind-induced responses, in addition to the use of the white noise excitations to verify the theoretical derivations. Based on the resulting wind-induced responses, the RD signatures of the responses were constructed to compare their analytical free vibration responses. The new challenge was created in the comparison procedure, since the analytical free vibration responses were difficult to achieve without knowledge of the initial displacement and velocity conditions. Therefore, the procedure proposed in the previous chapter by taking advantage of the concept of the RD technique was used to

determine such initial conditions from the synchronous RD signatures of a set of responses. The feasibility of such a procedure should be discussed from the theoretical viewpoint and then verified in the numerical simulations.

4.2 Correlation Functions of a Linear MDOF Dynamic System

The governing equations of motion for a linear time-invariant n DOF discrete dynamic system can be expressed in a matrix form as:

$$M\ddot{X}(t) + C\dot{X}(t) + KX(t) = f(t) \qquad t \geq 0 \tag{4.2.1}$$

in which M, C, and K denote mass, damping, and stiffness matrices of the dynamic system, respectively, and $f(t)$ represents an input force vector. It is assumed herein that M and K are symmetric and positive definite $n \times n$ matrices, and C is a positive semi-definite non-proportional damping $n \times n$ matrix.

In order to solve the responses of the dynamic system with the non-proportional damping matrix, Equation (4.2.1) can be transformed into a set of $2n$ uncoupled linear first-order differential equations as the following Equation (4.2.2), which is called the state space formulation [Hart and Wang, 2000].

$$\dot{z}(t) = Az(t) + \tilde{F}(t) \tag{4.2.2}$$

in which

$$z(t) = \begin{bmatrix} X(t) \\ \dot{X}(t) \end{bmatrix}_{2n\times 1}, A = \begin{bmatrix} 0 & I \\ -M^{-1}K & -M^{-1}C \end{bmatrix}_{2n\times 2n}, \tilde{F}(t) = \begin{bmatrix} 0 \\ M^{-1}f(t) \end{bmatrix}_{2n\times 1} \tag{4.2.3}$$

Making use of the normal mode approach to represent the responses as a superposition of the contributions from each normal mode, the state vector $z(t)$ can be written as:

$$z(t) = \begin{bmatrix} X(t) \\ \dot{X}(t) \end{bmatrix} = \sum_{i=1}^{2n} \hat{\phi}_i q_i(t) = \Phi Q(t) \tag{4.2.4}$$

in which the modal matrix $\Phi = \begin{bmatrix} \hat{\phi}_1 & \hat{\phi}_2 & \dots & \hat{\phi}_{2n} \end{bmatrix}_{2n \times 2n}$ represents the eigenvectors of the matrix A and $Q(t) = \begin{bmatrix} q_1(t) & q_2(t) & \dots & q_{2n}(t) \end{bmatrix}^T_{2n \times 1}$ denotes a new $2n \times 1$ vector of modal coordinates. The modal matrix Φ has been normalized so as to satisfy the orthogonal condition $\Phi^T \Phi = I$, where I is a $2n \times 2n$ identity matrix. Substitution of Equation (4.2.4) into Equation (4.2.2) and then pre-multiplication by the transpose of the modal matrix Φ^T give:

$$\dot{Q}(t) = \Phi^T A \Phi Q(t) + \Phi^T \tilde{F}(t) \tag{4.2.5}$$

in which the superscript T stands for the transpose of a matrix. Since each column of Φ is an eigenvector of A, it follows that the other orthogonality condition is:

$$\Phi^T A \Phi = \begin{bmatrix} \lambda_1 & 0 & \cdots & 0 \\ 0 & \lambda_2 & \ddots & \vdots \\ \vdots & \ddots & \ddots & 0 \\ 0 & \cdots & 0 & \lambda_{2n} \end{bmatrix}_{2n \times 2n} = \Lambda \tag{4.2.6}$$

in which λ_i is the i^{th} eigenvalue of A and the eigenvalues are assumed to be a distinct and negative real part making the dynamic system stable. By virtue of such an orthogonality condition, Equation (4.2.5) can be reduced as:

$$\dot{Q}(t) = \Lambda Q(t) + \Phi^T \tilde{F}(t) \tag{4.2.7}$$

The eigenvalues and corresponding eigenvectors have to be in pairs of complex conjugates, if both of them are complex-valued. As a consequence, Equation (4.2.6) can be partitioned as:

$$\Lambda = \begin{bmatrix} \lambda & 0 \\ 0 & \lambda^* \end{bmatrix} \tag{4.2.8}$$

The corresponding modal matrix and the vector of the modal coordinates are expressed respectively as:

$$\Phi = \begin{bmatrix} \phi & \phi^* \\ \phi\lambda & \phi^*\lambda^* \end{bmatrix} \tag{4.2.9}$$

$$Q(t) = \begin{bmatrix} q(t) & q^*(t) \end{bmatrix}^T \tag{4.2.10}$$

in which the superscript * denotes the complex conjugate operator.

Substituting Equations (4.2.9) and (4.2.10) into Equation (4.2.4), it becomes that

$$X(t) = \phi q(t) + \phi^* q^*(t) = 2\,\mathrm{Re}\{\phi q(t)\} \tag{4.2.11}$$

$$\dot{X}(t) = \phi\lambda q(t) + \phi^*\lambda^* q^*(t) = 2\,\mathrm{Re}\{\phi\lambda q(t)\} \tag{4.2.12}$$

, and also the second derivative of $X(t)$ may be obtained as:

$$\ddot{X}(t) = \phi\lambda\dot{q}(t) + \phi^*\lambda^*\dot{q}^*(t) = 2\,\mathrm{Re}\{\phi\lambda\dot{q}(t)\} \tag{4.2.13}$$

in which Re{ } denotes the real component of the complex function. Correspondingly, based on Equations (4.2.8-10), Equation (4.2.7) becomes:

$$\begin{bmatrix} \dot{q}(t) \\ \dot{q}^*(t) \end{bmatrix} = \begin{bmatrix} \lambda & 0 \\ 0 & \lambda^* \end{bmatrix} \begin{bmatrix} q(t) \\ q^*(t) \end{bmatrix} + \begin{bmatrix} \phi & \phi^* \\ \phi\lambda & \phi^*\lambda^* \end{bmatrix}^T \begin{bmatrix} M^{-1}f(t) \\ 0 \end{bmatrix} \tag{4.2.14}$$

or

$$\dot{q}(t) - \lambda q(t) = \phi M^{-1} f(t) \tag{4.2.15}$$

$$\dot{q}^*(t) - \lambda^* q^*(t) = \phi^* M^{-1} f(t) \tag{4.2.16}$$

In general, the solution of Equation (4.2.15) with the zero initial conditions for $q(t)$ can be expressed in the more general form as [Soong and Grigoriu, 1993]:

$$q(t) = \int_{-\infty}^{t} H(t-\tau)\phi^T M^{-1} f(\tau) d\tau = \int_{0}^{\infty} H(s) G f(t-s) ds \tag{4.2.17}$$

in which $G = \phi^T M^{-1}$, $H(t) = \begin{bmatrix} e^{\lambda_1 t} & 0 & \cdots & 0 \\ 0 & e^{\lambda_2 t} & \cdots & 0 \\ \vdots & \vdots & \ddots & \vdots \\ 0 & 0 & \cdots & e^{\lambda_n t} \end{bmatrix}$ and $H(t) \equiv 0$ for $t < 0$, and transformation of variables $s = t - \tau$. The first derivative of $q(t)$ with respect to t are obtained as follows:

$$\begin{aligned} \dot{q}(t) &= \int_{-\infty}^{t} \dot{H}(t-\tau) G f(\tau) d\tau + H(0) G f(t) \\ &= \int_{0}^{\infty} \dot{H}(s) G f(t-s) ds + G f(t) \\ &= \int_{0}^{\infty} \dot{H}^a(s) G f(t-s) ds \end{aligned} \tag{4.2.18}$$

in which

$$\dot{H}^a(t) = \begin{bmatrix} \lambda_1 e^{\lambda_1 t} + \delta(t) & 0 & \cdots & 0 \\ 0 & \lambda_2 e^{\lambda_2 t} + \delta(t) & \cdots & 0 \\ \vdots & \vdots & \ddots & \vdots \\ 0 & 0 & \cdots & \lambda_n e^{\lambda_n t} + \delta(t) \end{bmatrix} \tag{4.2.19}$$

, and $\delta(t)$ is the Dirac delta function.

The correlation matrices of the displacement, velocity, and acceleration for Equations (4.2.11-13) are subsequently defined by Equations (4.2.20-22).

$$R_{XX}(\tau) = E[X(t)X^{*T}(t+\tau)] = 2\,\mathrm{Re}\left\{\phi R_{qq}(\tau)\phi^T + \phi^* R_{q^*q}(\tau)\phi^T\right\} \tag{4.2.20}$$

$$R_{X\dot{X}}(\tau) = 2\,\mathrm{Re}\left\{\phi\lambda R_{qq}(\tau)\lambda^T\phi^T + \phi^*\lambda^* R_{q^*q}(\tau)\lambda^T\phi^T\right\} \tag{4.2.21}$$

$$R_{\dot{X}\ddot{X}}(\tau) = 2\,\mathrm{Re}\left\{\phi\lambda R_{\dot{q}\dot{q}}(\tau)\lambda^T\phi^T + \phi^*\lambda^* R_{\dot{q}^*\dot{q}}(\tau)\lambda^T\phi^T\right\} \tag{4.2.22}$$

in which

$$R_{qq}(\tau) = \int_0^\infty \int_0^\infty H(s_1) G R_{ff}(\tau + s_1 - s_2) G^T H^T(s_2) ds_1 ds_2 \tag{4.2.23}$$

$$R_{q^* q}(\tau) = \int_0^\infty \int_0^\infty H^*(s_1) G^* R_{ff}(\tau + s_1 - s_2) G^T H^T(s_2) ds_1 ds_2 \tag{4.2.24}$$

$$\begin{aligned} R_{\dot{q}\dot{q}}(\tau) = & \int_0^\infty \int_0^\infty \dot{H}(s_1) G R_{ff}(\tau + s_1 - s_2) G^T \dot{H}^T(s_2) ds_1 ds_2 \\ & + \int_0^\infty \dot{H}(s_1) G R_{ff}(\tau + s_1) G^T ds_1 + \int_0^\infty G R_{ff}(\tau - s_2) G^T \dot{H}^T(s_2) ds_2 \\ & + G R_{ff}(\tau) G^T \end{aligned} \tag{4.2.25}$$

$$\begin{aligned} R_{\dot{q}^* \dot{q}}(\tau) = & \int_0^\infty \int_0^\infty \dot{H}^*(s_1) G^* R_{ff}(\tau + s_1 - s_2) G^T \dot{H}^T(s_2) ds_1 ds_2 \\ & + \int_0^\infty \dot{H}^*(s_1) G^* R_{ff}(\tau + s_1) G^T ds_1 + \int_0^\infty G^* R_{ff}(\tau - s_2) G^T \dot{H}^T(s_2) ds_2 \\ & + G^* R_{ff}(\tau) G^T \end{aligned} \tag{4.2.26}$$

on condition that the input force vector $f(t)$ is stationary.

4.3 Free Vibration Responses of a Linear MDOF Dynamic System

The initial values of the modal coordinates $Q(t)$ is basically required to solve Equation (4.2.7) with $\widetilde{F} = 0$ for the free vibration responses, unless only the steady state responses are of interest. However, the initial displacement and velocity vectors, $X(0)$ and $\dot{X}(0)$, are usually specified for the dynamic system. In order to determine the initial values of the modal coordinates $Q(0)$, the definition of Equation (4.2.4) is used to establish the following expression [Ginsberg, 2001]:

$$z(0) = \begin{bmatrix} X(0) \\ \dot{X}(0) \end{bmatrix} = \Phi Q(0) = 2\,\mathrm{Re}\{\Phi_1 q_0\} \tag{4.3.1}$$

in which $\Phi_1 = \begin{bmatrix} \phi \\ \phi\lambda \end{bmatrix}$ and $q_0 = q(0)$. As a result, the initial values of the modal coordinates $Q(t)$ can be further obtained by pre-multiplying Equation (4.3.1) with the transpose of the modal matrix Φ^T as follows:

$$Q(0) = \begin{bmatrix} q_0 \\ q_0^* \end{bmatrix} = \Phi^T z(0) = \Phi^T \begin{bmatrix} X(0) \\ \dot{X}(0) \end{bmatrix} \tag{4.3.2}$$

or

$$q_0 = \phi X(0) + \phi\lambda \dot{X}(0) \tag{4.3.3}$$

$$q_0^* = \phi^* X(0) + \phi^* \lambda^* \dot{X}(0) \tag{4.3.4}$$

Therefore, the free vibration responses of the modal coordinates for Equation (4.2.15) starting with the modal initial conditions q_0 are given as:

$$q(t) = H(t) q_0 \tag{4.3.5}$$

in which the modal initial conditions, q_0, are obtained by Equation (4.3.3). Subsequently, from Equations (4.2.11-13), it follows that the free vibration responses of the system are described as follows for the purpose of comparison.

$$X(t) = 2\,\mathrm{Re}\{\phi H(t) q_0\} \tag{4.3.6}$$

$$\dot{X}(t) = 2\,\mathrm{Re}\{\phi \dot{H}(t) q_0\} \tag{4.3.7}$$

$$\ddot{X}(t) = 2\,\mathrm{Re}\{\phi \ddot{H}(t) q_0\} \tag{4.3.8}$$

4.4 Relationship between RD Signatures and Free Vibration Responses for a 2DOF Dynamic System Loaded by White Noise Excitations

Without loss of generality, a 2DOF linear dynamical system is commonly employed to demonstrate the theoretical relationship between the auto and cross RD

signatures of the responses and the free vibration responses of the dynamic system. Two individual derivations of the theoretical relationship for the 2DOF dynamical system when separately subjected to the uncorrelated and correlated Gaussian white noise processes on each DOF of two masses, m_1 and m_2, are discussed in detail as follows.

4.4.1 Uncorrelated Input Forces

The theoretical derivation of the relationship between the RD signatures and the free vibration responses starts the consideration of two forcing functions, $f_1(t)$ and $f_2(t)$, which are uncorrelated Gaussian white noises with zero means and uniform spectral density functions of one. The correlation function matrix of such forcing functions is given in a form as follows:

$$R_{ff}(\tau) = \begin{bmatrix} \delta(\tau) & 0 \\ 0 & \delta(\tau) \end{bmatrix} \tag{4.4.1}$$

in which $\delta(\tau)$ is denoted as the Dirac delta function. Equation (4.4.1) is substituted into Equations (4.2.23-26) to result in the following expressions:

$$\begin{Bmatrix} R_{X_1X_1}(\tau) \\ R_{X_1X_2}(\tau) \end{Bmatrix} = 2\,\mathrm{Re}\left\{ e^{\lambda_1\tau} A_1^d [\phi]_1 + e^{\lambda_2\tau} A_2^d [\phi]_2 \right\} \tag{4.4.2}$$

$$\begin{Bmatrix} R_{X_1\dot{X}_1}(\tau) \\ R_{X_1\dot{X}_2}(\tau) \end{Bmatrix} = 2\,\mathrm{Re}\left\{ e^{\lambda_1\tau} A_1^v [\phi]_1 + e^{\lambda_2\tau} A_2^v [\phi]_2 \right\} \tag{4.4.3}$$

$$\begin{Bmatrix} R_{\dot{X}_1\ddot{X}_1}(\tau) \\ R_{\dot{X}_1\ddot{X}_2}(\tau) \end{Bmatrix} = 2\,\mathrm{Re}\left\{ e^{\lambda_1\tau} A_1^a [\phi]_1 + e^{\lambda_2\tau} A_2^a [\phi]_2 + \Delta_1\delta(\tau)[\phi]_1 + \Delta_2\delta(\tau)[\phi]_2 \right\} \tag{4.4.4}$$

in which

$$A_1^d = -\left[\frac{\phi_{11}}{2\lambda_1} a_1 + \frac{\phi_{12}}{\lambda_1 + \lambda_2} a_2 + \frac{\phi_{11}^*}{\lambda_1^* + \lambda_1} a_3 + \frac{\phi_{12}^*}{\lambda_1 + \lambda_2^*} a_4 \right] \tag{4.4.5}$$

$$A_2^d = -\left[\frac{\phi_{11}}{\lambda_1+\lambda_2}b_1 + \frac{\phi_{12}}{2\lambda_2}b_2 + \frac{\phi_{11}^*}{\lambda_1^*+\lambda_2}b_3 + \frac{\phi_{12}^*}{\lambda_2^*+\lambda_2}b_4\right] \tag{4.4.6}$$

$$A_1^v = -\left[\frac{\lambda_1^2\phi_{11}}{2\lambda_1}a_1 + \frac{\lambda_1\lambda_2\phi_{12}}{\lambda_1+\lambda_2}a_2 + \frac{\lambda_1\lambda_1^*\phi_{11}^*}{\lambda_1+\lambda_1^*}a_3 + \frac{\lambda_1\lambda_2^*\phi_{12}^*}{\lambda_1+\lambda_2^*}a_4\right] \tag{4.4.7}$$

$$A_2^v = -\left[\frac{\lambda_1\lambda_2\phi_{11}}{\lambda_1+\lambda_2}b_1 + \frac{\lambda_2^2\phi_{12}}{2\lambda_2}b_2 + \frac{\lambda_1^*\lambda_2\phi_{11}^*}{\lambda_1^*+\lambda_2}b_3 + \frac{\lambda_2^*\lambda_2\phi_{12}^*}{\lambda_2^*+\lambda_2}b_4\right] \tag{4.4.8}$$

$$A_1^a = -\lambda_1^2 A_1^v, \quad A_2^a = -\lambda_2^2 A_2^v \tag{4.4.9}$$

$$\begin{aligned} a_1 &= \frac{\phi_{11}^2}{m_1^2} + \frac{\phi_{21}^2}{m_2^2}, \quad a_2 = \frac{\phi_{12}\phi_{11}}{m_1^2} + \frac{\phi_{22}\phi_{21}}{m_2^2}, \\ a_3 &= \frac{\phi_{11}^*\phi_{11}}{m_1^2} + \frac{\phi_{21}^*\phi_{21}}{m_2^2}, \quad a_4 = \frac{\phi_{12}^*\phi_{11}}{m_1^2} + \frac{\phi_{22}^*\phi_{21}}{m_2^2} \end{aligned} \tag{4.4.10}$$

$$\begin{aligned} b_1 &= \frac{\phi_{12}\phi_{11}}{m_1^2} + \frac{\phi_{22}\phi_{21}}{m_2^2}, \quad b_2 = \frac{\phi_{12}^2}{m_1^2} + \frac{\phi_{22}^2}{m_2^2}, \\ b_3 &= \frac{\phi_{11}^*\phi_{12}}{m_1^2} + \frac{\phi_{21}^*\phi_{22}}{m_2^2}, \quad b_4 = \frac{\phi_{12}^*\phi_{12}}{m_1^2} + \frac{\phi_{22}^*\phi_{22}}{m_2^2} \end{aligned} \tag{4.4.11}$$

$$\Delta_1 = \phi_{11}\lambda_1^2 a_1 + \phi_{12}\lambda_1\lambda_2 a_2 + \phi_{11}^*\lambda_1^*\lambda_1 a_3 + \phi_{12}^*\lambda_1\lambda_2^* a_4 \tag{4.4.12}$$

$$\Delta_2 = \phi_{11}\lambda_1\lambda_2 b_1 + \phi_{12}\lambda_2^2 b_2 + \phi_{11}^*\lambda_1^*\lambda_2 b_3 + \phi_{12}^*\lambda_2\lambda_2^* b_4 \tag{4.4.13}$$

$$[\phi]_1 = \begin{bmatrix}\phi_{11}\\ \phi_{21}\end{bmatrix}, \quad [\phi]_2 = \begin{bmatrix}\phi_{12}\\ \phi_{22}\end{bmatrix} \tag{4.4.14}$$

On the basis of Equations (3.4.20) and (3.4.21), the auto and cross RD signatures for the level-crossing triggering condition that is usually used in a practical data process are defined as:

$$\delta_{X_1X_1}(\tau) = E[X_1(\tau)|X_1(0) = x_0] = \frac{R_{X_1X_1}(\tau)}{R_{X_1X_1}(0)}x_0 \tag{4.4.15}$$

$$\delta_{X_2X_1}(\tau) = E[X_2(\tau)|X_1(0) = x_0] = \frac{R_{X_1X_2}(\tau)}{R_{X_1X_1}(0)}x_0 \tag{4.4.16}$$

in which X_1 is selected to be a leading response. Consequently, the following auto and cross RD signatures of the responses can be established, after Equations (4.4.2-4) are substituted into the preceding Equations (4.4.15) and (4.4.16). This result is similar to the derivation of Huang et al. [1998].

$$\begin{Bmatrix} \delta_{X_1X_1}(\tau) \\ \delta_{X_2X_1}(\tau) \end{Bmatrix} = \frac{2\,\mathrm{Re}\left\{ e^{\lambda_1\tau} A_1^d [\phi]_1 + e^{\lambda_2\tau} A_2^d [\phi]_2 \right\}}{2\,\mathrm{Re}\left\{ A_1^d \phi_{11} + A_2^d \phi_{12} \right\}} x_0 \tag{4.4.17}$$

$$\begin{Bmatrix} \delta_{\dot{X}_1X_1}(\tau) \\ \delta_{\dot{X}_2X_1}(\tau) \end{Bmatrix} = \frac{2\,\mathrm{Re}\left\{ e^{\lambda_1\tau} A_1^v [\phi]_1 + e^{\lambda_2\tau} A_2^v [\phi]_2 \right\}}{2\,\mathrm{Re}\left\{ A_1^v \phi_{11} + A_2^v \phi_{12} \right\}} \dot{x}_0 \tag{4.4.18}$$

$$\begin{Bmatrix} \delta_{\ddot{X}_1X_1}(\tau) \\ \delta_{\ddot{X}_2X_1}(\tau) \end{Bmatrix} = \frac{2\,\mathrm{Re}\left\{ \left[e^{\lambda_1\tau} A_1^a + \Delta_1\delta(\tau) \right][\phi]_1 + \left[e^{\lambda_2\tau} A_2^a + \Delta_2\delta(\tau) \right][\phi]_2 \right\}}{2\,\mathrm{Re}\left\{ \left[A_1^a + \Delta_1\delta(0) \right]\phi_{11} + \left[A_2^a + \Delta_2\delta(0) \right]\phi_{12} \right\}} \ddot{x}_0 \tag{4.4.19}$$

The comparison of the auto and cross RD signatures with the corresponding free vibration responses in Equations (4.3.6) and (4.3.7) indicates that the free vibration displacement and velocity responses are identical to the RD displacement and velocity signatures, respectively, when the corresponding modal initial conditions are given in Equations (4.4.20) and (4.4.21) [Huang, 1998].

$$q_0 = \frac{x_0}{2\,\mathrm{Re}\left\{ A_1^d \phi_{11} + A_2^d \phi_{12} \right\}} \begin{Bmatrix} A_1^d \\ A_2^d \end{Bmatrix} \tag{4.4.20}$$

$$\lambda q_0 = \frac{\dot{x}_0}{2\,\mathrm{Re}\left\{ A_1^v \phi_{11} + A_2^v \phi_{12} \right\}} \begin{Bmatrix} A_1^v \\ A_2^v \end{Bmatrix} \tag{4.4.21}$$

However, it is apparent that the RD acceleration signatures are not equivalent to the corresponding free vibration responses, because of the existence of the Dirac delta function [Huang and Yeh, 1999]. If the RD acceleration signatures with $\tau > 0$ are taken into account, the second summation terms in the numerator of Equation (4.4.19) become

zero, according to the properties of the Dirac delta function. It turns out that the equivalent relationship between the RD signatures and the free vibration responses for the acceleration responses is also valid [Huang, 2001]. Hence, the modal initial conditions for the identity between the free vibration responses of Equation (4.3.8) and the RD acceleration signatures of Equation (4.4.19) further proposed in the present study can be formulated by the following formulation with a requirement of $\tau > 0$,

$$\lambda^2 q_0 = \frac{\ddot{x}_0}{2\,\mathrm{Re}\left\{\left[A_1^a + \Delta_1\delta(0)\right]\phi_{11} + \left[A_2^a + \Delta_2\delta(0)\right]\phi_{12}\right\}} \begin{Bmatrix} A_1^a \\ A_2^a \end{Bmatrix} \tag{4.4.22}$$

The advantage to use Equation (4.4.22) is that the given initial accelerations $\ddot{x}_0$ yield the initial conditions $z(0)$ in Equation (4.3.1) through the modal initial conditions q_0. This treatment can facilitate the calculation of the analytical free vibration acceleration responses of the dynamic system in a numerical simulation.

4.4.2 Correlated Input Forces

It is interesting to realize whether the RD signatures from the corresponding responses of the linear 2DOF system subjected to the correlated forcing functions are able to appropriately represent the free vibration responses of the 2DOF system. For the sake of simplification, the correlated forcing functions are assumed to be the Gaussian white noise processes with the zero means and the condition of the time shift, τ_d , which can be expressed as $f(t)$ and $\gamma f(t - \tau_d)$. The correlation matrix of such two forcing functions can be given as:

$$R_{ff}(\tau) = \begin{bmatrix} \delta(\tau) & \gamma\delta(\tau - \tau_d) \\ \gamma\delta(\tau + \tau_d) & \gamma^2\delta(\tau) \end{bmatrix} \qquad \text{when } \tau \geq \tau_d \tag{4.4.23}$$

and

$$R_{ff}(\tau)=\begin{bmatrix}\delta(\tau) & \gamma\delta(-(\tau-\tau_d))\\ \gamma\delta(\tau+\tau_d) & \gamma^2\delta(\tau)\end{bmatrix} \qquad \text{when } \tau\le\tau_d \qquad (4.4.24)$$

Similarly, the individual substitution of Equations (4.4.23) and (4.4.24) into Equations (4.2.23-26) yields the subsequent results of the correlation functions.

When $\tau\ge\tau_d$

$$\begin{Bmatrix}R_{X_1X_1}(\tau)\\ R_{X_1X_2}(\tau)\end{Bmatrix}=2\,\mathrm{Re}\left\{e^{\lambda_1\tau}\hat{A}_1^d[\phi]_1+e^{\lambda_2\tau}\hat{A}_2^d[\phi]_2\right\} \qquad (4.4.25)$$

$$\begin{Bmatrix}R_{\dot{X}_1\dot{X}_1}(\tau)\\ R_{\dot{X}_1\dot{X}_2}(\tau)\end{Bmatrix}=2\,\mathrm{Re}\left\{e^{\lambda_1\tau}\hat{A}_1^v[\phi]_1+e^{\lambda_2\tau}\hat{A}_2^v[\phi]_2\right\} \qquad (4.4.26)$$

$$\begin{Bmatrix}R_{\ddot{X}_1\ddot{X}_1}(\tau)\\ R_{\ddot{X}_1\ddot{X}_2}(\tau)\end{Bmatrix}=2\,\mathrm{Re}\left\{e^{\lambda_1\tau}\hat{A}_1^a[\phi]_1+e^{\lambda_2\tau}\hat{A}_2^a[\phi]_2+\tilde{\Delta}_{12}\delta(\tau-\tau_d)[\phi]_1+\tilde{\Delta}_{21}\delta(\tau-\tau_d)[\phi]_2\right\} \qquad (4.4.27)$$

in which

$$\hat{A}_1^d=-\left[\frac{\phi_{11}}{2\lambda_1}\hat{a}_1+\frac{\phi_{12}}{\lambda_1+\lambda_2}\hat{a}_2+\frac{\phi_{11}^*}{\lambda_1^*+\lambda_1}\hat{a}_3+\frac{\phi_{12}^*}{\lambda_1+\lambda_2^*}\hat{a}_4\right] \qquad (4.4.28)$$

$$\hat{A}_2^d=-\left[\frac{\phi_{11}}{\lambda_1+\lambda_2}\hat{b}_1+\frac{\phi_{12}}{2\lambda_2}\hat{b}_2+\frac{\phi_{11}^*}{\lambda_1^*+\lambda_2}\hat{b}_3+\frac{\phi_{12}^*}{\lambda_2^*+\lambda_2}\hat{b}_4\right] \qquad (4.4.29)$$

$$\hat{A}_1^v=-\left[\frac{\lambda_1^2\phi_{11}}{2\lambda_1}\hat{a}_1+\frac{\lambda_1\lambda_2\phi_{12}}{\lambda_1+\lambda_2}\hat{a}_2+\frac{\lambda_1\lambda_1^*\phi_{11}^*}{\lambda_1+\lambda_1^*}\hat{a}_3+\frac{\lambda_1\lambda_2^*\phi_{12}^*}{\lambda_1+\lambda_2^*}\hat{a}_4\right] \qquad (4.4.30)$$

$$\hat{A}_2^v=-\left[\frac{\lambda_1\lambda_2\phi_{11}}{\lambda_1+\lambda_2}\hat{b}_1+\frac{\lambda_2^2\phi_{12}}{2\lambda_2}\hat{b}_2+\frac{\lambda_1^*\lambda_2\phi_{11}^*}{\lambda_1^*+\lambda_2}\hat{b}_3+\frac{\lambda_2\lambda_2^*\phi_{12}^*}{\lambda_2+\lambda_2^*}\hat{b}_4\right] \qquad (4.4.31)$$

$$\hat{A}_1^a=-\lambda_1^2\hat{A}_1^v,\quad \hat{A}_2^a=-\lambda_2^2\hat{A}_2^v \qquad (4.4.32)$$

$$\hat{a}_1 = \frac{\phi_{11}^2}{m_1^2} + \frac{\gamma\phi_{11}\phi_{21}}{m_1 m_2}(e^{\lambda_1\tau_d} + e^{-\lambda_1\tau_d}) + \frac{\gamma^2\phi_{21}^2}{m_2^2} \tag{4.4.33}$$

$$\hat{a}_2 = \frac{\phi_{11}\phi_{12}}{m_1^2} + \frac{\gamma e^{\lambda_1\tau_d}\phi_{11}\phi_{22}}{m_1 m_2} + \frac{\gamma e^{-\lambda_1\tau_d}\phi_{12}\phi_{21}}{m_1 m_2} + \frac{\gamma^2\phi_{21}\phi_{22}}{m_2^2} \tag{4.4.34}$$

$$\hat{a}_3 = \frac{\phi_{11}\phi_{11}^*}{m_1^2} + \frac{\gamma e^{\lambda_1\tau_d}\phi_{11}\phi_{21}^*}{m_1 m_2} + \frac{\gamma e^{-\lambda_1\tau_d}\phi_{21}\phi_{11}^*}{m_1 m_2} + \frac{\gamma^2\phi_{21}\phi_{21}^*}{m_2^2} \tag{4.4.35}$$

$$\hat{a}_4 = \frac{\phi_{11}\phi_{12}^*}{m_1^2} + \frac{\gamma e^{\lambda_1\tau_d}\phi_{11}\phi_{22}^*}{m_1 m_2} + \frac{\gamma e^{-\lambda_1\tau_d}\phi_{12}^*\phi_{21}}{m_1 m_2} + \frac{\gamma^2\phi_{21}\phi_{22}^*}{m_2^2} \tag{4.4.36}$$

$$\hat{b}_1 = \frac{\phi_{11}\phi_{12}}{m_1^2} + \frac{\gamma e^{\lambda_2\tau_d}\phi_{12}\phi_{21}}{m_1 m_2} + \frac{\gamma e^{-\lambda_2\tau_d}\phi_{11}\phi_{22}}{m_1 m_2} + \frac{\gamma^2\phi_{21}\phi_{22}}{m_2^2} \tag{4.4.37}$$

$$\hat{b}_2 = \frac{\phi_{12}^2}{m_1^2} + \frac{\gamma\phi_{12}\phi_{22}}{m_1 m_2}(e^{\lambda_2\tau_d} + e^{-\lambda_2\tau_d}) + \frac{\gamma^2\phi_{22}^2}{m_2^2} \tag{4.4.38}$$

$$\hat{b}_3 = \frac{\phi_{11}^*\phi_{12}}{m_1^2} + \frac{\gamma e^{\lambda_2\tau_d}\phi_{12}\phi_{21}^*}{m_1 m_2} + \frac{\gamma e^{-\lambda_2\tau_d}\phi_{11}^*\phi_{22}}{m_1 m_2} + \frac{\gamma^2\phi_{21}^*\phi_{22}}{m_2^2} \tag{4.4.39}$$

$$\hat{b}_4 = \frac{\phi_{12}\phi_{12}^*}{m_1^2} + \frac{\gamma e^{\lambda_2\tau_d}\phi_{12}\phi_{22}^*}{m_1 m_2} + \frac{\gamma e^{-\lambda_2\tau_d}\phi_{12}^*\phi_{22}}{m_1 m_2} + \frac{\gamma^2\phi_{22}\phi_{22}^*}{m_2^2} \tag{4.4.40}$$

$$\tilde{\Delta}_{12} = \frac{\gamma}{m_1 m_2}\left[\phi_{11}^2\phi_{12}\lambda_1^2 + \phi_{12}^2\phi_{21}\lambda_1\lambda_2 + \phi_{11}^{*\,2}\phi_{21}\lambda_1^*\lambda_1 + \phi_{12}^{*\,2}\phi_{21}\lambda_1\lambda_2^*\right] \tag{4.4.41}$$

$$\tilde{\Delta}_{21} = \frac{\gamma}{m_1 m_2}\left[\phi_{11}^2\phi_{22}\lambda_1\lambda_2 + \phi_{12}^2\phi_{22}\lambda_2^2 + \phi_{11}^{*\,2}\phi_{22}\lambda_1^*\lambda_2 + \phi_{12}^{*\,2}\phi_{22}\lambda_2\lambda_2^*\right] \tag{4.4.42}$$

When $\tau \le \tau_d$

$$\begin{Bmatrix} R_{X_1X_1}(\tau) \\ R_{X_1X_2}(\tau) \end{Bmatrix} = 2\,\mathrm{Re}\Big\{e^{\lambda_1\tau}\tilde{A}_1^d[\phi]_1 + e^{\lambda_2\tau}\tilde{A}_2^d[\phi]_2 + \Big(\tilde{B}_1^d e^{-\lambda_1(\tau-\tau_d)} + \tilde{B}_2^d e^{-\lambda_2(\tau-\tau_d)} + \tilde{B}_3^d e^{-\lambda_1^*(\tau-\tau_d)} + \tilde{B}_4^d e^{-\lambda_2^*(\tau-\tau_d)}\Big)[\phi]_1 + \Big(\tilde{C}_1^d e^{-\lambda_1(\tau-\tau_d)} + \tilde{C}_2^d e^{-\lambda_2(\tau-\tau_d)} + \tilde{C}_3^d e^{-\lambda_1^*(\tau-\tau_d)} + \tilde{C}_4^d e^{-\lambda_2^*(\tau-\tau_d)}\Big)[\phi]_2\Big\} \tag{4.4.43}$$

$$\begin{Bmatrix} R_{\dot{X}_1\dot{X}_1}(\tau) \\ R_{\dot{X}_1\dot{X}_2}(\tau) \end{Bmatrix} = 2\,\mathrm{Re}\Big\{ e^{\lambda_1\tau}\widetilde{A}_1^v[\phi]_1 + e^{\lambda_2\tau}\widetilde{A}_2^v[\phi]_2 + \Big(\widetilde{B}_1^v e^{-\lambda_1(\tau-\tau_d)} + \widetilde{B}_2^v e^{-\lambda_2(\tau-\tau_d)} + \widetilde{B}_3^v e^{-\lambda_1^*(\tau-\tau_d)} + \widetilde{B}_4^v e^{-\lambda_2^*(\tau-\tau_d)}\Big)[\phi]_1 + \Big(\widetilde{C}_1^v e^{-\lambda_1(\tau-\tau_d)} + \widetilde{C}_2^v e^{-\lambda_2(\tau-\tau_d)} + \widetilde{C}_3^v e^{-\lambda_1^*(\tau-\tau_d)} + \widetilde{C}_4^v e^{-\lambda_2^*(\tau-\tau_d)}\Big)[\phi]_2 \Big\} \tag{4.4.44}$$

$$\begin{Bmatrix} R_{\ddot{X}_1\dot{X}_1}(\tau) \\ R_{\ddot{X}_1\dot{X}_2}(\tau) \end{Bmatrix} = 2\,\mathrm{Re}\Big\{ e^{\lambda_1\tau}\widetilde{A}_1^a[\phi]_1 + e^{\lambda_2\tau}\widetilde{A}_2^a[\phi]_2 + \Big(\widetilde{B}_1^a e^{-\lambda_1(\tau-\tau_d)} + \widetilde{B}_2^a e^{-\lambda_2(\tau-\tau_d)} + \widetilde{B}_3^a e^{-\lambda_1^*(\tau-\tau_d)} + \widetilde{B}_4^a e^{-\lambda_2^*(\tau-\tau_d)}\Big)[\phi]_1 + \Big(\widetilde{C}_1^a e^{-\lambda_1(\tau-\tau_d)} + \widetilde{C}_2^a e^{-\lambda_2(\tau-\tau_d)} + \widetilde{C}_3^a e^{-\lambda_1^*(\tau-\tau_d)} + \widetilde{C}_4^a e^{-\lambda_2^*(\tau-\tau_d)}\Big)[\phi]_2 + \Big(\widetilde{\Delta}_{11}\delta(\tau) + \widetilde{\Delta}_{12}\delta(-\tau+\tau_d)\Big)[\phi]_1 + \Big(\widetilde{\Delta}_{22}\delta(\tau) + \widetilde{\Delta}_{21}\delta(-\tau+\tau_d)\Big)[\phi]_2 \Big\} \tag{4.4.45}$$

in which

$$\widetilde{A}_1^d = -\left[\frac{\phi_{11}}{2\lambda_1}\widetilde{a}_1 + \frac{\phi_{12}}{\lambda_1+\lambda_2}\widetilde{a}_2 + \frac{\phi_{11}^*}{\lambda_1^*+\lambda_1}\widetilde{a}_3 + \frac{\phi_{12}^*}{\lambda_1+\lambda_2^*}\widetilde{a}_4\right] \tag{4.4.46}$$

$$\widetilde{A}_2^d = -\left[\frac{\phi_{11}}{\lambda_1+\lambda_2}\widetilde{b}_1 + \frac{\phi_{12}}{2\lambda_2}\widetilde{b}_2 + \frac{\phi_{11}^*}{\lambda_1^*+\lambda_2}\widetilde{b}_3 + \frac{\phi_{12}^*}{\lambda_2^*+\lambda_2}\widetilde{b}_4\right] \tag{4.4.47}$$

$$\widetilde{A}_1^v = -\left[\frac{\lambda_1^2\phi_{11}}{2\lambda_1}\widetilde{a}_1 + \frac{\lambda_1\lambda_2\phi_{12}}{\lambda_1+\lambda_2}\widetilde{a}_2 + \frac{\lambda_1\lambda_1^*\phi_{11}^*}{\lambda_1+\lambda_1^*}\widetilde{a}_3 + \frac{\lambda_1\lambda_2^*\phi_{12}^*}{\lambda_1+\lambda_2^*}\widetilde{a}_4\right] \tag{4.4.48}$$

$$\widetilde{A}_2^v = -\left[\frac{\lambda_1\lambda_2\phi_{11}}{\lambda_1+\lambda_2}\widetilde{b}_1 + \frac{\lambda_2^2\phi_{12}}{2\lambda_2}\widetilde{b}_2 + \frac{\lambda_1^*\lambda_2\phi_{11}^*}{\lambda_1^*+\lambda_2}\widetilde{b}_3 + \frac{\lambda_2\lambda_2^*\phi_{12}^*}{\lambda_2+\lambda_2^*}\widetilde{b}_4\right] \tag{4.4.49}$$

$$\widetilde{A}_1^a = -\lambda_1^2\widetilde{A}_1^v, \quad \widetilde{A}_2^a = -\lambda_2^2\widetilde{A}_2^v \tag{4.4.50}$$

$$\begin{aligned} \widetilde{B}_1^d &= -\frac{\gamma\phi_{11}^2\phi_{21}}{2\lambda_1 m_1 m_2}, \quad \widetilde{B}_2^d = -\frac{\gamma\phi_{12}^2\phi_{21}}{(\lambda_1+\lambda_2)m_1 m_2}, \\ \widetilde{B}_3^d &= -\frac{\gamma\phi_{11}^{*\,2}\phi_{21}}{(\lambda_1+\lambda_1^*)m_1 m_2}, \quad \widetilde{B}_4^d = -\frac{\gamma\phi_{12}^{*\,2}\phi_{21}}{(\lambda_1+\lambda_2^*)m_1 m_2} \end{aligned} \tag{4.4.51}$$

$$\tilde{C}_1^d = -\frac{\gamma\phi_{11}^2\phi_{22}}{(\lambda_1+\lambda_2)m_1m_2},\quad \tilde{C}_2^d = -\frac{\gamma\phi_{12}^2\phi_{22}}{2\lambda_2 m_1m_2},$$
$$\tilde{C}_3^d = -\frac{\gamma\phi_{11}^{*\,2}\phi_{22}}{(\lambda_1^*+\lambda_2)m_1m_2},\quad \tilde{C}_4^d = -\frac{\gamma\phi_{12}^{*\,2}\phi_{22}}{(\lambda_2+\lambda_2^*)m_1m_2} \tag{4.4.52}$$

$$\tilde{B}_1^v = \lambda_1^2\tilde{B}_1^d,\ \tilde{B}_2^v = \lambda_1\lambda_2\tilde{B}_2^d,\ \tilde{B}_3^v = \lambda_1\lambda_1^*\tilde{B}_3^d,\ \tilde{B}_4^v = \lambda_1\lambda_2^*\tilde{B}_4^d \tag{4.4.53}$$

$$\tilde{C}_1^v = \lambda_1\lambda_2\tilde{C}_1^d,\ \tilde{C}_2^v = \lambda_2^2\tilde{C}_2^d,\ \tilde{C}_3^v = \lambda_1^*\lambda_2\tilde{C}_3^d,\ \tilde{C}_4^v = \lambda_2\lambda_2^*\tilde{C}_4^d \tag{4.4.54}$$

$$\tilde{B}_1^a = -\lambda_1^2\tilde{B}_1^v,\ \tilde{B}_2^a = -\lambda_2^2\tilde{B}_2^v,\ \tilde{B}_3^a = -\lambda_1^{*2}\tilde{B}_3^v,\ \tilde{B}_4^a = -\lambda_2^{*2}\tilde{B}_4^v \tag{4.4.55}$$

$$\tilde{C}_1^a = -\lambda_1^2\tilde{C}_1^v,\ \tilde{C}_2^a = -\lambda_2^2\tilde{C}_2^v,\ \tilde{C}_3^a = -\lambda_1^{*2}\tilde{C}_3^v,\ \tilde{C}_4^a = -\lambda_2^{*2}\tilde{C}_4^v \tag{4.4.56}$$

$$\tilde{a}_1 = \frac{\phi_{11}^2}{m_1^2} + \frac{\gamma e^{\lambda_1\tau_d}\phi_{11}\phi_{21}}{m_1m_2} + \frac{\gamma^2\phi_{21}^2}{m_2^2} \tag{4.4.57}$$

$$\tilde{a}_2 = \frac{\phi_{11}\phi_{12}}{m_1^2} + \frac{\gamma e^{\lambda_1\tau_d}\phi_{11}\phi_{22}}{m_1m_2} + \frac{\gamma^2\phi_{21}\phi_{22}}{m_2^2} \tag{4.4.58}$$

$$\tilde{a}_3 = \frac{\phi_{11}\phi_{11}^*}{m_1^2} + \frac{\gamma e^{\lambda_1\tau_d}\phi_{11}\phi_{21}^*}{m_1m_2} + \frac{\gamma^2\phi_{21}\phi_{21}^*}{m_2^2} \tag{4.4.59}$$

$$\tilde{a}_4 = \frac{\phi_{11}\phi_{12}^*}{m_1^2} + \frac{\gamma e^{\lambda_1\tau_d}\phi_{11}\phi_{22}^*}{m_1m_2} + \frac{\gamma^2\phi_{21}\phi_{22}^*}{m_2^2} \tag{4.4.60}$$

$$\tilde{b}_1 = \frac{\phi_{11}\phi_{12}}{m_1^2} + \frac{\gamma e^{\lambda_2\tau_d}\phi_{12}\phi_{21}}{m_1m_2} + \frac{\gamma^2\phi_{21}\phi_{22}}{m_2^2} \tag{4.4.61}$$

$$\tilde{b}_2 = \frac{\phi_{12}^2}{m_1^2} + \frac{\gamma e^{\lambda_2\tau_d}\phi_{12}\phi_{22}}{m_1m_2} + \frac{\gamma^2\phi_{22}^2}{m_2^2} \tag{4.4.62}$$

$$\tilde{b}_3 = \frac{\phi_{11}^*\phi_{12}}{m_1^2} + \frac{\gamma e^{\lambda_2\tau_d}\phi_{12}\phi_{21}^*}{m_1m_2} + \frac{\gamma^2\phi_{21}^*\phi_{22}}{m_2^2} \tag{4.4.63}$$

$$\tilde{b}_4 = \frac{\phi_{12}\phi_{12}^*}{m_1^2} + \frac{\gamma e^{\lambda_2\tau_d}\phi_{12}\phi_{22}^*}{m_1m_2} + \frac{\gamma^2\phi_{22}\phi_{22}^*}{m_2^2} \tag{4.4.64}$$

$$\tilde{\Delta}_{11} = \lambda_1^2\left(\frac{\phi_{11}^3}{m_1^2}+\frac{\gamma^2\phi_{11}\phi_{21}^2}{m_2^2}\right)+\lambda_1\lambda_2\phi_{12}\left(\frac{\phi_{11}\phi_{12}}{m_1^2}+\frac{\gamma^2\phi_{21}\phi_{22}}{m_2^2}\right)$$
$$+\lambda_1\lambda_1^*\phi_{11}^*\left(\frac{\phi_{11}\phi_{11}^*}{m_1^2}+\frac{\gamma^2\phi_{21}\phi_{21}^*}{m_2^2}\right)+\lambda_1\lambda_2^*\phi_{12}^*\left(\frac{\phi_{11}\phi_{12}^*}{m_1^2}+\frac{\gamma^2\phi_{21}\phi_{22}^*}{m_2^2}\right) \quad (4.4.65)$$

$$\tilde{\Delta}_{22} = \lambda_1\lambda_2\phi_{11}\left(\frac{\phi_{11}\phi_{12}}{m_1^2}+\frac{\gamma^2\phi_{21}\phi_{22}}{m_2^2}\right)+\lambda_2^2\phi_{12}\left(\frac{\phi_{12}^2}{m_1^2}+\frac{\gamma^2\phi_{22}^2}{m_2^2}\right)$$
$$+\lambda_1^*\lambda_2\phi_{11}^*\left(\frac{\phi_{11}^*\phi_{12}}{m_1^2}+\frac{\gamma^2\phi_{21}^*\phi_{22}}{m_2^2}\right)+\lambda_2\lambda_2^*\phi_{12}^*\left(\frac{\phi_{12}\phi_{12}^*}{m_1^2}+\frac{\gamma^2\phi_{22}\phi_{22}^*}{m_2^2}\right) \quad (4.4.66)$$

The substitution of Equations (4.4.25-27) and (4.4.43-45) into Equations (4.4.15) and (4.4.16) can further lead to the auto and cross RD signatures of the responses. In comparison with the corresponding free vibration responses as described in Equations (4.3.6-8), Huang and Yeh [1999] indicated that when $\tau \leq \tau_d$, the RD signatures are not equivalent to the corresponding free vibration responses, since the terms of $e^{-\lambda(\tau-\tau_d)}$ are particularly present in Equations (4.4.43-45). However, Huang and Yeh neglected the inherent truth in the preceding derivation procedure that the format of the exponential term, -(τ-τ_d), is intended to maintain positive in the range of $\tau \leq \tau_d$ because the timing of the forcing functions are assumed to start at $\tau = 0$. It means that one point in the range of $\tau \leq \tau_d$ basically gives the same results as the corresponding one in the range of $\tau \geq \tau_d$ in a calculation procedure when comparing Equations (4.4.25-27) to Equations (4.4.43-45). Basically, the equivalence between the RD signatures and the free vibration responses for the case of the correlated white noise processes is valid.

From the other point of view to support such equivalence, because each of the forcing functions still maintains the properties of the white noise process no matter how correlated they are between each other provides a simple reason. As a consequence of the reason, the requirement of the equivalence between the RD signatures and the free

vibration responses is still fulfilled. This also leads to the following outcome that there exists a set of the initial conditions starting at $t = 0$ in order to make the analytical free vibration responses equivalent to the overall RD displacement or velocity signatures. It is especially noted in Equations (4.4.27) and (4.4.45) that the RD acceleration signatures consist of the Dirac delta functions giving rise to the singularity at $\tau = 0$ and $\tau = \tau_d$. Similar to the case of the uncorrelated white noise excitations, the equivalence between the RD acceleration signatures and the free vibration responses may be acceptable on condition that such a singularity at these two points is neglected.

4.5 Numerical Simulations of a 2DOF Dynamic System

The demonstration of numerical simulations is devoted to enhancing the better understanding of the theoretical foundation in the RD technique. In this respect, a 2DOF linear dynamical system with non-proportional damping as follows plays a pivotal role in the following numerical simulations.

$$\begin{bmatrix} 1 & 0 \\ 0 & 1 \end{bmatrix} \begin{Bmatrix} \ddot{X}_1 \\ \ddot{X}_2 \end{Bmatrix} + \begin{bmatrix} 0.04 & 0.01 \\ 0.01 & 0.03 \end{bmatrix} \begin{Bmatrix} \dot{X}_1 \\ \dot{X}_2 \end{Bmatrix} + \begin{bmatrix} 2 & -1 \\ -1 & 1 \end{bmatrix} \begin{Bmatrix} X_1 \\ X_2 \end{Bmatrix} = \begin{Bmatrix} f_1(t) \\ f_2(t) \end{Bmatrix} \tag{4.5.1}$$

Such a 2DOF system contains the natural frequencies of 0.2575 Hz and 0.0984 Hz and the damping ratios of 0.87 % and 3.37 %.

The forcing functions $f_1(t)$ and $f_2(t)$ applied on the 2DOF system were two various forms of force simulations, including Gaussian white noise excitations and practical wind forces. For the Gaussian white noise excitations, two independent sets of the excitations with zero mean and one variance were simulated for the two forcing functions. Each forcing function generated the total number of 400000 points at a time interval of 0.02 second. For the wind forces, the simulation procedure developed in Chapter 2 was used

to generate the fluctuating alongwind and crosswind forces. The time interval was set as 0.2 second to generate the total number of 40000 points for both simulations of the fluctuating wind forces.

The procedure of the wind force simulation was established on a multivariate autoregressive moving average model in accordance with a target spectral density matrix in which the temporal and spatial correlations of the wind forces were taken into consideration. The simulation of the fluctuating alongwind forces emphasized the property of a time delay in the spatial correlation between the two simulated forces as illustrated in Figure 2.3.4. On the other hand, the simulation of the fluctuating crosswind forces only concentrated on the spatial correlation without a time delay between two simulated forces as illustrated in Figure 2.3.5.

When the simulated forcing functions were applied on the 2DOF dynamic system, the dynamic responses of displacement, velocity, and acceleration were numerically analyzed by the Newmark-β method with the assumption of linear acceleration [Cheng, 2001]. The resulting responses for the total time length of 8000 seconds were provided to give rise to the estimated auto and cross RD signatures of the responses by means of the RD technique. Such RD signatures were constructed by the traditional level crossing triggering condition in which one standard deviation of a leading response at the 1DOF of X_1 was selected as a triggering level for each superimposed segment. Each selected segment demanded a time length for ten times the minimum of the natural periods of the dynamic system.

In fact, the auto and cross RD signatures of the dynamic responses and the input forcing functions are simultaneously extracted in each numerical simulation. The main

purpose to do so is attempted to enhance the procedure developed in Chapter 3 to determine the initial conditions of the analytical free vibration responses of a MDOF dynamic system in a straightforward and feasible way. The procedure selects the starting points at $t = 0$ from the synchronically formed RD displacement and velocity signatures as the initial conditions, when one kind of the dynamic responses is specified to give the pivotal RD signatures. The basic principle of the procedure is based primarily on the equivalent relations between the RD signatures and the corresponding free vibration responses, if the external excitations are given as white noises. Therefore, the selected initial conditions can comprehend the free vibration characteristics of the dynamic system without involving any external disturbance, so that the analytical free vibration responses are implemented to compare the pivotal RD signatures.

With such a solid theoretical foundation, Table 4.5.1 displays the selected initial conditions from the starting points of the associated RD displacement and velocity signatures, when the dynamic system is subjected to the white noise excitations. The parenthesized values in Table 4.5.1 represent the theoretical initial conditions calculated from Equations (4.3.1) and (4.4.20-22). The compared results reveal that the selected initial conditions are basically fulfilled with the theoretical initial conditions. The slight discrepancy of the selected initial conditions from the theoretical initial conditions is noticed when the acceleration response at the 1DOF is the leading response. However, such a discrepancy may not cause the analytical free vibration acceleration responses much deviated from the formed RD acceleration signatures in a numerical analysis. It can be shown in Figure 4.5.4 that the first point in the RD acceleration residuals defined by the difference of the RD acceleration signature and the corresponding free vibration

response has the same value as the RD force signatures. It means that the theoretical initial accelerations are identical to the initial acceleration conditions identified from the corrected RD acceleration signatures after extracting the RD force signatures from them.

Table 4.5.1 Initial Conditions of Free Vibration Responses from White Noise Case

Leading Response	Displacement Responses		Velocity Responses		Acceleration Responses	
Locations	1DOF	2DOF	1DOF	2DOF	1DOF	2DOF
Initial Displacements	0.52136 (0.52195)	0.46280 (0.42408)	0.00219 (0)	0.01312 (-0.00404)	-0.22765 (-0.20792)	0.02389 (0.03288)
Initial Velocities	-0.00378 (0)	0.00209 (-0.00456)	0.54765 (0.54842)	-0.05636 (-0.08672)	-0.00200 (0.00646)	0.00529 (0.00262)

Note: 1. The values in parentheses denote the theoretical initial conditions.

In Tables 4.5.2 and 4.5.3, the theoretical initial conditions for the case of the wind forces, however, are available only for the first degree-of-freedom of the dynamic system on which the triggering level for the leading response is selected. Whether the initial conditions are properly selected by the proposed procedure cannot be completely realized because of the lack of the theoretical proof. On the other hand, if the selected initial conditions by the procedure can exceptionally make their free vibration responses equivalent to specified RD signatures, it is perhaps reasonable to conclude that the RD signatures have the free vibration behavior.

The primary advantage of the proposed procedure contributes to the ease of the selection of the initial conditions over the theoretical ones. Either, there is no change in the definition of the free vibration response since the system characteristics of the selected initial points are essentially correlated to one another in numerical analysis. In the following numerical simulations, the proposed procedure is utilized to gain better understanding of the RD technique.

Table 4.5.2 Initial Conditions of Free Vibration Responses from Alongwind Force Case

Leading Response	Displacement Responses		Velocity Responses		Acceleration Responses	
Locations	1DOF	2DOF	1DOF	2DOF	1DOF	2DOF
Initial Displacements	27804 (27844)	41511	-935.73 (0)	-1257.2	-16832	-15078
Initial Velocities	-58.849 (0)	-395.87	18836 (18820)	18760	344.04	913.55

Table 4.5.3 Initial Conditions of Free Vibration Responses from Crosswind Force Case

Leading Response	Displacement Responses		Velocity Responses		Acceleration Responses	
Locations	1DOF	2DOF	1DOF	2DOF	1DOF	2DOF
Initial Displacements	2.86502 (2.87100)	3.93845	0.08883 (0)	0.15991	-1.46440	-0.89252
Initial Velocities	0.01970 (0)	0.18301	2.27399 (2.27929)	1.31178	0.04133	-0.05540

4.5.1 Effects of White Noise Excitations

The illustrations of Figures 4.5.1-3 focus on the case of the uncorrelated white noise excitations. The comparisons of the estimated RD signatures and the free vibration responses emphasize on sufficient understanding of the theoretical derivation in the RD technique and evaluate if the RD acceleration signatures are relevant to the free vibration responses. As anticipated from the previous theoretical derivations, the RD displacement and velocity signatures are equivalent to the corresponding free vibration responses. The compared results in Figure 4.5.3 appear with interest that the RD acceleration signatures and the free vibration responses with the specified initial conditions are satisfactorily matched, though a sharp jump in the first DOF of the RD signatures, $\hat{\delta}_{\ddot{X}_1\ddot{X}_1}(\tau)$, is found at $\tau = 0$.

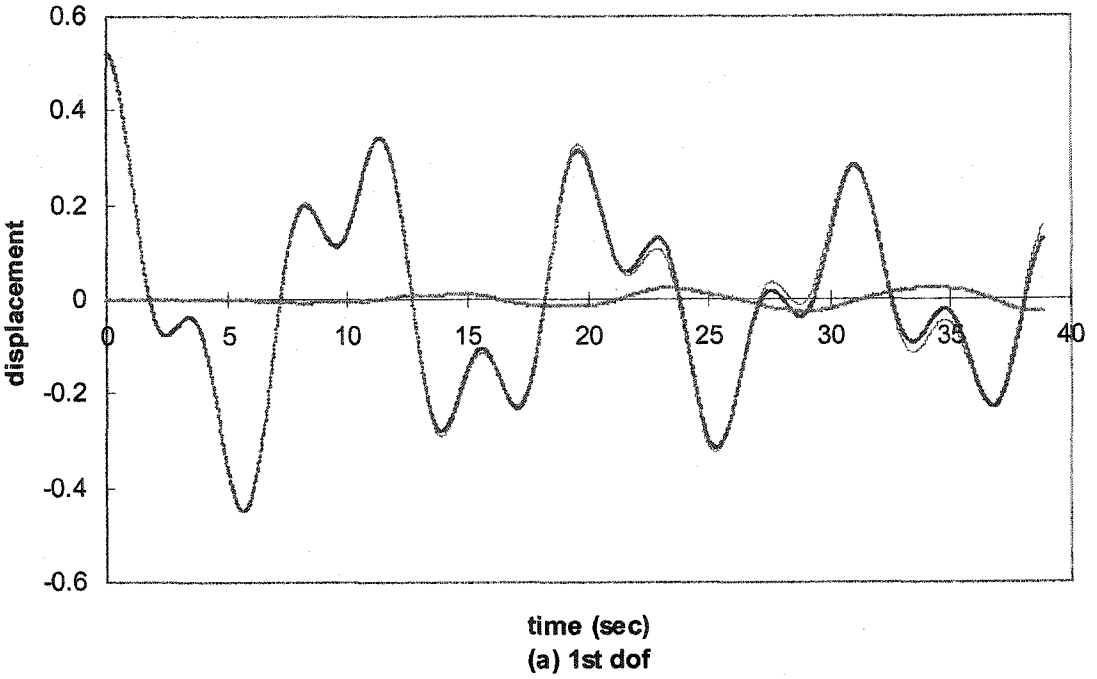

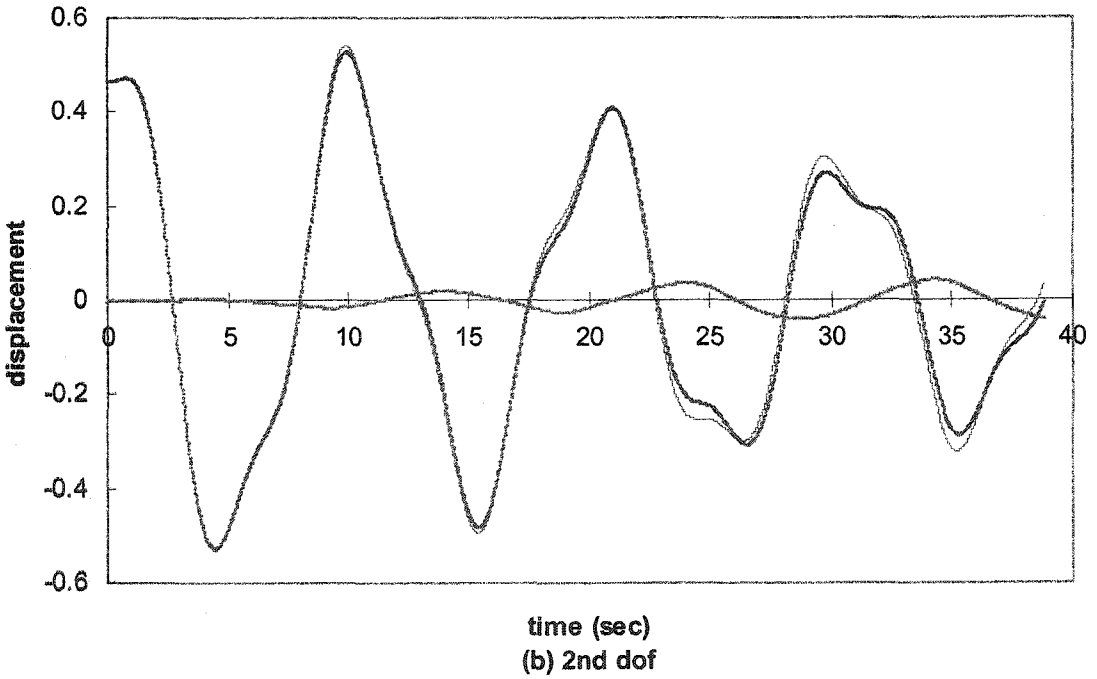

Figure 4.5.1 Random Decrement Displacement Signatures

——, Free Vibration Response; ♦♦♦♦♦, RD signature; ▲▲▲▲▲, Residuals

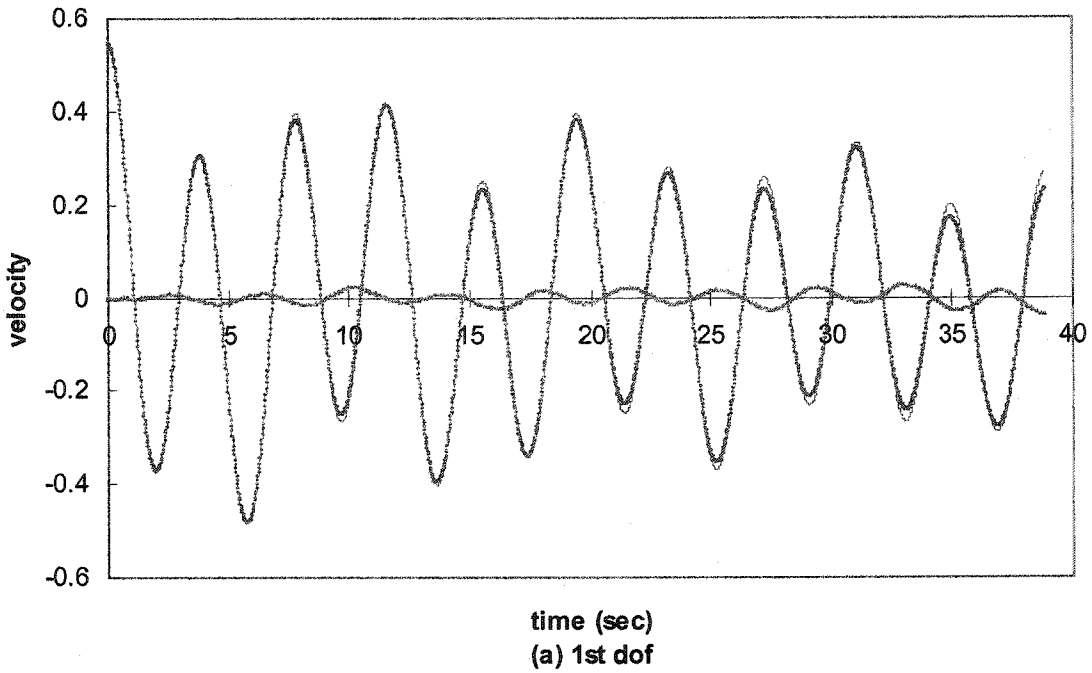

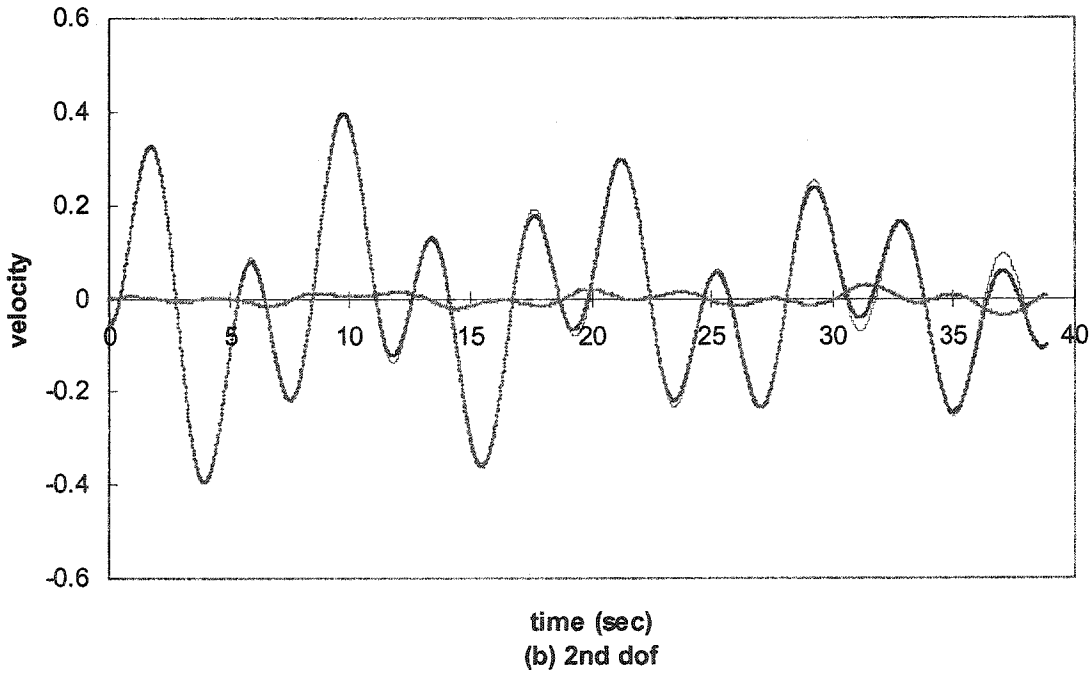

Figure 4.5.2 Random Decrement Velocity Signatures

——, Free Vibration Response; ♦♦♦♦♦, RD signature; ▲▲▲▲▲, Residuals

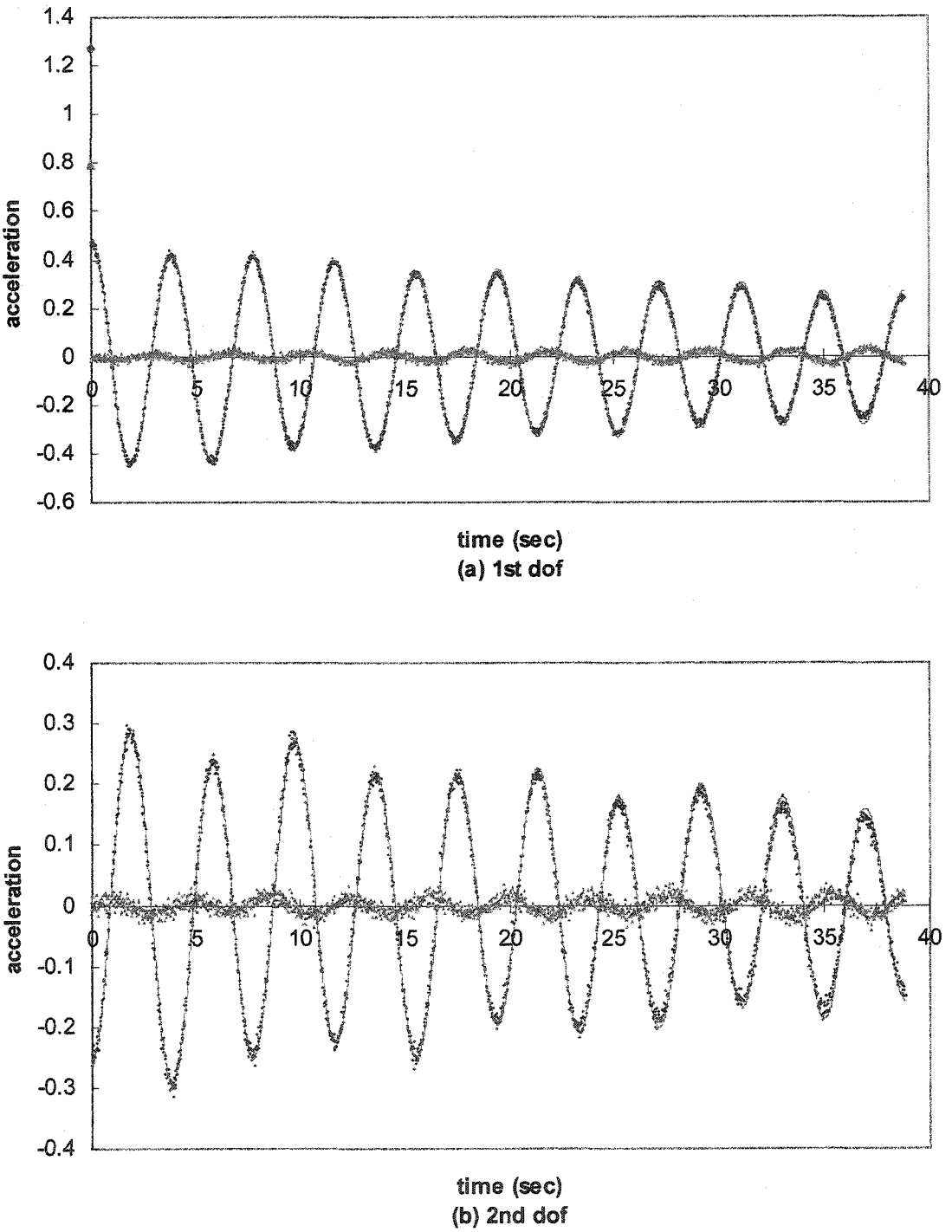

Figure 4.5.3 Random Decrement Acceleration Signatures

——, Free Vibration Response; ♦♦♦♦♦, RD signature; ▲▲▲▲▲, Residuals

In fact, the observation of such a singular point at $\tau = 0$ is related to the property of the Dirac delta function for the white noise excitations, as mentioned by Huang and Yeh [1999]. Such a phenomenon is also consistent with Equation (4.4.19) in which the Dirac delta function is substantially included. However, it seems that there should be a singular point at $\tau = 0$ expected to be found in the second DOF of Figure 4.5.3, since the estimated cross RD signature, $\hat{\delta}_{\ddot{X}_2\ddot{X}_1}(\tau)$, in Equation (4.4.19) contains the Dirac delta functions as well. In this regard, Huang and Yeh [1999] especially indicated that the singularities of the acceleration correlation matrix depend not only on the singularities of the correlation matrix of the input forces, but also on the mass matrix of the system.

To best elucidate how the mass matrix affects such a singularity in certain specified circumstance, the following derivation is introduced by taking only the diagonal mass matrix into consideration. A natural starting point is given to carefully examine Equations (4.2.25) and (4.2.26), within which the singularities of the correlation matrices of the first derivative modal coordinates are completely governed by the last term with $R_{ff}(\tau)$. It means that it may be allowed to establish the following expression, based on Equation (4.2.7),

$$R^{S}_{\dot{Q}\dot{Q}} = \Phi^{T} R_{\tilde{F}\tilde{F}} \Phi \tag{4.5.2}$$

, in which $R^{S}_{\dot{Q}\dot{Q}}$ signifies the portion of the singularity in the correlation matrix of $\dot{Q}$, and

$$R_{\tilde{F}\tilde{F}}(\tau) = E[\tilde{F}(t)\tilde{F}^{T}(t+\tau)] = \begin{bmatrix} 0 & 0 \\ 0 & M^{-1}R_{ff}(\tau)M^{-1} \end{bmatrix} \tag{4.5.3}$$

Furthermore, by virtue of the established relationship between $[z]$ and $[Q]$ as given in Equation (4.2.4), it yields that

$$R^S_{\ddot{z}\ddot{z}} = \Phi R^S_{\dot{Q}\dot{Q}} \Phi^T = \Phi\Phi^T R_{\tilde{F}\tilde{F}} \Phi\Phi^T = R_{\tilde{F}\tilde{F}} \tag{4.5.4}$$

After the substitution of Equation (4.5.3) into Equation (4.5.4), it turns out that

$$R^S_{\ddot{z}\ddot{z}} = \begin{bmatrix} R^S_{\ddot{X}\ddot{X}} & 0 \\ 0 & R^S_{\ddot{X}\ddot{X}} \end{bmatrix} = \begin{bmatrix} 0 & 0 \\ 0 & M^{-1} R_{ff} M^{-1} \end{bmatrix} \tag{4.5.5}$$

Since the correlation matrix of the forcing functions is a diagonal matrix, *i.e.* Equation (4.4.1), it follows that the singularities take place only at the diagonal elements of the acceleration correlation matrix as shown below:

$$R^S_{\ddot{X}\ddot{X}} = \begin{bmatrix} R^S_{\ddot{X}_1\ddot{X}_1} & R^S_{\ddot{X}_1\ddot{X}_2} \\ R^S_{\ddot{X}_2\ddot{X}_1} & R^S_{\ddot{X}_2\ddot{X}_2} \end{bmatrix} = \begin{bmatrix} \dfrac{\delta(\tau)}{m_1^2} & 0 \\ 0 & \dfrac{\delta(\tau)}{m_2^2} \end{bmatrix} \tag{4.5.6}$$

Equation (4.5.6) can explain the reason why a sharp jump displays on $\hat{\delta}_{\ddot{X}_1\ddot{X}_1}(\tau)$, but not on $\hat{\delta}_{\ddot{X}_2\ddot{X}_1}(\tau)$. In addition to verifying the factors of the singularity in the acceleration correlation matrix, Equation (4.5.5) also reveals obviously the other fact that such a singularity does not exist in the velocity correlation matrix [Huang and Yeh, 1999]. Similarly, if the correlated forcing functions such as Equation (4.4.23) are taken into consideration, the singularities of the acceleration correlation matrix can be further proposed in this study as:

$$R^S_{\ddot{X}\ddot{X}} = \begin{bmatrix} \dfrac{\delta(\tau)}{m_1^2} & \dfrac{\gamma\delta(\tau-\tau_d)}{m_1 m_2} \\ \dfrac{\gamma\delta(\tau+\tau_d)}{m_1 m_2} & \dfrac{\gamma^2\delta(\tau)}{m_2^2} \end{bmatrix} \tag{4.5.7}$$

It can be realized immediately from Equation (4.5.7) that a sharp jump on $\hat{\delta}_{\ddot{X}_1\ddot{X}_1}(\tau)$ and $\hat{\delta}_{\ddot{X}_2\ddot{X}_1}(\tau)$ is occurred at $\tau = 0$ and $\tau = \tau_d$, respectively.

Further investigations based on the time domain and frequency domain analyses are shown in Figures 4.5.4 and 4.5.5, respectively, for the comparison between the RD acceleration residuals and the associated RD force signatures. The RD residuals are defined by the difference between the estimated RD signatures and their analytical free vibration responses. The initial two points of each RD acceleration residuals and each RD force signature in Figure 4.5.4 are marked by triangle and square, respectively. It is found that the first marked point in the RD residuals and the RD force signatures has the same value as anticipated in the derivation of Equation (4.4.19) for the properties of the white noise excitations. The examination of Equations (4.2.25) and (4.2.26) can explain theoretically the added effect of the correlation matrix of the forcing functions existed in the correlation matrix of the acceleration responses. This explanation is further fostered by the results in Figure 4.5.5, after transferring the RD residuals and RD force signatures into the frequency domain data by the FFT based approach.

According to the foregoing results, the RD acceleration signature substantially consists of two portions. One portion represents the free vibration acceleration response of a linear dynamic system and the other portion results from the contribution of the white noise excitation acting on the DOF of the dynamic system. Hence, the following relationships can be established:

$$\delta_{\ddot{X}_1\ddot{X}_1}(\tau) = \delta^F_{\ddot{X}_1\ddot{X}_1}(\tau) + \delta^L_{\ddot{X}_1\ddot{X}_1}(\tau) \tag{4.5.8}$$

$$\delta_{\ddot{X}_2\ddot{X}_1}(\tau) = \delta^F_{\ddot{X}_2\ddot{X}_1}(\tau) + \delta^L_{\ddot{X}_2\ddot{X}_1}(\tau) \tag{4.5.9}$$

in which the superscripts of the RD acceleration signatures, F and L, naturally correspond to the free vibration portion and the forcing function portion in the RD signatures.

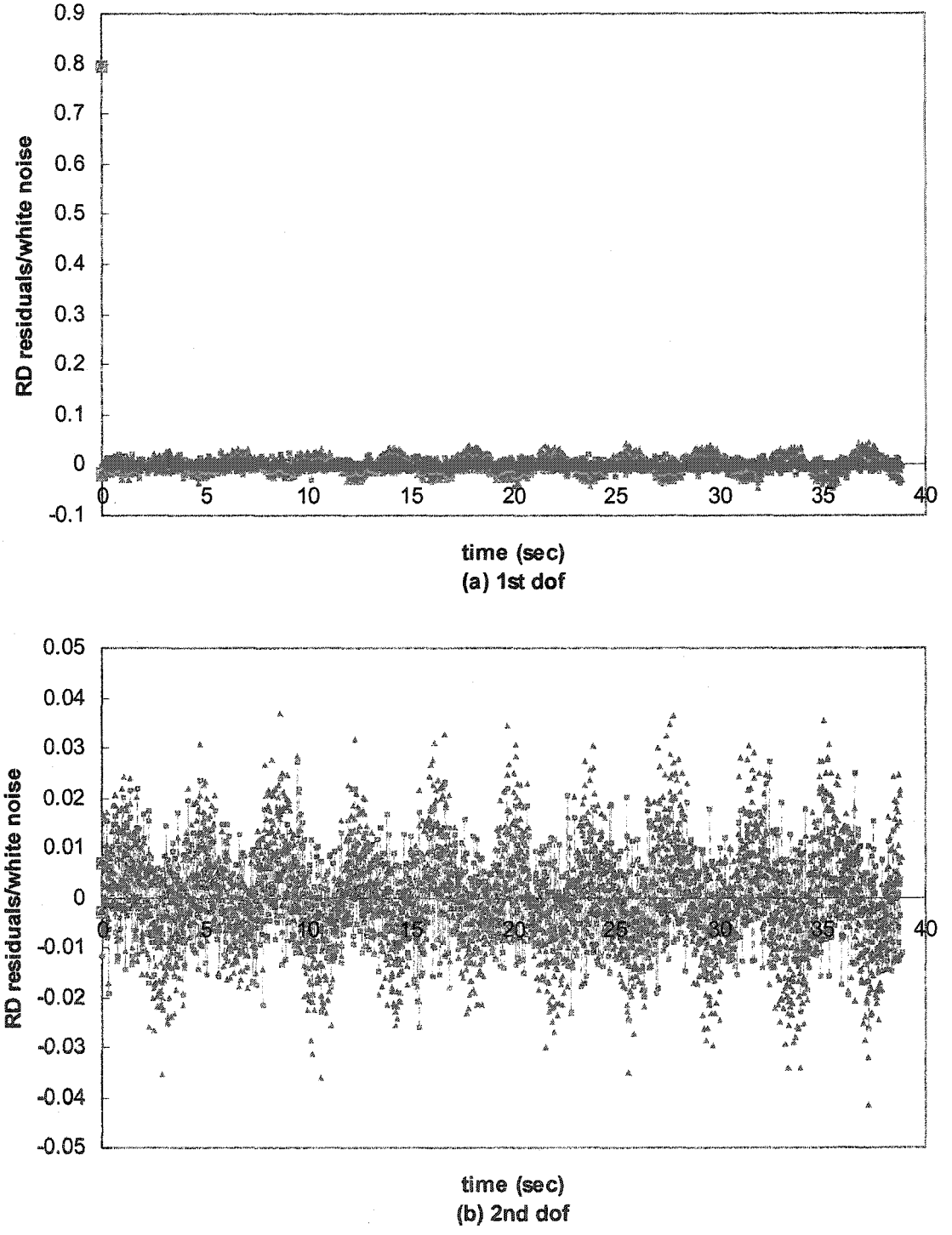

Figure 4.5.4 Relation of RD Acceleration Residuals and White Noises

-□-□-, RD White Noise Signature; ▲▲▲▲▲, RD Acceleration Residuals

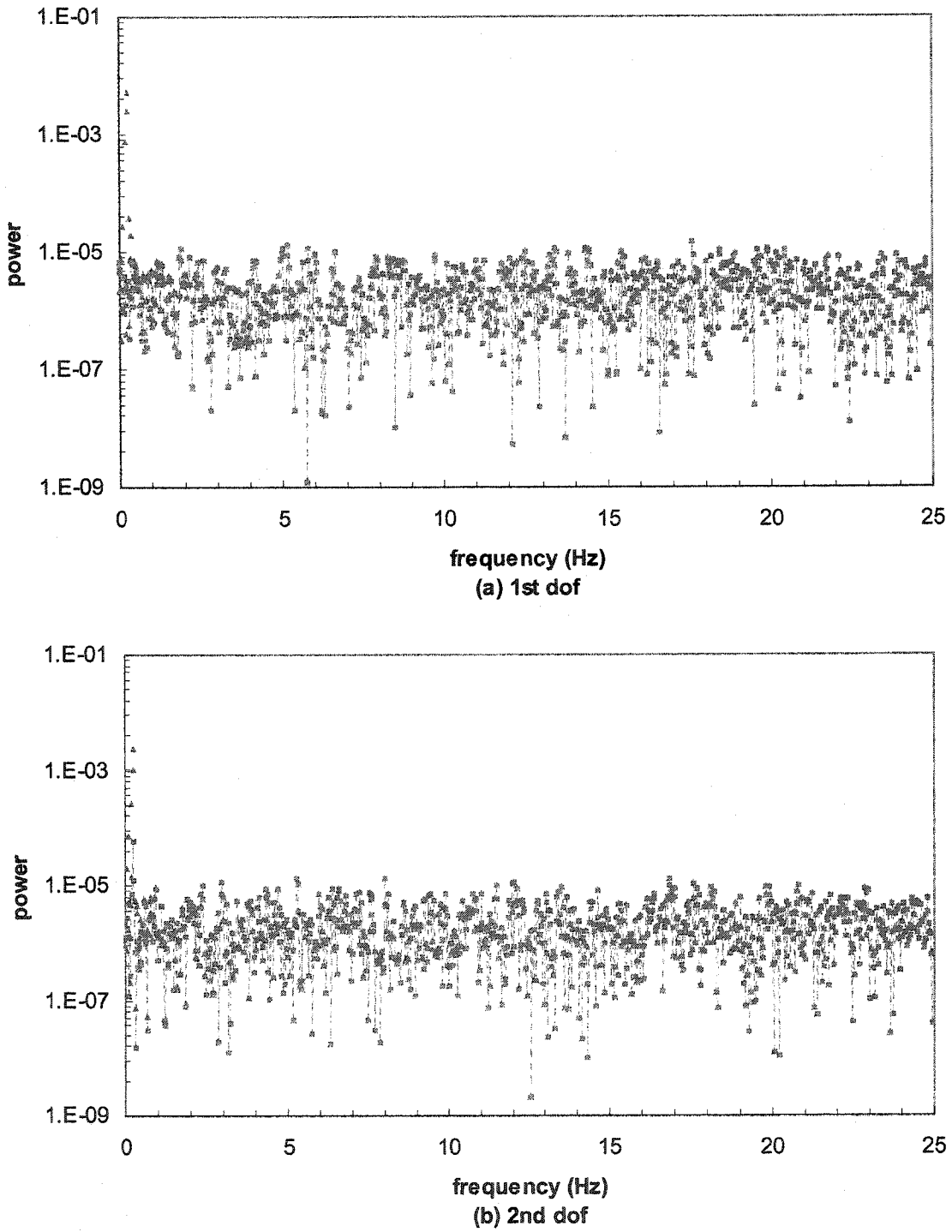

Figure 4.5.5 Relation of RD Acceleration Residuals and White Noises

-□-□-, RD White Noise Signature; ▲▲▲▲▲, RD Acceleration Residuals

4.5.2 Effects of Simulated Wind Forces

The RD signatures of the responses resulting from the dynamic system subjected to the fluctuating alongwind and crosswind forces are shown in Figures 4.5.6-8 and 4.5.11-13, respectively, in comparison with the corresponding free vibration responses. Surprisingly, the compared results appear to prove that the RD displacement and velocity signatures are congruous with the free vibration responses for both cases of the simulated wind forces, though the theoretical development is restrained for the white noise inputs. It may be explained that wind forces can be regarded as a broadband process in certain practical applications, when compared to a system transfer function. In this sense, the simulated wind forces in these cases are treated as good approximations of the white noise processes.

Nevertheless, common to both of Figures 4.5.8 and 4.5.13 are the RD acceleration signatures, which illustrate the significant deviation in the first several points from the corresponding free vibration response. Again, it reflects the added effect of the RD force signatures in the RD acceleration signatures, in contrast with the results of the RD displacement and velocity signatures. The comparisons between the RD acceleration residuals and the RD force signatures in Figures 4.5.9-10 and Figures 4.5.14-15 reveal such an effect. Such a result is sufficient to reconfirm the relationships in Equations (4.5.8) and (4.5.9) and further establish the following expressions:

$$\delta_{\ddot{X}_1\ddot{X}_1}(\tau) = \delta^R_{\ddot{X}_1\ddot{X}_1}(\tau) + \delta^L_{\ddot{X}_1\ddot{X}_1}(\tau) \tag{4.5.10}$$

$$\delta_{\ddot{X}_2\ddot{X}_1}(\tau) = \delta^R_{\ddot{X}_2\ddot{X}_1}(\tau) + \delta^L_{\ddot{X}_2\ddot{X}_1}(\tau) \tag{4.5.11}$$

in which R and L stand for the two portions in the RD acceleration signatures from the non-forced acceleration responses and the forcing functions, respectively.

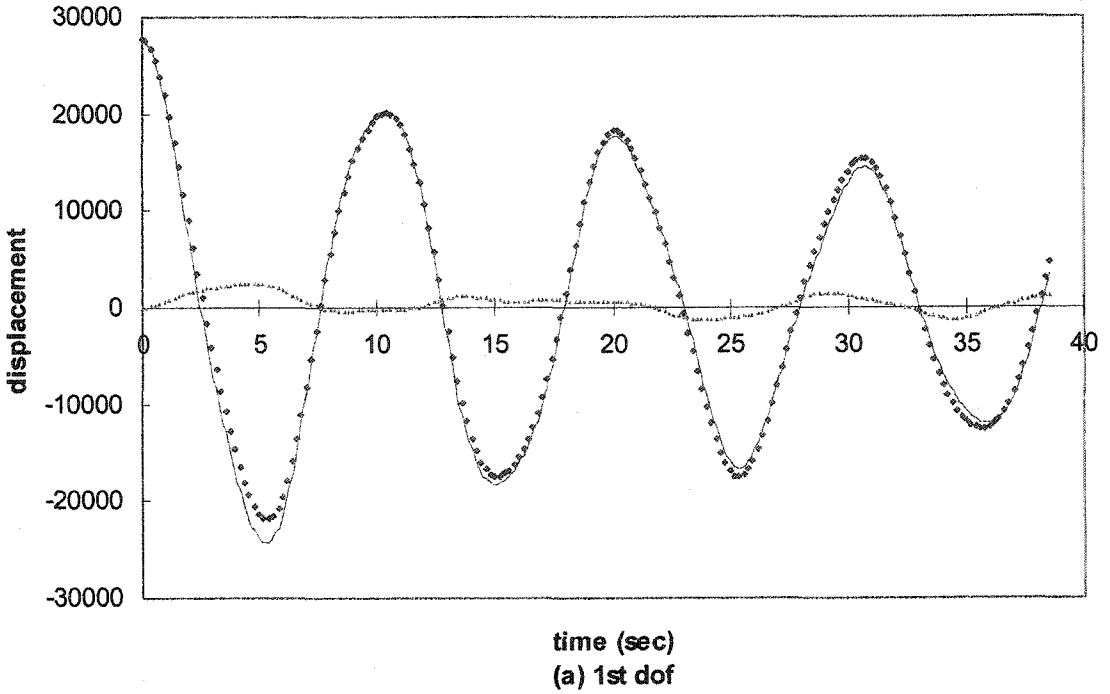

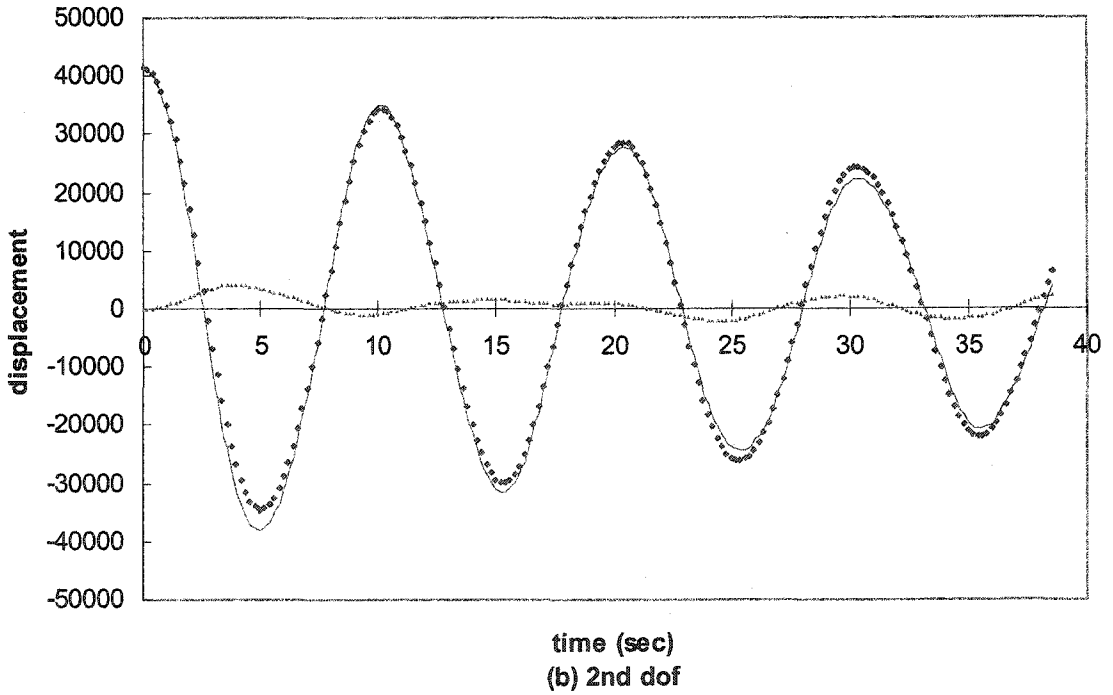

Figure 4.5.6 Random Decrement Displacement Signatures

——, Free Vibration Response; ♦♦♦♦♦, RD signature; ▲▲▲▲▲, Residuals

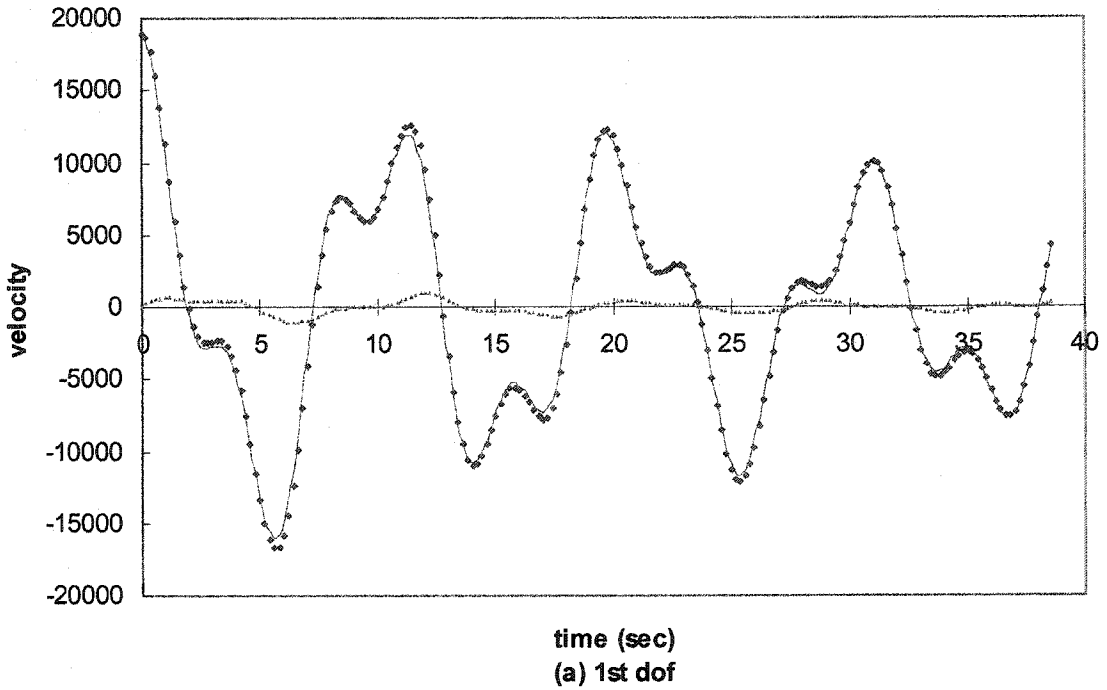

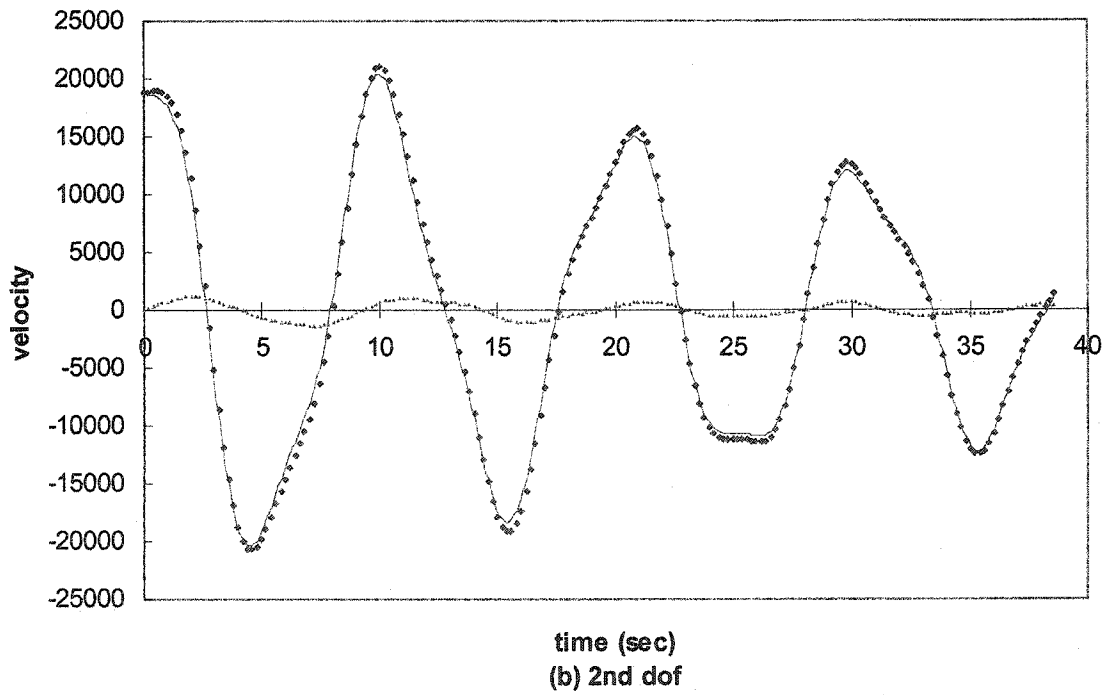

Figure 4.5.7 Random Decrement Velocity Signatures

——, Free Vibration Response; ♦♦♦♦♦, RD signature; ▲▲▲▲▲, Residuals

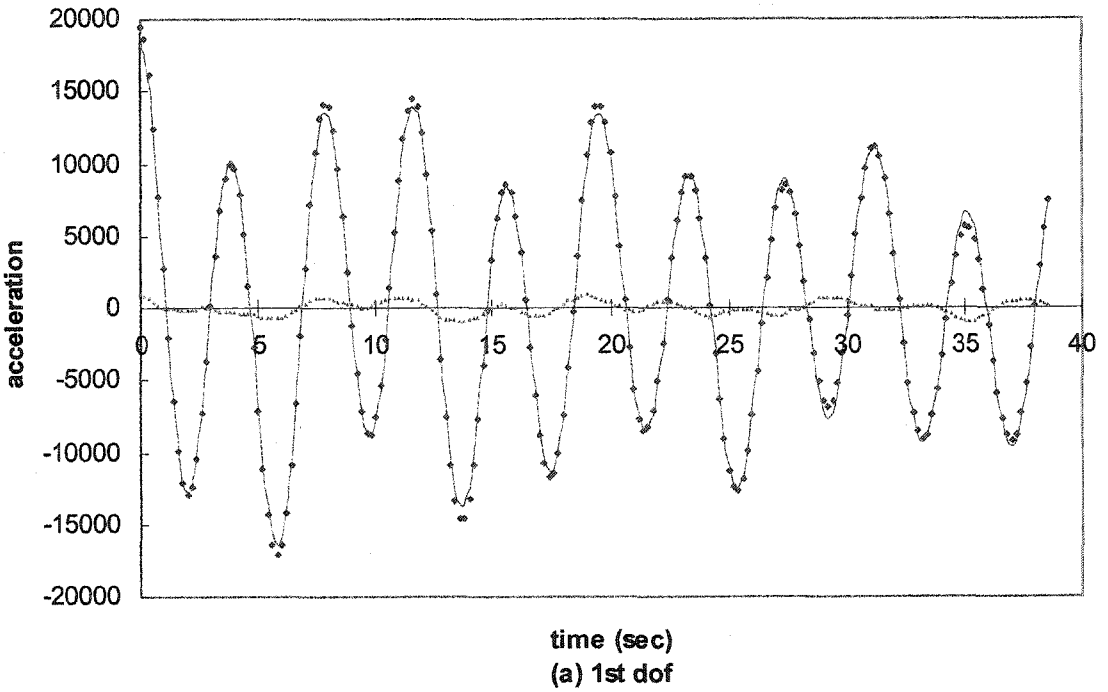

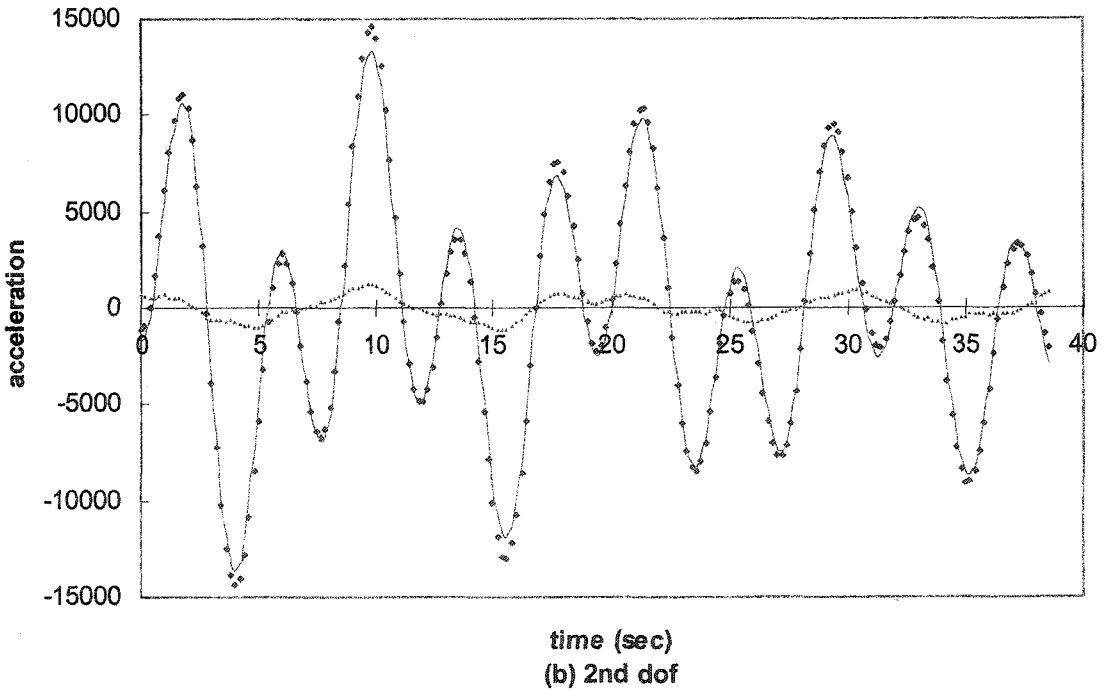

Figure 4.5.8 Random Decrement Acceleration Signatures

——, Free Vibration Response; ♦♦♦♦♦, RD signature; ▲▲▲▲▲, Residuals

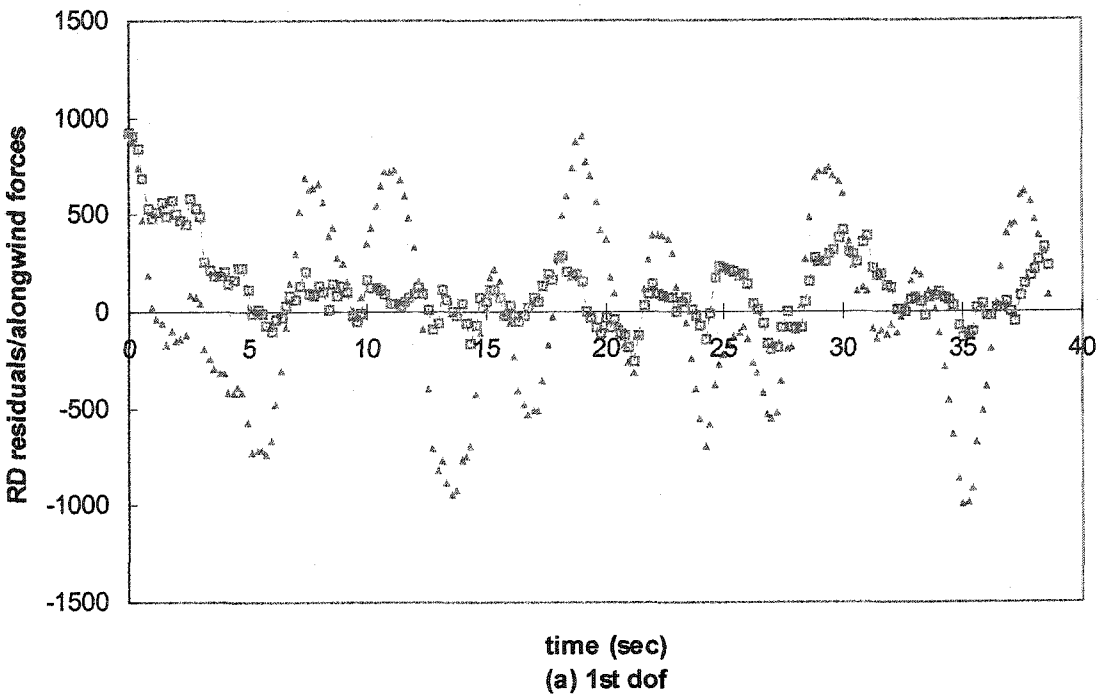

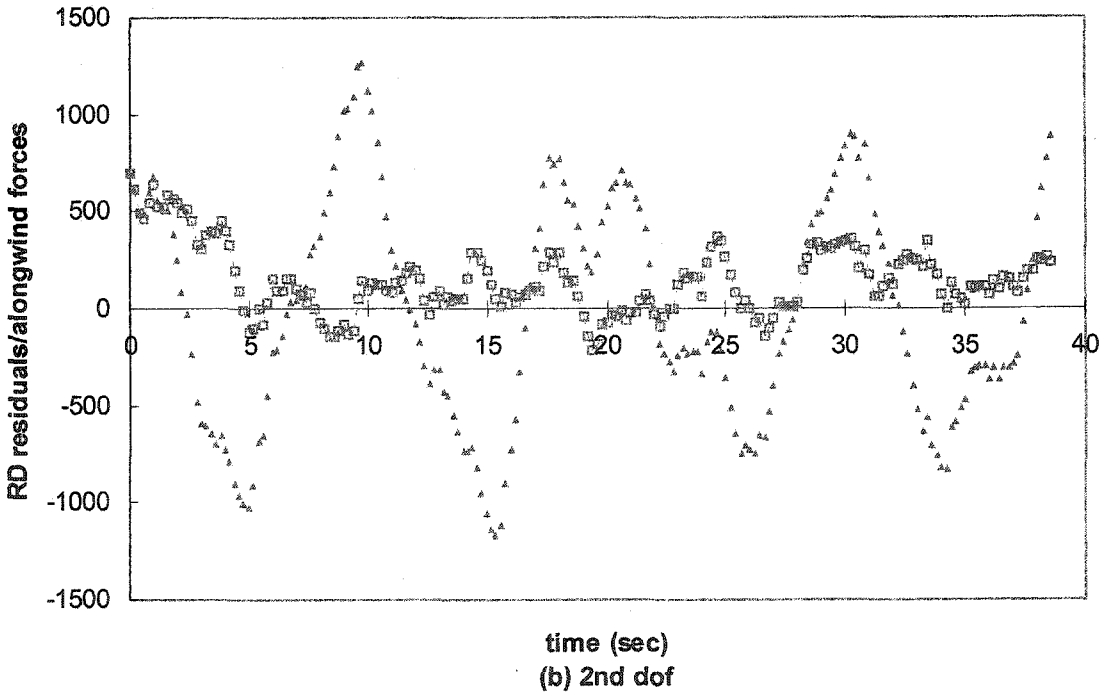

Figure 4.5.9 Relation of RD Acceleration Residuals and Alongwind Forces

-□-□-, RD Force Signature; ▲▲▲▲▲, Acceleration Residuals

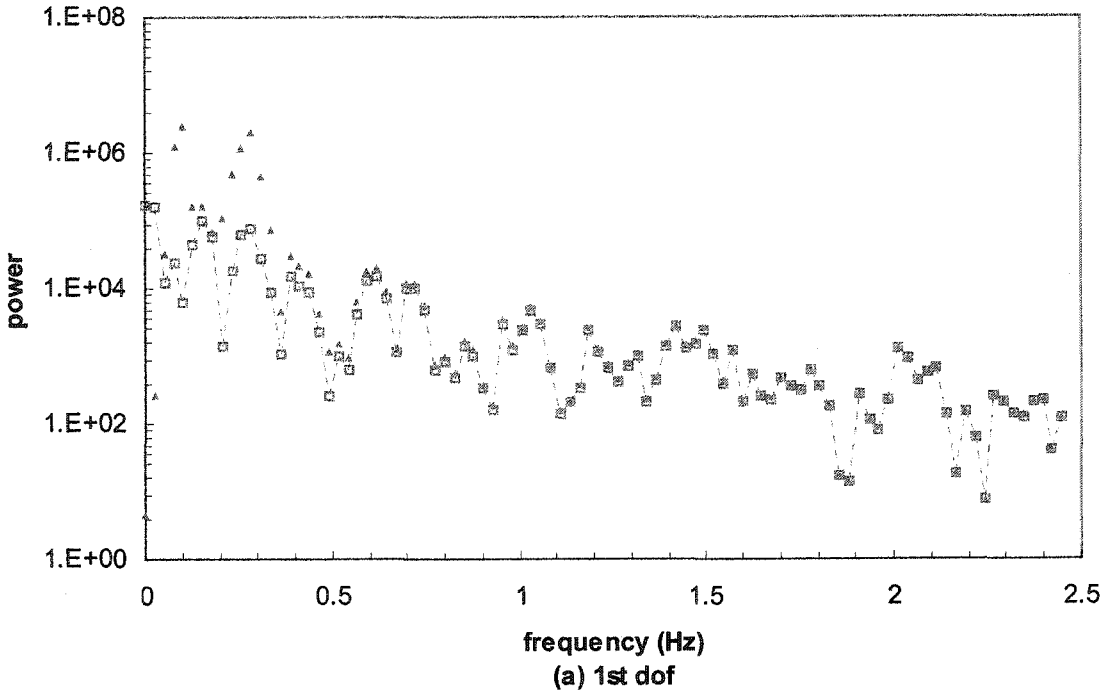

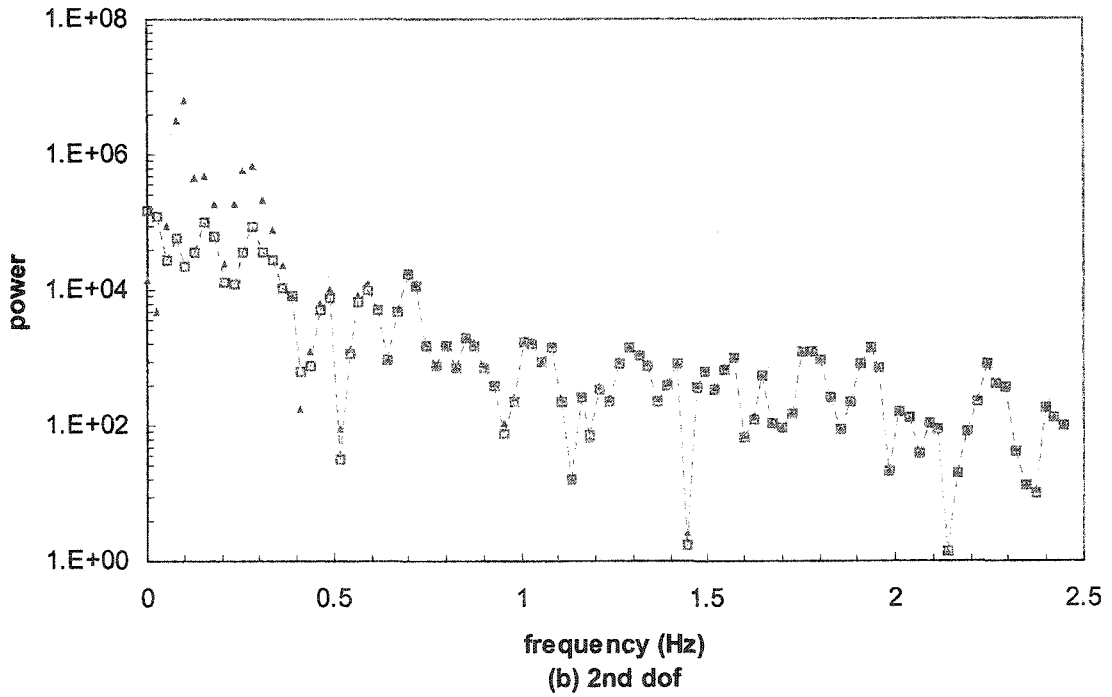

Figure 4.5.10 Relation of RD Acceleration Residuals and Alongwind Forces

-□-□-, RD Force Signature; ▲▲▲▲▲, Acceleration Residuals

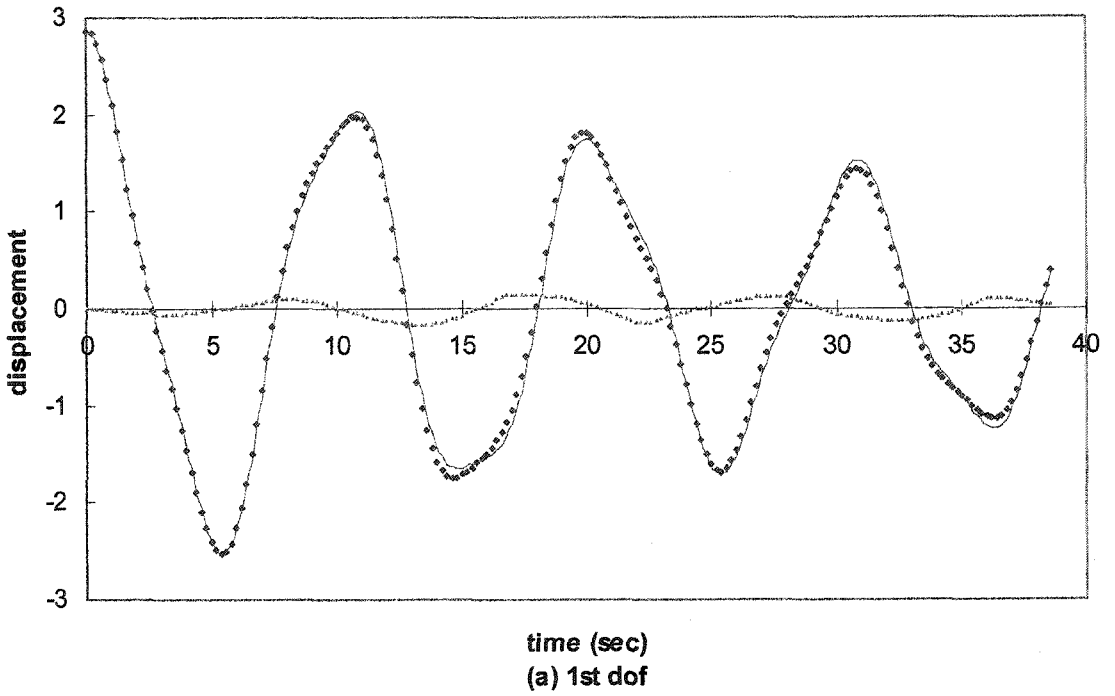

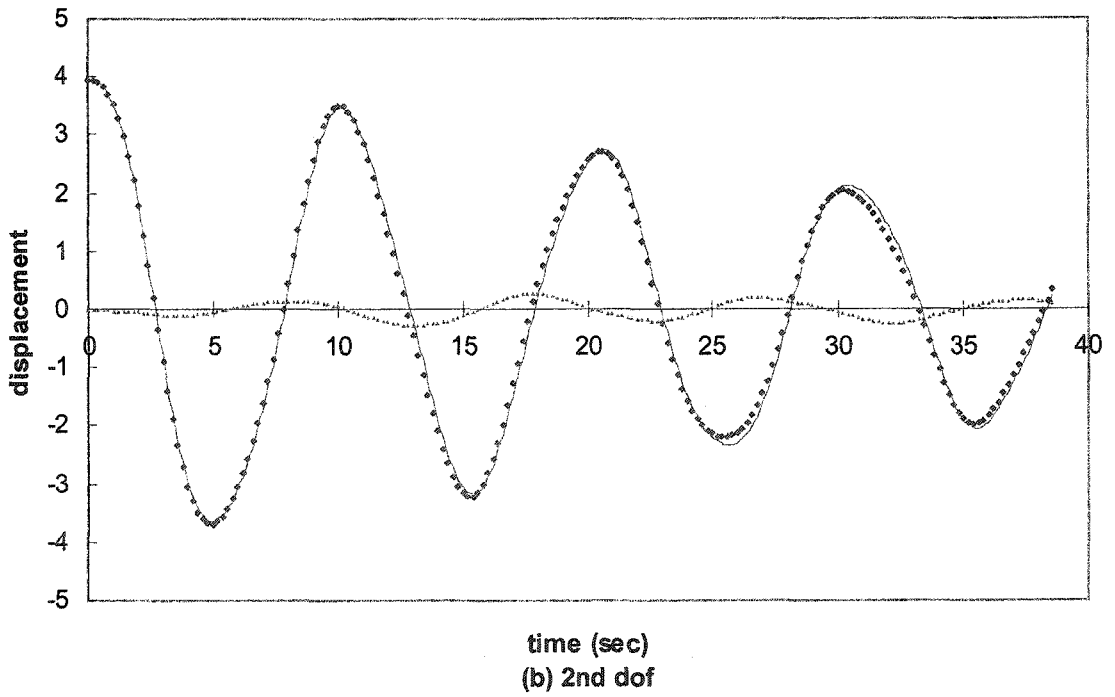

Figure 4.5.11 Random Decrement Displacement Signatures

——, Free Vibration Response; ♦♦♦♦♦, RD signature; ▲▲▲▲▲, Residuals

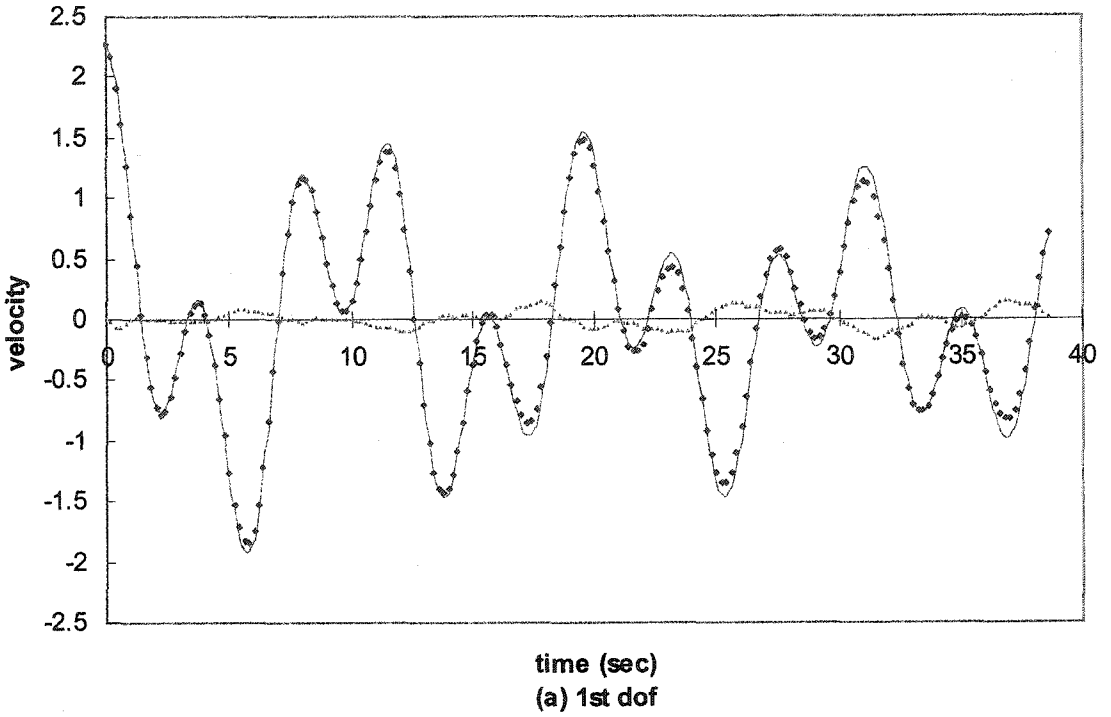

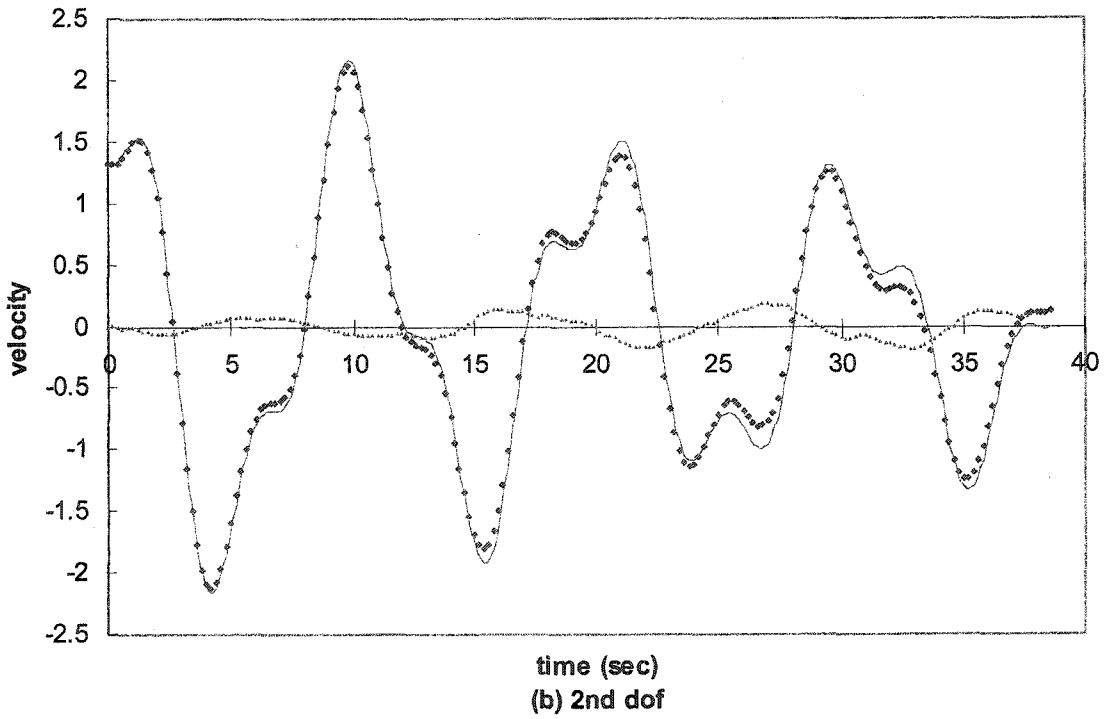

Figure 4.5.12 Random Decrement Velocity Signatures

——, Free Vibration Response; ♦♦♦♦♦, RD signature; ▲▲▲▲▲, Residuals

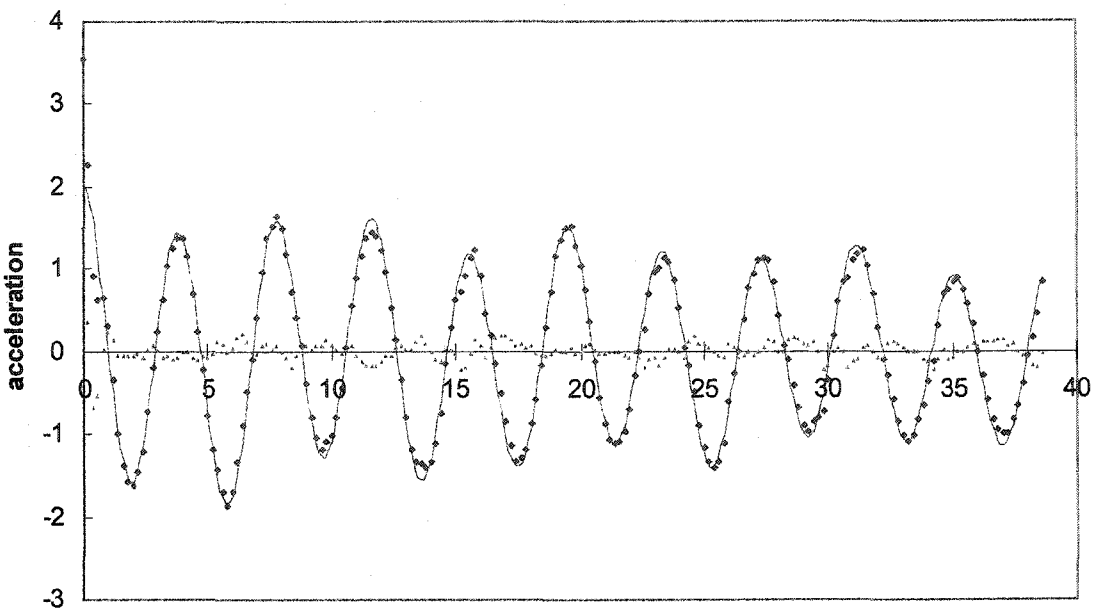

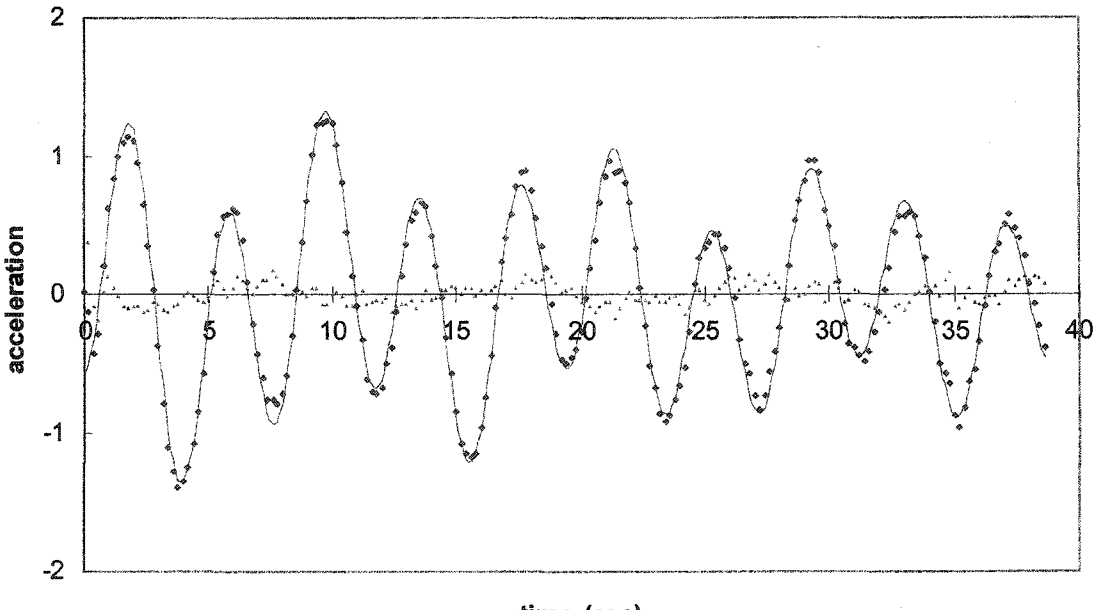

Figure 4.5.13 Random Decrement Acceleration Signatures

——, Free Vibration Response; ♦♦♦♦♦, RD signature; ▲▲▲▲▲, Residuals

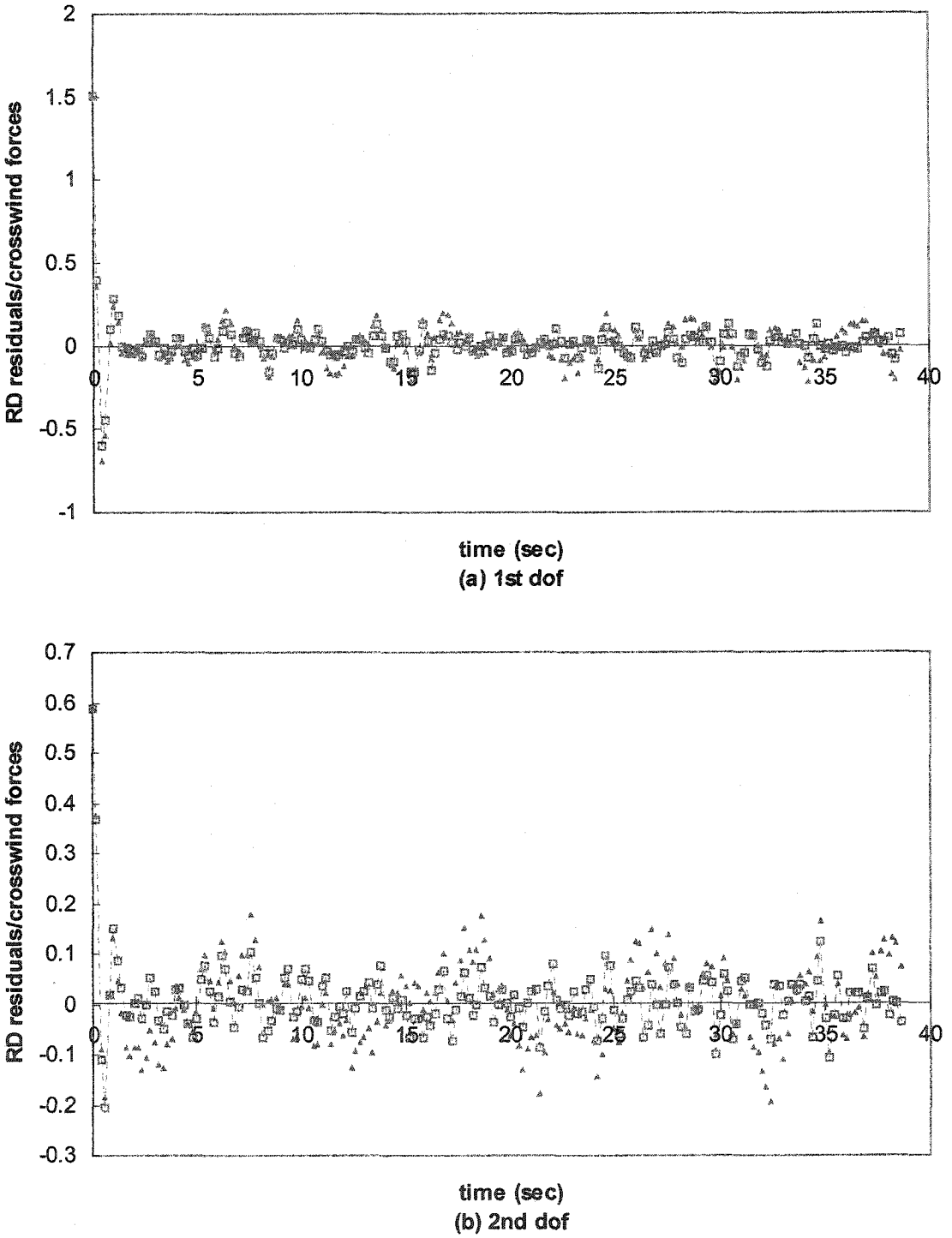

Figure 4.5.14 Relation of RD Acceleration Residuals and Crosswind Forces

-□-□-, RD Force Signature; ▲▲▲▲▲, Acceleration Residuals

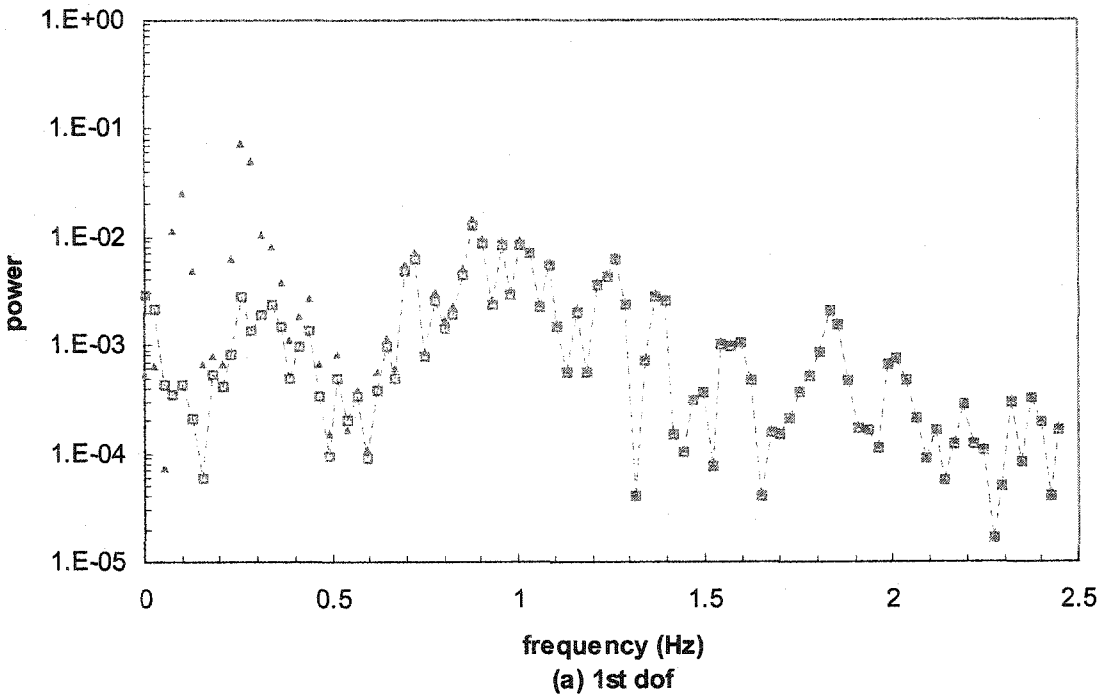

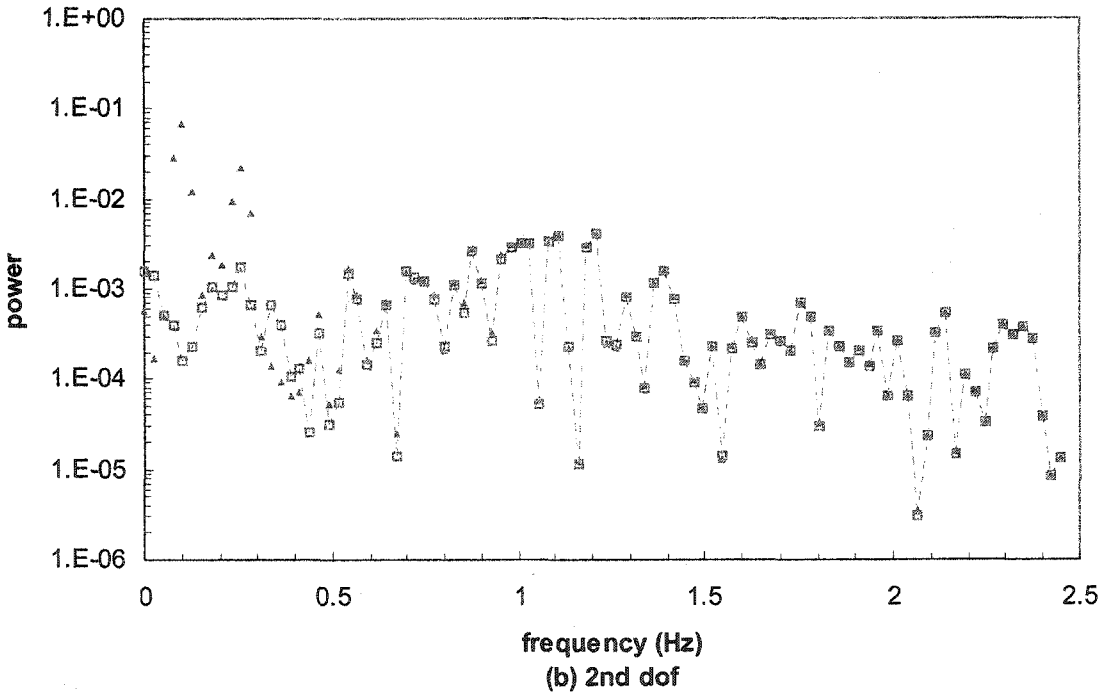

Figure 4.5.15 Relation of RD Acceleration Residuals and Crosswind Forces

-□-□-, RD Force Signature; ▲▲▲▲▲, Acceleration Residuals

4.6 Concluding Remarks

The theoretical foundation of the multiple-signal RD technique has been enhanced to access further information of the RD signatures on the basis of the theoretical studies of Huang, et al. and Bedewi. The development of the theoretical foundation takes advantage of the state space formulation to represent the auto and cross RD signatures of dynamic responses in an elegant way. Making use of such a representation in connection with the free vibration responses of a linear dynamic system can help define a set of the theoretical initial conditions so that the RD signatures satisfy the requirement of the free vibration behavior. In this theoretical development, each forcing function is assumed to possess the properties of the Gaussian white noise process, but the correlation is capable of existing between the forcing functions.

A previously proposed procedure was extensively used in this study together with the developed theory of the RD technique to give rise to the MDOF analytical free vibration responses. Such a procedure adopts the concept behind the RD technique in order to facilitate the determination of the initial conditions through the formed RD signatures of displacement and velocity responses from a dynamic system.

To verify the proposed procedure, numerical simulations of a 2DOF dynamic system separately loaded by the uncorrelated white noise excitations and the two simulated wind forces were carried out. Verification was assessed on the basis of comparison between the estimated RD signatures and the deterministic free vibration responses. Figures 4.5.1 and 4.5.2 reconfirmed that the RD displacement and velocity signatures are equivalent to their free vibration responses for the dynamic system subjected to the white noise excitations. For the cases of the fluctuating wind forces

shown in Figures 4.5.6-7, and 4.5.11-12, the compared results give an excellent agreement, which also indicate the applicability of the RD technique to the real wind-induced responses. Moreover, the comparisons in Figures 4.5.4, 4.5.9, and 4.5.14 reveal that the first points of the RD acceleration residuals have the same values as those of the related RD force signatures, despite the RD acceleration signatures do not resemble the free vibration responses. These compared results above naturally support the feasibility of the procedure described in this study.

Correspondingly, the contribution of the proposed procedure to the RD signatures brings a better understanding of the theoretical foundation on the RD technique. In particular, the primary concerns in this study are to realize the RD acceleration signatures in comparison with the free vibration responses and further establish the generalized relation between the RD acceleration signatures and the RD force signatures. Common to the numerical simulations for the RD acceleration signatures, the RD force signatures apparently influence the RD acceleration signatures, which is evident from inspecting visually Figures 4.5.3-5, 4.5.8-10, and 4.5.13-15. In fact, the added effect of the RD force signatures on the RD acceleration signatures is consistent with Equations (4.2.25) and (4.2.26), where the correlation matrix of the forcing functions is essentially included. Hence, it follows that the RD acceleration signature consists of two portions contributed from the non-forced acceleration response and the applied forcing function, as formulated in Equations (4.5.10) and (4.5.11).

The experiences from this study recommend that force measurement may be required to accompany acceleration measurement in practical tests to achieve the more accurate modal parameters of a numerical model for a dynamic system.

References

Bedewi, N. E. (1986), The Mathematical Foundation of the Auto and Cross- Random Decrement Techniques and the Development of a System Identification Technique for the Detection of Structural Deterioration, Ph.D. Dissertation, Department of Mechanical Engineering, University of Maryland.

Cheng, F. Y. (2001), Matrix Analysis of Structural Dynamics Applications and Earthquake Engineering, 1st Edition, Marcel Dekker.

Cole, H. A. (1971), "Method And Apparatus For Measuring The Damping Characteristic Of A Structure", United State Patent No.: 3,620,069.

Ginsberg, J. H. (2001), Mechanical and Structural Vibrations Theory and Applications, 1st Edition, John Wiley & Sons, pp. 580-582.

Hart, G. C. and Wong, K. (2000), Structural Dynamics for Structural Engineers, 1st Edition, John Wiley & Sons, pp. 196-201.

Huang, C. S. (1998), Theoretical Investigation of the Application of Random Decrement Technique to Ambient Vibration Measurement of a Linear System with Non-proportional Damping, Report of National Center for Research on Earthquake Engineering, Taiwan, NCREE-98-003.

Huang, C. S. (2001), "Structural Identification From Ambient Vibration Measurement Using The Multivariate AR Model", Journal of Sound and Vibration, Vol. 241, No. 3, pp. 337-359.

Huang, C. S. and Yeh, C. H. (1999), "Some Properties Of Randomdec Signatures", Mechanical Systems and Signal Processing, Vol. 13, No. 3, pp. 491-507.

Huang, C. S., Yeh, C. H., and Tsai, I. C. (1998), "Random Decrement Technique For Ambient Vibration Test In Time-domain System Identification", Journal of the Chinese Institute of Civil and Hydraulic Engineering, Vol. 10, No. 3, pp. 537-547. (In Chinese)

Huang, C. S., Yeh, C. H., Lin, S. C., and Yeh, K. T. (1996), The Application of Random Decrement Technique to Ambient Vibration Measurement – A Proportional Damping System, Report of National Center for Research on Earthquake Engineering, Taiwan, NCREE-96-013.

Ibrahim, S. R. (1977), "Random Decrement Technique For Modal Identification Of Structures", Journal of Spacecraft, AIAA, Vol. 14, No. 11, pp. 696-700.

Soong, T. T. and Grigoriu, M. (1993), Random Vibration of Mechanical and Structural System, 1st Edition, Prentice Hall, pp. 191-194.

Chapter 5

RANDOM DECREMENT BASED METHOD

5.1 Introduction

Many time domain identification techniques, developed to determine unknown modal parameters from multiple-output responses only, are available, such as the Ibrahim time domain identification technique [Ibrahim, 1977; Pappa and Ibrahim, 1981], the poly-reference least squares complex exponential method [Vold and Rocklin, 1982; Vold and Russell, 1983], the eigen-system realization algorithms (ERA) [Juang and Pappa, 1985; Juang et al., 1988] or fast ERA method [Liu and Zhang, 1999], the autoregressive moving average model [Wang and Fang, 1986], the stochastic subspace method [Van Overschee and De Moor, 1996] and so on. The use of these techniques generally requires the form of impulse or free decay response functions including correlation functions. As shown in the previous chapters, however, the impulse and free decay response functions involve the additional information from the applied forcing functions, when the acceleration responses measured from forced vibration tests are taken into consideration. Hence, the use of these time domain identification techniques on such forced acceleration responses, without knowledge of the applied forcing functions, may draw a significant biased estimation of the modal parameters for the dynamic system. This problem is a major concern of this chapter.

In response to such a problem, the random decrement (RD) based method, which elaborates response data in the time and, then, frequency domains by cooperating the RD

technique with the fast Fourier transform (FFT) based algorithms, is proposed in this study. In fact, the RD based method used for the acceleration responses, irrespective of whether the analysis procedure is in the time domain or frequency domain, still needs to overcome the influence of the applied forcing functions. As already underlined, the use of the RD technique encounters the same drawback of involving the RD force signatures in the RD acceleration signatures. Instead, the task of evaluating the frequency response functions (FRFs) with the FFT based algorithms from the RD acceleration signatures is therefore managed to make it possible to determine the modal parameters of the dynamic system. To accomplish this task, a new FRF approach for the acceleration responses, which is a modification of the traditional one, has to be verified in advance, leading to the crucial theoretical foundation for deriving the FRFs of the RD acceleration signatures.

Numerical simulations of 2DOF and 3DOF linear dynamic systems subjected to white noise excitations in theory and simulated wind forces in practice, separately, are carried out to corroborate the applicability of the RD based method. The results of the RD based method evaluated only from the acceleration responses are naturally compared with those of the FRF approach to understand their relative merits to the parameter identification of a dynamic system. The performance of the RD based method and the FRF approach is mainly discussed in relation to the accuracy of natural frequencies and corresponding mode shapes. In the course of these simulations, an innovation of the RD technique to effectively avoid the added effect of the RD force signatures in the RD acceleration signatures is discovered. The innovated RD technique is based on a new manipulation of selecting a leading response that is isolated from the direct application of input forces and associated with the diagonal mass matrix of a dynamic system. Besides,

the identification accuracy of the mode shapes can be further enhanced, when a proper time length is selected from the formed RD signatures to evaluate their FRFs.

5.2 Frequency Response Function Approach

A starting point for the theory of the output-only FRFs is based on the solution of multiple-degree-of-freedom (MDOF) differential equations of motion. Using the modal superposition method [Paz, 1997], the displacement responses for an n DOF discrete linear dynamic system, in terms of the normal modes of the system, can be expressed by Equation (5.2.1).

$$X(t) = \varphi_1 q_1(t) + \varphi_2 q_2(t) + \cdots + \varphi_n q_n(t) = \Phi Q(t) \tag{5.2.1}$$

in which the modal matrix Φ and the modal coordinates $Q(t)$ are respectively denoted by:

$$\Phi = \begin{bmatrix} \varphi_1 & \varphi_2 & \cdots & \varphi_j & \cdots & \varphi_n \end{bmatrix} = \begin{bmatrix} \phi_{11} & \phi_{12} & \cdots & \phi_{1j} & \cdots & \phi_{1n} \\ \phi_{21} & \phi_{22} & \cdots & \phi_{2j} & \cdots & \phi_{2n} \\ \vdots & \vdots & \cdots & \vdots & \cdots & \vdots \\ \phi_{n-1,1} & \phi_{n-1,2} & \cdots & \phi_{n-1,j} & \cdots & \phi_{n-1,n} \\ \phi_{n1} & \phi_{n2} & \cdots & \phi_{nj} & \cdots & \phi_{nn} \end{bmatrix} \tag{5.2.2}$$

$$Q(t) = \begin{Bmatrix} q_1(t) \\ q_2(t) \\ \vdots \\ q_j(t) \\ \vdots \\ q_n(t) \end{Bmatrix} \tag{5.2.3}$$

The use of Equation (5.2.1) can convert the n coupled equations of motion, as follows:

$$M\ddot{X}(t) + C\dot{X}(t) + KX(t) = f(t) \tag{5.2.4}$$

to a set of n uncoupled equations, which are given by:

$$\ddot{q}_j(t) + 2\zeta_j \omega_j \dot{q}_j(t) + \omega_j^2 q_j(t) = F_j(t) \qquad j = 1, 2, \ldots, n \tag{5.2.5}$$

In this study, M, C and K are $n \times n$ symmetric mass, damping, and stiffness matrices, and

$$\varphi_j^T M \varphi_j = 1 \tag{5.2.6}$$

$$F_j(t) = \varphi_j^T f(t) \tag{5.2.7}$$

The solution of Equation (5.2.5) for the modal displacement response $q_j(t)$ with its zero initial conditions is following [Crandall and Mark, 1963]:

$$q_j(t) = \int_{-\infty}^{t} h_j(t-\tau) F_j(\tau) d\tau \tag{5.2.8}$$

in which an impulse displacement response function is defined by:

$$h_j(t) = \frac{e^{-\zeta_j \omega_j t} \sin(\sqrt{1-\zeta_j^2}\,\omega_j t)}{\sqrt{1-\zeta_j^2}\,\omega_j} \tag{5.2.9}$$

The transformation of Equation (5.2.1) with the aid of Equation (5.2.8) into the frequency domain yields subsequently:

$$X(f) = \varphi_1 H_1(f) F_1(f) + \varphi_2 H_2(f) F_2(f) + \cdots + \varphi_n H_n(f) F_n(f) \tag{5.2.10}$$

in which the i^{th} frequency response function $H_i(f)$ is the Fourier transform of $h_i(t)$, and $F(f)$ is the Fourier transform of the forcing function vector $F(t)$.

The corresponding acceleration response is formulated by Equation (5.2.11), consisting of a superposition of its normal modes.

$$\ddot{X}(t) = \varphi_1 \ddot{q}_1(t) + \varphi_2 \ddot{q}_2(t) + \cdots + \varphi_n \ddot{q}_n(t) = \Phi \ddot{Q}(t) \tag{5.2.11}$$

In Equation (5.2.11), the modal acceleration response is resulted from the double differentiation of Equation (5.2.8) with respect to t:

$$\begin{aligned}\ddot{q}_j(t) &= \int_{-\infty}^{t} \ddot{h}_j(t-\tau)F_j(\tau)d\tau + \dot{h}_j(0)F_j(t) \\ &= \int_{-\infty}^{t} h_j^a(t-\tau)F_j(\tau)d\tau\end{aligned} \tag{5.2.12}$$

in which

$$h_j^a(t) = \ddot{h}_j(t) + \delta_j(t) \tag{5.2.13}$$

$h_j^a(t)$ is the impulse acceleration response function that contains the Dirac delta function $\delta_j(t)$ in order to satisfy the theoretical definition of the impulse response function. It is noted that the formation of Equation (5.2.13) is different from other literatures that use the impulse acceleration response function without the term of the Dirac delta function. Similarly, the transformation of Equation (5.2.11) into the frequency domain yields:

$$\ddot{X}(f) = \varphi_1 H_1^a(f)F_1(f) + \varphi_2 H_2^a(f)F_2(f) + \cdots + \varphi_n H_n^a(f)F_n(f) \tag{5.2.14}$$

It is apparent from Equations (5.2.10) and (5.2.14) that the displacement and acceleration responses at the i^{th} DOF of the system can be given by the subsequent equations:

$$X_i(f) = \phi_{i1}H_1(f)F_1(f) + \phi_{i2}H_2(f)F_2(f) + \cdots + \phi_{in}H_n(f)F_n(f) \tag{5.2.15}$$

$$\ddot{X}_i(f) = \phi_{i1}H_1^a(f)F_1(f) + \phi_{i2}H_2^a(f)F_2(f) + \cdots + \phi_{in}H_n^a(f)F_n(f) \tag{5.2.16}$$

Under the assumptions that vibration modes are well separated and modal damping ratios are small, the dynamic response at a resonant frequency is dominated by the contribution of the corresponding vibration mode, and the contributions of other vibration modes are negligible [Bao and Ko, 1991]. As a result, the responses at the k^{th} natural frequency, f_k, can be approximately evaluated as:

$$X_i(f_k) = \phi_{ik}H_k(f_k)F_k(f_k) \tag{5.2.17}$$

$$\ddot{X}_i(f_k) = \phi_{ik} H_k^a(f_k) F_k(f_k) \tag{5.2.18}$$

From Equations (5.2.17) and (5.2.18), it follows that a modal ratio between two simultaneously resulting responses at the i^{th} DOF and the j^{th} DOF of the dynamic system can be obtained using:

$$\frac{X_j(f_k)}{X_i(f_k)} = \frac{\phi_{jk} H_k(f_k) F_k(f_k)}{\phi_{ik} H_k(f_k) F_k(f_k)} = \frac{\phi_{jk}}{\phi_{ik}} \tag{5.2.19}$$

$$\frac{\ddot{X}_j(f_k)}{\ddot{X}_i(f_k)} = \frac{\phi_{jk} H_k^a(f_k) F_k(f_k)}{\phi_{ik} H_k^a(f_k) F_k(f_k)} = \frac{\phi_{jk}}{\phi_{ik}} \tag{5.2.20}$$

In addition, Equations (5.2.19) and (5.2.20) are also the definition of the traditional frequency response function (FRF), which is essentially the ratio of the output to input, that is,

$$H_{ij}(f) = \frac{X_j(f)}{X_i(f)} \tag{5.2.21}$$

In this study, $X_i(f)$ and $X_j(f)$ represent the Fourier transforms of two ergodic stochastic responses $X_i(t)$ and $X_j(t)$, respectively, as illustrated in Figure 5.2.1, and f denotes the natural frequency. The FRFs of the displacement and acceleration responses at the k^{th} natural frequency f_k can be further expressed, respectively, as following:

$$H_{ij}^{(I)}(f_k) = \frac{G_{X_i X_j}(f_k)}{G_{X_i X_i}(f_k)} = \frac{\phi_{jk}}{\phi_{ik}} \tag{5.2.22}$$

$$H_{ij}^{(II)}(f_k) = \frac{G_{X_j X_j}(f_k)}{G_{X_i X_j}(f_k)} = \frac{\phi_{jk}}{\phi_{ik}} \tag{5.2.23}$$

$$H_{ij}^{(III)}(f_k) = \sqrt{\frac{G_{X_j X_j}(f_k)}{G_{X_i X_i}(f_k)}} = \left|\frac{\phi_{jk}}{\phi_{ik}}\right| \tag{5.2.24}$$

and

$$H_{ij}^{(I)}(f_k) = \frac{G_{\ddot{X}_i\ddot{X}_j}(f_k)}{G_{\ddot{X}_i\ddot{X}_i}(f_k)} = \frac{\phi_{jk}}{\phi_{ik}} \tag{5.2.25}$$

$$H_{ij}^{(II)}(f_k) = \frac{G_{\ddot{X}_j\ddot{X}_j}(f_k)}{G_{\ddot{X}_i\ddot{X}_j}(f_k)} = \frac{\phi_{jk}}{\phi_{ik}} \tag{5.2.26}$$

$$H_{ij}^{(III)}(f_k) = \sqrt{\frac{G_{\ddot{X}_j\ddot{X}_j}(f_k)}{G_{\ddot{X}_i\ddot{X}_i}(f_k)}} = \left|\frac{\phi_{jk}}{\phi_{ik}}\right| \tag{5.2.27}$$

, in terms of the one-sided estimated spectral density functions defined by the following Equations (5.2.28-30):

$$G_{X_iX_i}(f) = \frac{2}{T}[X_i^*(f,T)X_i(f,T)] \tag{5.2.28}$$

$$G_{X_jX_j}(f) = \frac{2}{T}[X_j^*(f,T)X_j(f,T)] \tag{5.2.29}$$

$$G_{X_iX_j}(f) = \frac{2}{T}[X_i^*(f,T)X_j(f,T)] \tag{5.2.30}$$

in which the superscript * denotes the complex conjugate and T is the time length of the responses, $X_i(t)$ and $X_j(t)$ [Bendat and Piersol, 2000].

The introduction of such FRFs can be used to determine the mode shapes of the dynamic system. When a set of responses at different locations of a dynamic system is available, the mode shapes of the dynamic system can be evaluated from the amplitude and phase of a FRF between any response and a common reference response. Crucially, this can be carried out not only from displacement or velocity responses, but also from acceleration responses irrespective of the additional effect of the applied forcing function on the impulse acceleration response function.

It is known that $\left|H_{ij}^{(I)}(f_k)\right| = \left|H_{ij}^{(II)}(f_k)\right| = \left|H_{ij}^{(III)}(f_k)\right|$ at any value of the natural frequency, when a tested dynamic system fulfills the linear and time invariant assumptions and when noise and measurement errors do not exist. Hence, the ordinary coherence function, which is basically defined by Equation (5.2.31), is equal to 1.

$$\gamma_{ij}^2(f_k) = \frac{H_{ij}^{(I)}(f_k)}{H_{ij}^{(II)}(f_k)} = \frac{\left|G_{X_iX_j}(f_k)\right|^2}{G_{X_iX_i}(f_k)G_{X_jX_j}(f_k)} = 1 \tag{5.2.31}$$

In contrast, if both noises are present in the input and output responses, as illustrated in Figure 5.2.2, the corrupted FRFs can be derived as follows:

$$\hat{H}_{ij}^{(I)}(f_k) = \frac{\hat{G}_{X_i^E X_j^E}(f_k)}{\hat{G}_{X_i^E X_i^E}(f_k)} = H_{ij}^{(I)}(f_k)\left(1 + \frac{G_{MM}(f_k)}{G_{X_iX_i}(f_k)}\right)^{-1} \tag{5.2.32}$$

$$\hat{H}_{ij}^{(II)}(f_k) = \frac{\hat{G}_{X_j^E X_j^E}(f_k)}{\hat{G}_{X_i^E X_j^E}(f_k)} = H_{ij}^{(I)}(f_k)\left(1 + \frac{G_{NN}(f_k)}{G_{X_jX_j}(f_k)}\right) \tag{5.2.33}$$

$$\hat{H}_{ij}^{(III)}(f_k) = \sqrt{\frac{\hat{G}_{X_j^E X_j^E}(f_k)}{\hat{G}_{X_i^E X_i^E}(f_k)}} = \left|H_{ij}^{(I)}(f_k)\right| \sqrt{\frac{1 + \frac{G_{NN}(f_k)}{G_{X_jX_j}(f_k)}}{1 + \frac{G_{MM}(f_k)}{G_{X_iX_i}(f_k)}}} \tag{5.2.34}$$

in which

$$\hat{G}_{X_i^E X_i^E}(f_k) = G_{X_iX_i}(f_k) + G_{MM}(f_k) \tag{5.2.35}$$

$$\hat{G}_{X_j^E X_j^E}(f_k) = G_{X_jX_j}(f_k) + G_{NN}(f_k) \tag{5.2.36}$$

$$\hat{G}_{X_i^E X_j^E}(f_k) = G_{X_iX_j}(f_k) \tag{5.2.37}$$

assuming that the noise terms, $M(t)$ and $N(t)$, are uncorrelated with each other and with the input and output responses. It is manifest that the subsequent relations of Equations (5.2.38) and (5.2.39) can be established [He and Fu, 2001]:

$$\hat{H}_{ij}^{(I)}(f) \le \hat{H}_{ij}^{(III)}(f) \le \hat{H}_{ij}^{(II)}(f) \tag{5.2.38}$$

$$\hat{H}_{ij}^{(I)}(f) \le H_{ij}^{(I)}(f) \le \hat{H}_{ij}^{(II)}(f) \tag{5.2.39}$$

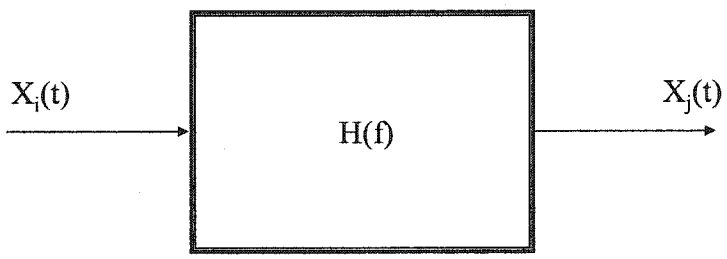

Figure 5.2.1 A Linear System with Single Input and Single Output

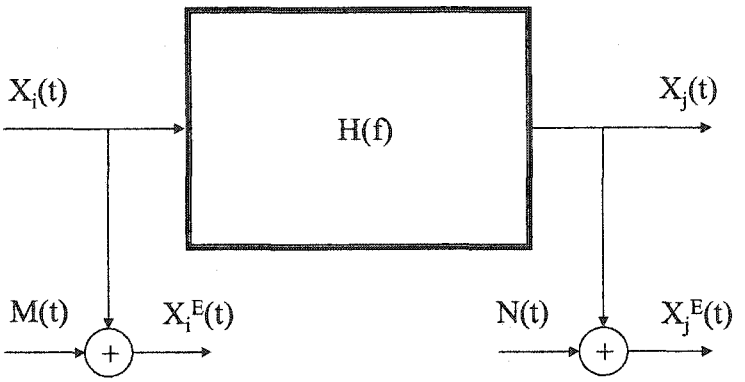

Figure 5.2.2 FRF Estimations with Input and Output Noises

5.3 Random Decrement Based Method

The random decrement (RD) technique, a time domain approach, was initially developed to form a characteristic signature, a RD signature of a dynamic system, based on the ensemble average of pre-selected sample segments from random response signals. Such a RD signature attempts to represent the free vibration response of the dynamic system, which can be used to continue with the parameter identification for the modal analysis. The fundamental definitions of the auto and cross RD signatures for the two ergodic stochastic responses, $X_i(t)$ and $X_j(t)$, are given by Equations (5.3.1) and (5.3.2).

$$\delta_{X_i X_i}(\tau) = E[X_i(t+\tau)|T_{X_i(t)}] \tag{5.3.1}$$

$$\delta_{X_j X_i}(\tau) = E[X_j(t+\tau)|T_{X_i(t)}] \tag{5.3.2}$$

where $E[|]$ denotes the conditional expectation operator and $T_{X_i(t)}$ designates a triggering condition, selected in a leading response $X_i(t)$ at a time of t.

The RD based method is introduced by combining the RD technique with the FFT based algorithms to investigate system dynamic characteristics through the output-only responses. Based on the Fourier transform of the RD signature as following:

$$\Delta_{X_j X_i}(f) = \int_{-\infty}^{\infty} \delta_{X_j X_i}(\tau) e^{-j2\pi f\tau} d\tau \tag{5.3.3}$$

, the RD based method transforms the formed RD signatures into the frequency domain in order to produce their spectral density functions. As a consequence of these spectral density functions, the definition of the FRFs for the RD signatures can be formulated as follows:

$$H_{ij}^{(I)}(f_k)|_{T_{X_i(t)}} = \frac{G^{RD}_{\Delta_{X_i X_i}\Delta_{X_j X_i}}(f_k)}{G^{RD}_{\Delta_{X_i X_i}\Delta_{X_i X_i}}(f_k)} \tag{5.3.4}$$

$$H_{ij}^{(II)}(f_k)|_{T_{X_i(t)}} = \frac{G^{RD}_{\Delta_{X_j X_i}\Delta_{X_j X_i}}(f_k)}{G^{RD}_{\Delta_{X_j X_i}\Delta_{X_i X_i}}(f_k)} \tag{5.3.5}$$

$$H_{ij}^{(III)}(f_k)|_{T_{X_i(t)}} = \sqrt{\frac{G^{RD}_{\Delta_{X_j X_i}\Delta_{X_j X_i}}(f_k)}{G^{RD}_{\Delta_{X_i X_i}\Delta_{X_i X_i}}(f_k)}} \tag{5.3.6}$$

$G^{RD}_{\Delta_{X_i X_i}\Delta_{X_i X_i}}(f)$ and $G^{RD}_{\Delta_{X_j X_i}\Delta_{X_j X_i}}(f)$ are the auto-spectral density functions of the RD signatures for $\delta_{X_i X_i}(\tau)$ and $\delta_{X_j X_i}(\tau)$, respectively, and $G^{RD}_{\Delta_{X_i X_i}\Delta_{X_j X_i}}(f)$ and $G^{RD}_{\Delta_{X_j X_i}\Delta_{X_i X_i}}(f)$ are the cross-spectral density functions between the RD signatures, $\delta_{X_i X_i}(\tau)$ and $\delta_{X_j X_i}(\tau)$.

As mentioned in the previous studies, the RD acceleration signatures are affected from the RD signatures of the forcing functions applied on the dynamic system. The use of the RD acceleration signatures may cause a biased estimation of the system dynamic properties especially for the time domain system identification techniques, relying on free vibration responses. Nonetheless, it is not quite tractable to distinguish the RD forcing function signatures, without knowledge of their characteristics, from the RD acceleration signatures in order to yield the free vibration responses of the dynamic system. With this in mind, the emphasis in this study is therefore addressed on verifying the applicability of the RD based method to evaluate the system parameters from the acceleration responses.

It has been indicated that the RD acceleration signature essentially consists of two portions contributed from the acceleration response of a dynamic system and the forcing function acting on the dynamic system. As a consequence, it follows that the subsequent expressions are allowed to give:

$$\delta_{\ddot{X}_i\ddot{X}_i}(\tau) = \delta^R_{\ddot{X}_i\ddot{X}_i}(\tau) + \delta^L_{\ddot{X}_i\ddot{X}_i}(\tau) \tag{5.3.7}$$

$$\delta_{\ddot{X}_j\ddot{X}_i}(\tau) = \delta^R_{\ddot{X}_j\ddot{X}_i}(\tau) + \delta^L_{\ddot{X}_j\ddot{X}_i}(\tau) \tag{5.3.8}$$

in which the superscripts of the RD acceleration signatures, R and L, naturally correspond to the non-forced acceleration response portion and the forcing function portion of the RD signatures, respectively.

At this stage, it is intended to transform Equations (5.3.7) and (5.3.8) into their frequency domain as follows:

$$\Delta_{\ddot{X}_i\ddot{X}_i}(f) = \Delta^R_{\ddot{X}_i\ddot{X}_i}(f) + \Delta^L_{\ddot{X}_i\ddot{X}_i}(f) \tag{5.3.9}$$

$$\Delta_{\ddot{X}_j\ddot{X}_i}(f) = \Delta^R_{\ddot{X}_j\ddot{X}_i}(f) + \Delta^L_{\ddot{X}_j\ddot{X}_i}(f) \tag{5.3.10}$$

Correspondingly, the use of Equations (5.2.28-30) can give rise to the auto-spectral density function, $G^{RD}_{\Delta_{\ddot{X}_i\ddot{X}_i}\Delta_{\ddot{X}_i\ddot{X}_i}}(f)$ and $G^{RD}_{\Delta_{\ddot{X}_j\ddot{X}_i}\Delta_{\ddot{X}_j\ddot{X}_i}}(f)$, and the cross-spectral density function $G^{RD}_{\Delta_{\ddot{X}_i\ddot{X}_i}\Delta_{\ddot{X}_j\ddot{X}_i}}(f)$ of $\Delta_{\ddot{X}_i\ddot{X}_i}(f)$ and $\Delta_{\ddot{X}_j\ddot{X}_i}(f)$ as follows:

$$G^{RD}_{\Delta_{\ddot{X}_i\ddot{X}_i}\Delta_{\ddot{X}_i\ddot{X}_i}}(f)=\frac{2}{T}\left[\Delta^{R}_{\ddot{X}_i\ddot{X}_i}(f)+\Delta^{L}_{\ddot{X}_i\ddot{X}_i}(f)\right]^2 \tag{5.3.11}$$

$$G^{RD}_{\Delta_{\ddot{X}_j\ddot{X}_i}\Delta_{\ddot{X}_j\ddot{X}_i}}(f)=\frac{2}{T}\left[\Delta^{R}_{\ddot{X}_j\ddot{X}_i}(f)+\Delta^{L}_{\ddot{X}_j\ddot{X}_i}(f)\right]^2 \tag{5.3.12}$$

$$\begin{aligned} G^{RD}_{\Delta_{\ddot{X}_i\ddot{X}_i}\Delta_{\ddot{X}_j\ddot{X}_i}}(f)&=\frac{2}{T}\left[\Delta^{R}_{\ddot{X}_i\ddot{X}_i}(f)+\Delta^{L}_{\ddot{X}_i\ddot{X}_i}(f)\right]^*\left[\Delta^{R}_{\ddot{X}_j\ddot{X}_i}(f)+\Delta^{L}_{\ddot{X}_j\ddot{X}_i}(f)\right] \\ &=G^{RD}_{\Delta_{\ddot{X}_j\ddot{X}_i}\Delta_{\ddot{X}_i\ddot{X}_i}}{}^*(f) \end{aligned} \tag{5.3.13}$$

Upon substituting the spectral density functions in Equations (5.3.11-13) into Equations (5.3.4-6), it comes out that the FRFs of the RD acceleration signatures become:

$$\begin{aligned} H^{(I)}_{ij}(f_k)|_{T_{\ddot{X}_i(t)}}&=\frac{G^{RD}_{\Delta_{\ddot{X}_i\ddot{X}_i}\Delta_{\ddot{X}_j\ddot{X}_i}}(f_k)}{G^{RD}_{\Delta_{\ddot{X}_i\ddot{X}_i}\Delta_{\ddot{X}_i\ddot{X}_i}}(f_k)} \\ &=\frac{\Delta^{R}_{\ddot{X}_j\ddot{X}_i}(f_k)+\Delta^{L}_{\ddot{X}_j\ddot{X}_i}(f_k)}{\Delta^{R}_{\ddot{X}_i\ddot{X}_i}(f_k)+\Delta^{L}_{\ddot{X}_i\ddot{X}_i}(f_k)}=H_{ij}(f_k)\frac{1+\dfrac{\Delta^{L}_{\ddot{X}_j\ddot{X}_i}(f_k)}{\Delta^{R}_{\ddot{X}_j\ddot{X}_i}(f_k)}}{1+\dfrac{\Delta^{L}_{\ddot{X}_i\ddot{X}_i}(f_k)}{\Delta^{R}_{\ddot{X}_i\ddot{X}_i}(f_k)}} \end{aligned} \tag{5.3.14}$$

$$\begin{aligned} H^{(II)}_{ij}(f_k)|_{T_{\ddot{X}_i(t)}}&=\frac{G^{RD}_{\Delta_{\ddot{X}_j\ddot{X}_i}\Delta_{\ddot{X}_j\ddot{X}_i}}(f_k)}{G^{RD}_{\Delta_{\ddot{X}_j\ddot{X}_i}\Delta_{\ddot{X}_i\ddot{X}_i}}(f_k)} \\ &=\frac{\Delta^{R}_{\ddot{X}_j\ddot{X}_i}(f_k)+\Delta^{L}_{\ddot{X}_j\ddot{X}_i}(f_k)}{\Delta^{R}_{\ddot{X}_i\ddot{X}_i}(f_k)+\Delta^{L}_{\ddot{X}_i\ddot{X}_i}(f_k)}=H_{ij}(f_k)\frac{1+\dfrac{\Delta^{L}_{\ddot{X}_j\ddot{X}_i}(f_k)}{\Delta^{R}_{\ddot{X}_j\ddot{X}_i}(f_k)}}{1+\dfrac{\Delta^{L}_{\ddot{X}_i\ddot{X}_i}(f_k)}{\Delta^{R}_{\ddot{X}_i\ddot{X}_i}(f_k)}} \end{aligned} \tag{5.3.15}$$

$$H_{ij}^{(III)}(f_k)|_{T_{\ddot{X}_i(t)}} = \sqrt{\frac{G^{RD}_{\Delta_{\ddot{X}_j\ddot{X}_i}\Delta_{\ddot{X}_j\ddot{X}_i}}(f_k)}{G^{RD}_{\Delta_{\ddot{X}_i\ddot{X}_i}\Delta_{\ddot{X}_i\ddot{X}_i}}(f_k)}}$$

$$= \left|\frac{\Delta^R_{\ddot{X}_j\ddot{X}_i}(f_k) + \Delta^L_{\ddot{X}_j\ddot{X}_i}(f_k)}{\Delta^R_{\ddot{X}_i\ddot{X}_i}(f_k) + \Delta^L_{\ddot{X}_i\ddot{X}_i}(f_k)}\right| = \left|H_{ij}(f_k)\frac{1+\dfrac{\Delta^L_{\ddot{X}_j\ddot{X}_i}(f_k)}{\Delta^R_{\ddot{X}_j\ddot{X}_i}(f_k)}}{1+\dfrac{\Delta^L_{\ddot{X}_i\ddot{X}_i}(f_k)}{\Delta^R_{\ddot{X}_i\ddot{X}_i}(f_k)}}\right| \quad (5.3.16)$$

in which

$$H_{ij}(f_k) = \frac{\Delta^R_{\ddot{X}_j\ddot{X}_i}(f_k)}{\Delta^R_{\ddot{X}_i\ddot{X}_i}(f_k)} \quad (5.3.17)$$

Paralleling the development of Equations (5.3.15-17), the other theoretical derivation is intended to link the FRFs of the RD signatures in terms of the spectral density functions of the original responses. Since the RD signatures are theoretically proportional to the correlation functions of their own responses, Equations (5.3.9) and (5.3.10) may be rewritten in the following formations:

$$\delta_{\ddot{X}_i\ddot{X}_i}(\tau) = C\left[R^R_{\ddot{X}_i\ddot{X}_i}(\tau) + R^L_{\ddot{X}_i\ddot{X}_i}(\tau)\right] \quad (5.3.18)$$

$$\delta_{\ddot{X}_j\ddot{X}_i}(\tau) = C\left[R^R_{\ddot{X}_i\ddot{X}_j}(\tau) + R^L_{\ddot{X}_i\ddot{X}_j}(\tau)\right] \quad (5.3.19)$$

in which C is a common proportional factor and $\ddot{X}_i(t)$ is assigned to be the leading response for the acceleration responses, $\ddot{X}_i(t)$ and $\ddot{X}_j(t)$.

Similarly, Equations (5.3.18) and (5.3.19) are converted into their frequency domain formulations:

$$\Delta_{\ddot{X}_i\ddot{X}_i}(f) = \int_{-\infty}^{\infty} C\left[R^R_{\ddot{X}_i\ddot{X}_i}(\tau) + R^L_{\ddot{X}_i\ddot{X}_i}(\tau)\right]e^{-2\pi f\tau}d\tau = \frac{C}{2}\left[G^R_{\ddot{X}_i\ddot{X}_i}(f) + G^L_{\ddot{X}_i\ddot{X}_i}(f)\right] \quad (5.3.20)$$

$$\Delta_{\ddot{X}_j\ddot{X}_i}(f) = \int_{-\infty}^{\infty} C\left[R^R_{\ddot{X}_i\ddot{X}_j}(\tau) + R^L_{\ddot{X}_i\ddot{X}_j}(\tau)\right]e^{-2\pi f\tau}d\tau = \frac{C}{2}\left[G^R_{\ddot{X}_i\ddot{X}_j}(f) + G^L_{\ddot{X}_i\ddot{X}_j}(f)\right] \quad (5.3.21)$$

which are based on the definition of Equation (5.3.3). The spectral density functions of $\Delta_{\ddot{X}_i\ddot{X}_i}(f)$ and $\Delta_{\ddot{X}_i\ddot{X}_j}(f)$ are calculated in Equations (5.3.22-24) in order to formulate the FRFs in Equations (5.3.25-27).

$$G^{RD}_{\Delta_{\ddot{X}_i\ddot{X}_i}\Delta_{\ddot{X}_i\ddot{X}_i}}(f) = \frac{C^2}{T}\left[\left[G^R_{\ddot{X}_i\ddot{X}_i}(f) + G^L_{\ddot{X}_i\ddot{X}_i}(f)\right]\right]^2 \tag{5.3.22}$$

$$G^{RD}_{\Delta_{\ddot{X}_j\ddot{X}_i}\Delta_{\ddot{X}_j\ddot{X}_i}}(f) = \frac{C^2}{T}\left[\left[G^R_{\ddot{X}_i\ddot{X}_j}(f) + G^L_{\ddot{X}_i\ddot{X}_j}(f)\right]\right]^2 \tag{5.3.23}$$

$$\begin{aligned} G^{RD}_{\Delta_{\ddot{X}_i\ddot{X}_i}\Delta_{\ddot{X}_j\ddot{X}_i}}(f) &= \frac{C^2}{T}\left[\left(G^R_{\ddot{X}_i\ddot{X}_i}(f) + G^L_{\ddot{X}_i\ddot{X}_i}(f)\right)^*\left(G^R_{\ddot{X}_i\ddot{X}_j}(f) + G^L_{\ddot{X}_i\ddot{X}_j}(f)\right)\right] \\ &= G^{RD}_{\Delta_{\ddot{X}_j\ddot{X}_i}\Delta_{\ddot{X}_i\ddot{X}_i}}{}^*(f) \end{aligned} \tag{5.3.24}$$

$$\begin{aligned} H^{(I)}_{ij}(f_k)|_{T_{\ddot{X}_i(t)}} &= \frac{G^{RD}_{\Delta_{\ddot{X}_i\ddot{X}_i}\Delta_{\ddot{X}_j\ddot{X}_i}}(f_k)}{G^{RD}_{\Delta_{\ddot{X}_i\ddot{X}_i}\Delta_{\ddot{X}_i\ddot{X}_i}}(f_k)} \\ &= \frac{G^R_{\ddot{X}_i\ddot{X}_j}(f_k) + G^L_{\ddot{X}_i\ddot{X}_j}(f_k)}{G^R_{\ddot{X}_i\ddot{X}_i}(f_k) + G^L_{\ddot{X}_i\ddot{X}_i}(f_k)} = H^{(I)}_{ij}(f_k)\frac{1+\dfrac{G^L_{\ddot{X}_i\ddot{X}_j}(f_k)}{G^R_{\ddot{X}_i\ddot{X}_j}(f_k)}}{1+\dfrac{G^L_{\ddot{X}_i\ddot{X}_i}(f_k)}{G^R_{\ddot{X}_i\ddot{X}_i}(f_k)}} \end{aligned} \tag{5.3.25}$$

$$\begin{aligned} H^{(II)}_{ij}(f_k)|_{T_{\ddot{X}_i(t)}} &= \frac{G^{RD}_{\Delta_{\ddot{X}_j\ddot{X}_i}\Delta_{\ddot{X}_j\ddot{X}_i}}(f_k)}{G^{RD}_{\Delta_{\ddot{X}_j\ddot{X}_i}\Delta_{\ddot{X}_i\ddot{X}_i}}(f_k)} \\ &= \frac{G^R_{\ddot{X}_i\ddot{X}_j}(f_k) + G^L_{\ddot{X}_i\ddot{X}_j}(f_k)}{G^R_{\ddot{X}_i\ddot{X}_i}(f_k) + G^L_{\ddot{X}_i\ddot{X}_i}(f_k)} = H^{(I)}_{ij}(f_k)\frac{1+\dfrac{G^L_{\ddot{X}_i\ddot{X}_j}(f_k)}{G^R_{\ddot{X}_i\ddot{X}_j}(f_k)}}{1+\dfrac{G^L_{\ddot{X}_i\ddot{X}_i}(f_k)}{G^R_{\ddot{X}_i\ddot{X}_i}(f_k)}} \end{aligned} \tag{5.3.26}$$

$$H_{ij}^{(III)}(f_k)|_{T_{\ddot{X}_i(t)}} = \sqrt{\frac{G^{RD}_{\Delta_{\ddot{X}_j\ddot{X}_i}\Delta_{\ddot{X}_j\ddot{X}_i}}(f_k)}{G^{RD}_{\Delta_{\ddot{X}_i\ddot{X}_i}\Delta_{\ddot{X}_i\ddot{X}_i}}(f_k)}}$$

$$= \left|\frac{G^{R}_{\ddot{X}_i\ddot{X}_j}(f_k) + G^{L}_{\ddot{X}_i\ddot{X}_j}(f_k)}{G^{R}_{\ddot{X}_i\ddot{X}_i}(f_k) + G^{L}_{\ddot{X}_i\ddot{X}_i}(f_k)}\right| = \left|H_{ij}^{(I)}(f_k)\frac{1+\dfrac{G^{L}_{\ddot{X}_i\ddot{X}_j}(f_k)}{G^{R}_{\ddot{X}_i\ddot{X}_j}(f_k)}}{1+\dfrac{G^{L}_{\ddot{X}_i\ddot{X}_i}(f_k)}{G^{R}_{\ddot{X}_i\ddot{X}_i}(f_k)}}\right| \tag{5.3.27}$$

in which

$$H_{ij}^{(I)}(f_k) = \frac{G^{R}_{\ddot{X}_i\ddot{X}_j}(f_k)}{G^{R}_{\ddot{X}_i\ddot{X}_i}(f_k)} \tag{5.3.28}$$

Equations (5.3.14-16) or (5.3.25-27) provide an appreciation on the application of the FRFs of the RD acceleration signatures. First, it is found that the ordinary coherence function defined by Equation (5.2.31) is equal to 1 for each frequency component, in that an identity relation among the FRFs is obviously established as following:

$$\left|H_{ij}^{(I)}(f_k)|_{T_{\ddot{X}_i(t)}}\right| = \left|H_{ij}^{(II)}(f_k)|_{T_{\ddot{X}_i(t)}}\right| = \left|H_{ij}^{(III)}(f_k)|_{T_{\ddot{X}_i(t)}}\right| \tag{5.3.29}$$

The dominant natural frequencies of a dynamic system cannot be determined using the ordinary coherence function. In addition, Equation (5.3.29) implies that the true FRFs of the dynamic system under consideration may be not guaranteed to obtain from Equations (5.3.14-16) or (5.3.23-27), if the following relations are not satisfied.

$$\frac{\Delta^{L}_{\ddot{X}_i\ddot{X}_i}(f_k)}{\Delta^{F}_{\ddot{X}_i\ddot{X}_i}(f_k)} = \frac{\Delta^{L}_{\ddot{X}_j\ddot{X}_i}(f_k)}{\Delta^{F}_{\ddot{X}_j\ddot{X}_i}(f_k)} \tag{5.3.30}$$

$$\frac{G^{L}_{\ddot{X}_i\ddot{X}_i}(f_k)}{G^{F}_{\ddot{X}_i\ddot{X}_i}(f_k)} = \frac{G^{L}_{\ddot{X}_j\ddot{X}_i}(f_k)}{G^{F}_{\ddot{X}_j\ddot{X}_i}(f_k)} \tag{5.3.31}$$

Without the influence of the forcing terms, it follows immediately that the FRFs of the RD signatures are scaled versions of the true FRFs for the dynamic system. It means that

the measurement of the displacement or velocity responses for the RD signatures should be a reliable alternative for the estimates of the FRFs, without the added complexities of the RD acceleration signatures.

Whether or not the dynamic properties of a system are possible to be determined by the FRFs of the RD acceleration signatures is further investigated. The theoretical derivation for the FRFs of the RD signatures stems from the conceptual viewpoint of the FRF approach for the acceleration responses. Of course, the justification of such a derivation is amenable to follow the same assumptions of the FRF approach, which are summarized by:

1. Each stochastic process is Gaussian;
2. The dynamic system behaves linearly;
3. Vibration modes of interest are significantly excited;
4. Vibration modes are well separated and lightly damped.

From a different perspective on the feature of the normal mode superposition, the RD acceleration signatures can be obtained by the summation of the RD signatures of the individual normal modes as follows:

$$\delta_{\ddot{X}\ddot{X}_i}(t) = \varphi_1 \delta_{\ddot{q}_1\ddot{q}_i}(t) + \varphi_2 \delta_{\ddot{q}_2\ddot{q}_i}(t) + \cdots + \varphi_n \delta_{\ddot{q}_n\ddot{q}_i}(t) \tag{5.3.32}$$

or

$$\begin{bmatrix} \delta_{\ddot{X}_1\ddot{X}_i}(t) \\ \delta_{\ddot{X}_2\ddot{X}_i}(t) \\ \vdots \\ \delta_{\ddot{X}_n\ddot{X}_i}(t) \end{bmatrix} = \begin{bmatrix} \phi_{11} & \phi_{12} & \cdots & \phi_{1n} \\ \phi_{21} & \phi_{22} & \ddots & \phi_{2n} \\ \vdots & \ddots & \ddots & \vdots \\ \phi_{n1} & \phi_{n2} & \cdots & \phi_{nn} \end{bmatrix} \begin{bmatrix} \delta_{\ddot{q}_1\ddot{q}_i}(t) \\ \delta_{\ddot{q}_2\ddot{q}_i}(t) \\ \vdots \\ \delta_{\ddot{q}_n\ddot{q}_i}(t) \end{bmatrix} \tag{5.3.33}$$

The derivation for the RD signatures of the individual normal mode in Equation (5.3.32) or (5.3.33) begins from the substitution of variables, $t' = t + \tau$ and $\tau = \varepsilon + t'$ in Equation (5.2.12). Therefore, it turns out that Equation (5.2.12) becomes:

$$\ddot{q}_j(t'+\tau) = \int_{-\infty}^{\tau} h_j^a(\tau-\varepsilon)F_j(t'+\varepsilon)d\varepsilon \tag{5.3.34}$$

Subsequently, taking the conditional expectation of Equation (5.3.34) with a triggering condition $T_{q_i(t')}$ yields:

$$E[\ddot{q}_j(t'+\tau)|T_{\ddot{q}_i(t')}] = \int_{-\infty}^{\tau} h_j^a(\tau-\varepsilon)E[F_j(t'+\varepsilon)|T_{\ddot{q}_i(t')}]d\varepsilon \tag{5.3.35}$$

In fact, Equation (5.3.35) satisfies the definition of the RD signatures, which becomes:

$$\delta_{\ddot{q}_j\ddot{q}_i}(\tau) = \int_{-\infty}^{\tau} h_j^a(\tau-\varepsilon)\delta_{F_j\ddot{q}_i}(\varepsilon)d\varepsilon \tag{5.3.36}$$

The use of Equation (5.3.32) or (5.3.33) and Equation (5.3.36) in the frequency domain gives rise to Equation (5.3.37).

$$\begin{aligned}\Delta_{\ddot{X}\ddot{X}_i}(f) &= \varphi_1\Delta_{\ddot{q}_1\ddot{q}_i}(f) + \varphi_2\Delta_{\ddot{q}_2\ddot{q}_i}(f) + \cdots + \varphi_n\Delta_{\ddot{q}_n\ddot{q}_i}(f) \\ &= \varphi_1 H_1^a(f)\Delta_{F_1\ddot{q}_i}(f) + \varphi_2 H_2^a(f)\Delta_{F_2\ddot{q}_i}(f) + \cdots + \varphi_n H_n^a(f)\Delta_{F_n\ddot{q}_i}(f)\end{aligned} \tag{5.3.37}$$

As a result, the i^{th} and j^{th} RD signatures from Equation (5.3.37) are given by:

$$\Delta_{\ddot{X}_i\ddot{X}_i}(f) = \phi_{i1}H_1^a(f)\Delta_{F_1\ddot{q}_i}(f) + \phi_{i2}H_2^a(f)\Delta_{F_2\ddot{q}_i}(f) + \cdots + \phi_{in}H_n^a(f)\Delta_{F_n\ddot{q}_i}(f) \tag{5.3.38}$$

$$\Delta_{\ddot{X}_j\ddot{X}_i}(f) = \phi_{j1}H_1^a(f)\Delta_{F_1\ddot{q}_i}(f) + \phi_{j2}H_2^a(f)\Delta_{F_2\ddot{q}_i}(f) + \cdots + \phi_{jn}H_n^a(f)\Delta_{F_n\ddot{q}_i}(f) \tag{5.3.39}$$

Likewise, the modal ratio between the i^{th} and j^{th} RD signatures at the k^{th} natural frequency f_k can be approximately expressed as:

$$\frac{\Delta_{\ddot{X}_j\ddot{X}_i}(f_k)}{\Delta_{\ddot{X}_i\ddot{X}_i}(f_k)} = \frac{\phi_{jk}H_k^a(f_k)\Delta_{F_k\ddot{q}_i}(f_k)}{\phi_{ik}H_k^a(f_k)\Delta_{F_k\ddot{q}_i}(f_k)} = \frac{\phi_{jk}}{\phi_{ik}} \tag{5.3.40}$$

The FRFs of the RD acceleration signatures can therefore be defined by the spectral density functions as follows:

$$H_{ij}^{(I)}(f_k)=\frac{G_{\Delta_{\dot{X}_i\dot{X}_i}\Delta_{\dot{X}_j\dot{X}_i}}(f_k)}{G_{\Delta_{\dot{X}_i\dot{X}_i}\Delta_{\dot{X}_i\dot{X}_i}}(f_k)}=\frac{\phi_{jk}}{\phi_{ik}} \tag{5.3.41}$$

$$H_{ij}^{(II)}(f_k)=\frac{G_{\Delta_{\dot{X}_j\dot{X}_i}\Delta_{\dot{X}_j\dot{X}_i}}(f_k)}{G_{\Delta_{\dot{X}_i\dot{X}_i}\Delta_{\dot{X}_j\dot{X}_i}}(f_k)}=\frac{\phi_{jk}}{\phi_{ik}} \tag{5.3.42}$$

$$H_{ij}^{(III)}(f_k)=\sqrt{\frac{G_{\Delta_{\dot{X}_j\dot{X}_i}\Delta_{\dot{X}_j\dot{X}_i}}(f_k)}{G_{\Delta_{\dot{X}_i\dot{X}_i}\Delta_{\dot{X}_i\dot{X}_i}}(f_k)}}=\frac{\phi_{jk}}{\phi_{ik}} \tag{5.3.43}$$

This completes the theoretical developments of the FRFs of the RD acceleration signatures. The following numerical simulations are presented to foster the theoretical developments of the RD based method and the FRF approach for the acceleration responses. Among these simulations, two simulated wind forces are particularly used to realize the applicability of the RD based method in practical engineering projects.

5.4 Numerical Verifications

5.4.1 2DOF Dynamic System with Two Forcing Functions

To verify the applicability of the RD based method for the acceleration responses, numerical simulations of a discrete 2DOF dynamic system with the non-proportional damping, illustrated in Figure 5.4.1, were first carried out. The equations of motion for the 2DOF dynamic system are given by Equation (5.4.1) in which the linear and time-invariant assumptions are fulfilled.

$$\begin{bmatrix}1 & 0\\ 0 & 1\end{bmatrix}\begin{Bmatrix}\ddot{X}_1\\ \ddot{X}_2\end{Bmatrix}+\begin{bmatrix}0.04 & 0.01\\ 0.01 & 0.03\end{bmatrix}\begin{Bmatrix}\dot{X}_1\\ \dot{X}_2\end{Bmatrix}+\begin{bmatrix}2 & -1\\ -1 & 1\end{bmatrix}\begin{Bmatrix}X_1\\ X_2\end{Bmatrix}=\begin{Bmatrix}f_1(t)\\ f_2(t)\end{Bmatrix} \tag{5.4.1}$$

The theoretical modal parameters of the 2DOF dynamic system are listed in Table 5.4.1. Gaussian white noise excitations and two distinct types of wind forces were individually simulated for the forcing functions, $f_1(t)$ and $f_2(t)$, in Equation (5.4.1). The time intervals for the Gaussian white noise and the simulated wind forces are 0.02 and 0.2 seconds, respectively. Time series of 8000 seconds for each forcing function were generated and then applied on each mass of the dynamic system. The Newmark-β numerical integration scheme was used in this chapter to analyze the acceleration responses of the dynamic system. The resulting responses of 7985vseconds are adopted after the discard of their initial part to avoid non-stationary transient responses.

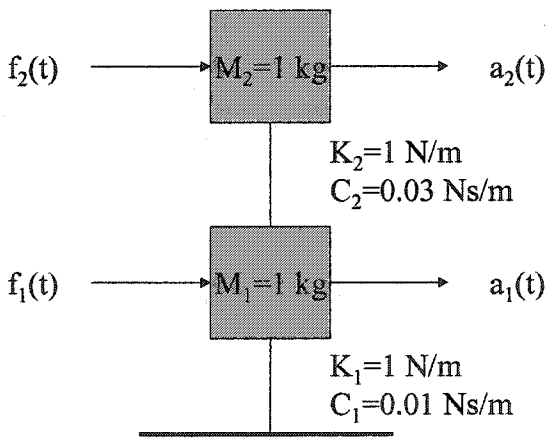

Figure 5.4.1 2DOF Dynamic System

Table 5.4.1 Theoretical Modal Parameters of a 2DOF Dynamic System

	Damped natural frequency	Damping ratio	$\lvert\phi_{1k}\rvert$	$\lvert\phi_{2k}\rvert$	$\angle\phi_{1k}$	$\angle\phi_{2k}$
Mode 1	0.0983 Hz	3.37 %	1	1.61753	0°	0.427°
Mode 2	0.2575 Hz	0.87 %	1	0.61817	0°	179.9°

The estimated RD signatures were pursued from such resulting responses by selecting a cross level in the leading response as the triggering condition of each sample segment, which was used throughout this chapter. The leading response was assigned to the location 1 of the two responses to form the RD signatures, corresponding to RDS1. Besides, 600, 150 and 75 seconds were individually specified to investigate the potential effect of the superimposed segment length required for the formation of the estimated RD signatures. Figures 5.4.2-4 illustrate the RD acceleration signatures from the three cases of the simulated forces, i.e. Gaussian white noises, alongwind forces and crosswind forces. To emphasize the significant influence of the input forces, the first point of each RD signature was particularly marked by a square in Figures 5.4.2-4, even though each RD signature looks like a free vibration response.

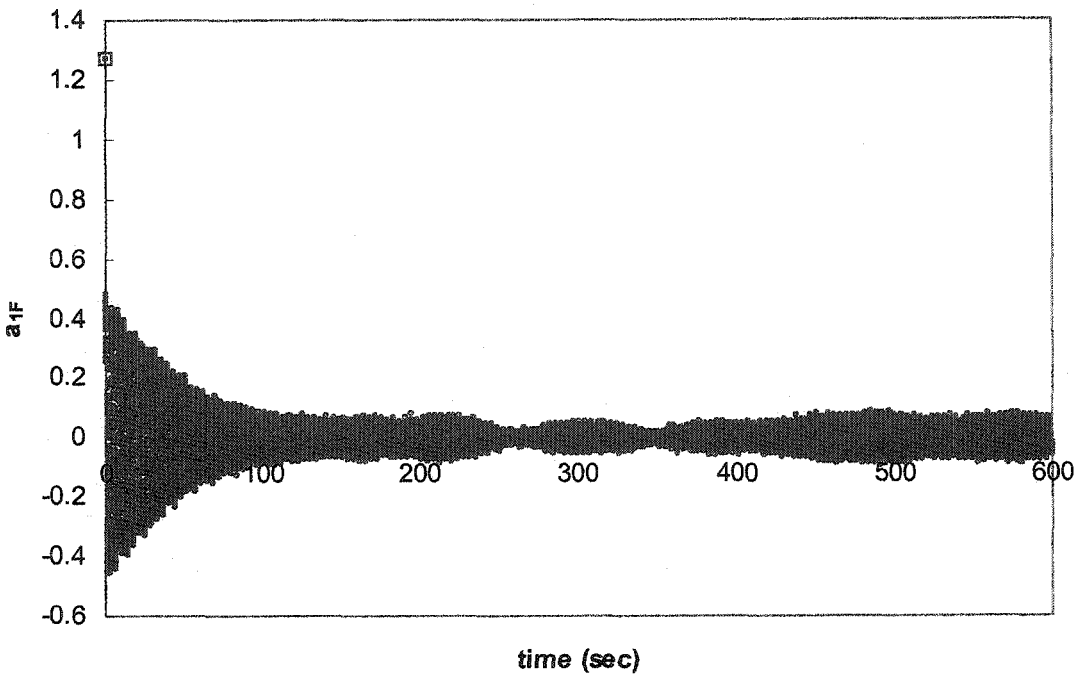

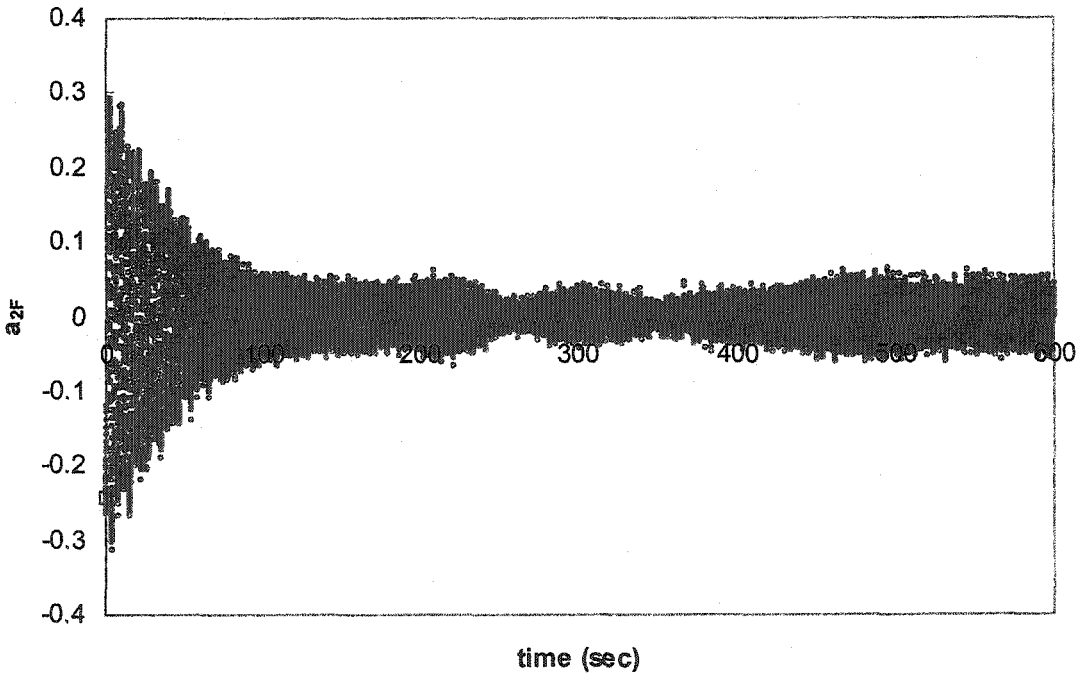

Figure 5.4.2 (a) 600 seconds

Figure 5.4.2 2DOF RD Acceleration Signatures to White Noise Excitations

○ RD Signatures; □ First Point of RD Signatures

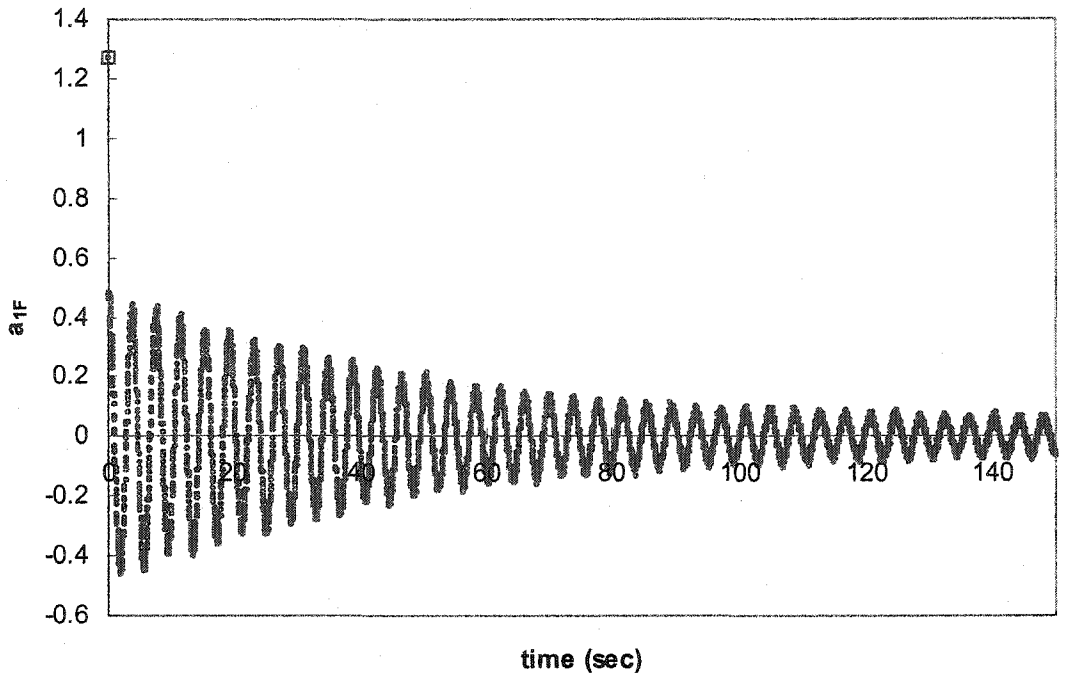

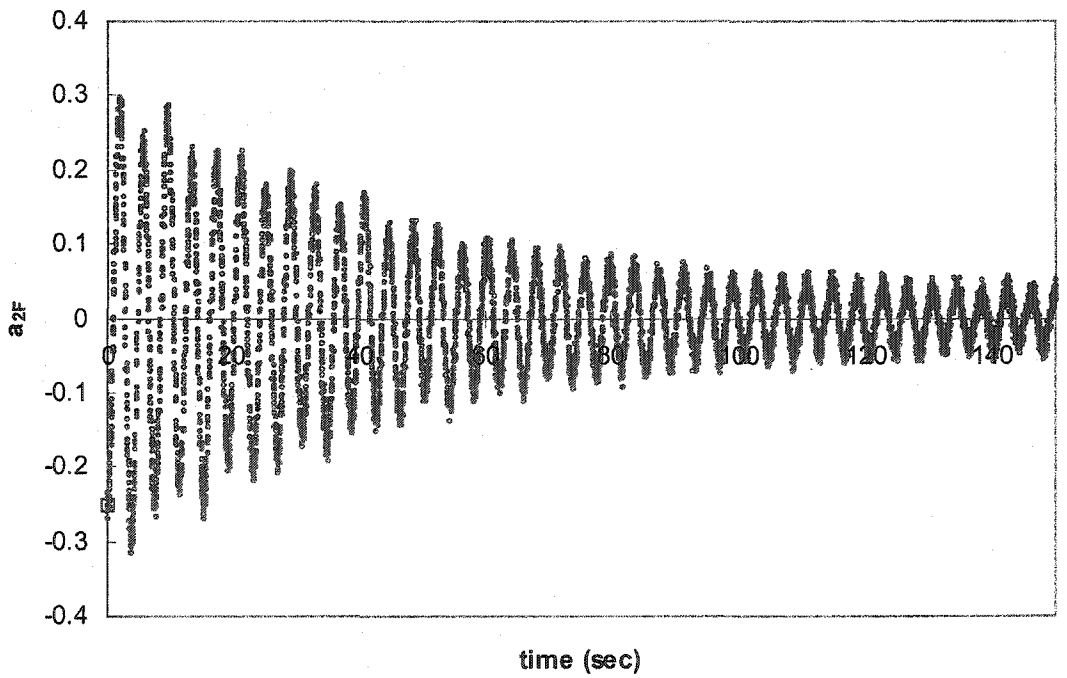

Figure 5.4.2 (b) 150 seconds

○ RD Signatures; □ First Point of RD Signatures

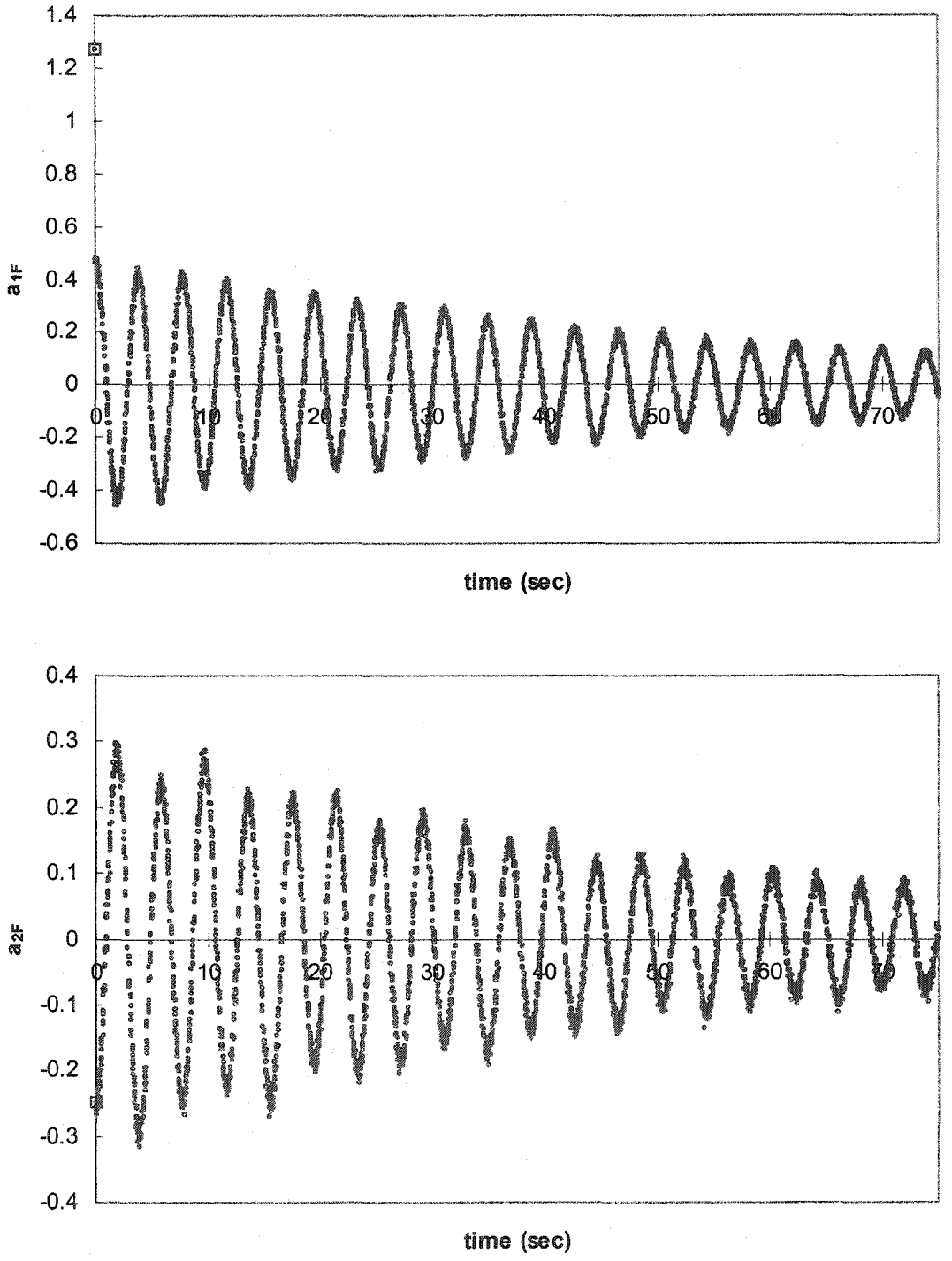

Figure 5.4.2 (c) 75 seconds

○ RD Signatures; □ First Point of RD Signatures

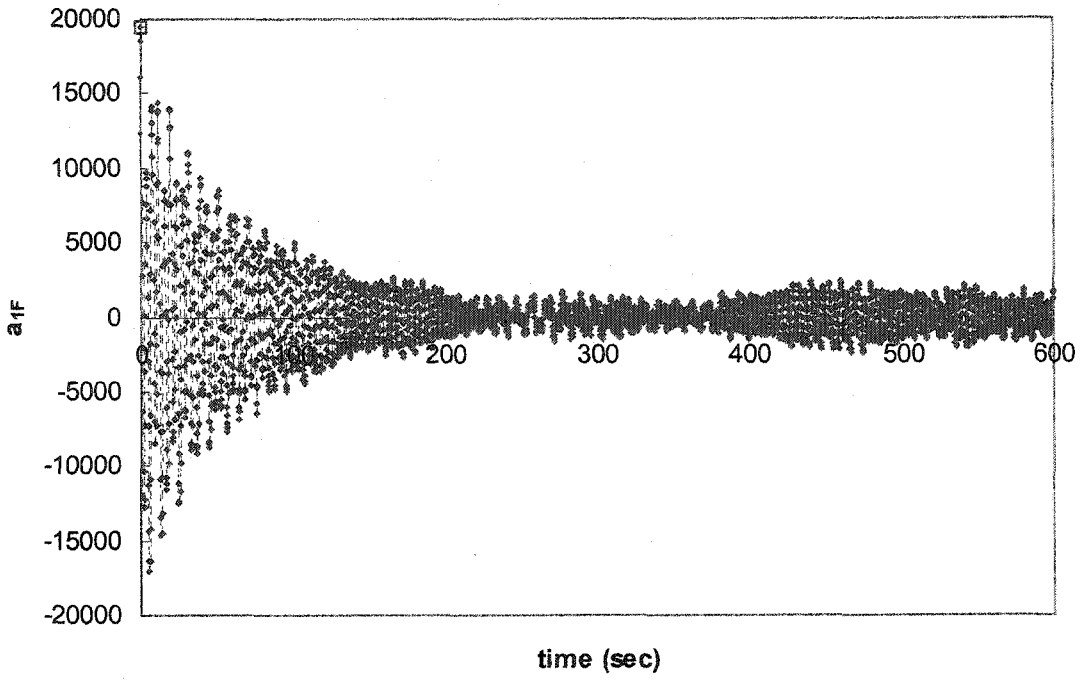

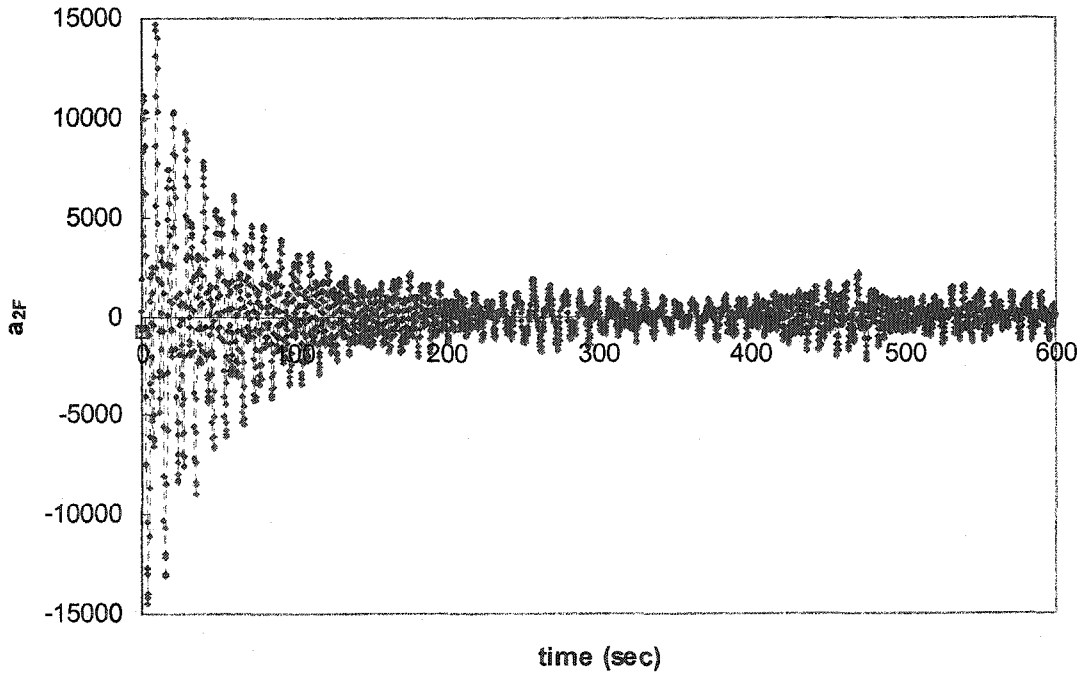

Figure 5.4.3 (a) 600 seconds

Figure 5.4.3 2DOF RD Acceleration Signatures to Simulated Alongwind Forces

-◊--◊- RD Signatures; □ First Point of RD Signatures

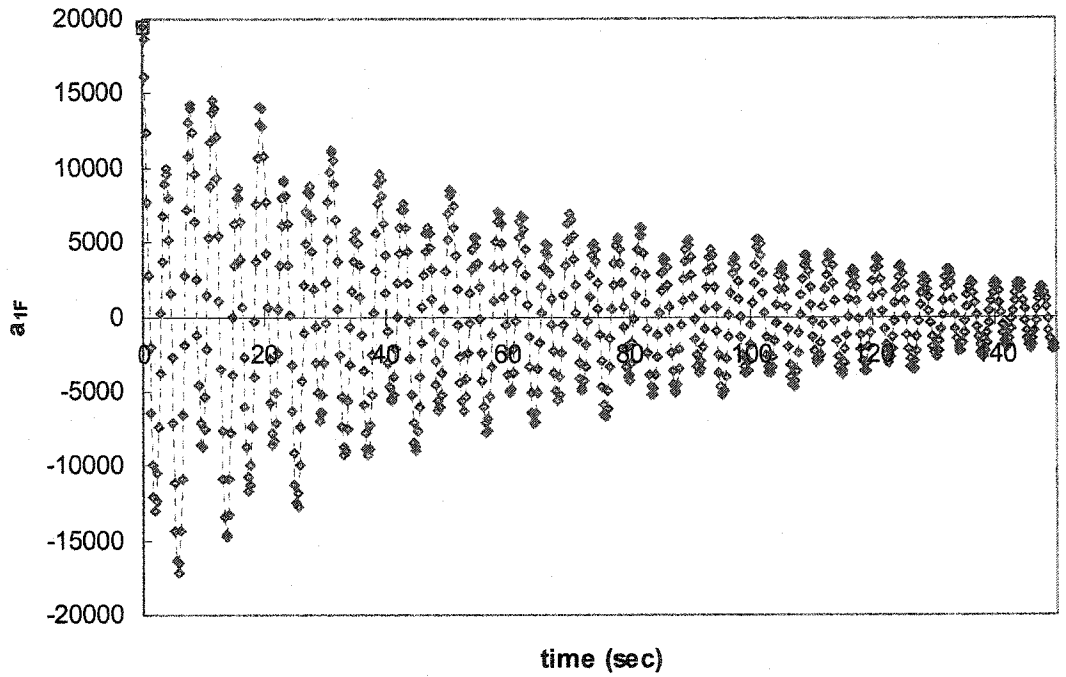

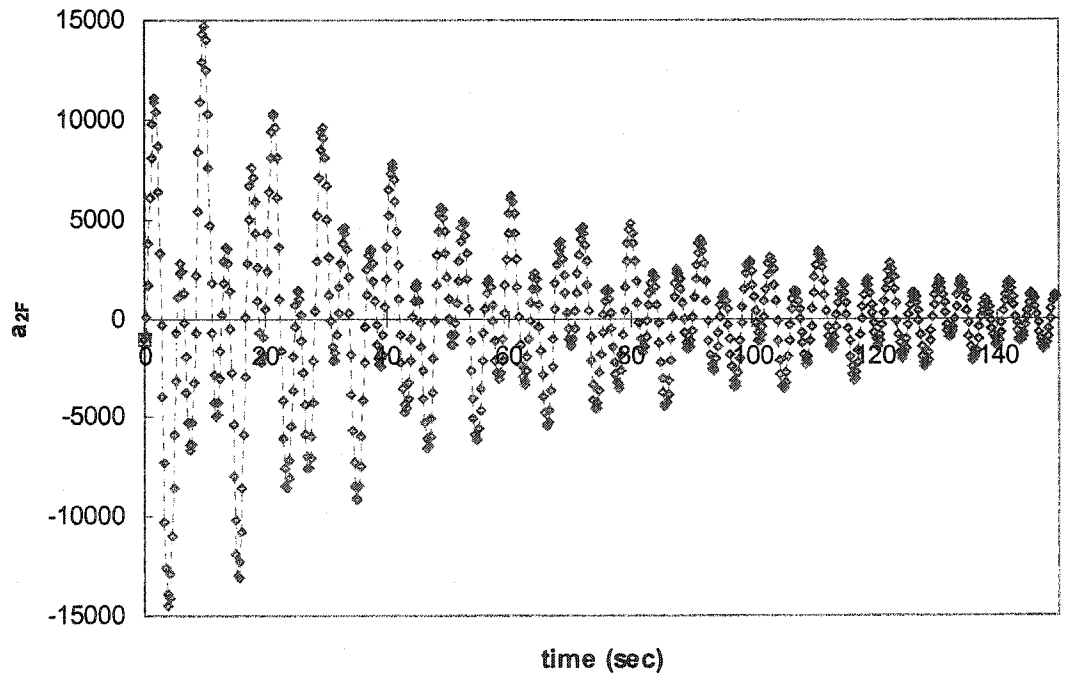

Figure 5.4.3 (b) 150 seconds

-◊--◊- RD Signatures; □ First Point of RD Signatures

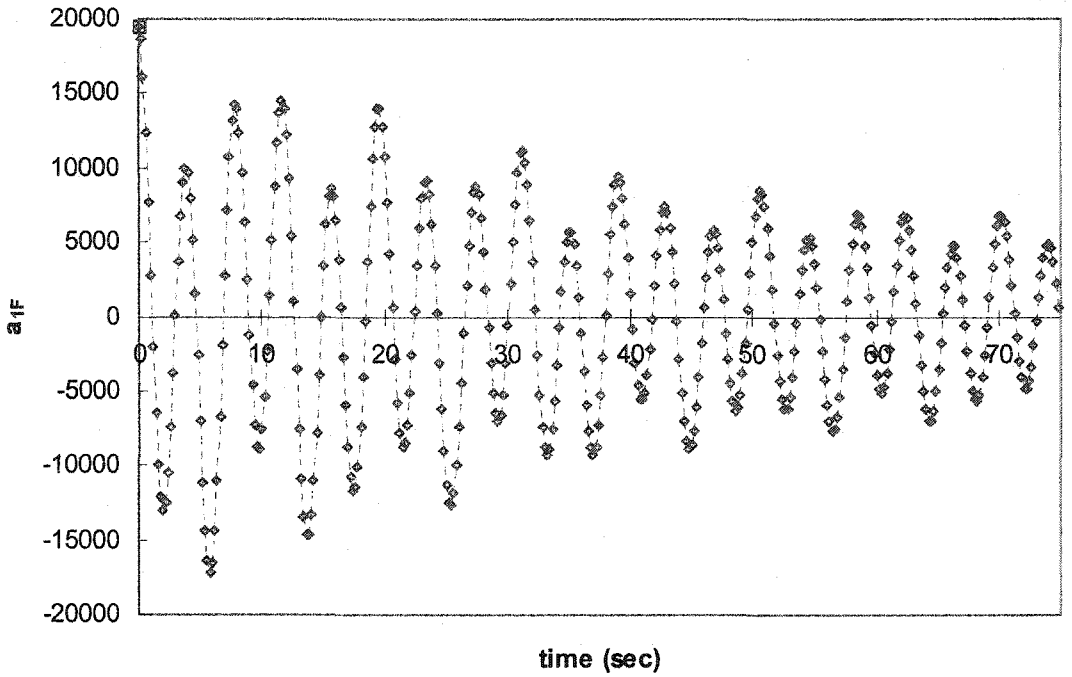

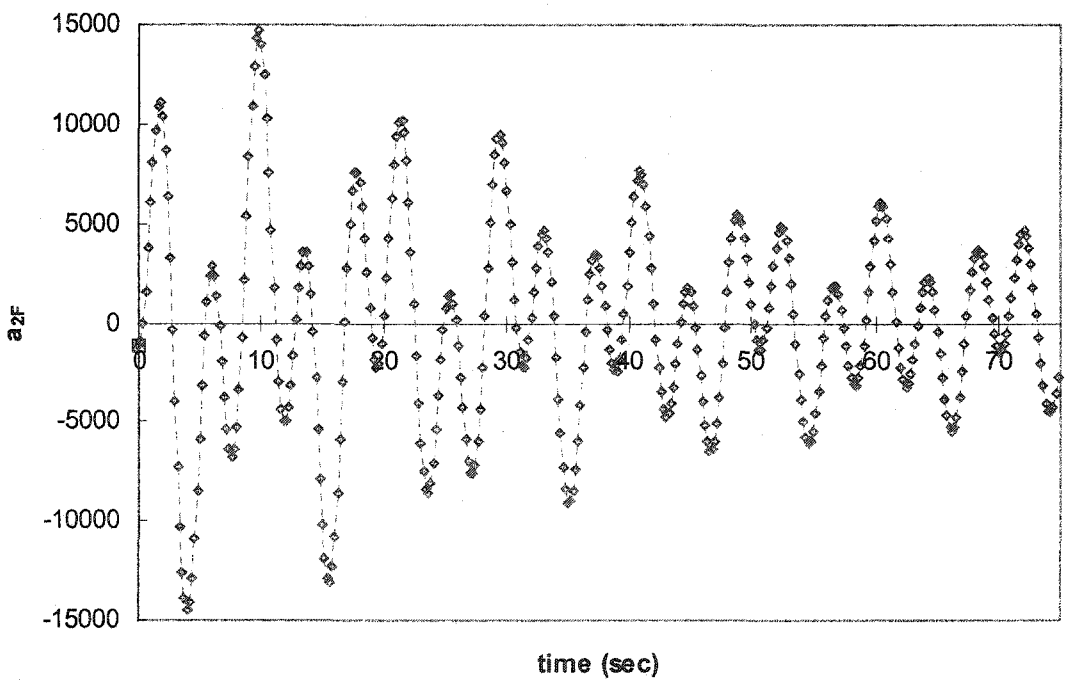

Figure 5.4.3 (c) 75 seconds

-◊--◊- RD Signatures; □ First Point of RD Signatures

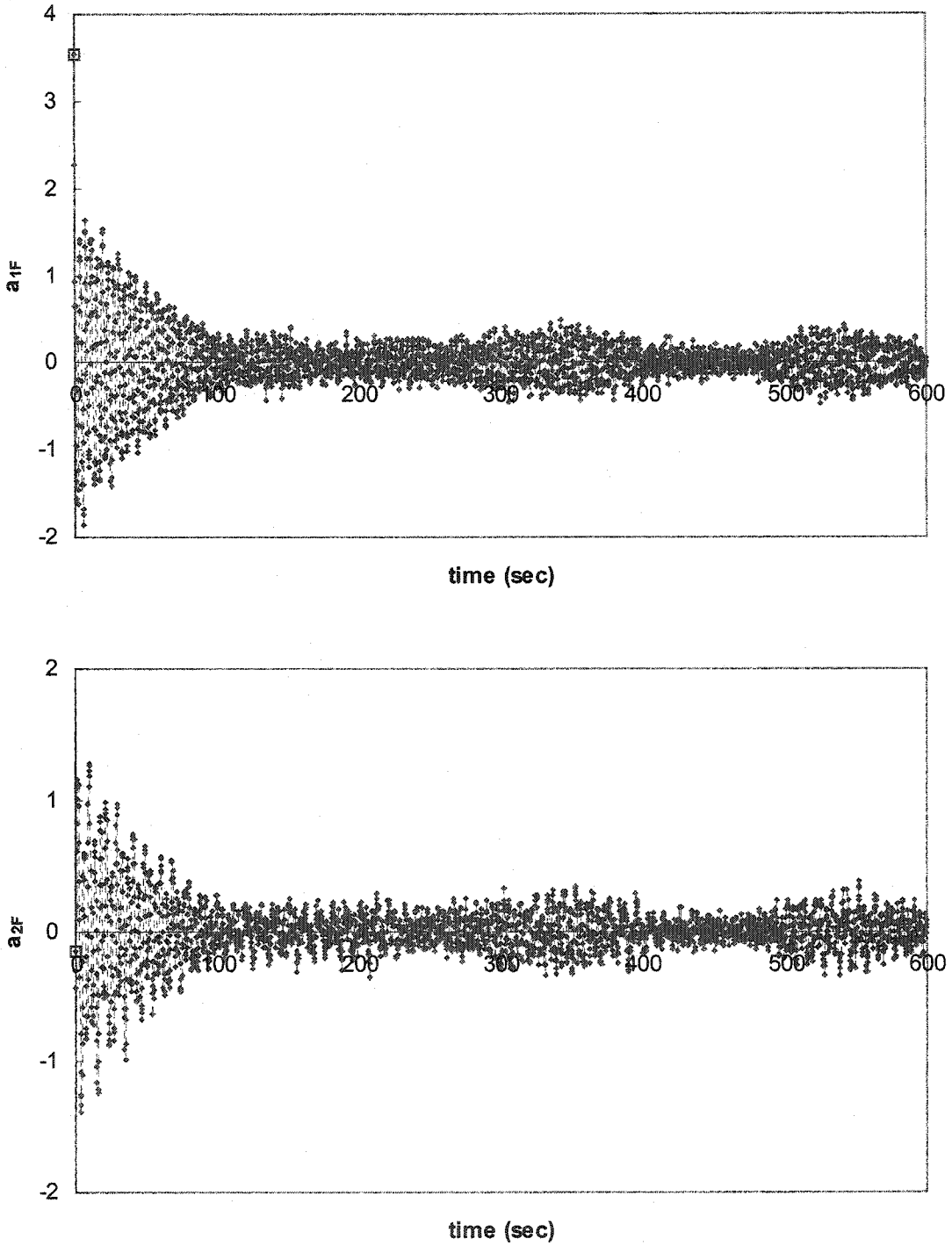

Figure 5.4.4 (a) 600 seconds

Figure 5.4.4 2DOF RD Acceleration Signatures to Simulated Crosswind Forces

-◊--◊- RD Signatures; □ First Point of RD Signatures

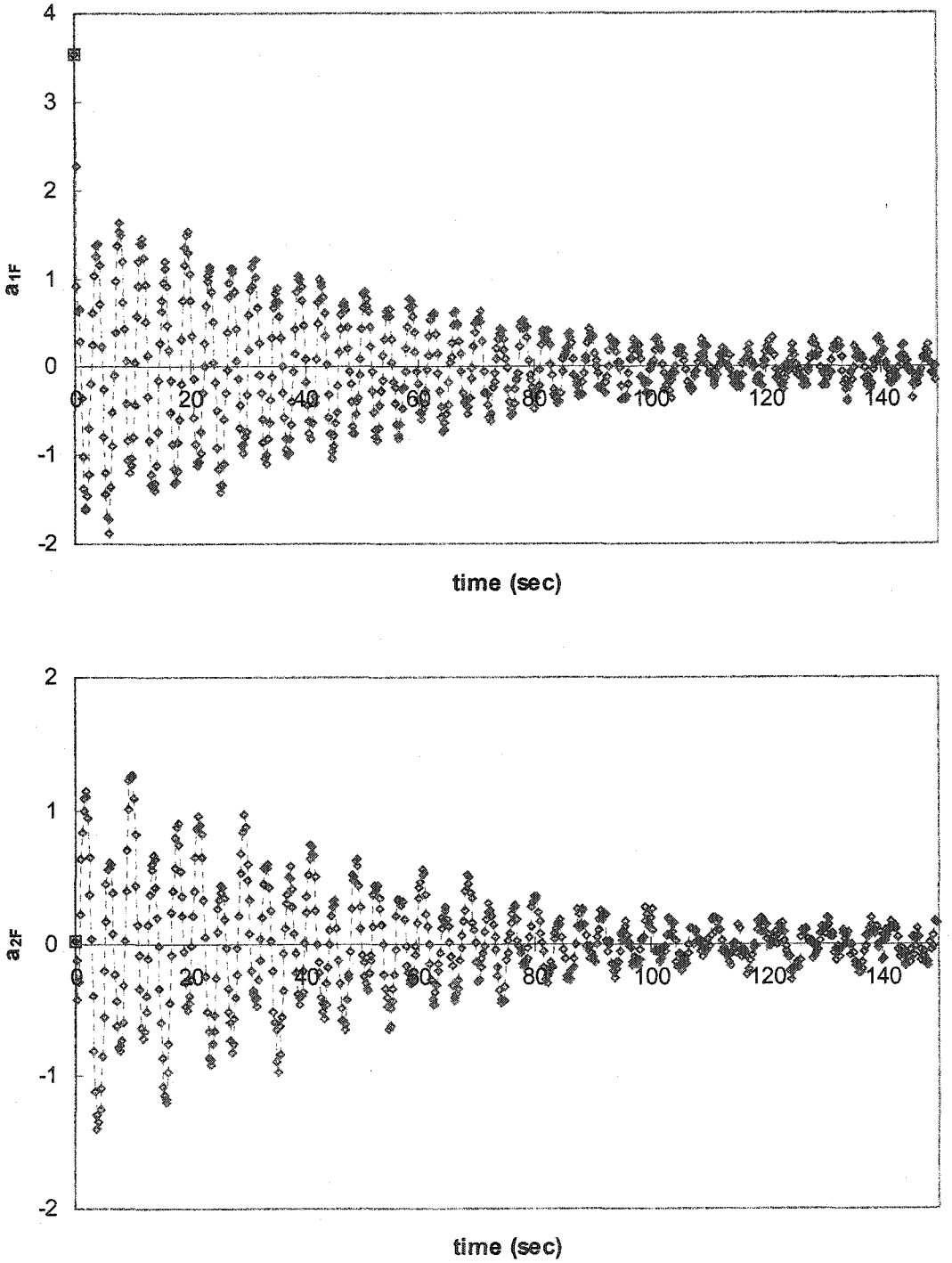

Figure 5.4.4 (b) 150 seconds

-◊--◊- RD Signatures; □ First Point of RD Signatures

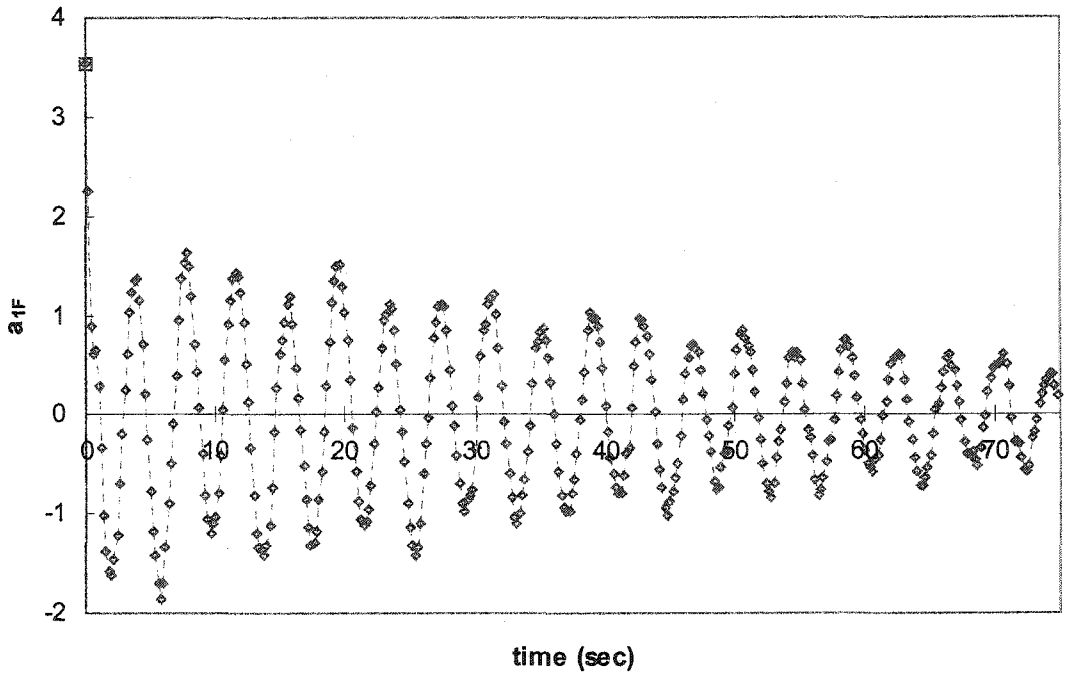

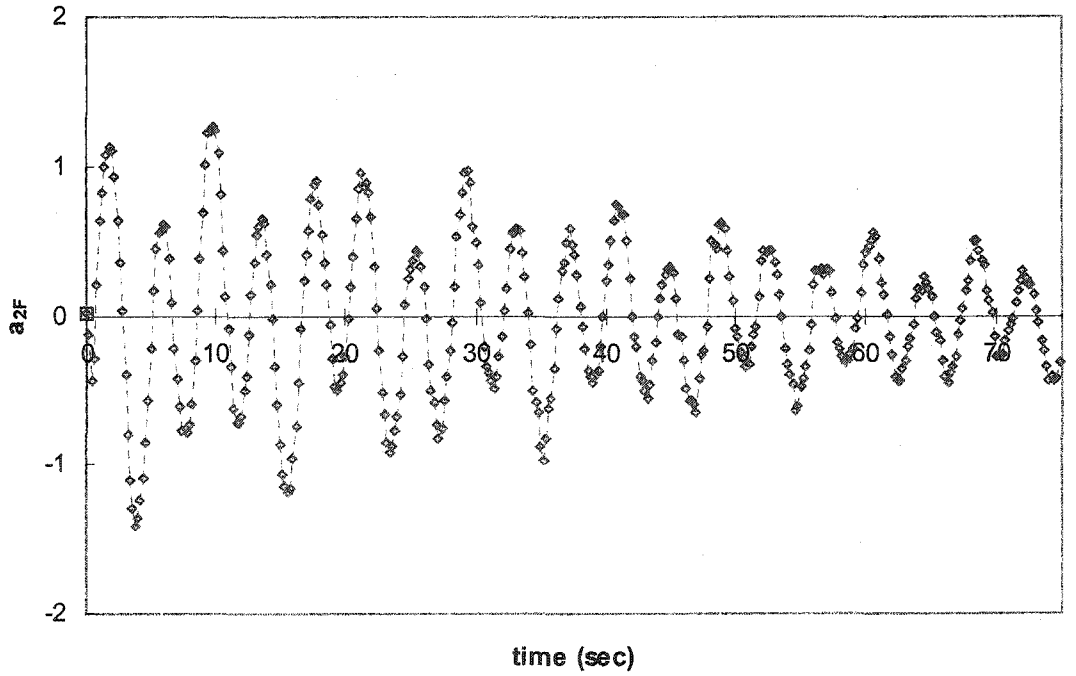

Figure 5.4.4 (c) 75 seconds

-◊--◊- RD Signatures; □ First Point of RD Signatures

The formed RD acceleration signatures gave rise to their estimated FRFs, which were used to compare with the estimated FRFs of the resulting acceleration responses at the dominant natural frequencies. To yield the FRFs, the auto- and cross- spectral density functions were estimated in advance using the traditional FFT based algorithm. For the acceleration responses, 600 seconds were used in each time segment for the computations of the Fourier transformation and the Hanning window, and then the total 13 segments were averaged to estimate the spectral density functions. Apparently, the main difference in calculating the spectral density functions of the RD signatures, in contrast to those of the responses, is that the averaging procedure is implemented in the time domain, before the FFT based algorithm is employed. The applications of the averaging procedure and the Hanning window as basis provide effective means of reducing random and systematic errors in the estimations of the spectral density functions.

The dominant natural frequencies of the dynamic system were first determined by direct observation from the estimated auto-spectral density functions of the original responses and the RD signatures, illustrated in Figures 5.4.5-7. However, the observed natural frequencies may be a result from the dominant frequencies of the input forces as well as the structural response frequencies. Accordingly, it is necessary to examine the estimated cross-spectral density functions and the estimated phase angles between the two responses of the dynamic system to verify such observed natural frequencies. The estimated cross-spectral density functions and phase angles for the various excitations are illustrated in Figures 5.4.8-10. Table 5.4.2 demonstrates the results of the dominant natural frequencies and the phase angles in the 2DOF dynamic system subjected to the various excitations. In review of the fact that the precision to identify natural frequencies

is greatly affected by the frequency resolution, the results with slight variances in Table 5.4.2 for all various cases, in comparison with the theoretical values in Table 5.4.1, are reasonably acceptable.

Table 5.4.2 Estimated Natural Frequencies and Phase Angles of a 2DOF System

		Natural Frequencies		**Phase Angles**			
		Mode 1 (Hz)	Mode 2 (Hz)	Mode 1		Mode 2	
				$\angle\phi_{1k}(°)$	$\angle\phi_{2k}(°)$	$\angle\phi_{1k}(°)$	$\angle\phi_{2k}(°)$
White Noises	Response (600s)	0.09666	0.25666	0	1.099	0	178.122
	RDS1 (600s)	0.10000	0.25499	0	1.600	0	178.958
	RDS1 (75s)	0.09333	0.25333	0	0.218	0	179.918
Alongwind Forces	Response (600s)	0.09663	0.25825	0	0.798	0	175.410
	RDS1 (600s)	0.09663	0.25991	0	0.359	0	177.103
	RDS1 (150s)	0.10000	0.26000	0	0.484	0	178.969
Crosswind Forces	Response (600s)	0.09997	0.25658	0	0.357	0	176.189
	RDS1 (600s)	0.09830	0.25658	0	0.135	0	178.560
	RDS1 (150s)	0.10000	0.25333	0	0.479	0	175.547

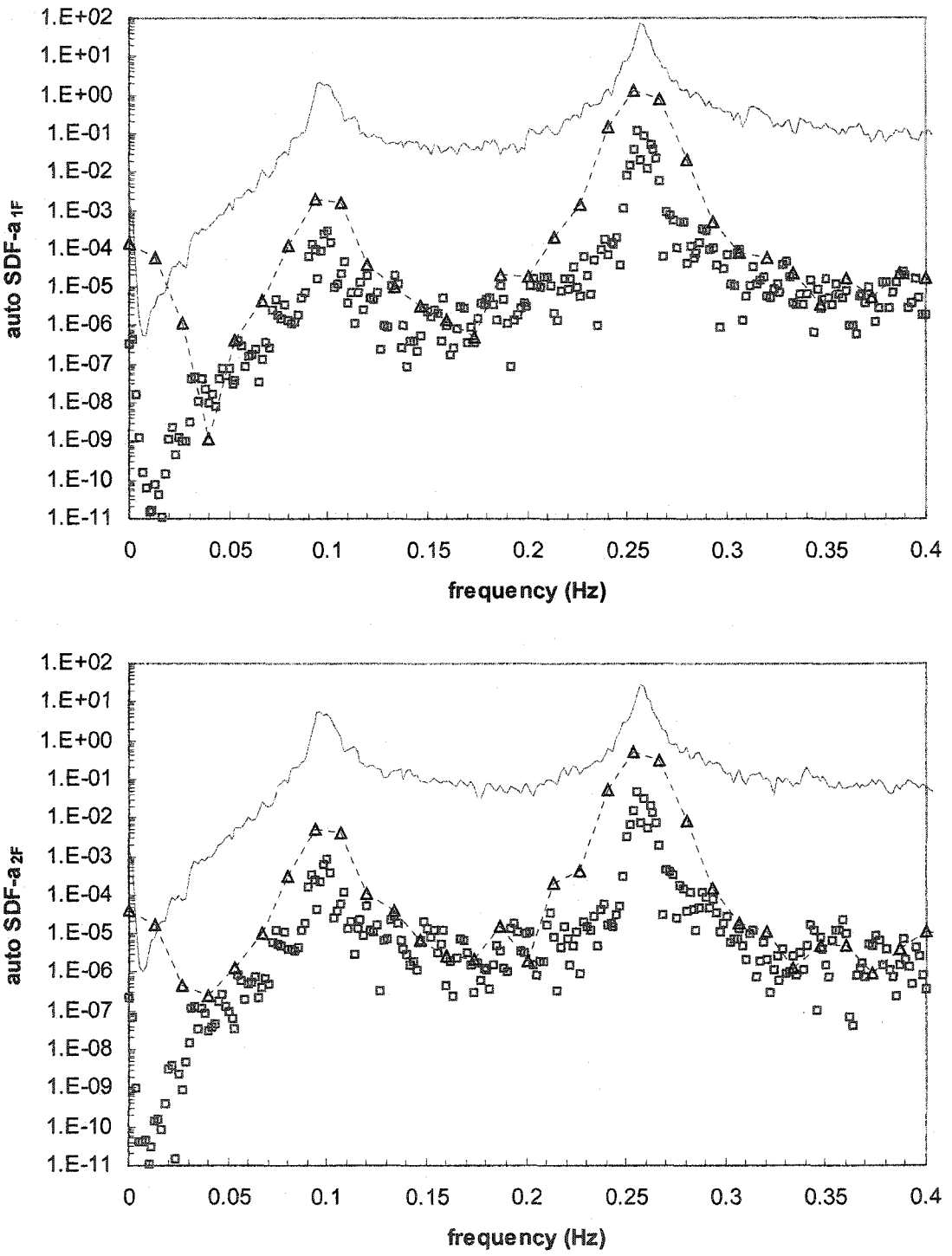

Figure 5.4.5 Auto-Spectral Density Functions of Acceleration Responses and RD Signatures to White Noise Excitations

— Acceleration Responses; RD Signatures: □ 600 sec; --Δ-- 75 sec

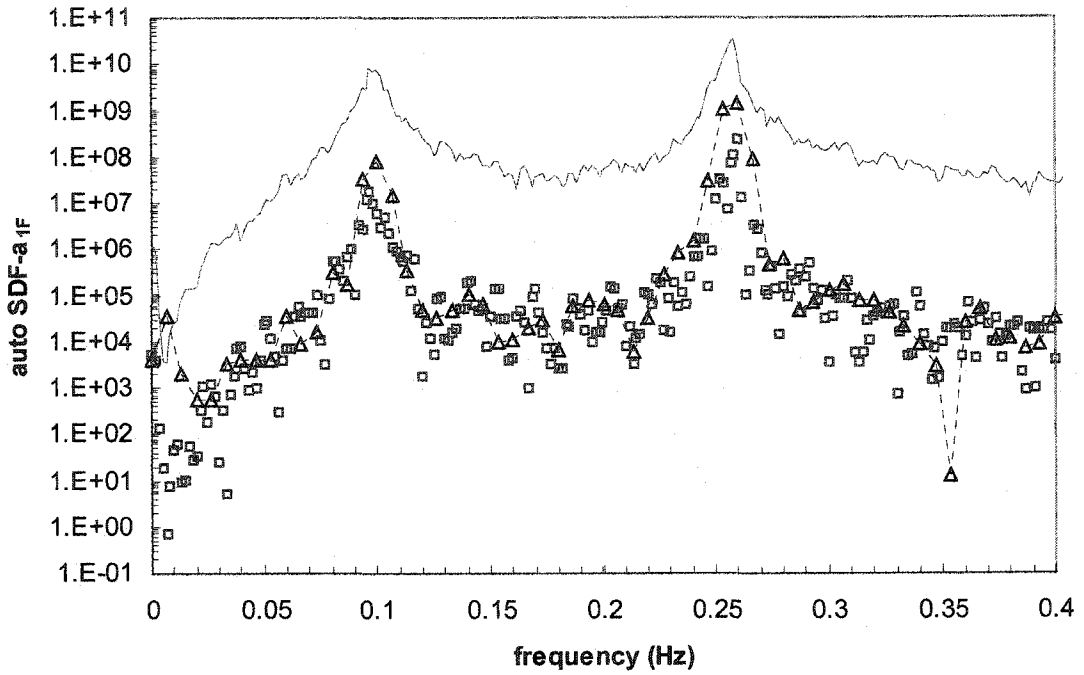

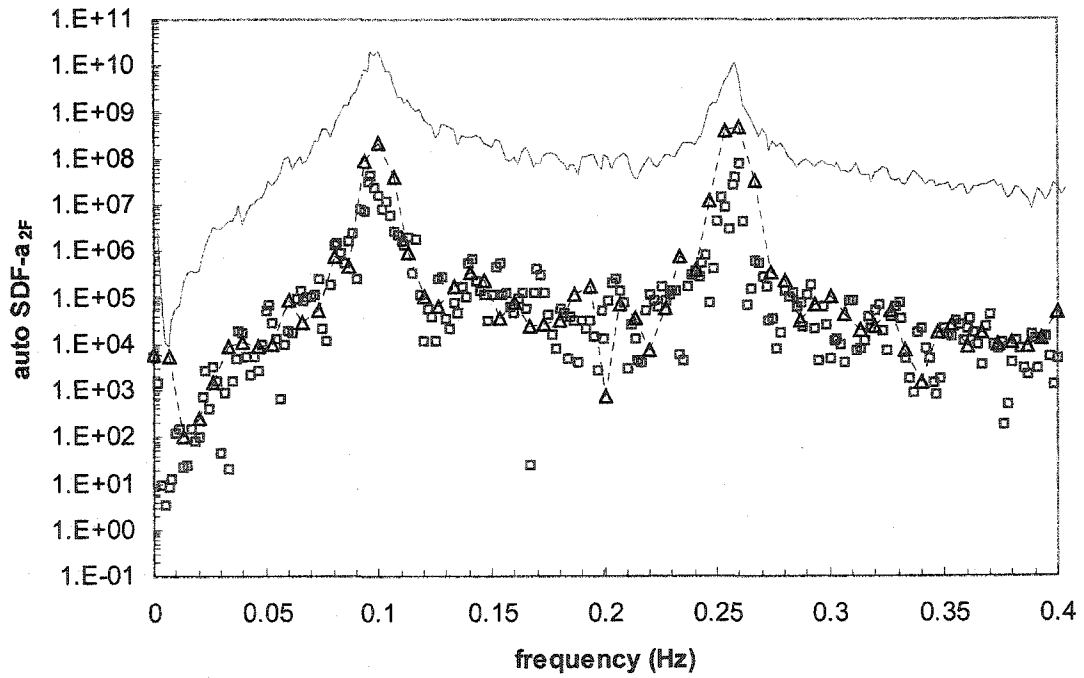

Figure 5.4.6 Auto-Spectral Density Functions of Acceleration Responses and RD Signatures to Simulated Alongwind Forces

— Acceleration Responses; RD Signatures: □ 600 sec; --Δ-- 150 sec

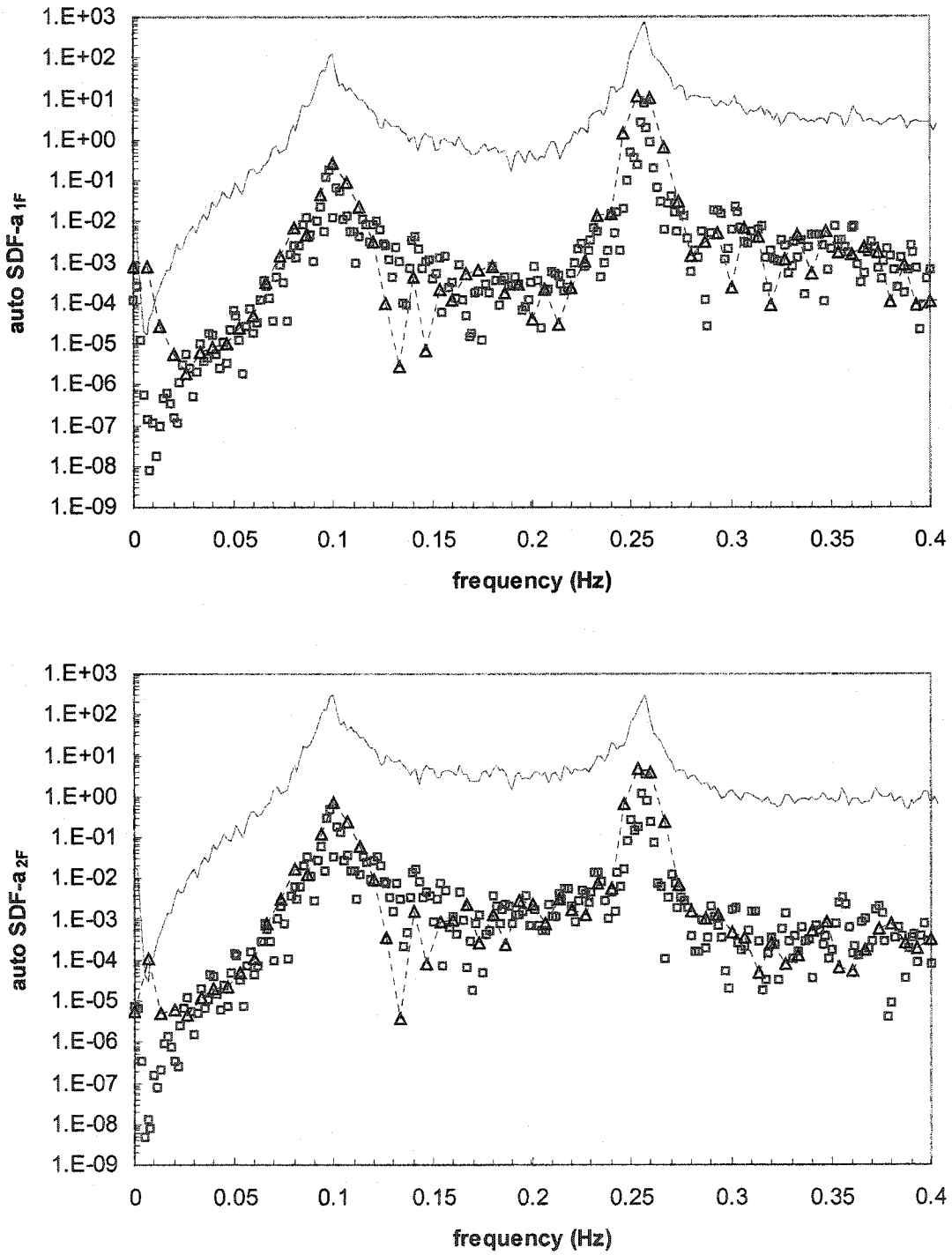

Figure 5.4.7 Auto-Spectral Density Functions of Acceleration Responses and RD Signatures to Simulated Crosswind Forces

— Acceleration Responses; RD Signatures: □ 600 sec; --Δ-- 150 sec

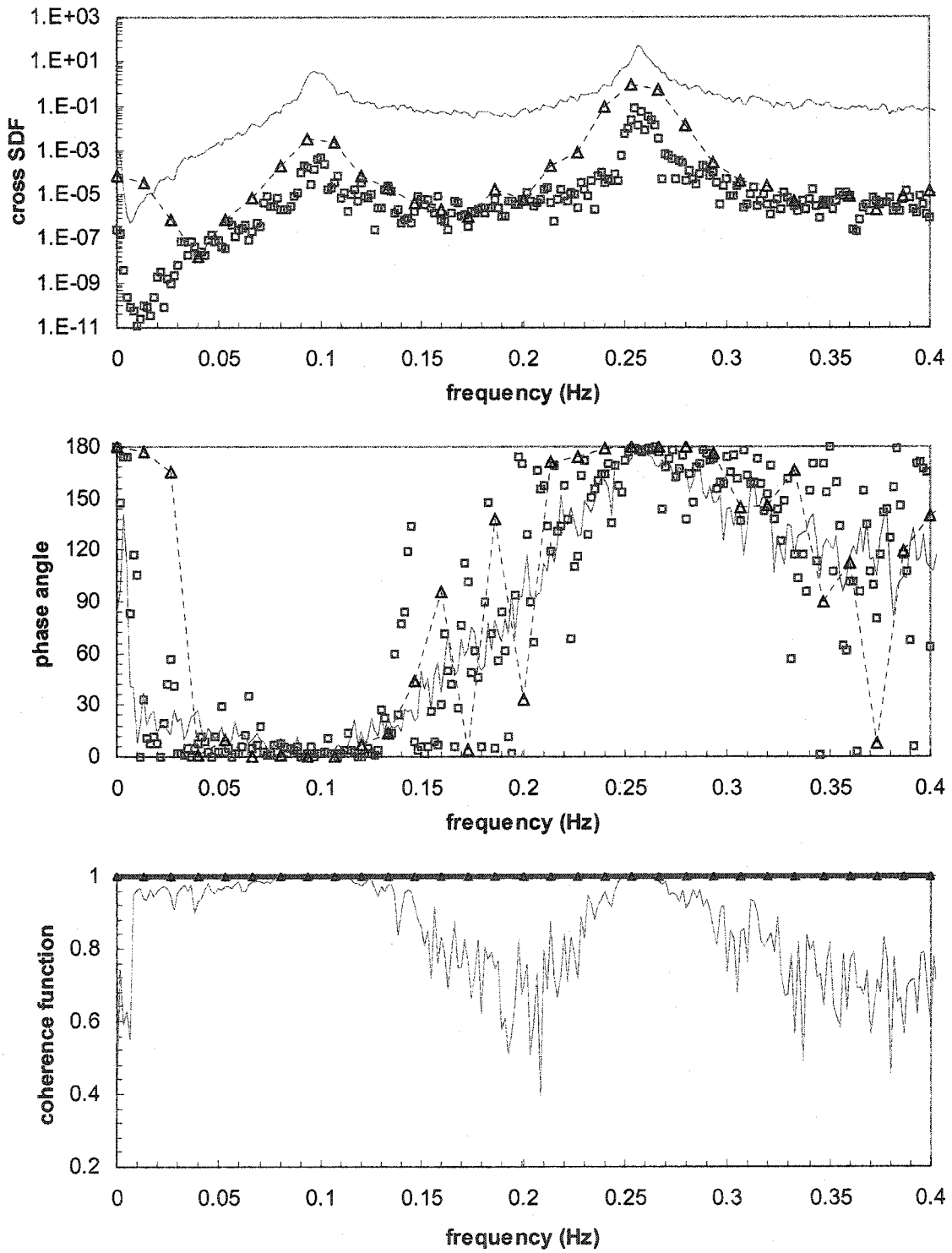

Figure 5.4.8 Cross-Spectral Density Function of Acceleration Responses and RD Signatures to White Noise Excitations

— Acceleration Responses; RD Signatures: □ 600 sec; --Δ-- 75 sec

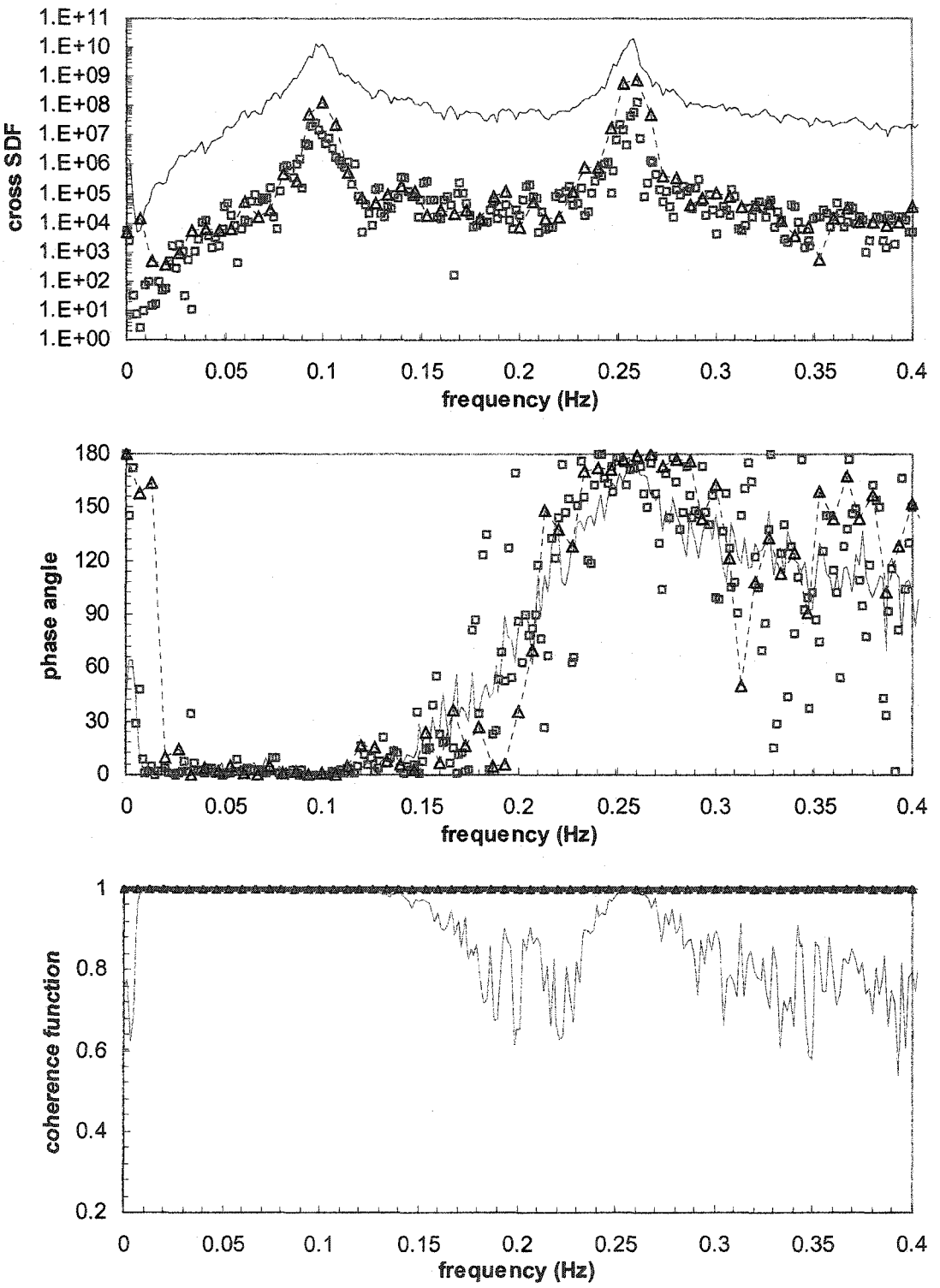

Figure 5.4.9 Cross-Spectral Density Function of Acceleration Responses and RD Signatures to Simulated Alongwind Forces

— Acceleration Responses; RD Signatures: □ 600 sec; --Δ-- 150 sec

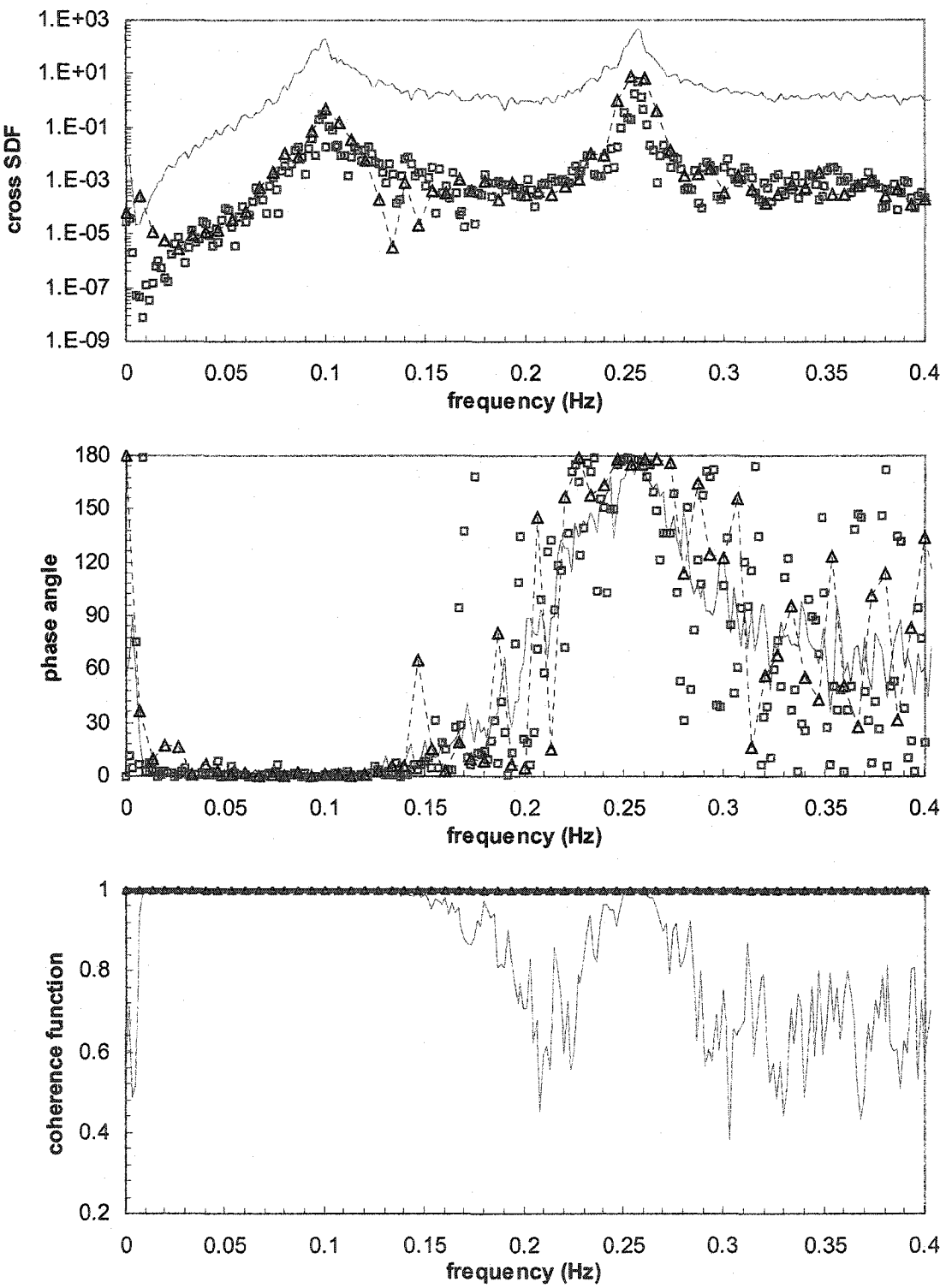

Figure 5.4.10 Cross-Spectral Density Function of Acceleration Responses and RD Signatures to Simulated Crosswind Forces

— Acceleration Responses; RD Signatures: □ 600 sec; --Δ-- 150 sec

With respect to the determined natural frequencies, the estimated FRFs in Table 5.4.3 were carried out using Equations (5.2.25-27) and (5.3.41-43) for the responses and the RD signatures, respectively. From the given results of the estimated FRFs, the corresponding modal ratios between the two locations of the dynamic system are also obtained. As recognized, because of the non-proportional damping nature of the dynamic system, the modal ratio components are usually complex. The quantities in Table 5.4.4 are therefore treated as the absolute values of the obtained modal ratios, in comparison with the theoretical absolute values of the modal ratios given in Table 5.4.1. To compare the degree of the accuracy in the modal ratios between the RD signatures and the responses, the quality measure is defined by the relative error in Equation (5.4.2):

$$\xi = \sum_{i=1}^{n} \frac{\left| \phi_{ik} - \hat{\phi}_{ik} \right|}{\phi_{ik}} \times 100\% \tag{5.4.2}$$

in which ϕ and $\hat{\phi}$ are the theoretical parameter and the estimated parameter of the modal component, respectively, and n is the total number of modes. Table 5.4.5 illustrates the relative errors of the modal ratios, following the results in Table 5.4.4.

The principal results in Tables 5.4.3 and 5.4.4 point out that the identity relation of the three estimated FRFs of the RD acceleration signatures in each mode, derived from Equations (5.3.14-16) or (5.3.25-27), is verified. This verification, based on the three different scenarios of the simulated forces, further reflects that the feature of the identity relation for the FRFs of the RD signatures in Equation (5.3.29) is also valid for any other Gaussian excitations.

Table 5.4.3 Frequency Response Functions of Responses and RD Signatures

		Frequency Response Functions					
		$\lvert H^{(I)}(f_k)\rvert$		$\lvert H^{(II)}(f_k)\rvert$		$\lvert H^{(III)}(f_k)\rvert$	
		Mode 1	Mode 2	Mode 1	Mode 2	Mode 1	Mode 2
White Noises	Response (600s)	1.61285	0.61373	1.61314	0.61430	1.61299	0.61402
	RDS1 (600s)	1.63299	0.63277	1.63299	0.63277	1.63299	0.63277
	RDS1 (75s)	1.62059	0.62133	1.62059	0.62133	1.62059	0.62133
Alongwind Forces	Response (600s)	1.61613	0.59233	1.61615	0.59283	1.61614	0.59258
	RDS1 (600s)	1.61076	0.60368	1.61076	0.60368	1.61076	0.60368
	RDS1 (150s)	1.61991	0.60179	1.61991	0.60179	1.61991	0.60179
Crosswind Forces	Response (600s)	1.62416	0.63007	1.62418	0.63297	1.62417	0.63152
	RDS1 (600s)	1.62221	0.65839	1.62221	0.65839	1.62221	0.65839
	RDS1 (150s)	1.61935	0.62493	1.61935	0.62493	1.61935	0.62493

The results in Table 5.4.5 reveals that the relative errors of the modal ratios are rather small, which supports the validation of the RD based method and the FRF approach to estimate the modal ratios of a dynamic system from the forced acceleration responses. When compared to the theoretical values of the modal ratios in Table 5.4.1, the relative errors for the responses of 600 seconds and the RD signatures of 75 seconds in the case of the white noise excitations are quite accurate with slight variances. It is believed that the white noise excitations having the property of the uniform frequency spectra can serve as a critical reason for such an excellent match. In the two cases of the simulated wind forces, the accuracy in the modal ratio of the 2nd mode for the RD signatures with 150 seconds is superior to that for the responses with 600 seconds. From this point, the superiority of the RD based method in contrast with the sole use of the traditional FRF approach to reliably estimate the higher modal ratios of a dynamic system can be expected in practical applications of wind engineering.

Table 5.4.4 Absolute Values of Modal Ratios for Frequency Response Functions

		Modal Ratios					
		$\left\lvert\frac{\phi_{2k}}{\phi_{1k}}\right\rvert_{H^{(I)}}$		$\left\lvert\frac{\phi_{2k}}{\phi_{1k}}\right\rvert_{H^{(II)}}$		$\left\lvert\frac{\phi_{2k}}{\phi_{1k}}\right\rvert_{H^{(III)}}$	
		Mode 1	Mode 2	Mode 1	Mode 2	Mode 1	Mode 2
White Noises	Response (600s)	1.61285 / 1	0.61373 / 1	1.61314 / 1	0.61430 / 1	1.61299 / 1	0.61402 / 1
	RDS1 (600s)	1.63299 / 1	0.63277 / 1	1.63299 / 1	0.63277 / 1	1.63299 / 1	0.63277 / 1
	RDS1 (75s)	1.62059 / 1	0.62133 / 1	1.62059 / 1	0.62133 / 1	1.62059 / 1	0.62133 / 1
Alongwind Forces	Response (600s)	1.61613 / 1	0.59233 / 1	1.61615 / 1	0.59283 / 1	1.61614 / 1	0.59258 / 1
	RDS1 (600s)	1.61076 / 1	0.60368 / 1	1.61076 / 1	0.60368 / 1	1.61076 / 1	0.60368 / 1
	RDS1 (150s)	1.61991 / 1	0.60179 / 1	1.61991 / 1	0.60179 / 1	1.61991 / 1	0.60179 / 1
Crosswind Forces	Response (600s)	1.62416 / 1	0.63007 / 1	1.62418 / 1	0.63297 / 1	1.62417 / 1	0.63152 / 1
	RDS1 (600s)	1.62221 / 1	0.65839 / 1	1.62221 / 1	0.65839 / 1	1.62221 / 1	0.65839 / 1
	RDS1 (150s)	1.61935 / 1	0.62493 / 1	1.61935 / 1	0.62493 / 1	1.61935 / 1	0.62493 / 1

Common to these three cases of the simulated forces in Table 5.4.5, the RD signatures with 75 and 150 seconds give better results for most modal ratios than those with 600 seconds. The reason is most likely because of the variance on the estimate of the RD signature, as opposed to the bias on the frequency resolution used for frequency domain analysis. Having been mentioned in Chapter 3, the variance of the estimated RD signature gradually increases with the increase of the time lags from its initial position.

As further seen in Figures 5.4.2-4, the longer lags in the RD signatures of 600 seconds are corrupted, owing to the increasing variances of the RD signatures and the additional effect of the RD force signatures, whereas the first several lags show a well decaying curve. Such corrupted lags in the RD signatures may give rise to the low signal to noise ratios, which adversely affect the estimates of the FRFs. On the other hand, the accuracy of the estimated FRFs relies upon a high resolution in frequency [Schmidt, 1985], which requires a longer segment length of the RD signatures. Constraints on the selected length of the RD signatures may necessitate a compromise between the resolution bias of the FRFs and the variance of the RD signatures. In this regard, the practice of a good engineering judgment to properly select the superimposed segment length is critical to enhance the accuracy of the FRFs of the RD signatures.

Table 5.4.5

Relative Errors of Modal Ratios for Acceleration Responses and RD Signatures

		Relative Errors ξ					
		$\left\|\frac{\phi_{2k}}{\phi_{1k}}\right\|_{H^{(I)}}$		$\left\|\frac{\phi_{2k}}{\phi_{1k}}\right\|_{H^{(II)}}$		$\left\|\frac{\phi_{2k}}{\phi_{1k}}\right\|_{H^{(III)}}$	
		Mode 1 (%)	Mode 2 (%)	Mode 1 (%)	Mode 2 (%)	Mode 1 (%)	Mode 2 (%)
White Noises	Response (600s)	0.289	0.717	0.271	0.625	0.280	0.671
	RDS1 (600s)	0.956	2.363	0.956	2.363	0.956	2.363
	RDS1 (75s)	0.189	0.511	0.189	0.511	0.189	0.511
Alongwind Forces	Response (600s)	0.087	4.180	0.085	4.100	0.086	4.140
	RDS1 (600s)	0.419	2.344	0.419	2.344	0.419	2.344
	RDS1 (150s)	0.148	2.649	0.148	2.649	0.148	2.649
Crosswind Forces	Response (600s)	0.410	1.926	0.411	2.395	0.410	2.160
	RDS1 (600s)	0.290	6.508	0.290	6.508	0.290	6.508
	RDS1 (150s)	0.113	1.095	0.113	1.095	0.113	1.095

5.4.2 2DOF Dynamic System with Single Forcing Function

The following study is to present an innovated RD technique. The argumentation of such an innovation is motivated by the conclusion of Huang and Yeh [1999], as shown in Equation (4.5.6). It was pointed out that the singularities of the RD acceleration signatures depend on the correlation functions of white noise excitations, as well as the mass matrix of a dynamic system. This result implies that the influence of the RD force signatures on the RD acceleration signatures may thus be eliminated, when the leading response assigned to a response is related with the diagonal mass matrix of a dynamic system and is behaved without the direct application of any forcing function. The target of such an innovated technique is managed to eliminate the RD signatures of the forcing functions in Equations (5.3.7) and (5.3.8), no matter if there is a correlation between the forcing functions.

To start, the preceding 2DOF dynamic system is adopted, but replacing $f_1(t)$ with the null element in the forcing function vector. That is,

$$\begin{bmatrix} 1 & 0 \\ 0 & 1 \end{bmatrix} \begin{Bmatrix} \ddot{X}_1 \\ \ddot{X}_2 \end{Bmatrix} + \begin{bmatrix} 0.04 & 0.01 \\ 0.01 & 0.03 \end{bmatrix} \begin{Bmatrix} \dot{X}_1 \\ \dot{X}_2 \end{Bmatrix} + \begin{bmatrix} 2 & -1 \\ -1 & 1 \end{bmatrix} \begin{Bmatrix} X_1 \\ X_2 \end{Bmatrix} = \begin{Bmatrix} 0 \\ f_2(t) \end{Bmatrix} \tag{5.4.3}$$

When the single forcing function is considered in connection with the diagonal mass matrix in Equation (5.4.3), the RD acceleration signature matrix of the forcing function portion $\delta^L_{\ddot{X}\ddot{Y}}(\tau)$ can be formulated by Equation (5.4.4). This formulation is based on the results from Equations (4.5.5) and (4.5.8-9) in Section 4.5.1.

$$\delta^L_{\ddot{X}\ddot{Y}}(\tau) = \begin{bmatrix} \delta^L_{\ddot{X}_1\ddot{X}_1}(\tau) & \delta^L_{\ddot{X}_1\ddot{X}_2}(\tau) \\ \delta^L_{\ddot{X}_2\ddot{X}_1}(\tau) & \delta^L_{\ddot{X}_2\ddot{X}_2}(\tau) \end{bmatrix} = \begin{bmatrix} 0 & 0 \\ 0 & \delta^L_{\ddot{X}_2\ddot{X}_2}(\tau) \end{bmatrix} \tag{5.4.4}$$

Apparently, the first row components of the RD signature matrix in Equation (5.4.4) are all zero when the dynamic response at the first location is chosen as the leading response. It explains that the effect of the forcing terms in Equations (5.3.7) and (5.3.8) disappears theoretically, according to the property of the diagonal mass matrix and the selection of the special leading response. In addition to verifying the innovated RD technique, the influence of the applied forcing function $f_2(t)$ is further exhibited in the second row of the RD signature matrix, when the leading response is specified at the second location.

To intensify more thoroughly the conceptual understanding of the proposed RD technique, simulated data with the length of 8000 seconds were generated. These data represent the acceleration responses of the dynamic system subjected to the single input force extracted from the various simulated forces used previously in Section 5.4.1. When the first DOF response was purposely selected to be the leading response to constitute the RD signatures in Figures 5.4.11-13, the added effect of the RD force signatures in the RD acceleration signatures is diminished in a great amount as anticipated. Particularly shown in Figure 5.4.11, the prominent jump at the first point of the RD acceleration signatures, based on the property of white noise excitations, has a dramatic decrease. Therefore, the proper selection of a measurement location for the leading response, which is isolated from the direct loading of any input force, may be an attractive alternative to effectively overcome the mentioned problem on the RD acceleration signatures.

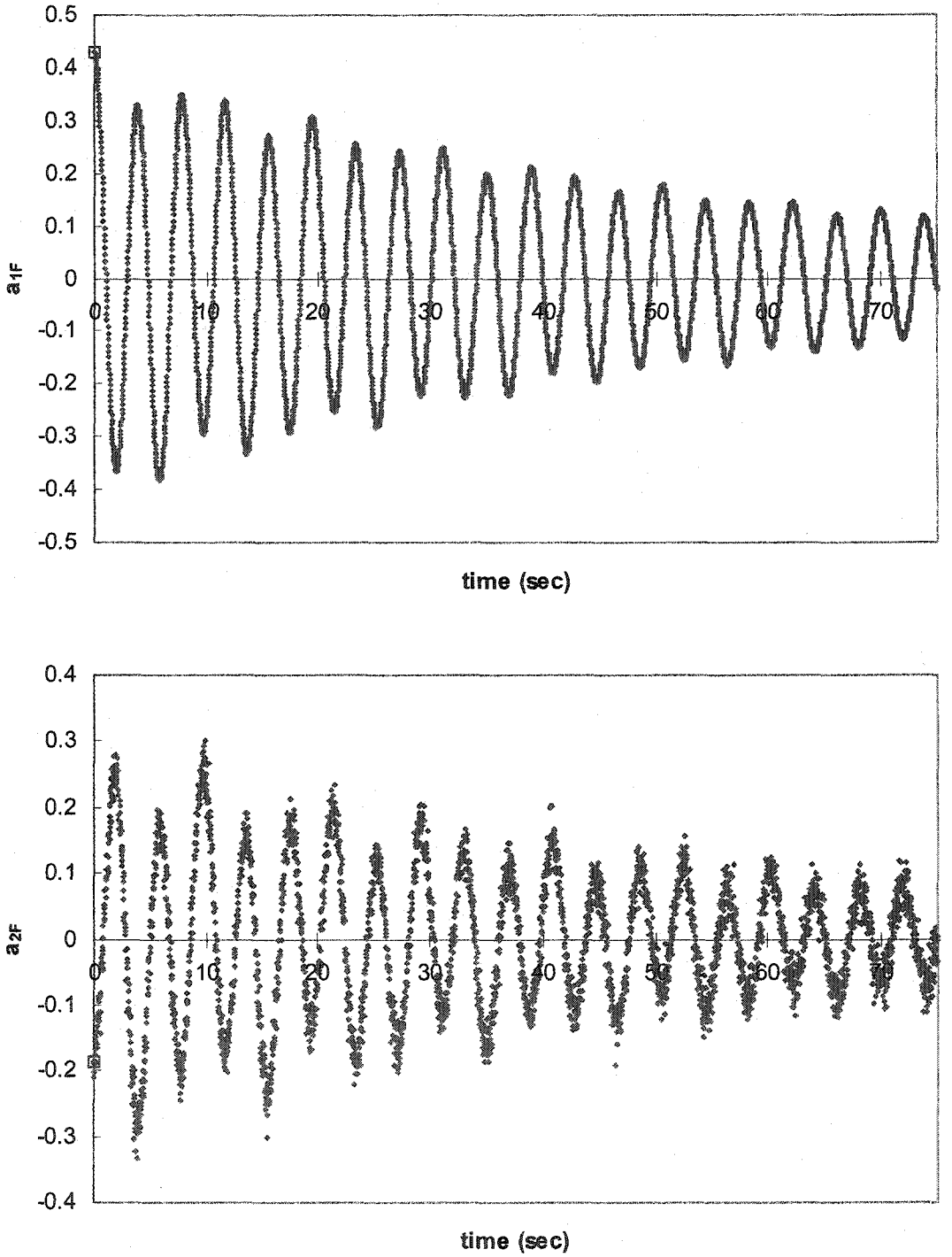

Figure 5.4.11 RD Acceleration Signatures to Single White Noise Excitation

◊ RD Signatures; □ First Point of RD Signatures

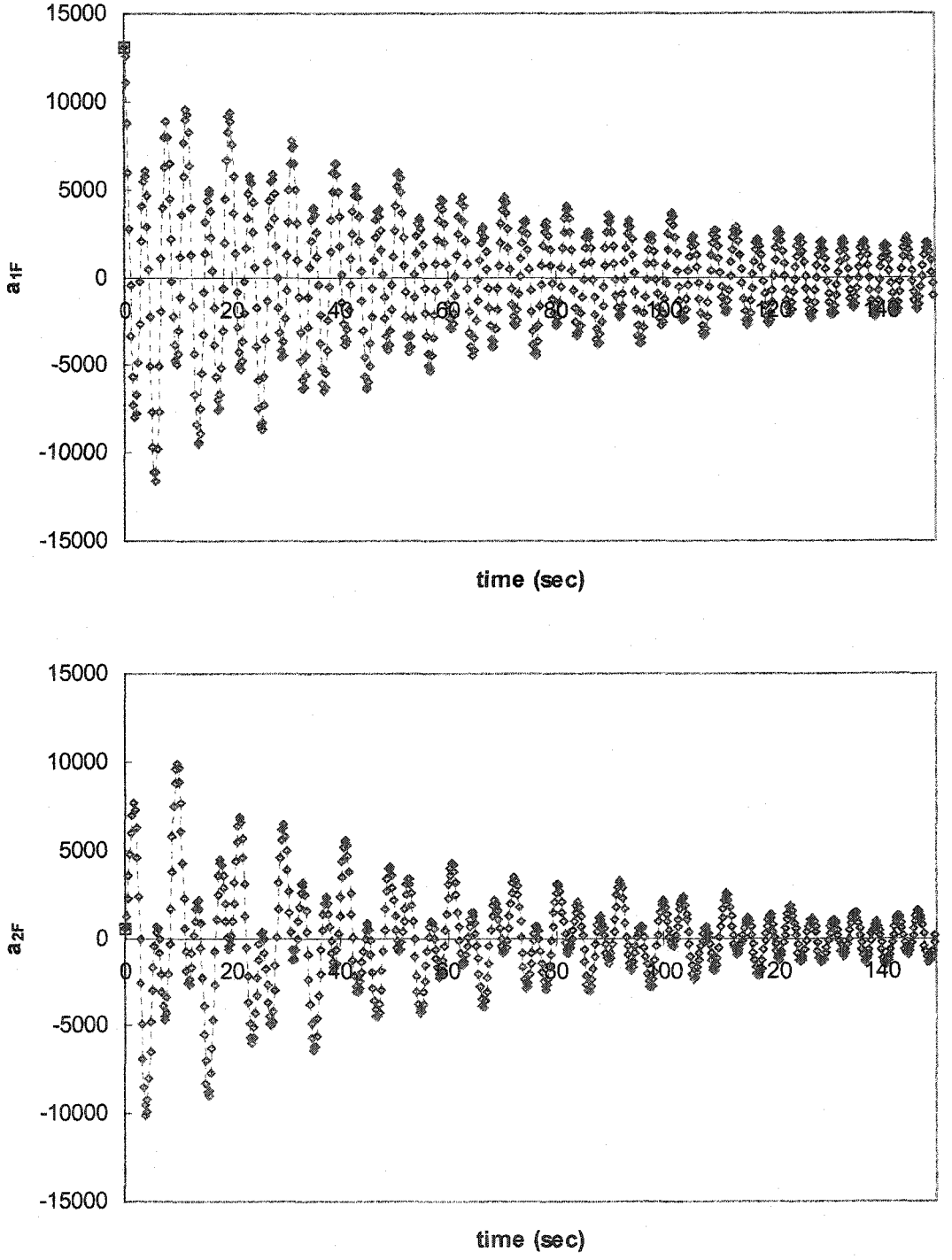

Figure 5.4.12 RD Acceleration Signatures to Single Simulated Alongwind Force

-◊--◊- RD Signatures; □ First Point of RD Signatures

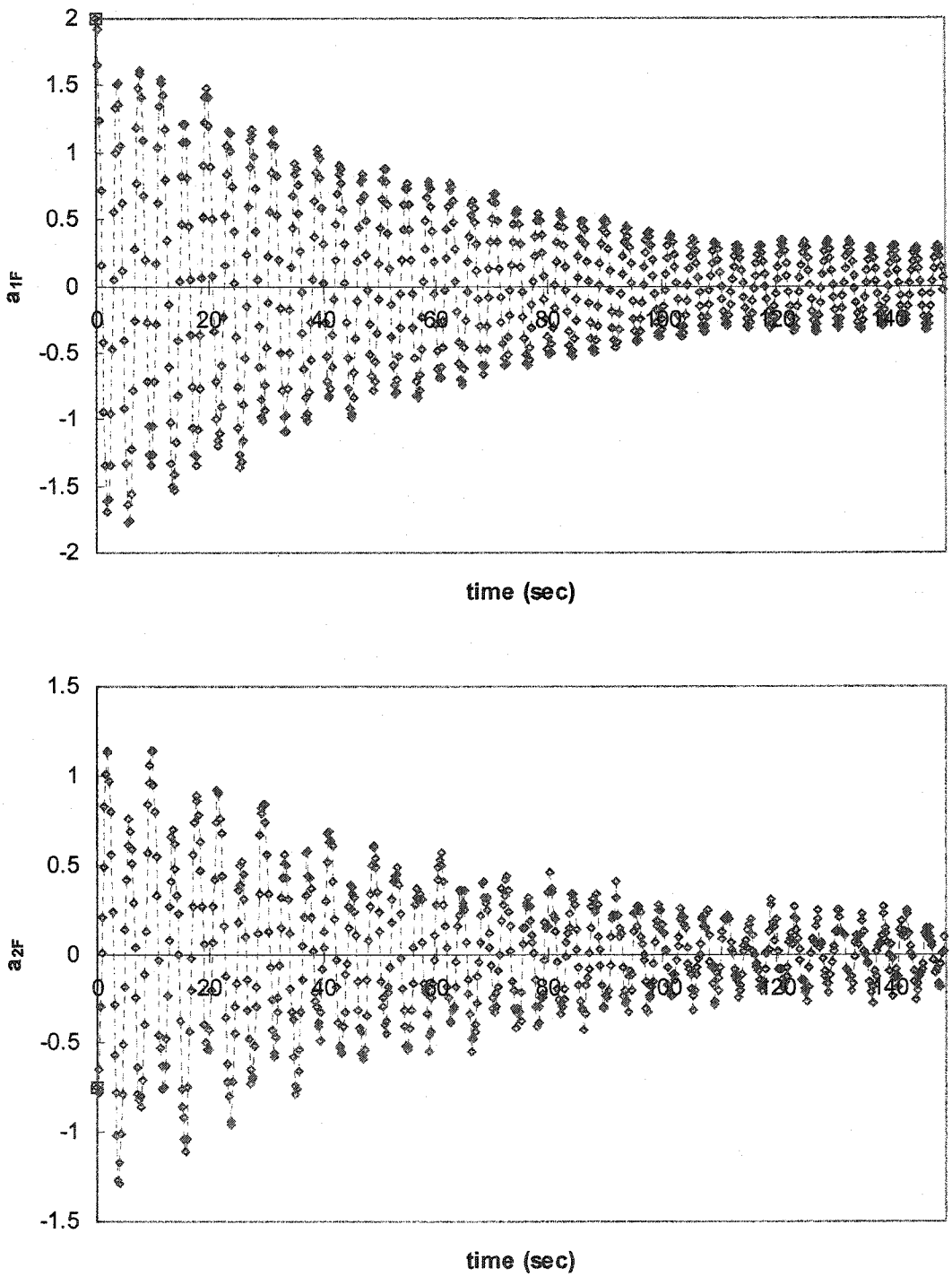

Figure 5.4.13 RD Acceleration Signatures to Single Simulated Crosswind Force

-◊--◊- RD Signatures; □ First Point of RD Signatures

Further investigation is implemented through the modal ratios and their relative errors resulting from the RD signatures and the acceleration responses. The results are illustrated in Table 5.4.6 by means of the $H^{(II)}(f)$ estimator, which is usually used other than the $H^{(I)}(f)$ and $H^{(III)}(f)$ estimators as it was found to give better noise rejection around the resonant frequency. RDS1_1F and RDS1_2F symbolize the results of the RD signatures from the simulation studies of the single forcing function and the two forcing functions, separately, applied on the 2DOF dynamic system.

The first observation from Table 5.4.6 is that the comparisons of all the relative errors between RDS1_1F and RDS1_2F seem not to support the theoretical development of the proposed method as it has been expected to. The other observation is that, for the two types of the simulated wind forces, the RD based method is not absolutely superior with respect to the accuracy of the modal ratio in the 2nd mode, when compared to the FRF approach. The problems in these two observations are probably caused from the difficulty that the selected leading response is not significantly excited and, thus, is not capable of giving the formation of the RD signatures a sufficient amount of the sample segments, in spite of the proper segment length. As a matter of fact, it can be observed in Figures 5.4.11-13 that the tail of the estimated RD signatures reveals a larger uncertainty. Especially, the uncertainty of the estimated cross RD signatures is usually higher than that of the estimated auto RD signatures, if the superimposed number of the sample segments is insufficient. Despite this, the theoretical justification essentially encourages a continuation with the proposed technique as another useful tool to analyze acceleration responses from structural measurements.

Table 5.4.6 Comparisons of Relative Errors for Modal Ratios between Cases of Single Forcing Function and Two Forcing Functions

		Modal Ratios $\left\lvert\frac{\phi_{2k}}{\phi_{1k}}\right\rvert_{H^{(II)}}$			
		Mode 1	Relative Error ξ (%)	Mode 2	Relative Error ξ (%)
White Noise Excitations	RESP_1F (600s)	$\frac{1.63068}{1}$	0.813	$\frac{0.60817}{1}$	1.618
	RDS1_1F (75s)	$\frac{1.62452}{1}$	0.432	$\frac{0.61261}{1}$	0.899
	RDS1_2F (75s)	$\frac{1.62059}{1}$	0.189	$\frac{0.62132}{1}$	0.511
Alongwind Forces	RESP_1F (600s)	$\frac{1.62851}{1}$	0.679	$\frac{0.62494}{1}$	1.096
	RDS1_1F (150s)	$\frac{1.62003}{1}$	0.155	$\frac{0.61208}{1}$	0.985
	RDS1_2F (150s)	$\frac{1.61991}{1}$	0.148	$\frac{0.60179}{1}$	2.649
Crosswind Forces	RESP_1F (600s)	$\frac{1.60653}{1}$	0.680	$\frac{0.62258}{1}$	0.714
	RDS1_1F (150s)	$\frac{1.61436}{1}$	0.196	$\frac{0.60776}{1}$	1.6832
	RDS1_2F (150s)	$\frac{1.61935}{1}$	0.113	$\frac{0.62493}{1}$	1.095

5.4.3 3DOF Dynamic System

The purpose of this section is to further document two individual methods on improving the accuracy of the RD based method by performing numerical simulations of a 3DOF dynamic system subjected to three and two forcing functions individually. The

equations of motion for the 3DOF dynamic system with the proportional damping are given by Equation (5.4.5):

$$\begin{bmatrix} 2 & 0 & 0 \\ 0 & 1 & 0 \\ 0 & 0 & 1 \end{bmatrix} \begin{Bmatrix} \ddot{X}_1 \\ \ddot{X}_2 \\ \ddot{X}_3 \end{Bmatrix} + \begin{bmatrix} 0.2 & -0.1 & 0 \\ -0.1 & 0.2 & -0.1 \\ 0 & -0.1 & 0.1 \end{bmatrix} \begin{Bmatrix} \dot{X}_1 \\ \dot{X}_2 \\ \dot{X}_3 \end{Bmatrix} + \begin{bmatrix} 4 & -2 & 0 \\ -2 & 4 & -2 \\ 0 & -2 & 2 \end{bmatrix} \begin{Bmatrix} X_1 \\ X_2 \\ X_3 \end{Bmatrix} = \begin{Bmatrix} f_1(t) \\ f_2(t) \\ f_3(t) \end{Bmatrix} \qquad (5.4.5)$$

in which the subscript numbers of 1, 2, and 3 stand for the first, second, and third DOF dynamic response, respectively. The theoretical modal parameters of the 3DOF dynamic system are listed in Table 5.4.7 for the purpose of comparison.

Table 5.4.7 Theoretical Modal Parameters of 3DOF Dynamic System

	Frequency (Hz)	Damping Ratio (%)	$\lvert\phi_{1k}\rvert$	$\lvert\phi_{2k}\rvert$	$\lvert\phi_{3k}\rvert$	$\angle\phi_{1k}°$	$\angle\phi_{2k}°$	$\angle\phi_{3k}°$
Mode 1	0.09473	1.49	1	1.64575	2	0	0	0
Mode 2	0.22508	3.54	1	0	1	0	0	180
Mode 3	0.37816	5.94	1	3.64575	2	0	180	0

The input forces used in Section 5.4.1, except that each point of the simulated alongwind forces was multiplied by 10^{-4} in advance, were applied on the 1st and 2nd DOFs of the 3DOF dynamic system to result in three sets of the acceleration responses referred as RESP_2F. Additional white noise excitation was independently generated and then applied on the 3rd DOF of the dynamic system, while the two used white noise excitations were applied on the other two DOFs, to yield another set of acceleration responses. Such responses with 8000 seconds are referred to be RESP_3F in comparison with their RD signatures, RDS3_3F, when the 3rd DOF response is assigned to be the leading response. The RD signatures, RDS3_2F and RDS3_3F, are shown in Figures 5.4.14-16 and 5.4.20.

First of all, special attention is given to the proposed RD technique by selecting a DOF response to be the leading response, which is isolated from the direct application of

any forcing function. Figures 5.4.14-16 display the RD signatures of the acceleration responses corresponding to the three types of the two simulated forces. The animated mode shapes of the 3DOF dynamic system are assembled in Figures 5.4.17-19, which were evaluated from the information of amplitudes and phase angles contained in the FRF, $H^{(ID)}(f_k) = \phi_{ik}/\phi_{jk}$, of the responses and the RD signatures.

The phase angles of the responses and the RD signatures with respect to the reference position of the 1st DOF for the three modes are illustrated in Tables 5.4.8-10, corresponding to Figures 5.4.17-19. In these tables, the 2nd mode phase angle between the 2nd DOF and the 1st DOF for the responses and RD signatures fails to be adequately identified. This is due to the fact that the measured signal of a dynamic mode at the location is quite small, when compared with those at the other locations. The presence of extraneous noises may lead to distortions and make the accurate estimation of phase angles difficult.

The relative errors of the identified modal ratios are evaluated in Table 5.4.11, in relation to the theoretical modal ratios in Table 5.4.7. A similar trend can be observed in Table 5.4.11 that the results of RESP_2F in the highest modal ratio have considerable discrepancies, as compared with those of RDS3_2F. Further examining the results of RDS3_3F, RDS1_2F, and RDS3_2F in the row of white noise excitations, the relative errors of RDS3_2F are comparatively low, even though the RD signatures of RDS3_3F and RDS1_2F have more superimposed segments. The potential advantage of using the innovated RD technique in the RD based method to prevent the disturbance of the input forces in the acceleration responses is overall recognized in this investigation.

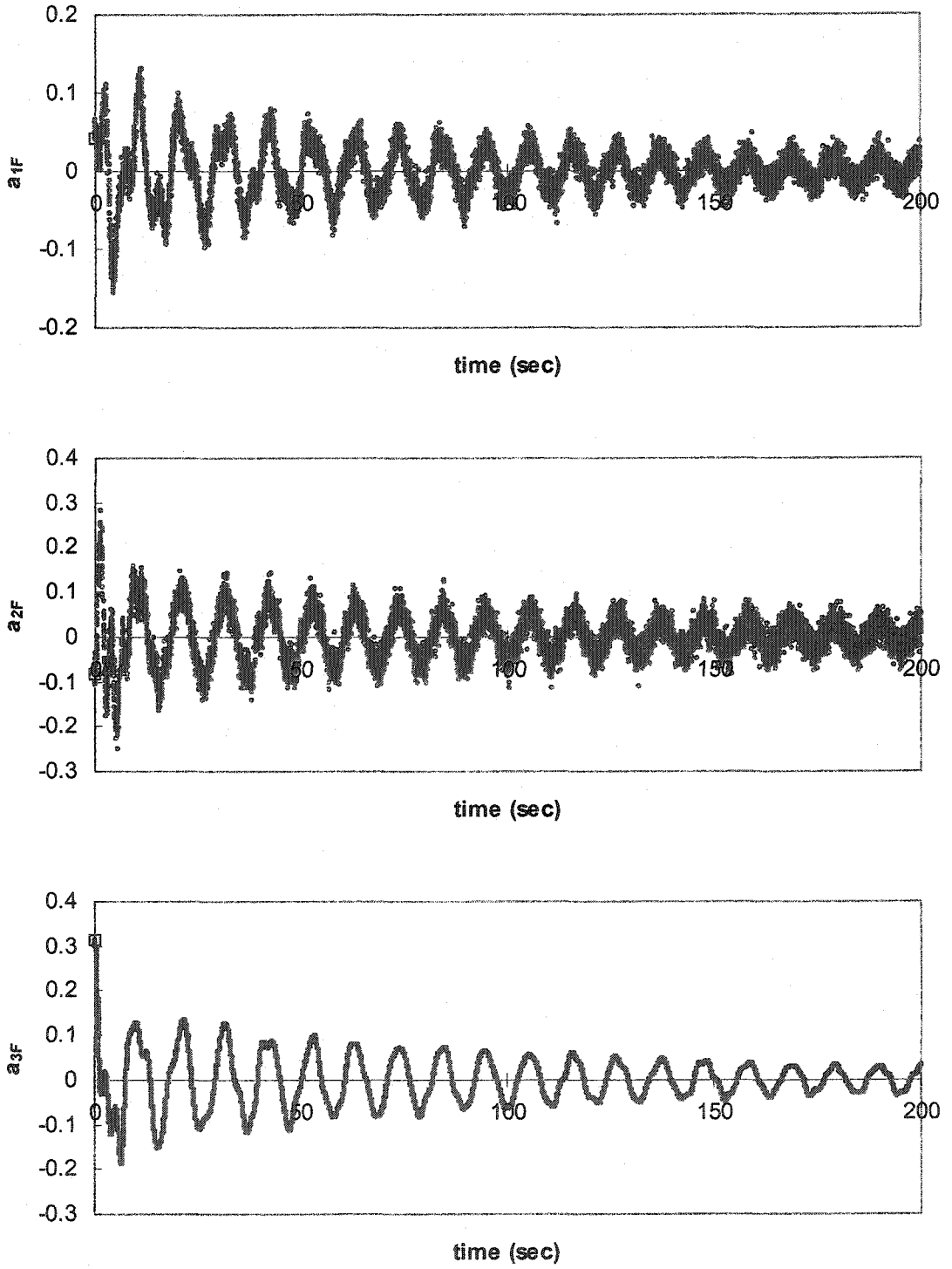

Figure 5.4.14 RD Acceleration Signatures to Two White Noise Excitations

• RD Signatures; □ First Point of RD Signatures

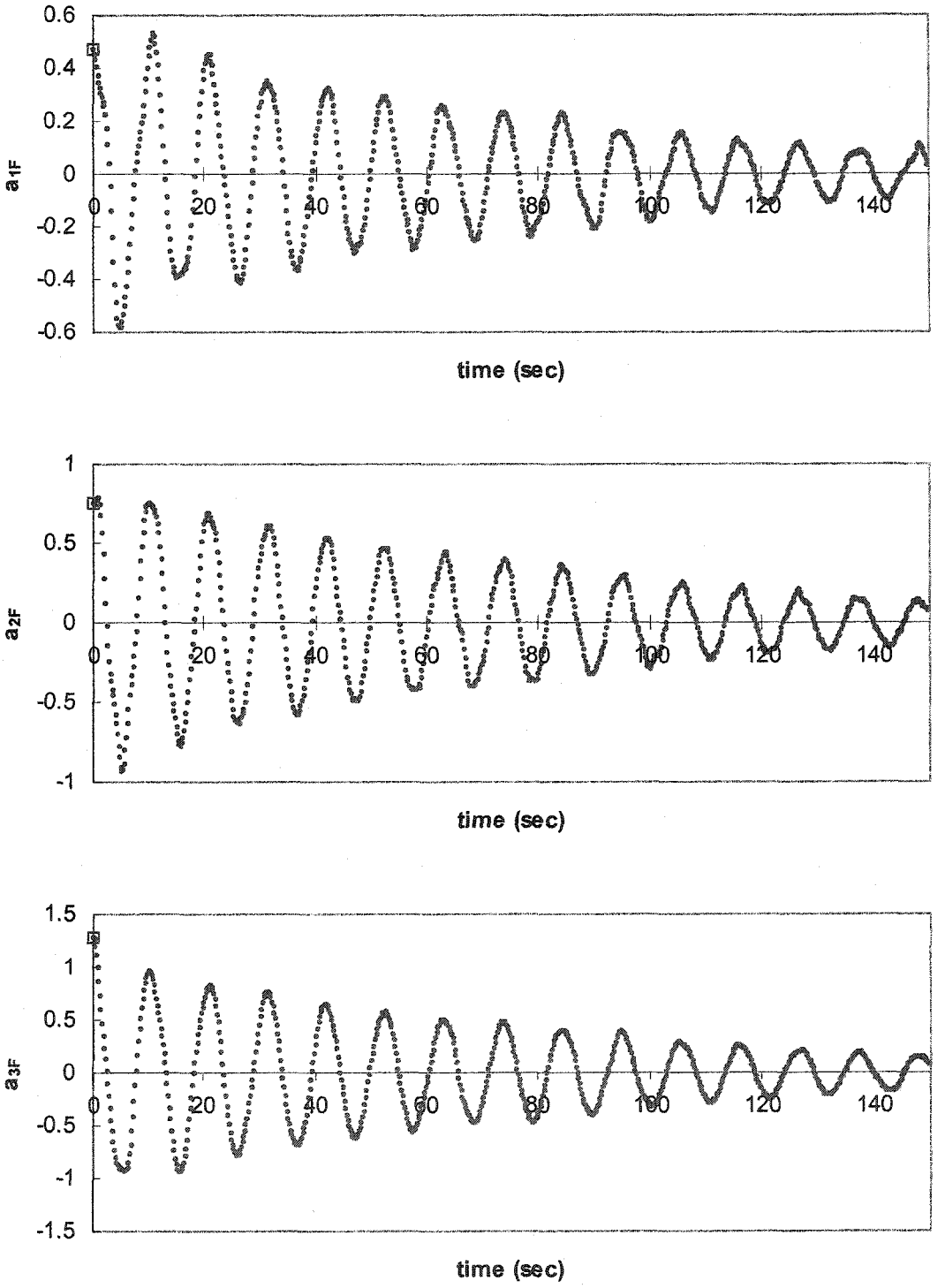

Figure 5.4.15 RD Acceleration Signatures to Two Alongwind Forces

• RD Signatures; □ First Point of RD Signatures

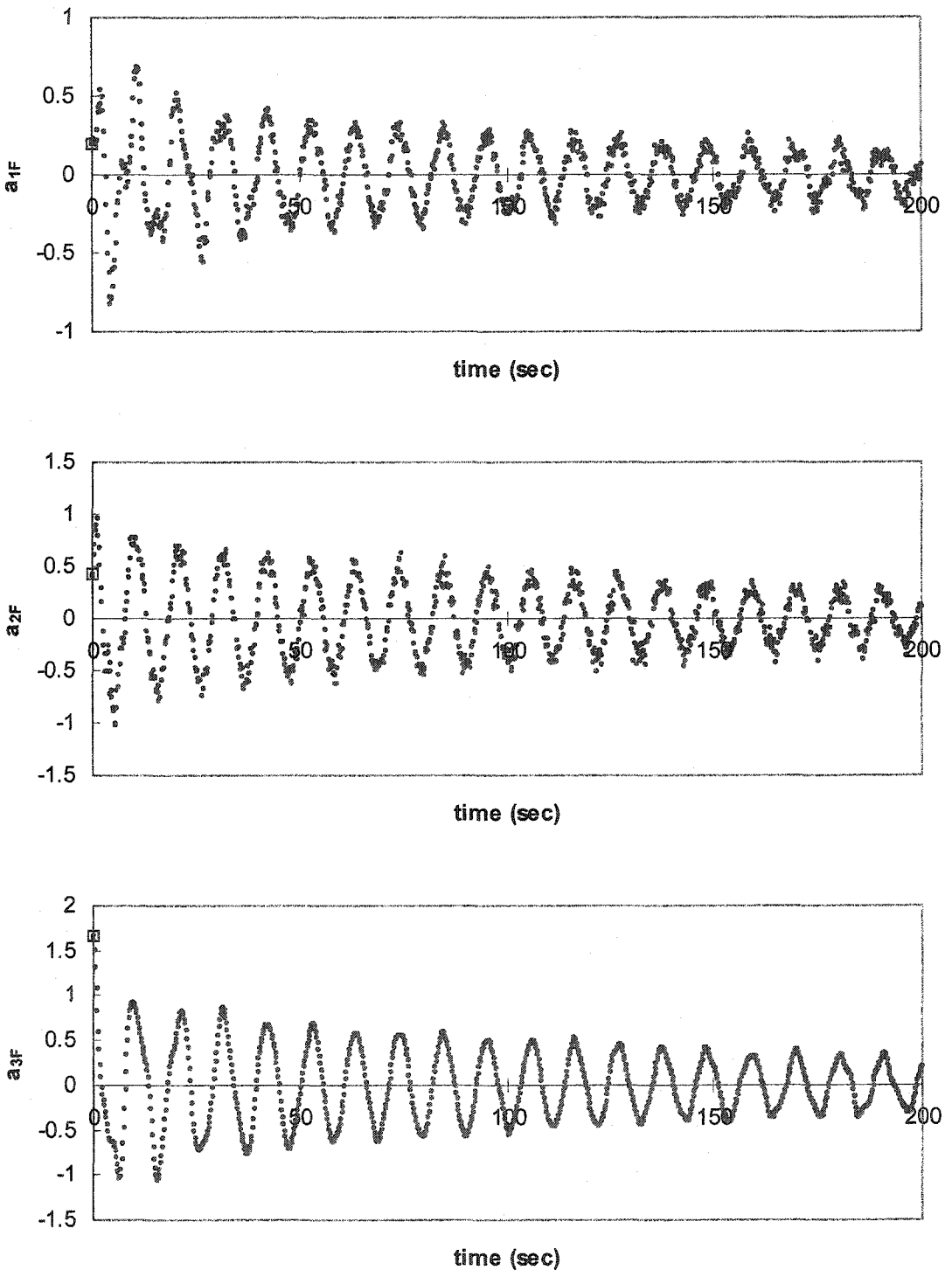

Figure 5.4.16 RD Acceleration Signatures to Two Crosswind Forces

• RD Signatures; □ First Point of RD Signatures

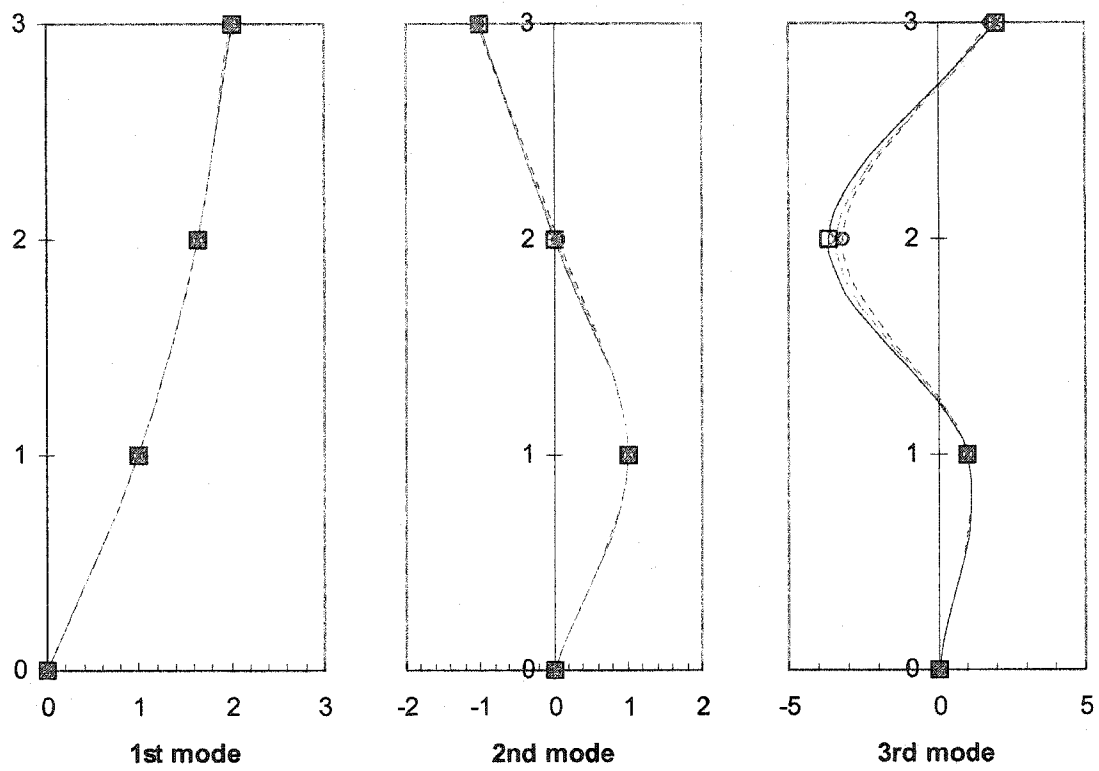

Figure 5.4.17 Estimated Mode Shapes of 3DOF System to Two White Noise Excitations

—□— Theoretical Values; --*-- RD Signatures; ---o--- Responses
(a) Responses: $f_1 = 0.095$ Hz, $f_2 = 0.22333$ Hz, $f_3 = 0.37665$ Hz
(b) RD Signatures: $f_1 = 0.095$ Hz, $f_2 = 0.225$ Hz, $f_3 = 0.37$ Hz

Table 5.4.8

Phase Angles of Modal Ratios of 3DOF System Excited by two White Noise Excitations

		Phase Angles of $\angle\left(\frac{\phi_{2k}}{\phi_{1k}}\right)_{H^{(II)}}$ and $\angle\left(\frac{\phi_{3k}}{\phi_{1k}}\right)_{H^{(II)}}$					
		Mode 1		Mode 2		Mode 3	
		$\angle\left(\frac{\phi_{21}}{\phi_{11}}\right)$	$\angle\left(\frac{\phi_{31}}{\phi_{11}}\right)$	$\angle\left(\frac{\phi_{22}}{\phi_{12}}\right)$	$\angle\left(\frac{\phi_{32}}{\phi_{12}}\right)$	$\angle\left(\frac{\phi_{23}}{\phi_{13}}\right)$	$\angle\left(\frac{\phi_{33}}{\phi_{13}}\right)$
White Noise Excitations	RESP_2F (600s)	0.54°	0.89°	100.42°	167.11°	163.45°	19.41°
	RDS3_2F (200s)	0.54°	0.57°	110.27°	177.84°	166.87°	3.27°
Theoretical Values		0°	0°	0°	180°	180°	0°

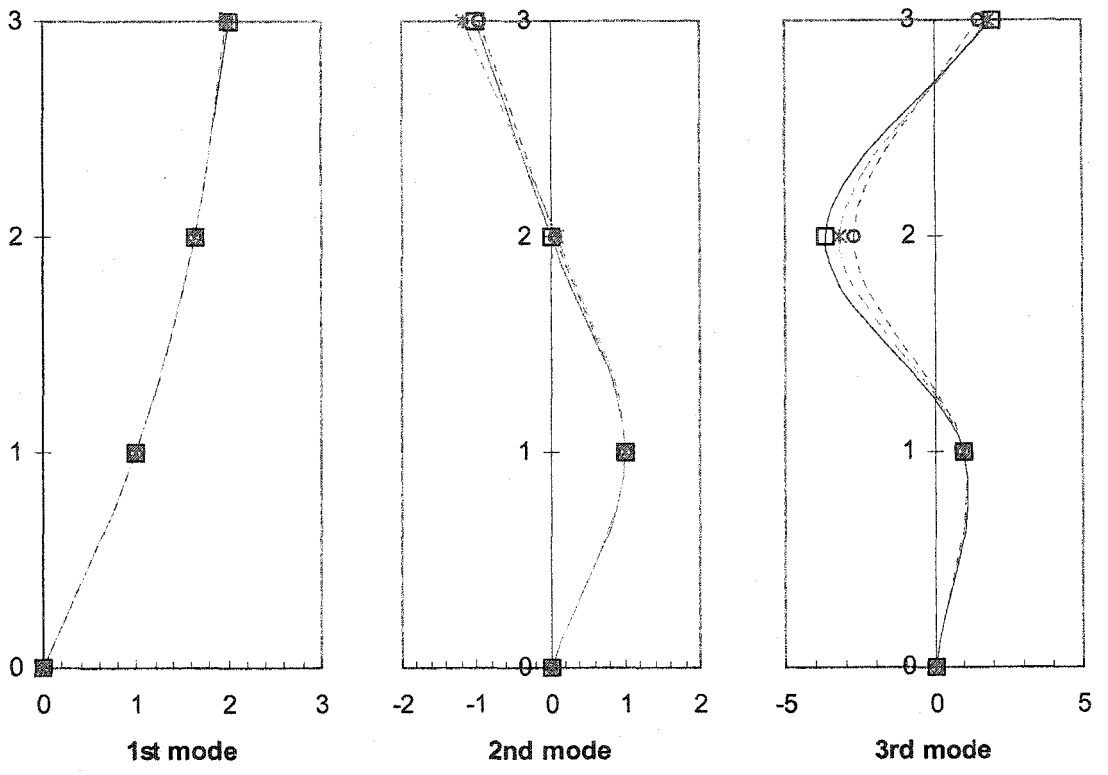

Figure 5.4.18 Estimated Mode Shapes of 3DOF System to Two Alongwind Forces

—□— Theoretical Values; --*-- RD Signatures; ---o--- Responses
(a) Responses: $f_1 = 0.0933$ Hz, $f_2 = 0.22659$ Hz, $f_3 = 0.37154$ Hz
(b) RD Signatures: $f_1 = 0.095$ Hz, $f_2 = 0.22$ Hz, $f_3 = 0.37$ Hz

Table 5.4.9

Phase Angles of Modal Ratios of 3DOF System Excited by two Alongwind Forces

		Phase Angles of $\angle\left(\frac{\phi_{2k}}{\phi_{1k}}\right)_{H^{(II)}}$ **and** $\angle\left(\frac{\phi_{3k}}{\phi_{1k}}\right)_{H^{(II)}}$					
		Mode 1		Mode 2		Mode 3	
		$\angle\left(\frac{\phi_{21}}{\phi_{11}}\right)$	$\angle\left(\frac{\phi_{31}}{\phi_{11}}\right)$	$\angle\left(\frac{\phi_{22}}{\phi_{12}}\right)$	$\angle\left(\frac{\phi_{32}}{\phi_{12}}\right)$	$\angle\left(\frac{\phi_{23}}{\phi_{13}}\right)$	$\angle\left(\frac{\phi_{33}}{\phi_{13}}\right)$
Alongwind Forces	RESP_2F (600s)	0.45°	0.74°	69.79°	165.89°	166.03°	16.68°
	RDS3_2F (150s)	0.10°	0.22°	135.62°	177.15°	158.94°	31.69°
Theoretical Values		0°	0°	0°	180°	180°	0°

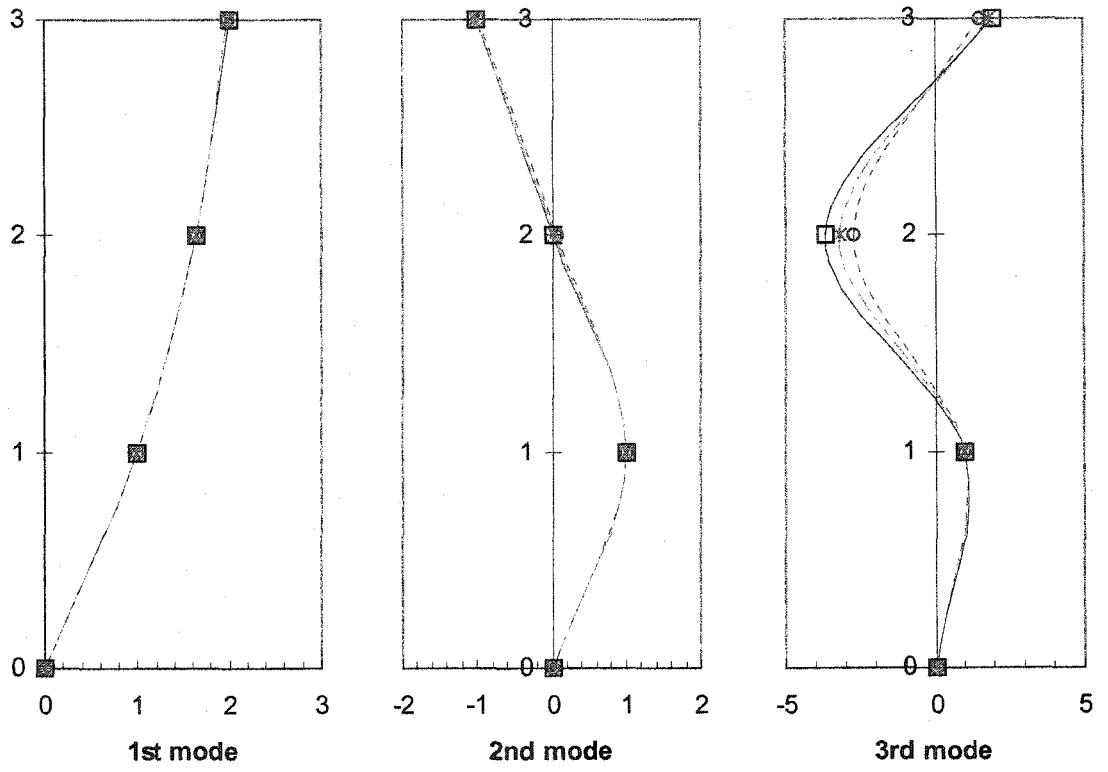

Figure 5.4.19 Estimated Mode Shapes of 3DOF System to Two Crosswind Forces

—□— Theoretical Values; --*-- RD Signatures; ---o--- Responses
(a) Responses: $f_1 = 0.09497$ Hz, $f_2 = 0.22659$ Hz, $f_3 = 0.37154$ Hz
(b) RD Signatures: $f_1 = 0.095$ Hz, $f_2 = 0.225$ Hz, $f_3 = 0.385$ Hz

Table 5.4.10

Phase Angles of Modal Ratios of 3DOF System Excited by two Crosswind Forces

		Phase Angles of $\angle\left(\frac{\phi_{2k}}{\phi_{1k}}\right)_{H^{(II)}}$ and $\angle\left(\frac{\phi_{3k}}{\phi_{1k}}\right)_{H^{(II)}}$					
		Mode 1		Mode 2		Mode 3	
		$\angle\left(\frac{\phi_{21}}{\phi_{11}}\right)$	$\angle\left(\frac{\phi_{31}}{\phi_{11}}\right)$	$\angle\left(\frac{\phi_{22}}{\phi_{12}}\right)$	$\angle\left(\frac{\phi_{32}}{\phi_{12}}\right)$	$\angle\left(\frac{\phi_{23}}{\phi_{13}}\right)$	$\angle\left(\frac{\phi_{33}}{\phi_{13}}\right)$
Crosswind Forces	RESP_2F (600s)	0.47°	0.99°	100.96°	168.83°	148.81°	21.86°
	RDS3_2F (200s)	0.12°	0.25°	86.25°	173.33°	124.52°	45.44°
Theoretical Values		0°	0°	0°	180°	180°	0°

Table 5.4.11

Relative Errors of Modal Ratios of 3DOF System Excited by two Forcing Functions

		Relative Error ξ of $\left\|\frac{\phi_{2k}}{\phi_{1k}}\right\|_{H^{(II)}}$ and $\left\|\frac{\phi_{3k}}{\phi_{1k}}\right\|_{H^{(II)}}$								
		Mode 1 (%)			Mode 2 (%)			Mode 3 (%)		
		$\left\|\frac{\phi_{21}}{\phi_{11}}\right\|$	$\left\|\frac{\phi_{31}}{\phi_{11}}\right\|$	ξ	$\left\|\frac{\phi_{22}}{\phi_{12}}\right\|$	$\left\|\frac{\phi_{32}}{\phi_{12}}\right\|$	ξ	$\left\|\frac{\phi_{23}}{\phi_{13}}\right\|$	$\left\|\frac{\phi_{33}}{\phi_{13}}\right\|$	ξ
White Noise Excitations	RESP_2F (600s)	0.002	0.037	0.039	N/A	3.748	3.748	11.71	10.26	21.97
	RDS3_3F (200s)	0.569	0.638	1.207	N/A	8.261	8.261	28.72	29.63	58.35
	RDS1_2F (200s)	0.343	0.218	0.561	N/A	13.90	13.90	37.86	48.59	86.46
	RDS3_2F (200s)	0.545	0.507	1.052	N/A	2.487	2.487	7.349	1.721	9.070
Alongwind Forces	RESP_2F (600s)	0.431	0.911	1.342	N/A	4.507	4.507	25.28	22.91	48.19
	RDS3_2F (150s)	0.069	0.137	0.206	N/A	13.21	13.21	6.396	8.954	15.35
Crosswind Forces	RESP_2F (600s)	0.013	0.054	0.067	N/A	2.185	2.185	14.01	11.36	25.37
	RDS3_2F (200s)	0.035	0.223	0.258	N/A	1.648	1.648	4.238	11.49	15.73

Secondly, the focus is put on the conclusion that the variance of the estimated RD signatures keeps increasing for the increasing time lags from the triggering position. The increasing variance can falsify the results in a parameter identification process such that it seems worthwhile to investigate its influence. Visual inspection in Figure 5.4.20 exhibits that there seems to exist a point on the RD signatures after which the use of more data makes the associated modal ratios less accurate, since the data taken from near the end of the RD signature may suffer from the variance. As a result, appropriately removing the undesired time lags from the formed RD signatures may be another improved method to effectively enhance the accuracy of their estimated modal ratios.

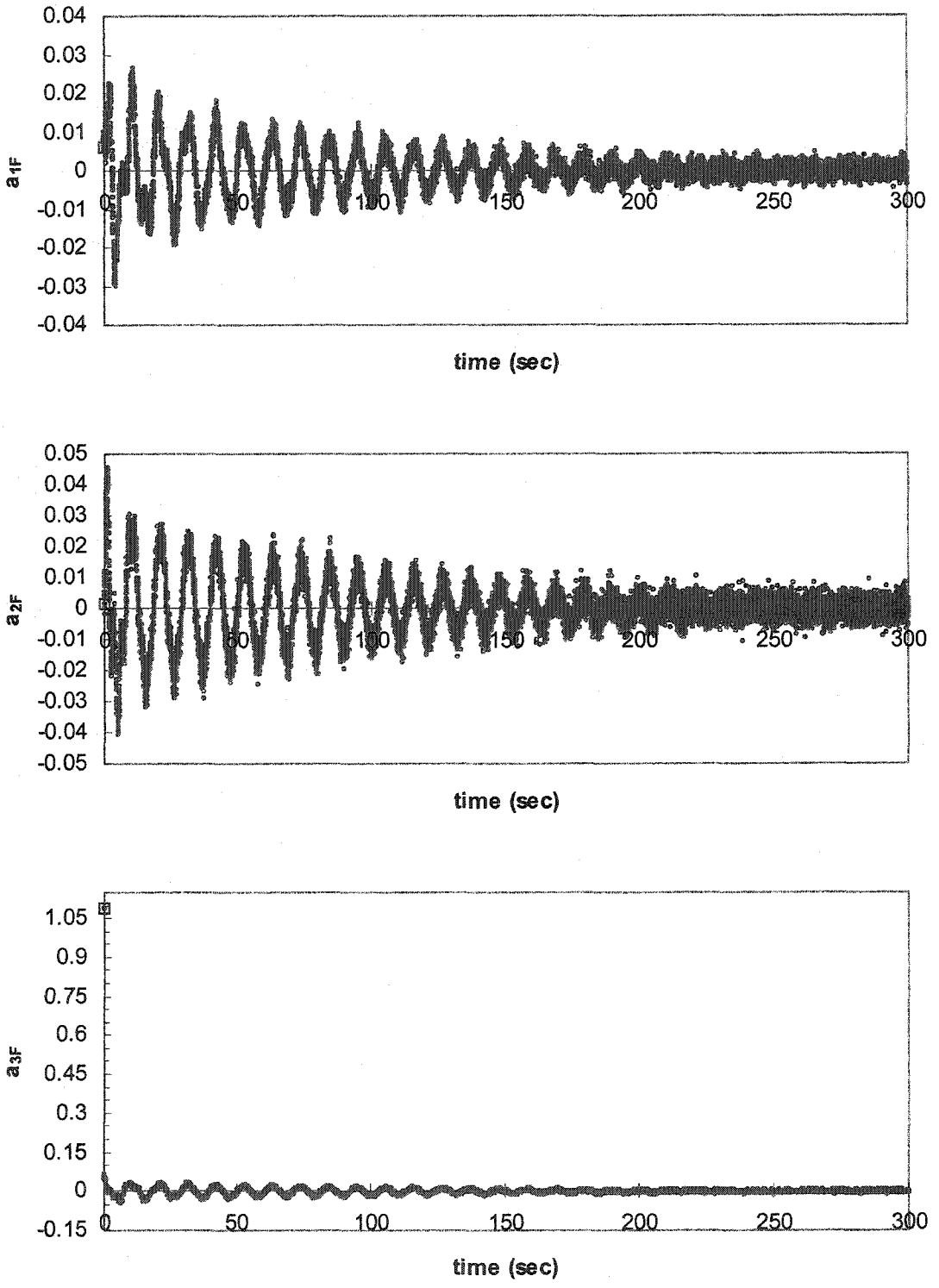

Figure 5.4.20 RD Acceleration Signatures to Three White Noise Excitations

• RD Signatures; □ First Point of RD Signatures

To assess this improved method, six time lengths of 300, 150, 75, 60, 45 and 30 seconds extracted from the figured RD signatures of 300 seconds are used. The results of the relative errors of the modal ratios for the six sets of the RD signatures are denoted as RDS_300 in Table 5.4.12. For the purpose of comparison, the other six sets are directly calculated by the RD signatures extracted from the responses with the segment lengths of 300, 150, 75, 60, 45, and 30 seconds, respectively. These sets are denoted as RDS_# in Table 5.4.12. The compared results in Table 5.4.12 reveal the advantage of the improved method that proves effective to return the better estimates of the modal ratios. However, the demand on how to optimally select the point in the formed RD signatures to make the RD signatures and their estimated FRFs more accurate is left for future investigations.

Table 5.4.12 Comparison of Relative Errors between RDS_300 and RDS_#

Specified Time Length	**Relative Error ε of $\left\|\frac{\phi_{2k}}{\phi_{1k}}\right\|_{H^{(II)}}$ and $\left\|\frac{\phi_{3k}}{\phi_{1k}}\right\|_{H^{(II)}}$**					
	Mode 1 (%)		Mode 2 (%)		Mode 3 (%)	
	RDS_300	RDS_#	RDS_300	RDS_#	RDS_300	RDS_#
300s	1.229	1.229	5.502	5.502	39.066	39.066
150s	0.959	0.994	4.052	3.852	62.281	67.662
75s	0.637	0.716	2.026	2.967	20.937	28.449
60s	0.541	0.609	0.277	1.280	37.029	42.513
45s	0.946	0.987	3.505	4.098	22.568	23.850
30s	0.061	0.093	7.685	7.666	4.520	7.422

5.5 Concluding Remarks

The RD based method was proposed for the modal parameter identification using the acceleration responses of a linear and time invariant dynamic system. However, the added effect of the applied forcing function in the impulse acceleration response function was emphasized. To overcome this problem, the theoretical development of the RD

based method was divided into two stages in this study. In first, the derivation of the traditional FRF approach for the stationary acceleration responses was modified, if the vibration modes are significantly excited, well separated and lightly damped. Second, the derivation of the RD based method, to establish the theoretical basis of the FRFs defined for the RD acceleration signatures, was achieved by adopting the concept of the derived FRF approach through use of the RD technique.

To verify the validity of the RD based method, the numerical simulations of the 2DOF and 3DOF dynamic systems individually subjected to the white noise excitations in theory and the simulated wind forces in practice were carried out. The results of these numerical simulations allow the following conclusions of this study to be made:

1. The identity relation in the estimated FRFs of the RD acceleration signatures for each mode in Table 5.4.3 validates Equations (5.3.14-16) or (5.3.25-27). Such a validation, based on the three different scenarios of the input forces, further reflects that the feature of the identity relation for the FRFs of the RD signatures is obtainable with respect to various types of Gaussian input excitations. In addition, such an underlying feature for the FRFs of the RD signatures of any kind is readily applicable to dynamic response measurements as a diagnostic indication of whether a prescribed linear dynamic model for the tested system is consistent or not.
2. The comparisons between the numerical and the theoretical modal ratios reveal a superior match for both the RD based method and the FRF approach, when the two dynamic systems were excited by the white noise excitations. The superiority of the RD based method over the FRF approach concerning the accuracy of the modal ratios is a notable finding, especially for the higher modes, when the simulated wind forces

were applied to the dynamic systems. Such a result not only fosters the substantial emphasis of simulating wind forces, but also verifies the critical reliability of using the RD based method to estimate the modal parameters of a dynamic system under environmental loadings.

3. To effectively circumvent the added effect of the RD force signatures in the RD acceleration signatures, the leading response can be assigned to a set of the collected response data in the location where any applied forcing function is isolated. It means that the location of the accelerometer is an important step to successfully yield the leading acceleration response. Such a ladder method conceptually innovates the use of the RD technique to acceleration responses and thus facilitates any other system identification procedure using the RD acceleration signatures.
4. Following the recognition on the increasing variance in the estimated RD signatures, the discard of the undesired section from the formed RD signatures is necessary to obtain the more accurate modal parameters. Nonetheless, in order to reduce the frequency resolution bias in the FRFs of the RD signatures, the time lags of each RD signature is required as longer as possible. These two contradictory requirements need a trade-off in the selected length from the formed RD signatures so that the use of the RD based method can include sufficient information regarding the dynamic system. In this respect, further research is recommended to focus on selecting the optimal section in the formed RD signatures in order to make the RD signatures and their estimated FRFs more desirable and accurate.

The success of the RD based method highlights the role of the FRF approach in such a method other than the RD technique to solve the difficulty of involving the

additional RD force signatures in the RD acceleration signatures. Similarly, the FRF approach might be combined with some other time domain identification techniques with respect to the same identification problem regarding this study. Since it is beyond the scope of this study, it will be the subject of future research.

References

Bao, Z. W. and Ko, J. M. (1991), "Determination Of Modal Parameters Of Tall Buildings With Ambient Vibration Measurements", The International Journal of Analytical and Experimental Modal Analysis, Vol. 6, No. 1, pp. 57-68.

Bendat, J. S. and Piersol, A. G. (2000), Random Data Analysis and Measurement Procedures, 3rd Edition, John Wiley & Sons, pp.138.

Crandall, S. H. and Mark, W. D. (1963), Random Vibration in Mechanical Systems, Academic Press, pp. 58-64.

He, J. M. and Fu, Z. F. (2001), Modal Analysis, 1st Edition, Butterworth-Heinemann, pp. 149-152.

Huang, C. S. and Yeh, C. H. (1999), "Some Properties Of Randomdec Signatures", Mechanical Systems and Signal Processing, Vol. 13, No. 3, pp. 491-507.

Ibrahim, S. R. (1977), "Random Decrement Technique For Modal Identification Of Structures", Journal of Spacecraft, Vol. 14, No. 11, pp. 696-700.

Juang, J. N. and Pappa, R. S. (1985), "An Eigensystem Realization Algorithm For Modal Parameter Identification And Model Reduction", Journal of Guidance, Control, and Dynamics, Vol. 8, pp. 620-627.

Juang, J. N., Cooper, J. E., and Wright, J. R. (1988), "An Eigensystem Realization Algorithm Using Data Correlation For Modal Parameter Identification", Journal of Control Theory and Advanced Techniques, Vol. 4, No. 1, pp. 5-14.

Liu, F. Q. and Zhang, L. M. (1999), "An Improved Eigensystem Realization Algorithm And Its Application To Modal Parameter Identification Of Intelligent Space Trusses", Journal of Vibration Engineering, Vol. 12, pp. 316-322.

Pappa, R. S. and Ibrahim, S. R. (1981), "A Parametric Study Of The Ibrahim Time Domain Modal Identification Algorithm", The Shock and Vibration Bulletin, Bulletin 51, Part 3, pp. 43-72.

Paz, M. (1997), Structural Dynamics: Theory and Computation, 4th Edition, Chapman & Hall, pp. 352-355.

Schmidt, H. (1985), "Resolution Bias Errors In Spectral Density, Frequency Response And Coherence Function Measurements, III: Application To Second-Order Systems (White Noise Excitation)", Journal of Sound and Vibration, Vol. 101, No. 3, pp. 377-404.

Schmidt, H. (1985), "Resolution Bias Errors In Spectral Density, Frequency Response And Coherence Function Measurements, V: Comparison Of Different Frequency Response Estimators", Journal of Sound and Vibration, Vol. 101, No. 3, pp. 413-418.

Van Overschee, P. and De Moor, B. (1996), Subspace Identification for Linear Systems, Kluwer.

Vold, H. and Rocklin, G. T. (1982), "The Numerical Implementation Of A Multi-Input Modal Estimation Method For Mini-Computers", Proceedings of the 1st International Modal Analysis Conference, pp. 542-548.

Vold, H. and Russell, R. (1983), "Advanced Analysis Methods Improve Modal Test Results", Sound and Vibration, Vol. 17, pp. 36-40.

Wang, Z. N. and Fang, T. (1986), "A Time-Domain Method For Identifying Modal Parameters", Journal of Applied Mechanics, ASME, Vol. 53, pp. 28-32.

Chapter 6

MODAL PARAMETER IDENTIFICATION OF AN MDOF AEROELASTIC BUILDING MODEL

6.1 Introduction

Experimental tests to characterize the dynamic behavior of proposed structural systems are ordinarily desirable during the development, design, or service stages of engineering projects. Prominent advances in measurement instrumentations and computational resources have contributed to increasing the capability and reliability of experimental tests for structural systems. Wind tunnel tests provide an effective and fast choice to investigate the dynamic behavior of structural systems under wind forces. Important information from wind tunnel tests of a linear structural system includes modal parameters, such as natural frequencies, damping ratios, and mode shapes. The modal parameters can be used to establish an analytical finite element model for a structural dynamic system in order to anticipate the behavior of the structural system in a specified wind environment.

To determine the reliable modal parameters, system identification techniques are essential in processing measured data from tests. Of particular concern in this study is the issue related to the identification of the modal parameters from forced acceleration responses without the use of quantitative information regarding the applied forces. The fact that the measured acceleration responses contain the added effect of the applied forces serves to complicate the identification problem. Given the previous theoretical

and numerical investigations, the random decrement based method, under certain conditions, is capable of processing such responses contaminated by the involvement of the applied forces.

The purpose of the study presented in Chapter 6 is therefore focused on verifying the feasibility of the RD based method in practical applications of acceleration responses. A five-story fully aeroelastic building model is used to measure its acceleration responses in a boundary layer wind tunnel. The RD based method combines the RD technique in cooperation with the fast Fourier transform (FFT) based algorithms to estimate the natural frequencies and mode shapes from the measured acceleration responses. Since there is the lack of reference parameters for the building model, the modal parameters estimated by the RD based method alone are perhaps not objective. In this respect, the frequency response function (FRF) approach that uses the FFT based algorithms for evaluating frequency response functions (FRFs) is also given for the purpose of a cross validation. The natural frequencies and corresponding mode shapes of the building model identified from the RD based method are compared with those identified from the FRF approach. The satisfaction of the orthogonality condition for the identified mode shapes to a lumped mass model is further inspected to validate the applicability of the proposed RD based method.

6.2 Wind Tunnel Measurements

6.2.1 Wind Characteristics in Wind Tunnel

The meteorological wind tunnel located at the wind engineering laboratory in Colorado State University was used for wind tunnel tests. The wind tunnel is a closed-

circuit system with a test section of 1.83 m × 1.83 m to 2.06 m × 2.06 m cross-section and 26.82 m long, as shown in Figure 6.2.1. The test model is mounted on the turntable located near the downstream end of the wind tunnel test section, which allows rotation for any approaching wind direction. Spires, low barriers and roughness elements can be set up through the test section in the wind tunnel to develop the anticipated turbulent boundary layer, as shown in Figure 6.2.2.

The profiles of mean wind velocity and longitudinal turbulent intensity, shown in Figure 6.2.3, were measured by a single hot-wire anemometer at the location of the turntable. In Figure 6.2.4, the logarithmic law and the power law, defined by Equations (6.2.1) and (6.2.2), respectively, were used to fit the mean wind velocity profile.

$$\overline{U}(z) = \frac{u_*}{\kappa} \ln \frac{z}{z_0} \tag{6.2.1}$$

$$\frac{\overline{U}(z)}{V_1(z_1)} = \left(\frac{z}{z_1} \right)^{\alpha} \tag{6.2.2}$$

in which $\kappa \approx 0.4$ is the von Karman constant, u_* is a surface friction velocity, z_0 is an aerodynamic roughness length, and $V_1(z_1)$ is a reference mean velocity at a height z_1 from the ground. The values, $u_* = 0.1644$ m/sec and $z_0 = 0.2597$ cm, were determined from Figure 6.2.4 (a) for the best fit of Equation (6.2.1). Besides, an exponent of $\alpha = 0.2173$ for Equation (6.2.2) was used to describe the mean velocity profile, as shown in Figure 6.2.4 (b). Furthermore, the normalized longitudinal velocity spectrum $fS_u(f)/\sigma_v^2$ at the top of a tested building model with respect to the normalized frequency fz/U is shown in Figure 6.2.5.

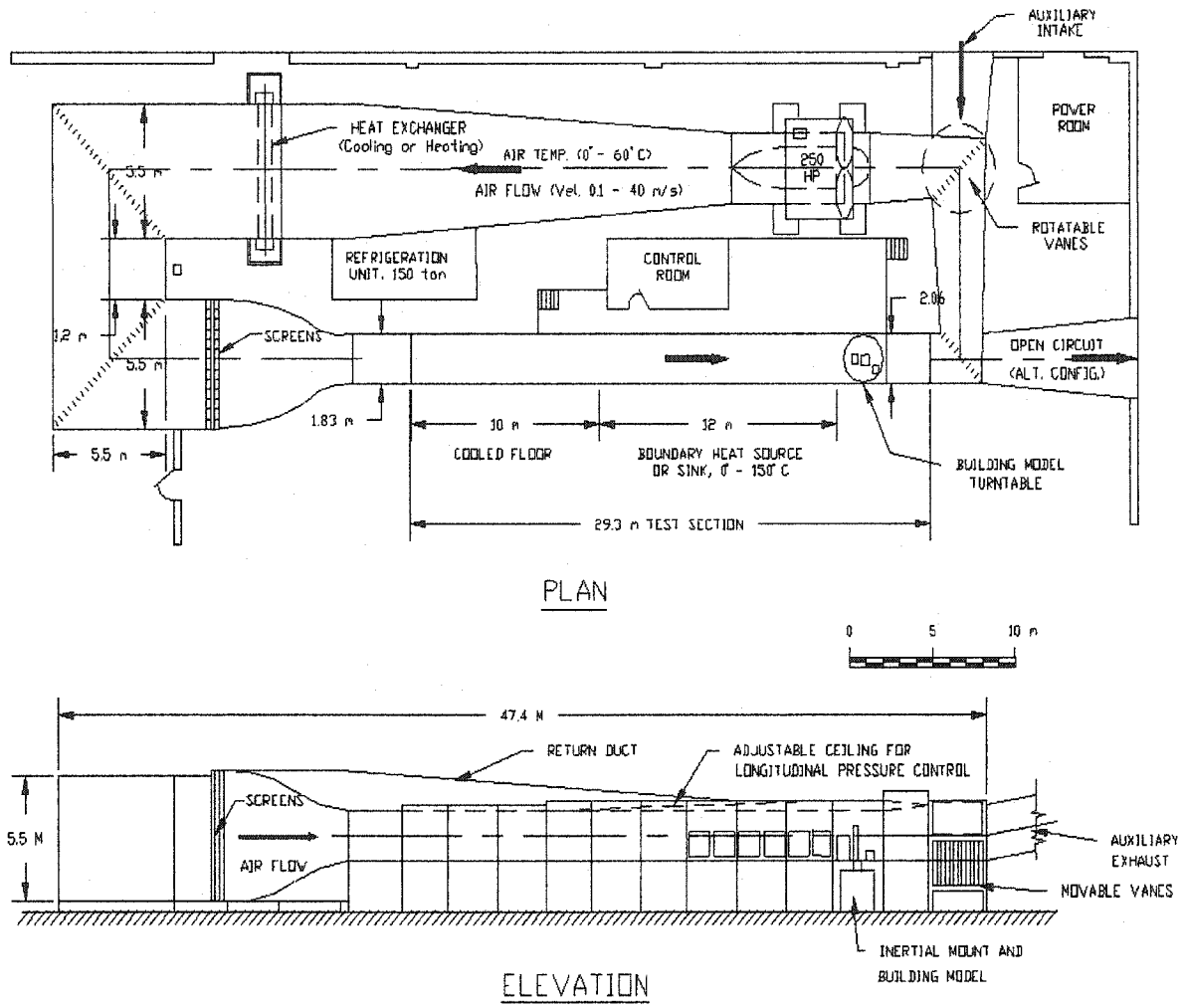

Figure 6.2.1 The Meteorological Wind Tunnel

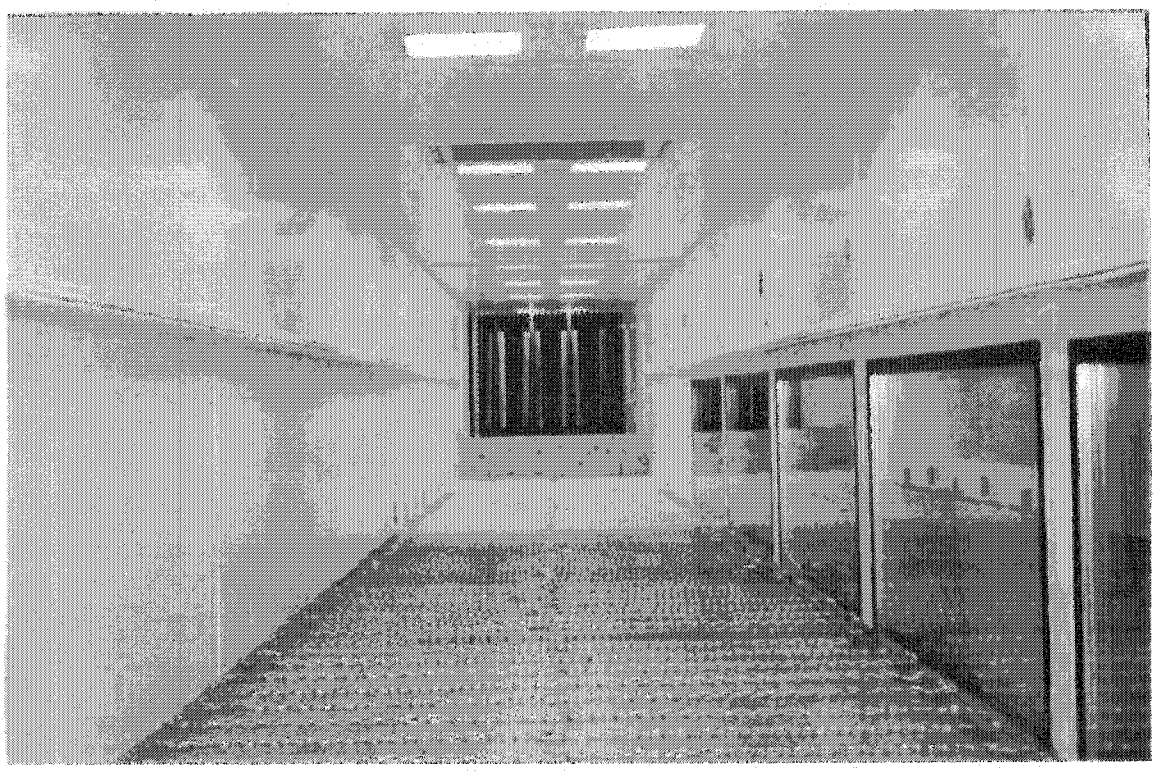

Figure 6.2.2 Arrangement of Upstream Setup

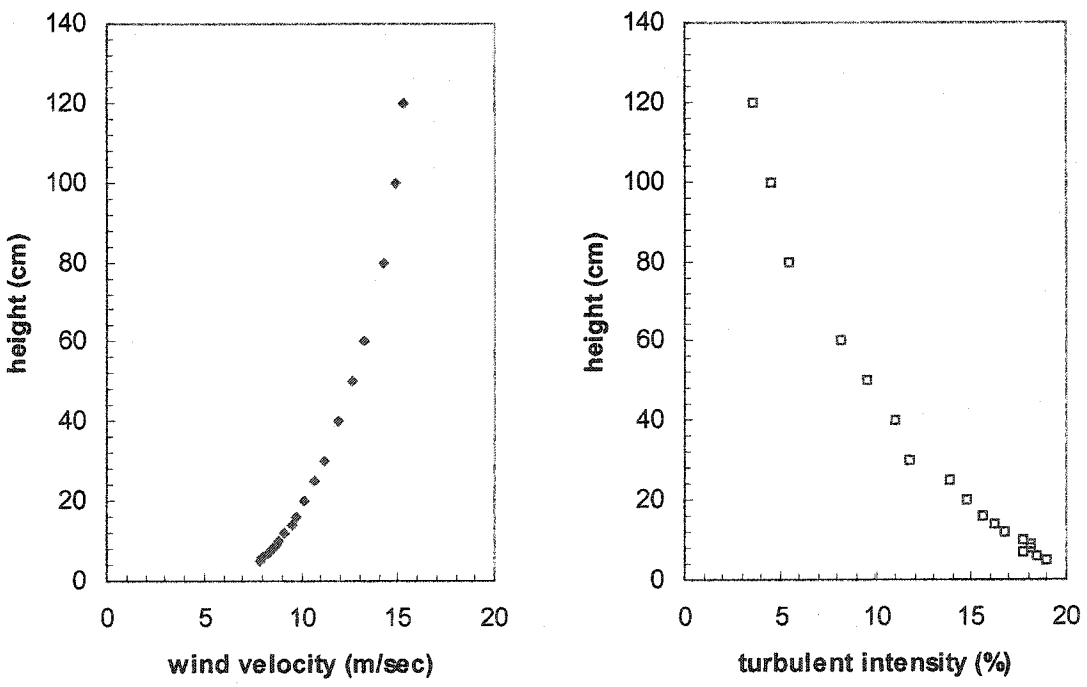

Figure 6.2.3 Profiles of Mean Velocity and Turbulent Intensity

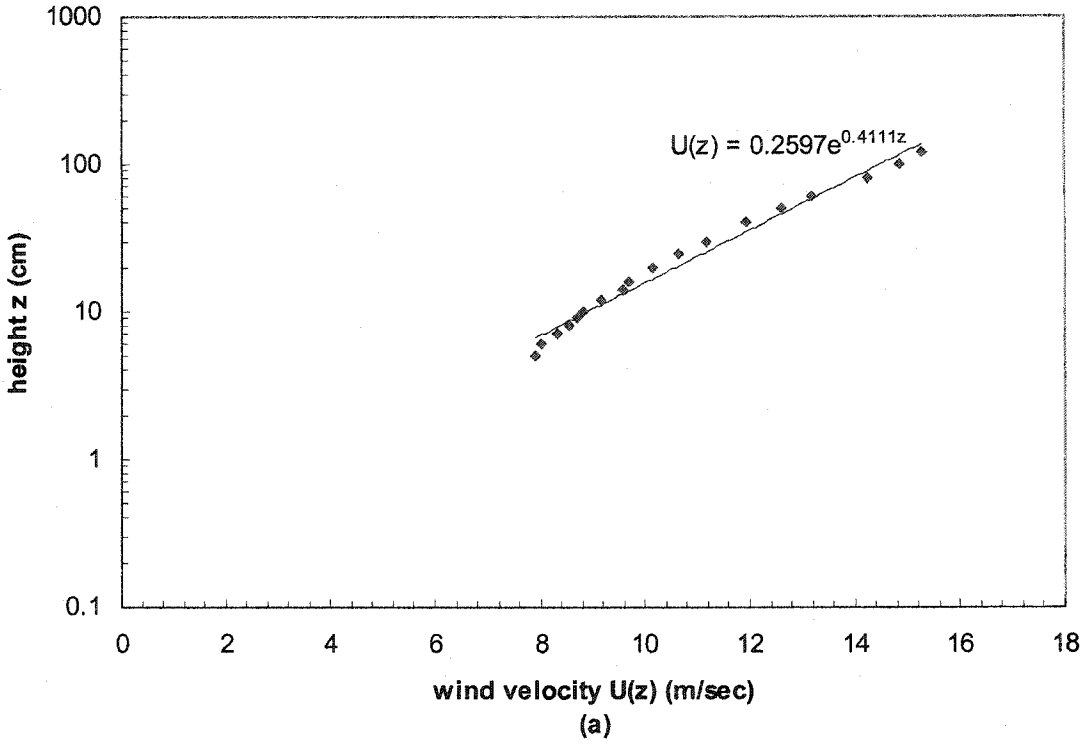

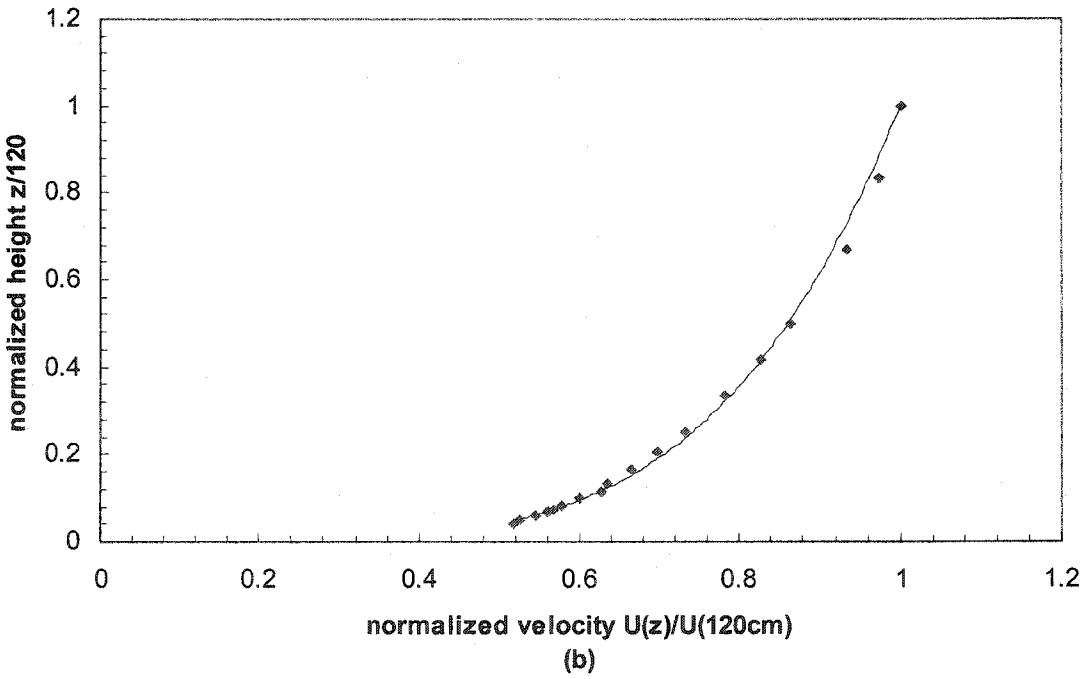

Figure 6.2.4 The Fits of (a) Logarithm Law and (b) Power Law for Mean Velocity Profile

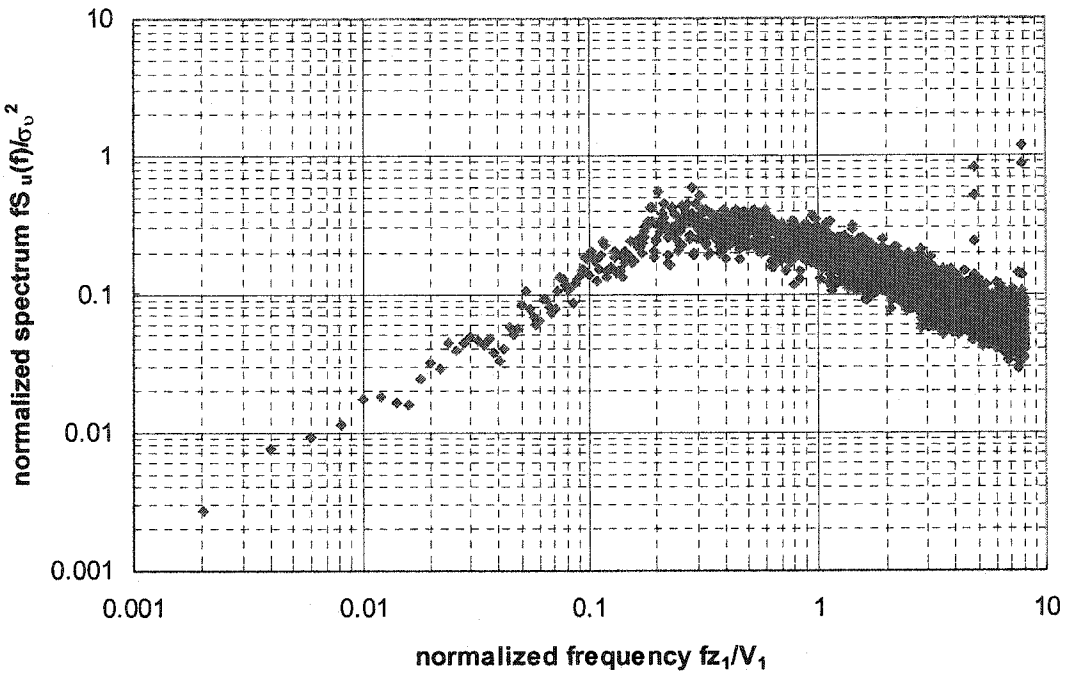

Figure 6.2.5 Normalized Longitudinal Wind Velocity Spectrum

6.2.2 Description of MDOF Aeroelastic Model

A MDOF aeroelastic model is required in wind tunnel tests, when the higher mode responses need to be examined. Such an aeroelastic model ordinarily uses lumped masses and each mass has two lateral and one rotational degrees-of-freedom (DOFs) responses, in order to simulate a number of coupled lateral and torsional modes of vibration in a tall building. Several MDOF aeroelastic building model tests have been carried out previously [Templin and Cooper, 1981; Isyumov, 1982; Katagiri, et al., 1998; Cho, 1999].

In this study, the model is a five-story aeroelastic brass frame representation of a rectangular building, which was originally built for a research of structural passive

motion control with bracings of viscoelastic damper. The model frame has a footprint of 500 mm × 330 mm and a height of 1167 mm, as shown in Figure 6.2.6. Removing the damper bracings and enclosing the exterior surface with 6.4 mm thick plastic sheets modified the aeroelastic building model for the use of this study. The exterior surface is separated by a 5 mm gap between two floors. The plastic sheets in each floor are attached to the diaphragm of the floor. The lumped masses of the first to fifth floor are estimated as 14.552 kg, 13.970 kg, 14.168 kg, 13.814 kg, and 13.858 kg, respectively, yielding a 5×5 lumped mass matrix. Each lumped mass consists of the floor girders, columns, plastic sheets, and an additional brass block on the center of the floor. The building model under test is shown in Figure 6.2.7.

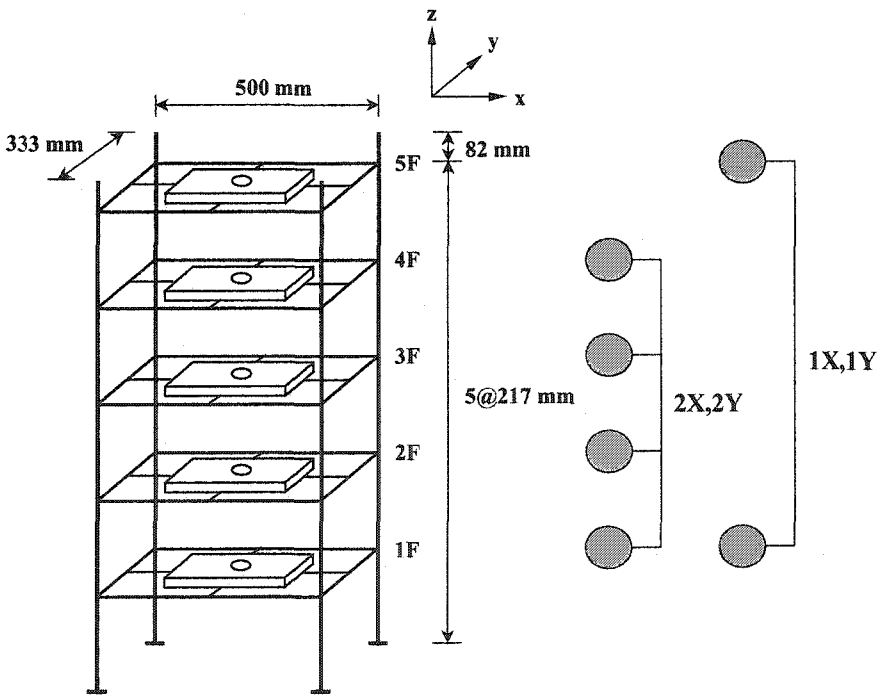

Figure 6.2.6 Sketch of a Five-Story Aeroelastic Building Model and Measurement Setup, 1X, Y and 2X, Y

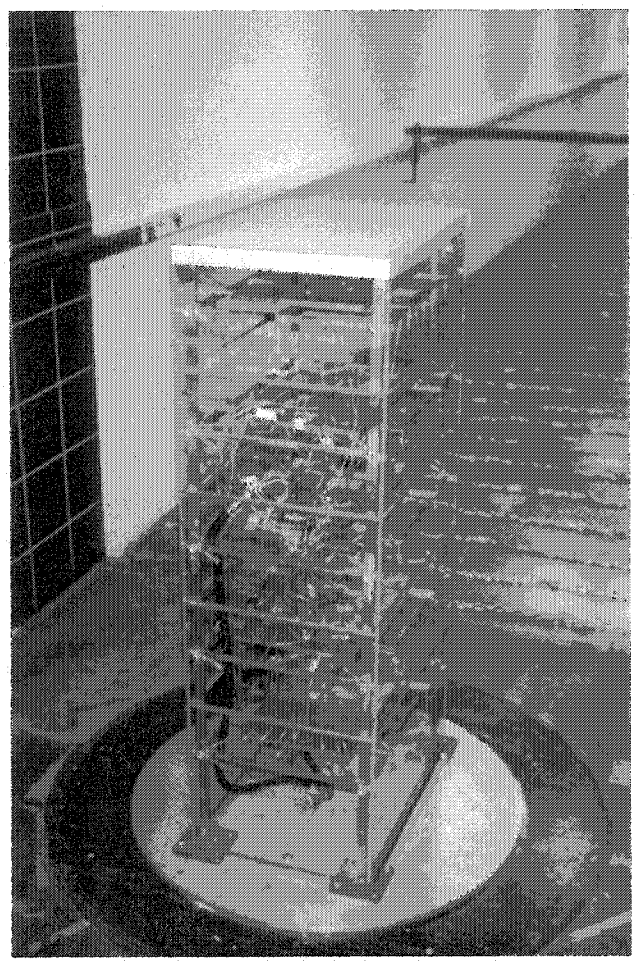

Figure 6.2.7 Tested Building Model

6.2.3 Instrumentation for Measurement

Four semiconductor-type accelerometers with a sufficient dynamic range of ±50g and an effective frequency band from 0 Hz to 360 Hz were used to measure a series of acceleration responses. These accelerometers were placed at locations of the building model so that the proper information could be extracted from the recorded acceleration responses. Each floor of the building model was instrumented to measure their lateral responses on account of wind-induced vibrations. In consequence of symmetry of the building model and high stiffness of the floor girders, it may be assumed that the lateral

and torsional responses in each floor are uncoupled when the approach wind is normal to the face of the building model. To minimize the response component associated with torsional motion, the accelerometer was attached at the geometrical center of each floor in the building model.

Given the limited number of the accelerometers available, the installation of the accelerometers in the building model was necessarily arranged into two groups of different floors, one with four accelerometers and the other with two accelerometers. From this arrangement, four sets of simultaneously measured acceleration responses in the perpendicular lateral directions were independently recorded, i.e. 1X, 1Y, 2X and 2Y, as schematically depicted in Figure 6.2.6. The overlapped position at the first floor for both groups was assigned to be a reference point, which was used to correlate the two sets of the measured responses in the same direction in order to assemble the complete mode shapes of the building model.

The analog signals generated simultaneously by the accelerometers have to be optimized for the maximum input range of a data acquisition board. Accordingly, four Honeywell Accudata 218 amplifiers were used to amplify low-level analog signals. The amplified signals were then filtered through three Wavetek model 852 filters to further enhance their quality. Finally, the amplified and filtered analog signals were converted to digital signals and recorded in a PC-based data acquisition system. According to the Nyquist theorem, the sampling frequency must be chosen over twice the maximum frequency component of interest in a signal to prevent the folding and aliasing problems when digitizing data. In this regard, the sampling frequency was set at 350.14 Hz in the data acquisition system for the acceleration measurement throughout the present study.

Correspondingly, the cutoff frequencies of the analogue anti-aliasing filter were selected at 60 Hz and 175 Hz for 1X, 1Y and 2X, 2Y, respectively, to eliminate all high frequency noises. The wind direction for each measurement set is defined in Figure 6.2.8. The data length of each measurement consisted of 32768 sample points corresponding to the time duration of 93.59 seconds. An example of a time history for the recorded measurement of the 1Y set is shown in Figure 6.2.9. The acceleration measurement for the wind tunnel tests was repeated six times to improve statistical estimates.

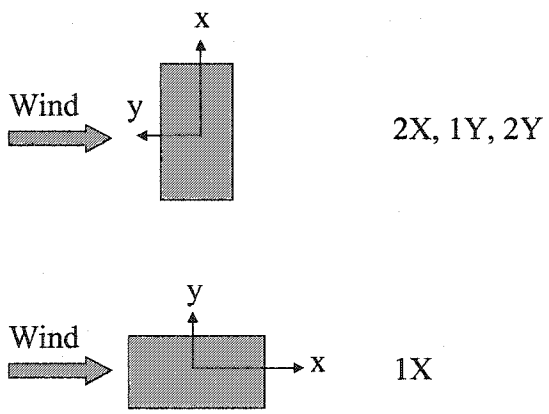

Figure 6.2.8 Approaching Wind Direction for each Measurement Set

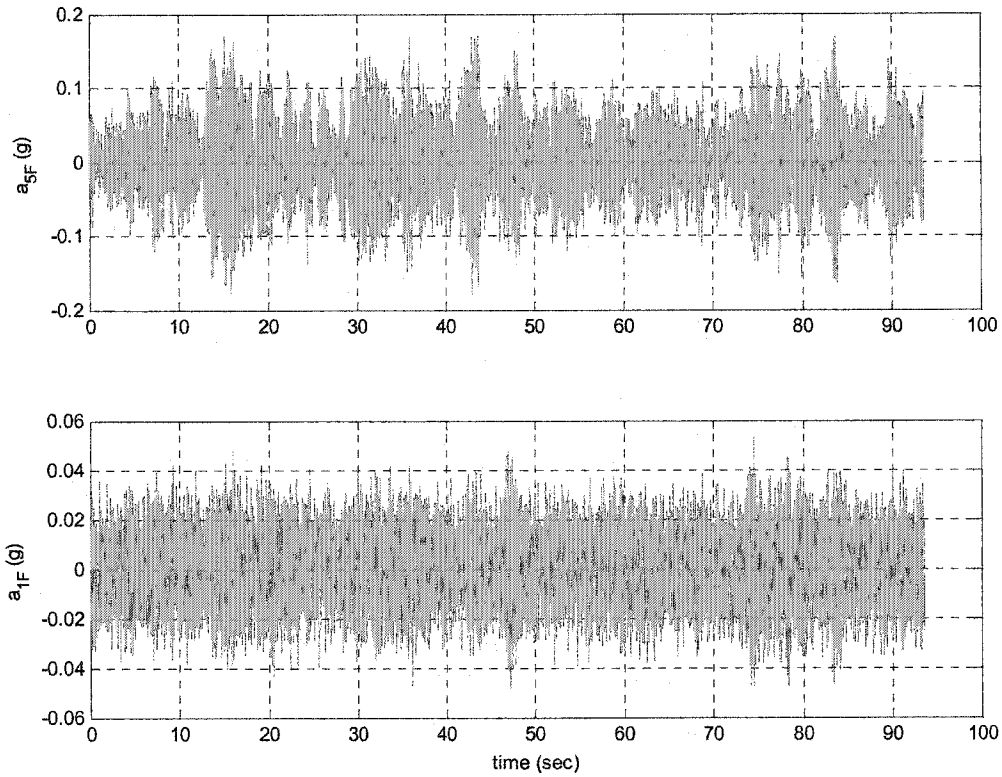

Figure 6.2.9 Time History of 1Y

In addition to the acceleration measurement, a Pitot-static tube and a single hot-wire anemometer were used for wind velocity measurement during the wind tunnel tests. The Pitot-static tube was installed 3.7 m upstream at the top of the building model to monitor a wind speed at 15 m/sec during the wind tunnel tests. When wind flow approached normally to the face of the building model, the hot-wire anemometer was located outside the wake region and at ¾ of the model height to explore the velocity fluctuations of the vortex shedding. The normalized spectra for the velocity fluctuations of the vortex shedding are illustrated in Figure 6.2.10.

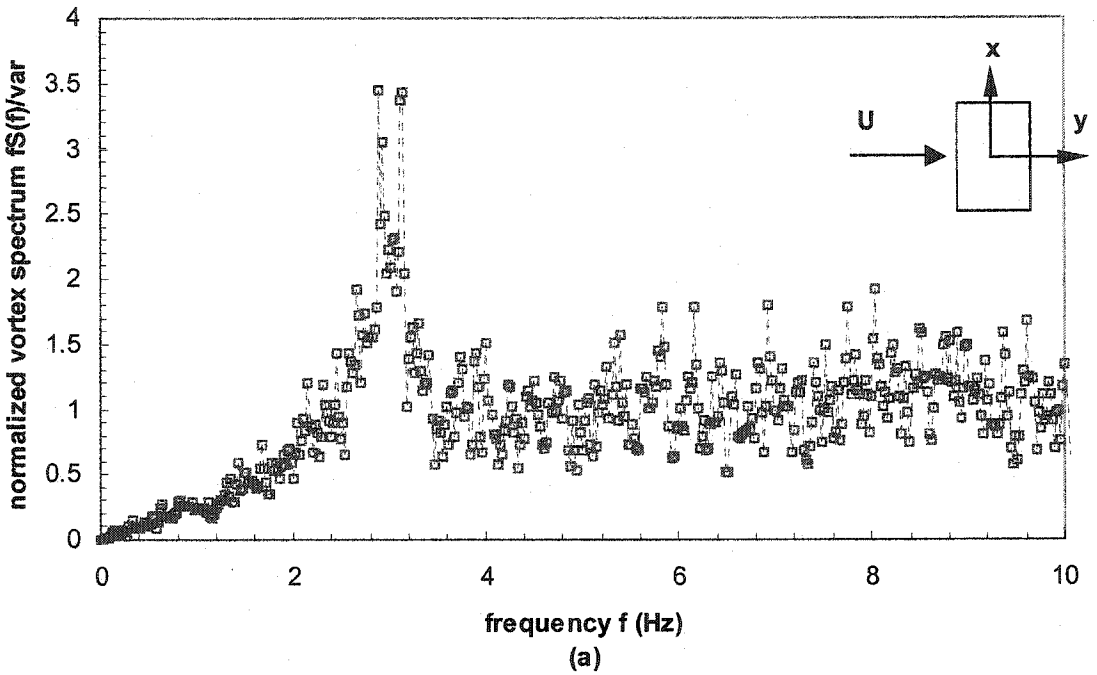

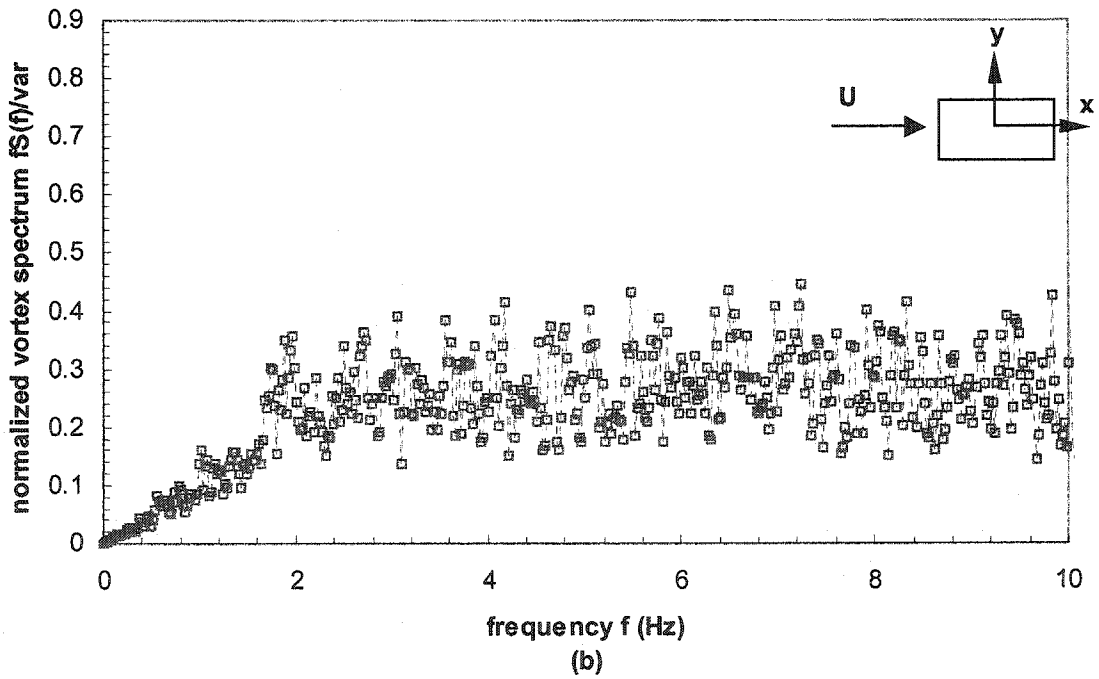

Figure 6.2.10 Normalized Spectra for Velocity Fluctuations of Vortex Shedding

6.3 Identification of Modal Parameters for a Building Model

The modal parameters of interest are natural frequencies and corresponding mode shapes for both lateral directions of the aeroelastic building model in the present study. Attention is focused primarily on system identification techniques, which can deal with the forced acceleration responses. The characteristics of such acceleration responses involving the applied forces may cause a biased problem in time domain identification techniques, when one takes into account only the acceleration responses. In this respect, frequency domain identification techniques were used in place of time domain identification techniques in this study.

The RD based method and the FRF approach were used to identify the modal parameters of the building model from the measured acceleration responses. The RD based method consists of the averaging procedure and the identification procedure. The averaging procedure implements the RD technique to remove random components and errors in measured responses and form the RD signatures. The identification procedure employs the FFT based algorithms to estimate the modal parameters from the formed RD signatures. In addition, the FRF approach is a fast and simple method only using the FFT based algorithms. The FRF approach identifies resonant frequencies virtually from peaks shown in spectral density functions. With the identified frequencies, the FRFs can be calculated via the spectral density functions between a designated reference response and other responses. The information of amplitude and phase angle contained in the FRFs can provide the estimates of the mode shapes. The identified modal parameters from these two methods can complement each other.

Notably, these two methods rely on the strict assumption that the dynamic response at a resonant frequency is dominated by the contribution of that vibration mode at the resonant frequency, and the contributions of other vibration modes are negligible. With the validity of such an assumption, the modal parameters can be determined in the frequency domain of the acceleration responses without further resolving the involved wind forces in such excited responses.

6.3.1 Random Decrement Signatures

The RD technique, a segment-based averaging procedure, is used to extract the RD signatures from their respective random responses induced by Gaussian random excitations with zero means. The unbiased estimates of the auto and cross RD signatures are, respectively, given by:

$$\hat{\delta}_{\ddot{X}_i\ddot{X}_i}(\tau) = \frac{1}{N}\sum_{k=1}^{N} \ddot{X}_i(t_k+\tau) | \ddot{X}_i(t_k) = \ddot{x}_0 \tag{6.3.1}$$

$$\hat{\delta}_{\ddot{X}_j\ddot{X}_i}(\tau) = \frac{1}{N}\sum_{k=1}^{N} \ddot{X}_j(t_k+\tau) | \ddot{X}_i(t_k) = \ddot{x}_0 \tag{6.3.2}$$

$$\tau \geq t_k$$

in which the concurrences of a threshold level $\ddot{x}_0$ and the response $\ddot{X}_i(t)$ are detected at t_k in order to select the stacking segments $\ddot{X}_i(t_k+\tau)$. With respect to $\ddot{X}_i(t_k+\tau)$, the stacking segments of the other responses $\ddot{X}_j(t_k+\tau)$ are also decided at the same time. As soon as the RD signatures are formed, their spectral density functions are evaluated with the FFT based algorithms in order to identify the modal parameters of a dynamic system.

In the following segment-based averaging procedure, the threshold level is specified as 0.8 times the root-mean-square value of the measured response at the 1st floor of the building model in which more information about the higher modes may be contained. Figures 6.3.1 and 6.3.2 illustrate the time histories of the four sets of the RD acceleration signatures with the total data length of 2500 points. The parenthesized terms in the title line of Figures 6.3.1 and 6.3.2 indicate the superimposed numbers of the selected segments used to constitute the RD signatures. The initial point of each RD acceleration signature is marked by a square to exhibit the possible influence from the RD signature of the applied force. It is observed that the first few points of the formed RD signatures deviate obviously from their own decay curves, especially for the RD signatures at the 1st floor. Such a deviation reflects the fact that the RD acceleration signature is influenced by the contribution of the RD force signature. Figures 6.3.3 and 6.3.4 reveal the averaged normalized spectral density functions of the RD signatures with 2048 data points prepared by the Hanning window.

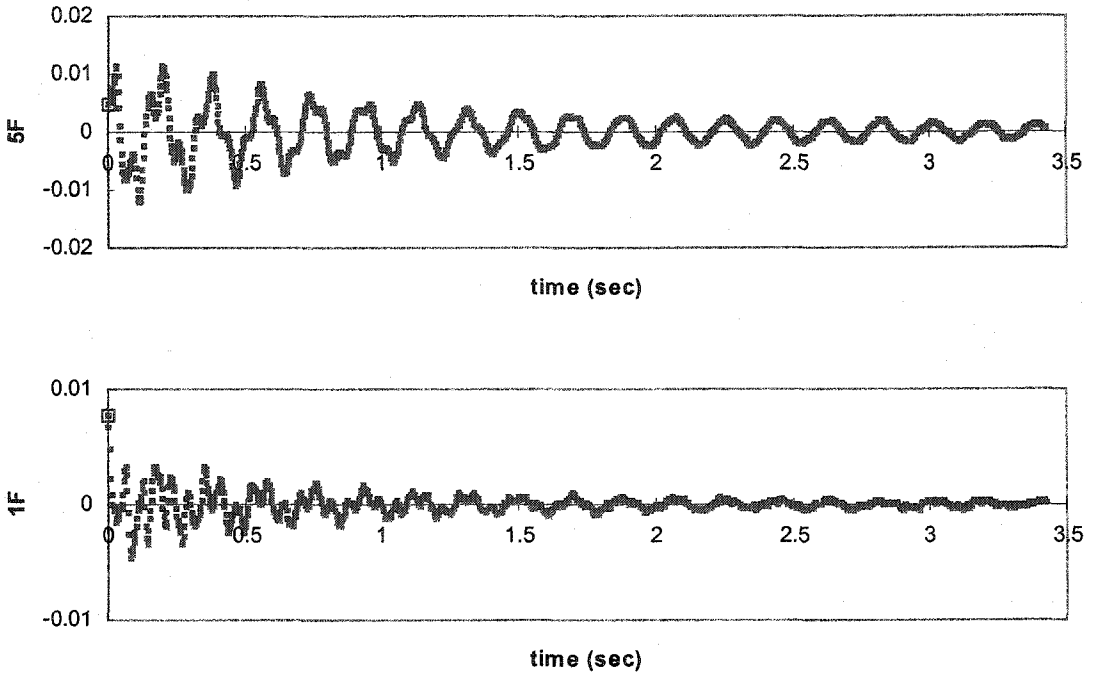

Figure 6.3.1 (a) RD Signatures for 1X (7347)

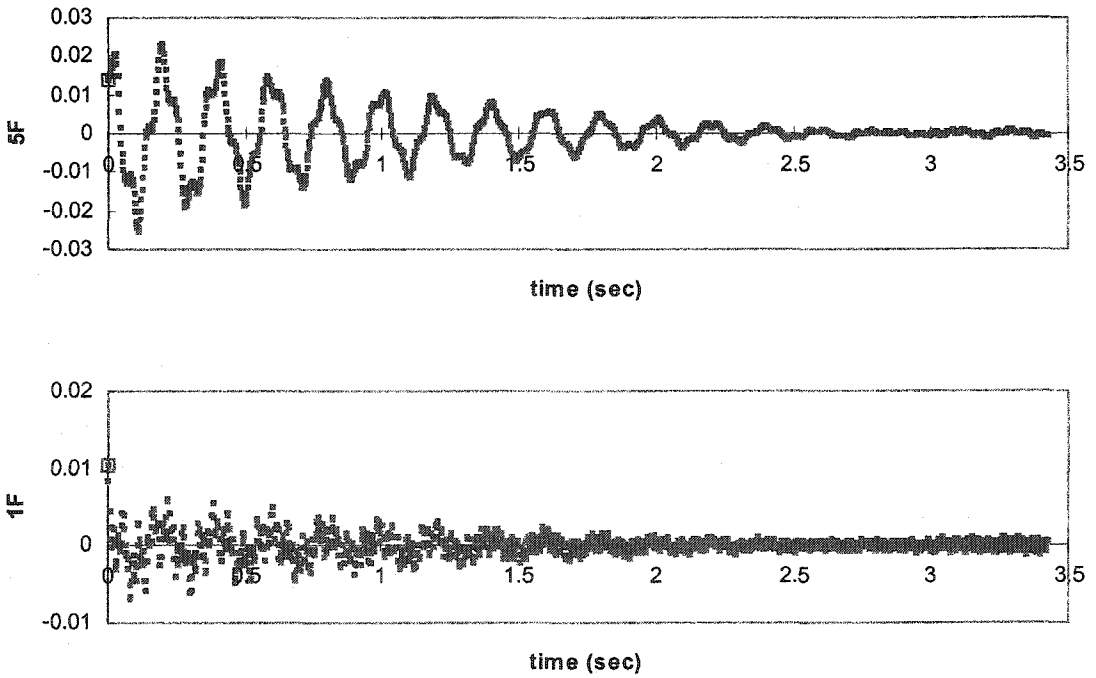

Figure 6.3.1 (b) RD Signatures for 1Y (7731)

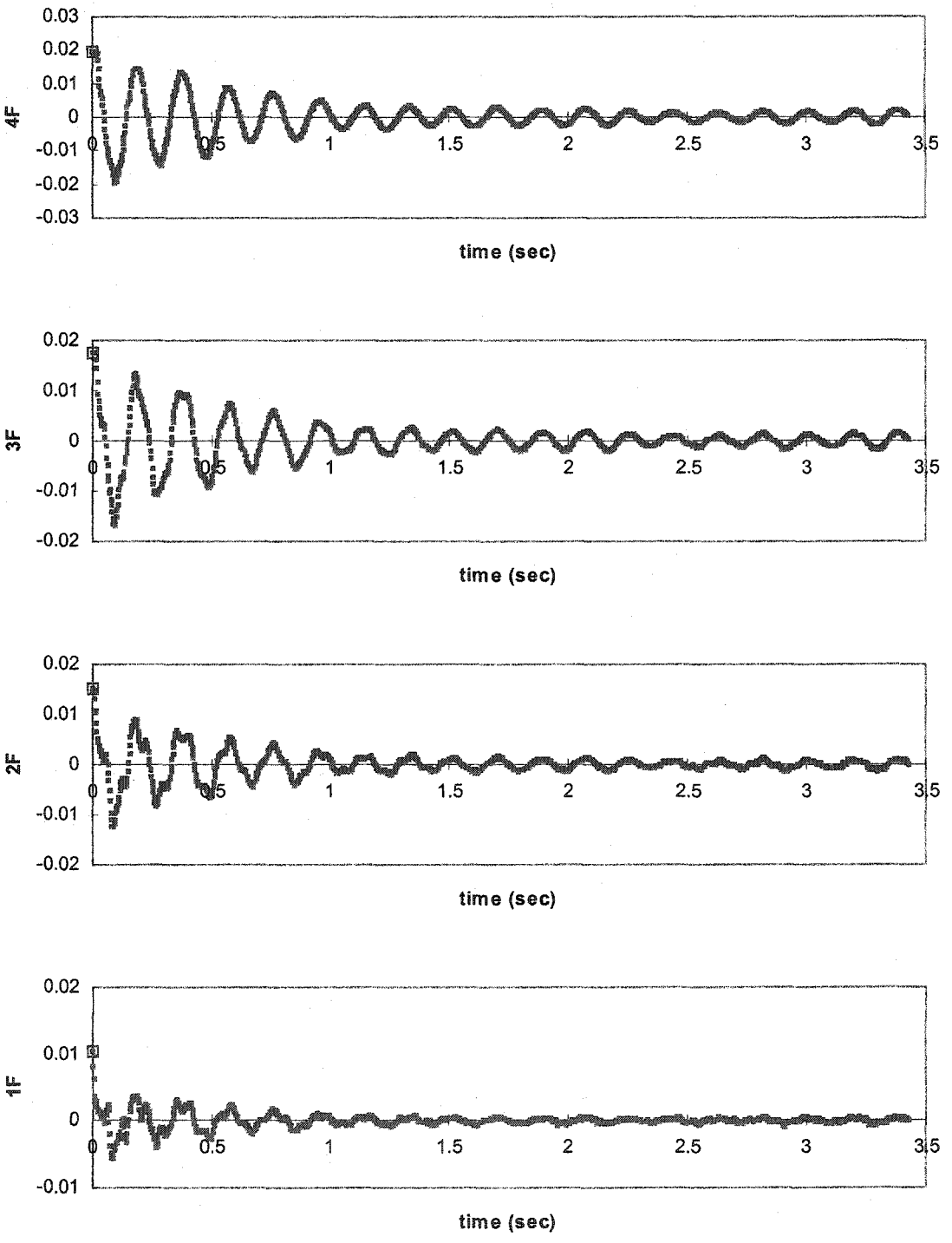

Figure 6.3.2 (a) RD Signatures for 2X (7761)

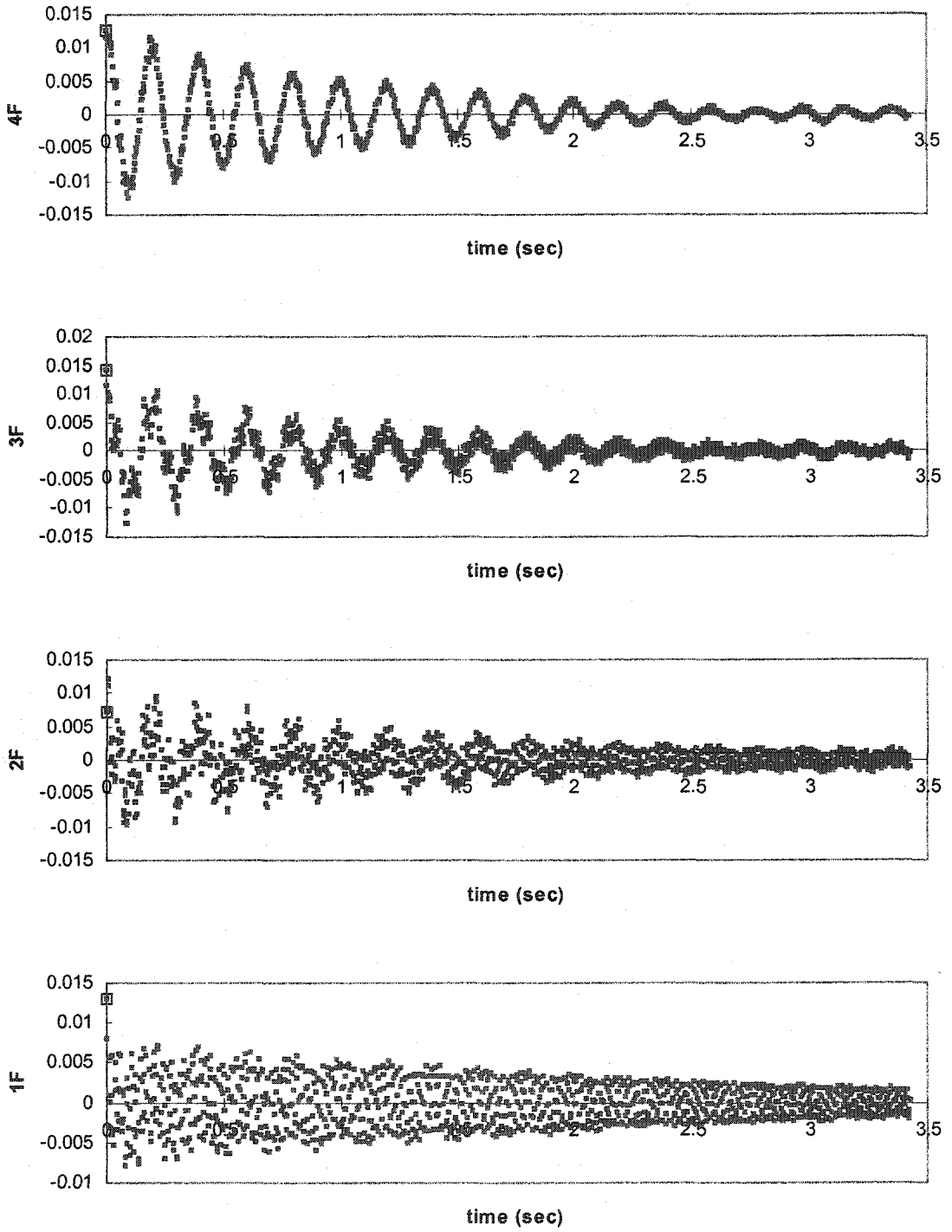

Figure 6.3.2 (b) RD Signatures for 2Y (7868)

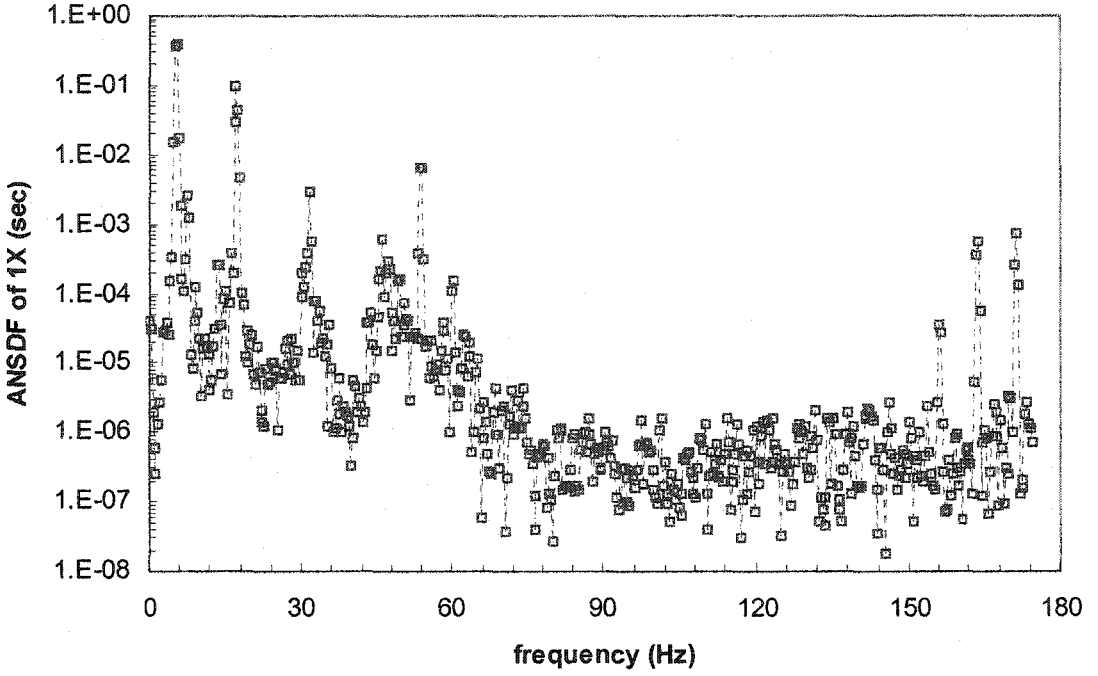

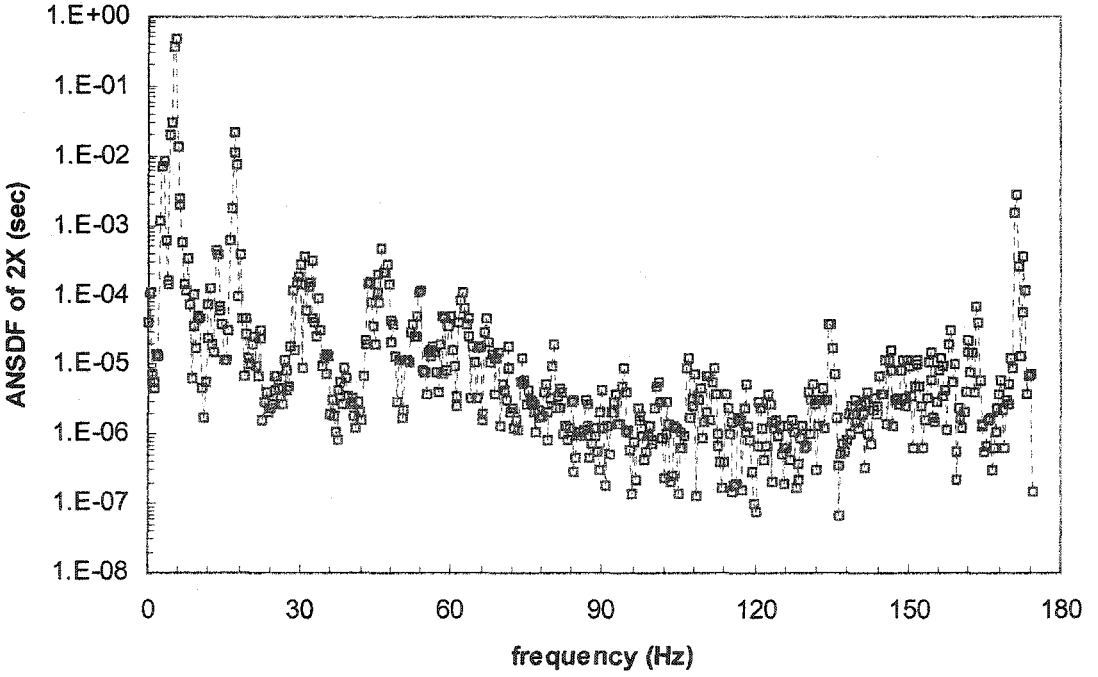

Figure 6.3.3

Averaged Normalized Spectral Density Functions of RD Signatures in X direction

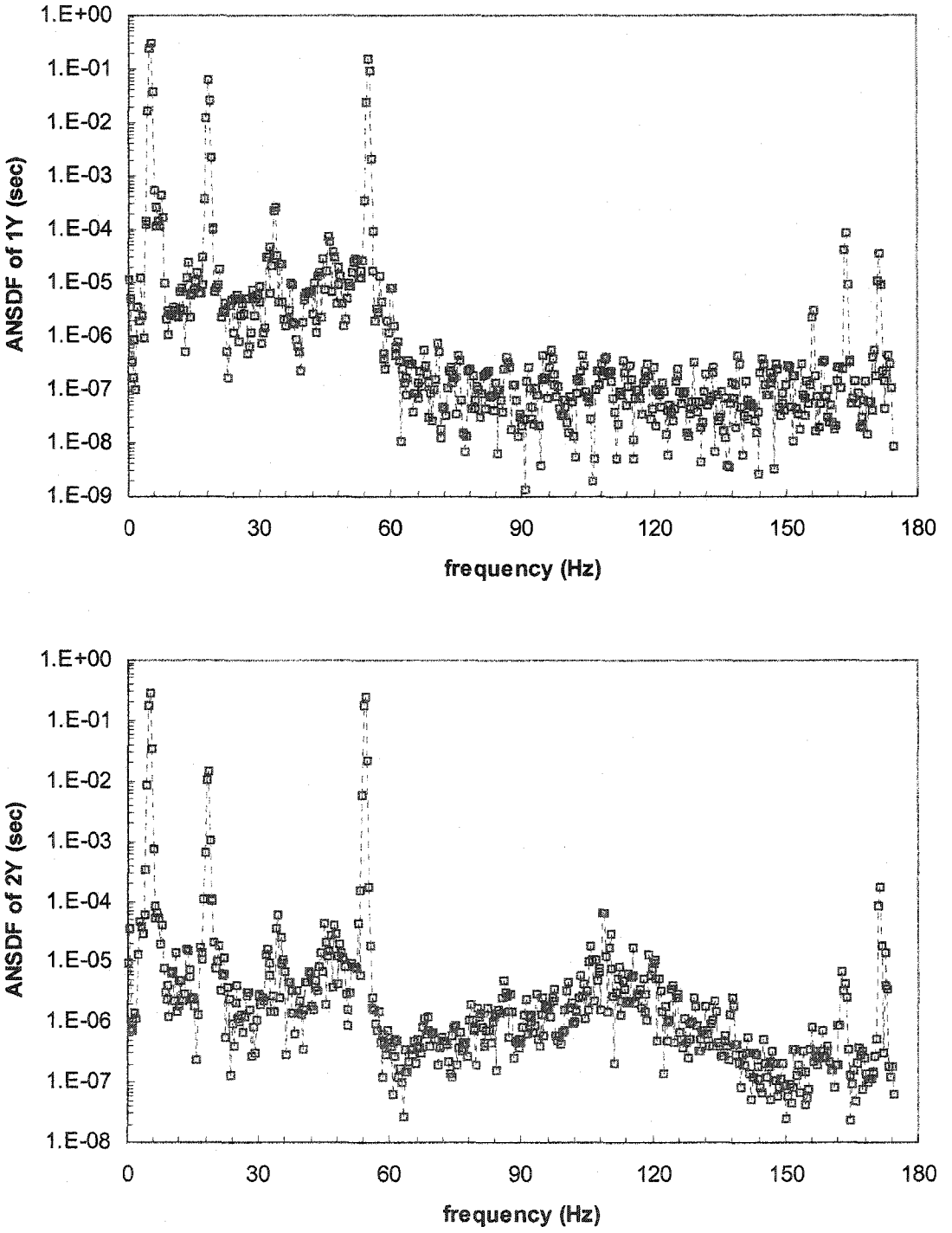

Figure 6.3.4

Averaged Normalized Spectral Density Functions of RD Signatures in Y direction

6.3.2 Natural Frequencies

The estimates of the resonant frequencies are based on direct observation of an averaged normalized spectral density function (ANSDF). The ANSDF collects a set of related auto-spectral density functions of measured data in a certain direction, and then normalizes and averages them [Felber, 1993]. Such a function facilitates the display of the resonant frequencies present in the set of the spectral density functions into one single plot. The expression of the ANSDF is given by:

$$\mathrm{ANSDF}(f_k) = \frac{1}{l}\sum_{i=1}^{l}\left[\frac{G_{\ddot{X}_i\ddot{X}_i}(f_k)}{\sigma^2_{\ddot{X}_i}}\right] \tag{6.3.3}$$

in which l is the number of the auto-spectral density functions of measured responses $G_{\ddot{X}_i\ddot{X}_i}(f_k)$ and $\sigma^2_{\ddot{X}_i} = \sum_{k=0}^{n} G_{\ddot{X}_i\ddot{X}_i}(f_k)$ is the variance. In Equation (6.3.3), the weight assigned to all of the auto-spectral density functions in a frequency distribution of interest is obviously even.

The observed frequencies are necessarily checked by means of the ordinary coherence function to confirm whether or not an observed peak is associated with a natural frequency in the building model. The ordinary coherence function integrates the information from the auto- and cross-spectral density functions, which varies between 0 and 1 to represent a measure of correlation between two simultaneously measured responses. For a given frequency, a high coherence suggests a linear relationship between the two responses, while a low coherence can be regarded as an indicator of non-linearity. Therefore, the dominant natural frequencies are verified as those having a high coherence value close to 1.

The spectral density functions of the measured responses were computed by the traditional FFT based algorithms with the sufficient segment length of 16384 data points providing a better frequency resolution of 0.0214 Hz. The Hanning window was applied to pre-process each segment to reduce a side lobe leakage problem when estimating the spectral density functions. However, since such a window could increase the effective bandwidth of the spectral density functions and the level of variance, a 50 percent overlap between each contiguous segment in the measured responses of 32768 points was employed. As a consequence, the total number of 18 data segments from the entire responses of 6×32768 points were individually transformed to the frequency domain and, subsequently, averaged to yield the spectral density functions.

Figures 6.3.5 and 6.3.6 illustrate the ANSDFs of the responses that were used to detect the possible locations of the natural frequencies of the building model. Figures 6.3.7 and 6.3.8 display the coherence functions and phase angles of the responses. The results of five natural frequencies identified from the ANSDFs of the original responses and the RD signatures for the four sets are summarized in Table 6.3.1. The four lowest natural frequencies of each set are judged to be accurate, based on their respective coherence functions and phase angles. Nevertheless, identifying the fifth mode natural frequency from the ANSDF alone is not an easy task owing to insufficient higher frequency components of the wind forces and corresponding responses.

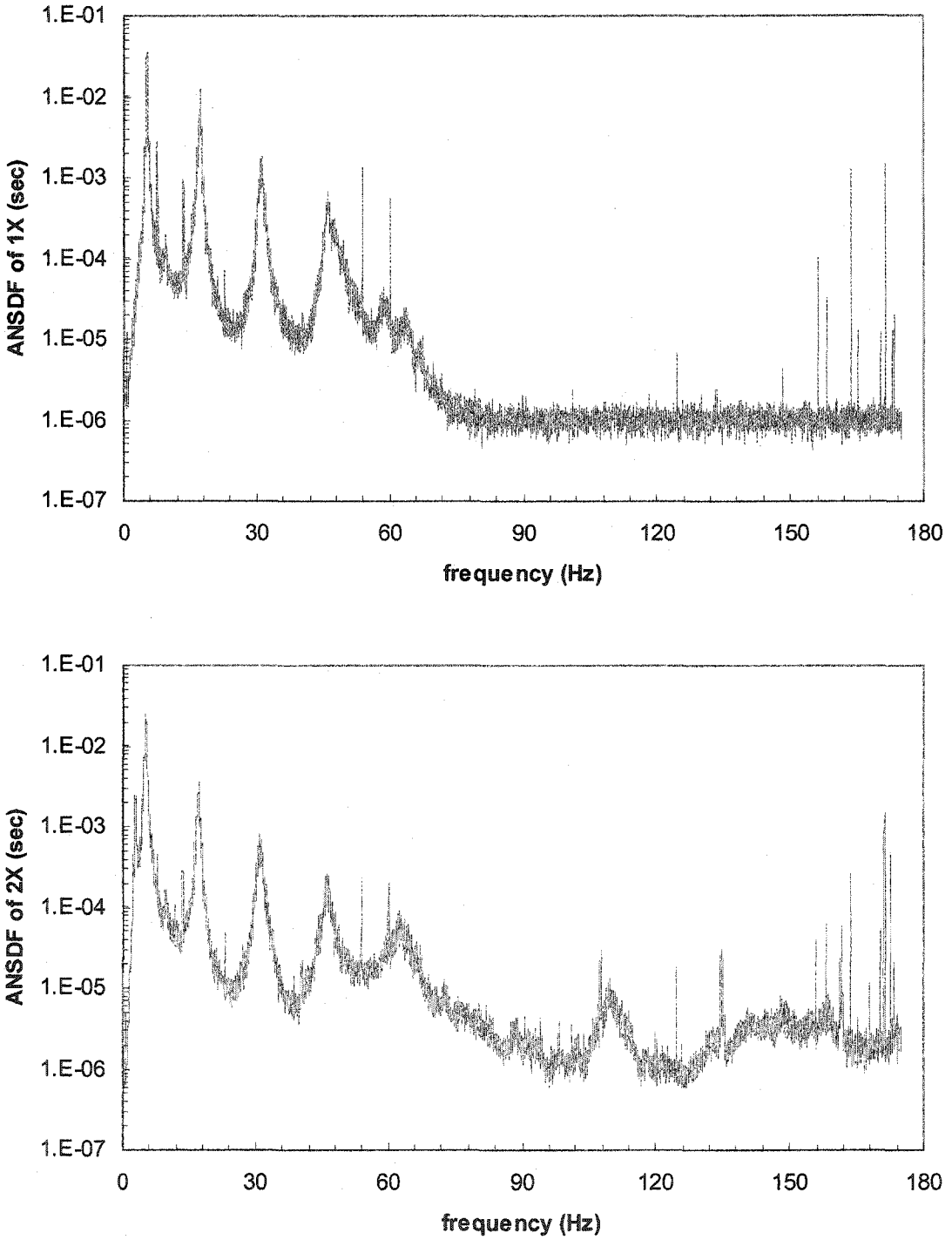

Figure 6.3.5

Averaged Normalized Spectral Density Functions of Responses for X direction

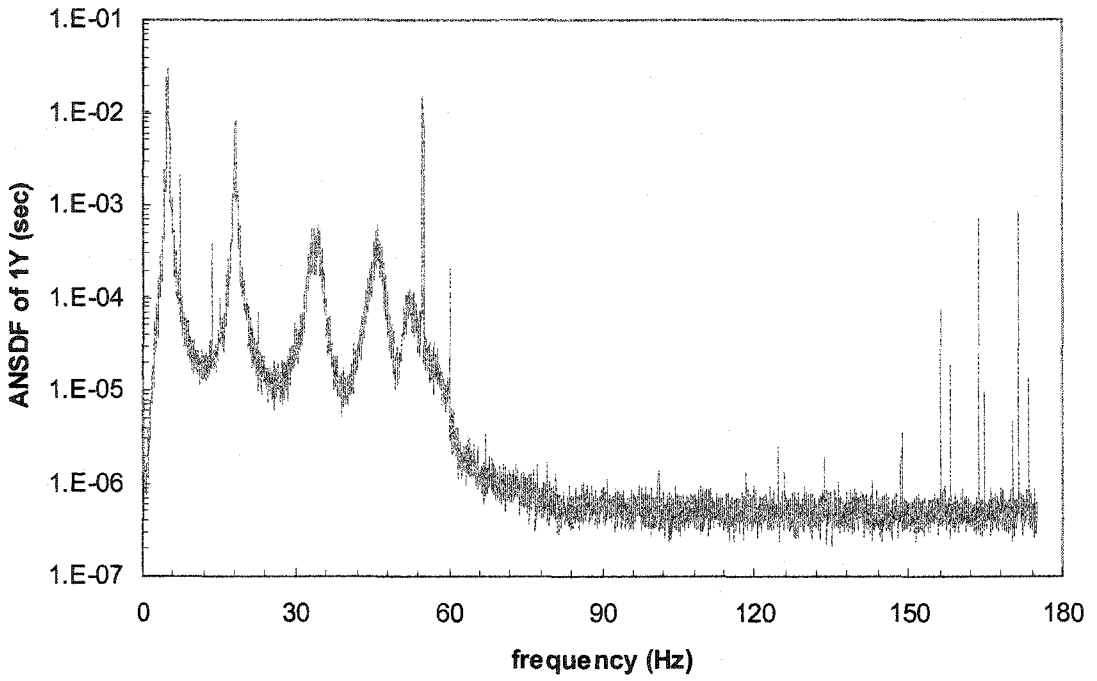

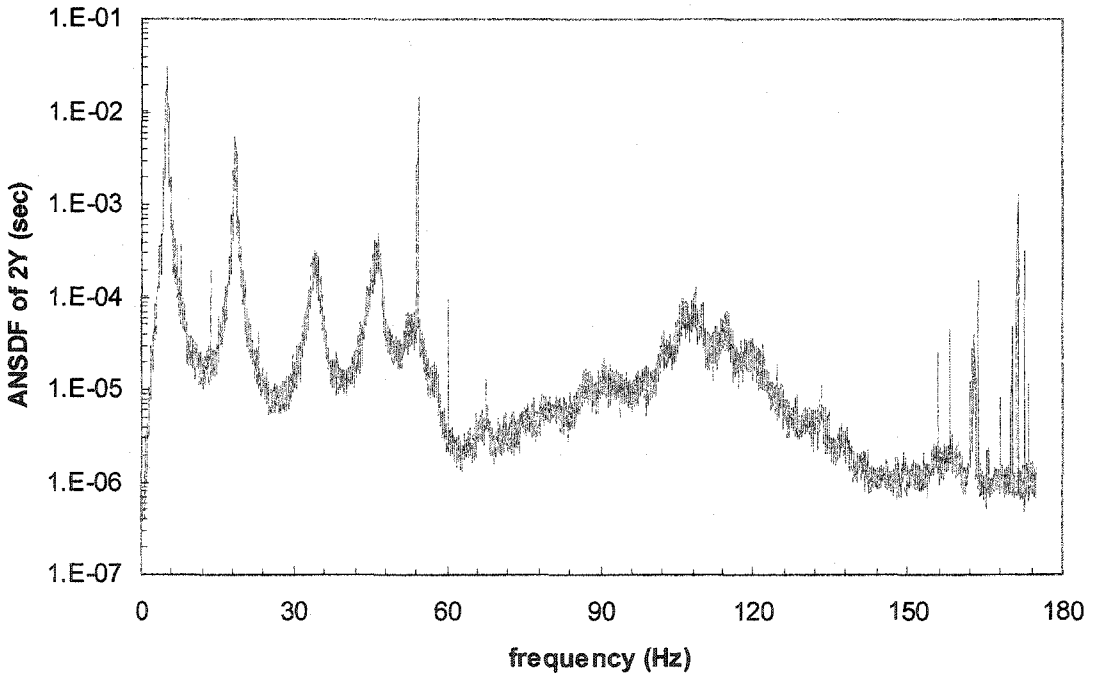

Figure 6.3.6

Averaged Normalized Spectral Density Functions of Responses for Y direction

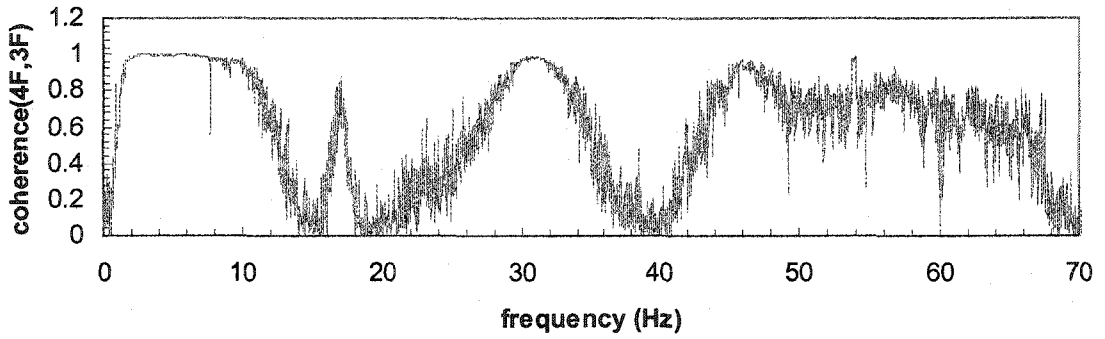

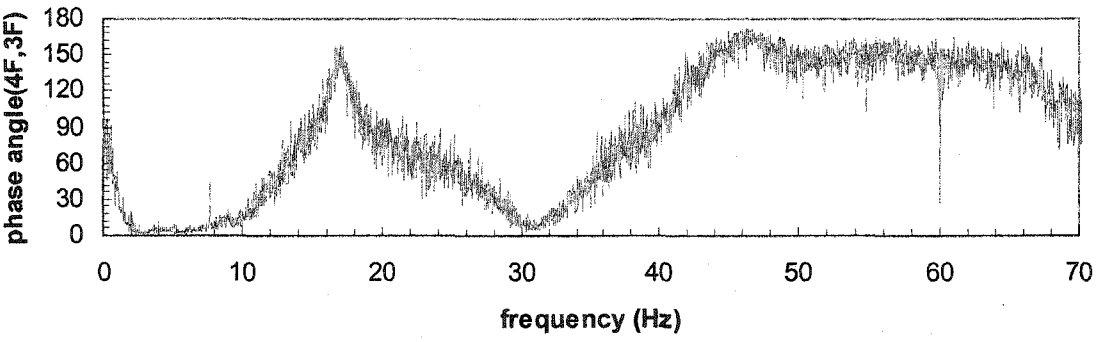

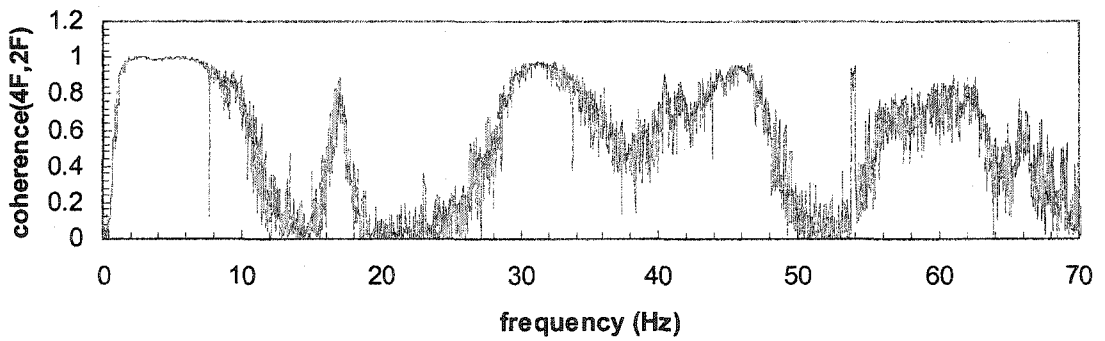

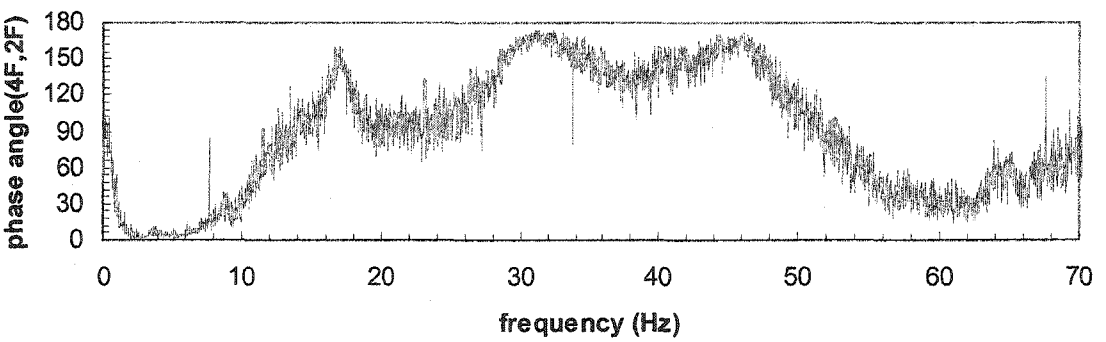

(Figure 6.3.7 continues next)

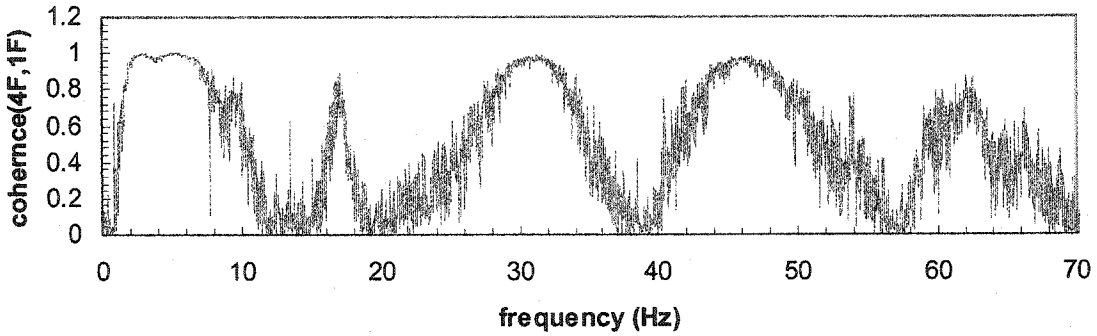

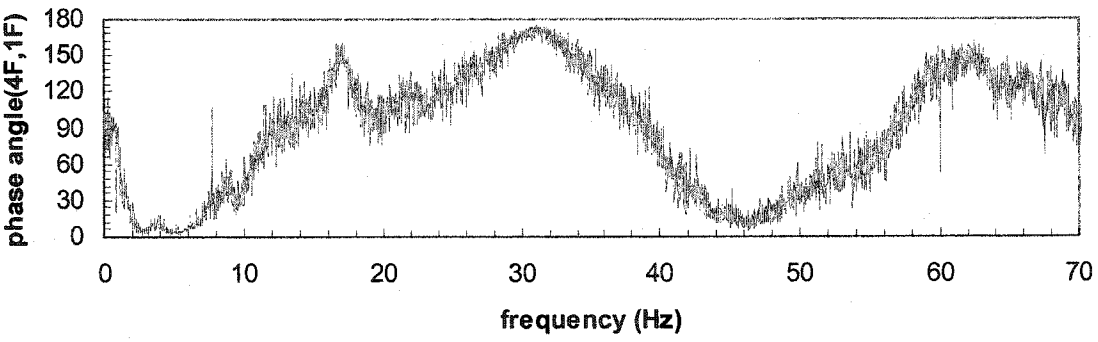

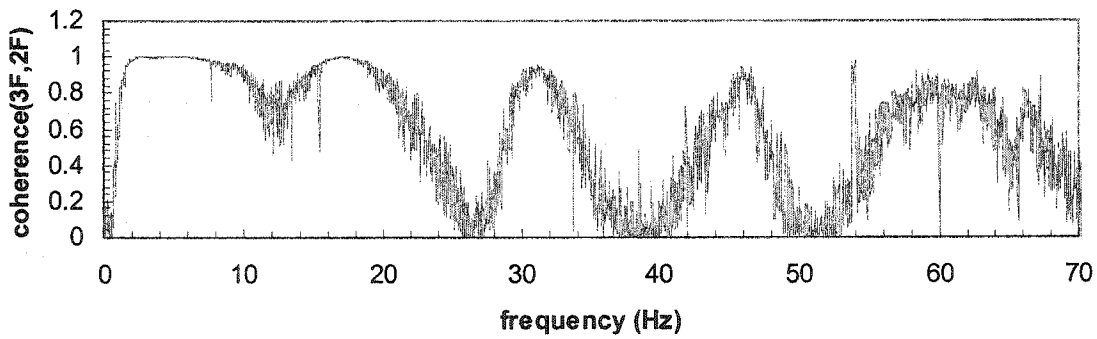

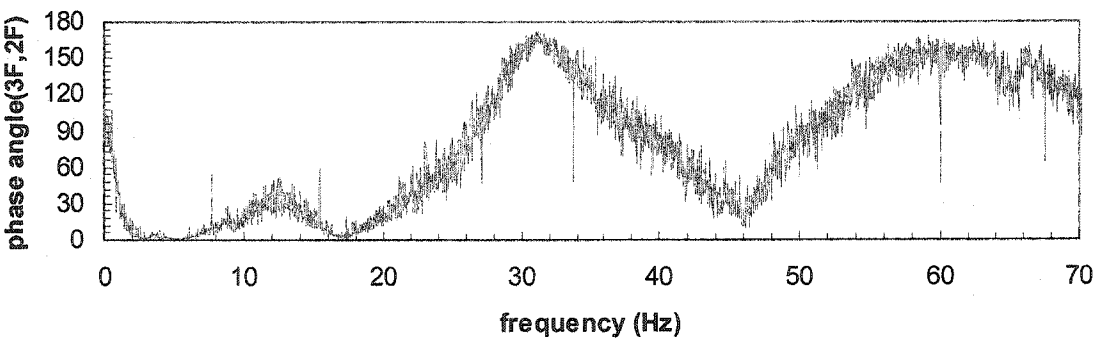

(Figure 6.3.7 continues next)

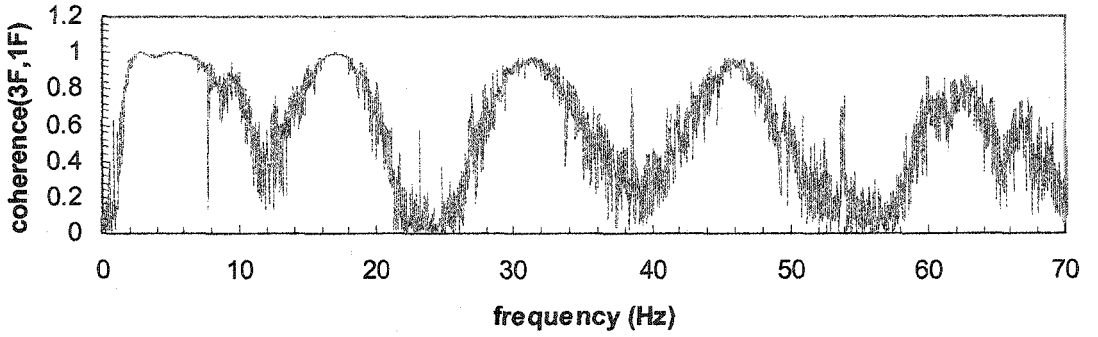

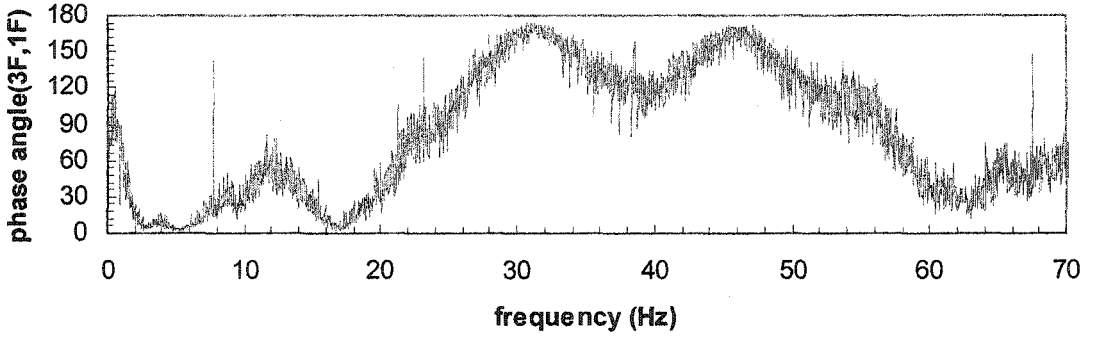

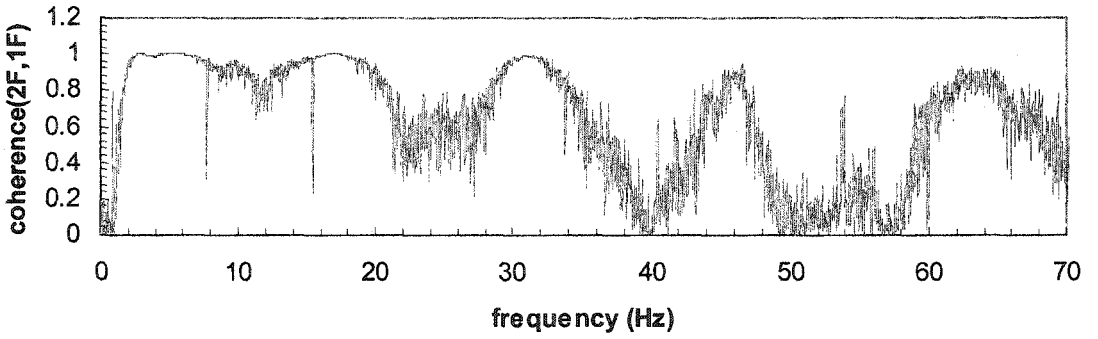

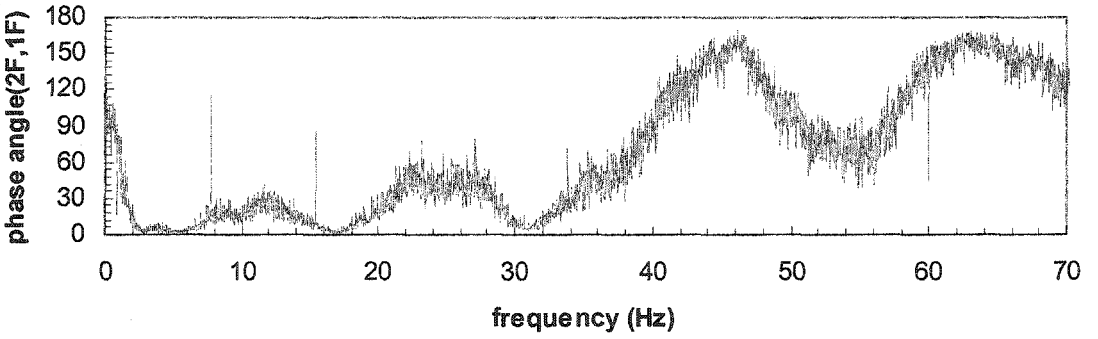

(Figure 6.3.7 continues next)

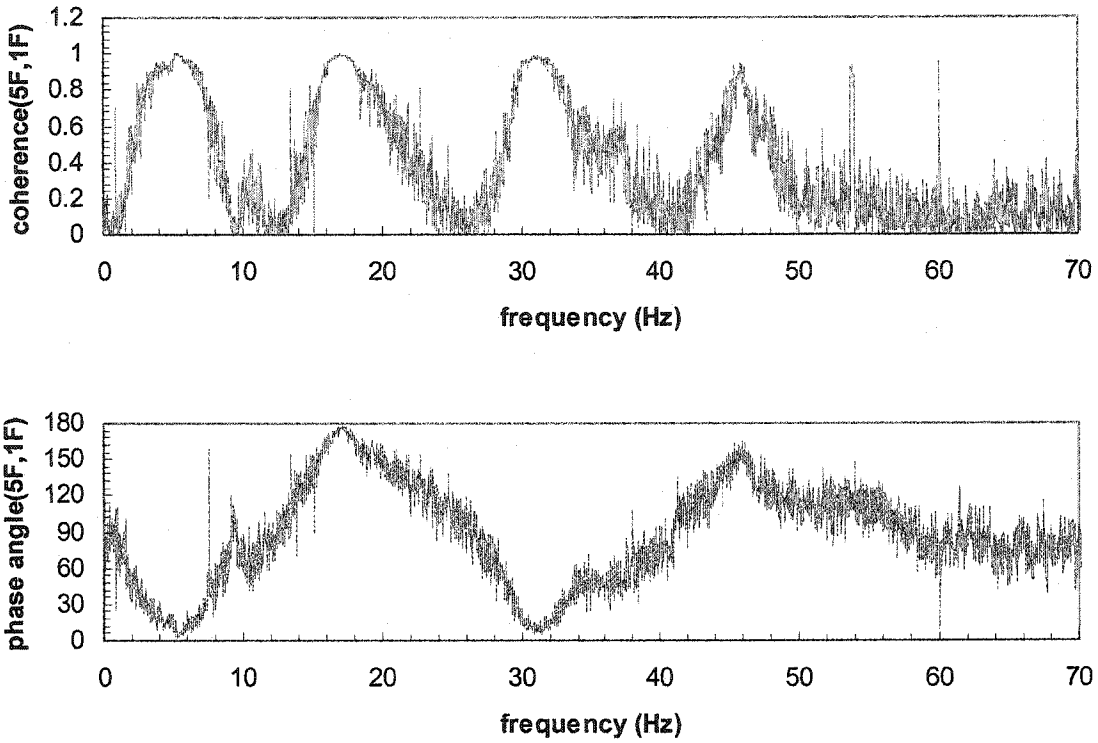

Figure 6.3.7 Coherence Functions and Phase Angles between Responses for X direction

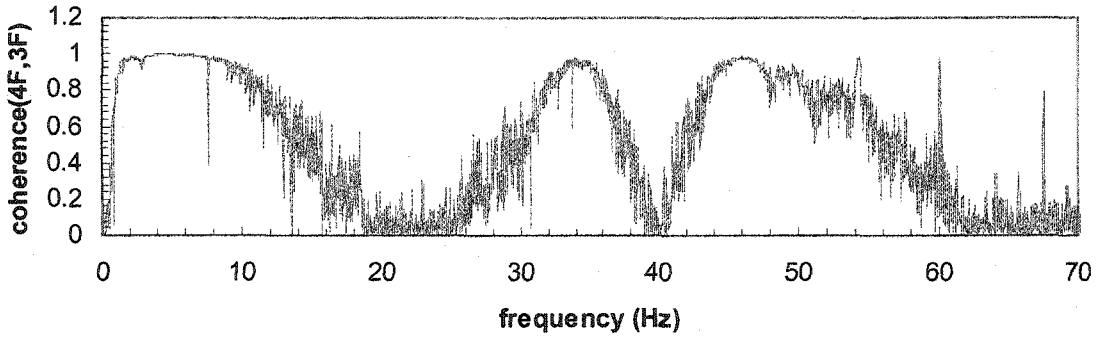

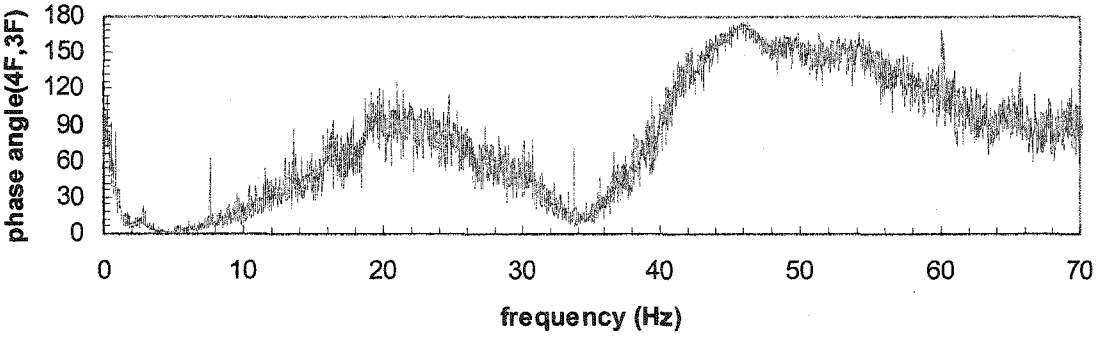

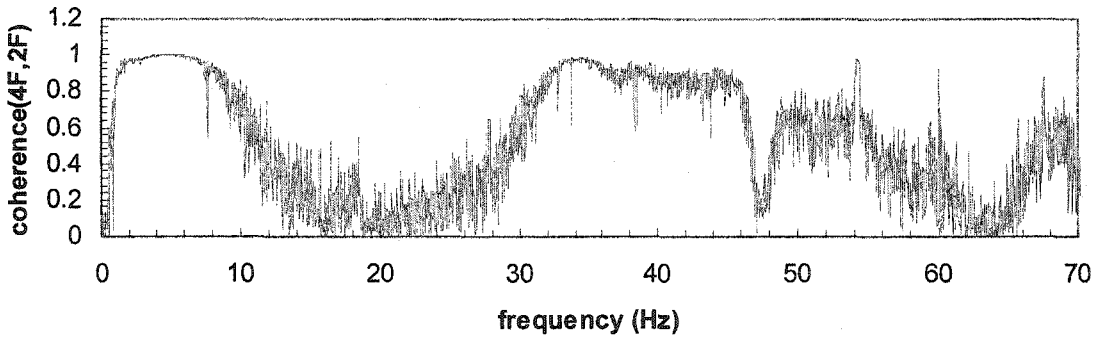

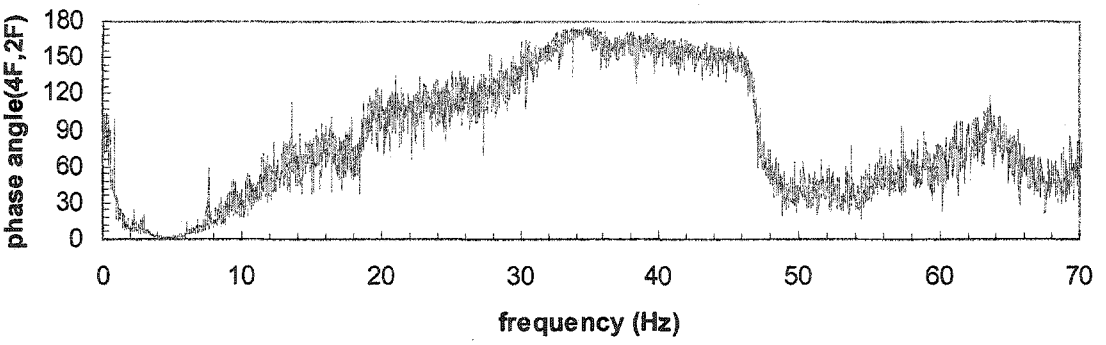

(Figure 6.3.8 continues next)

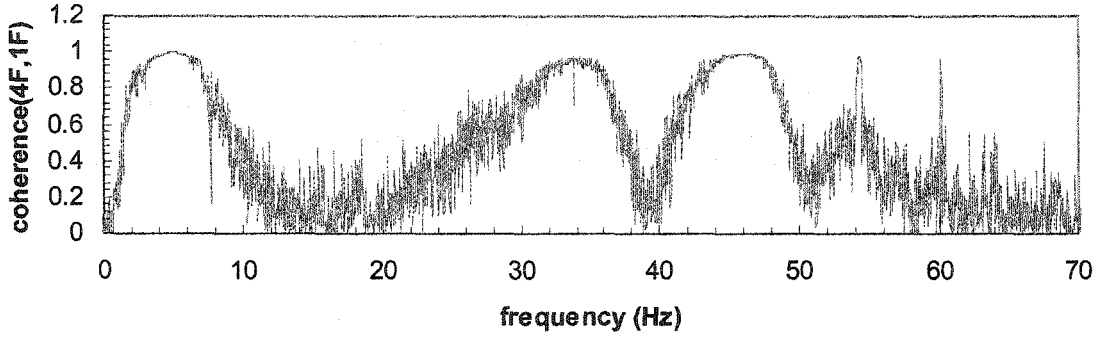

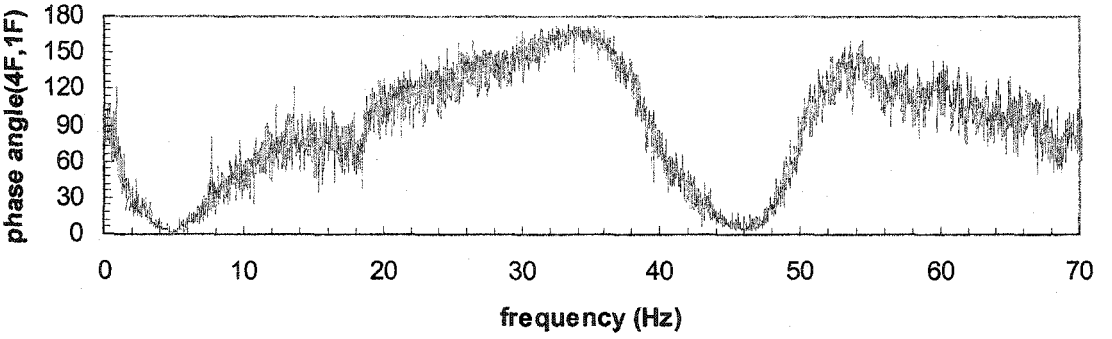

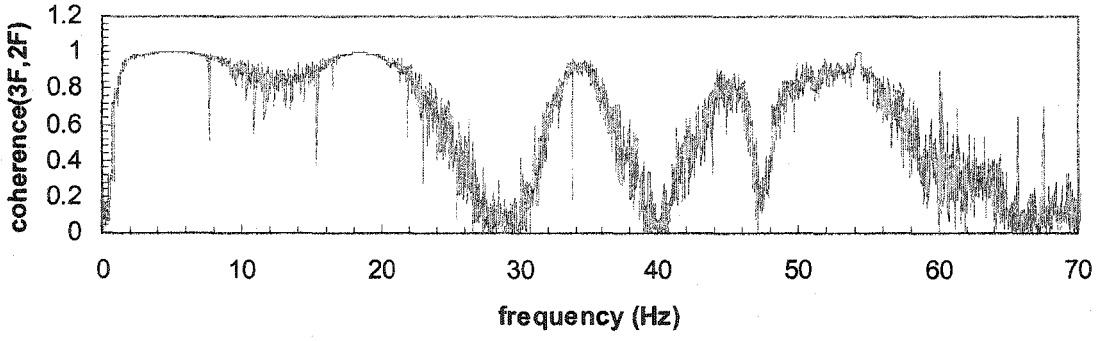

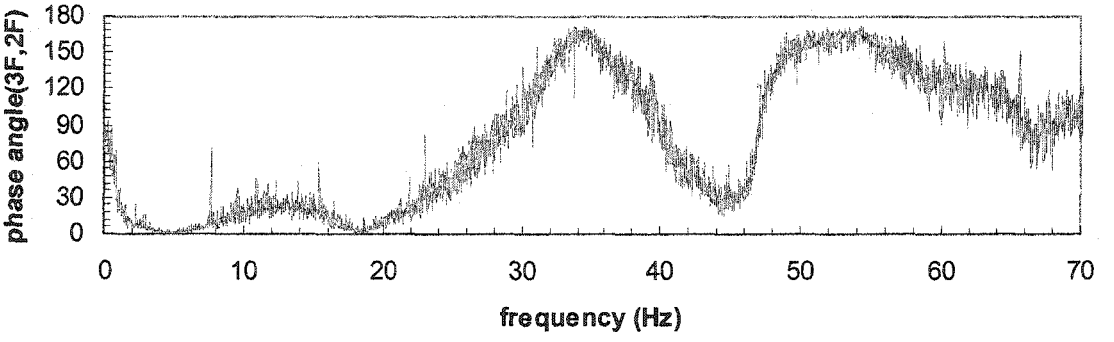

(Figure 6.3.8 continues next)

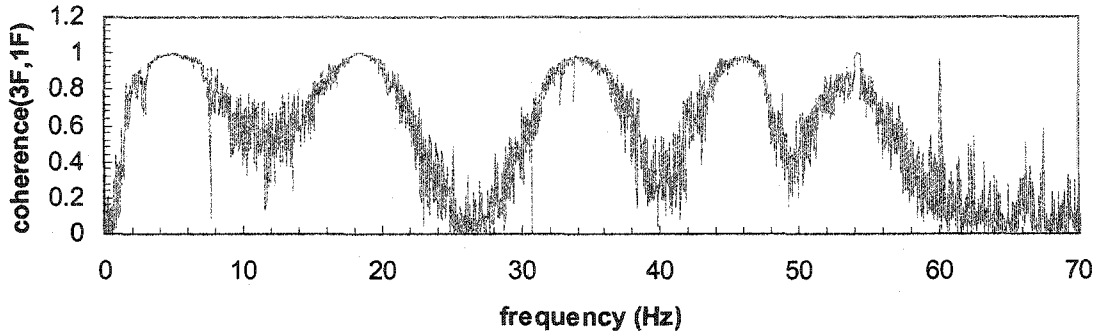

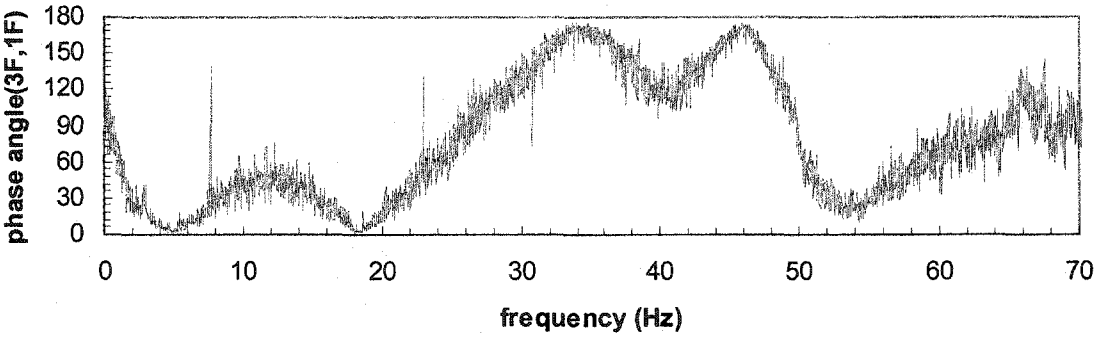

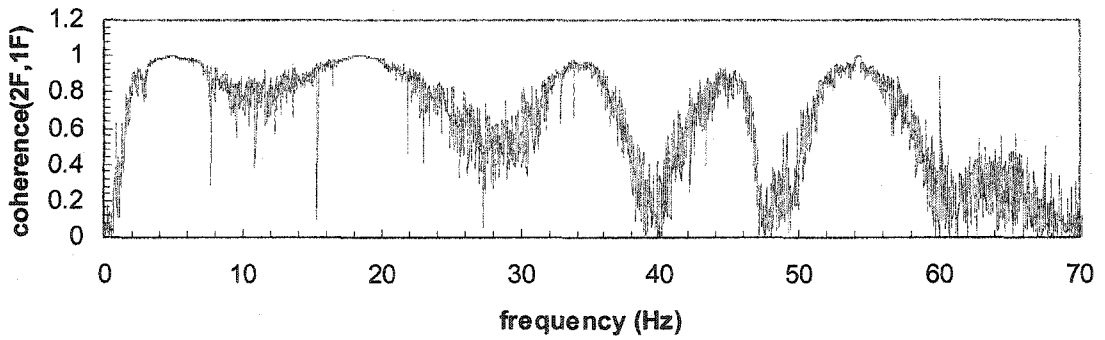

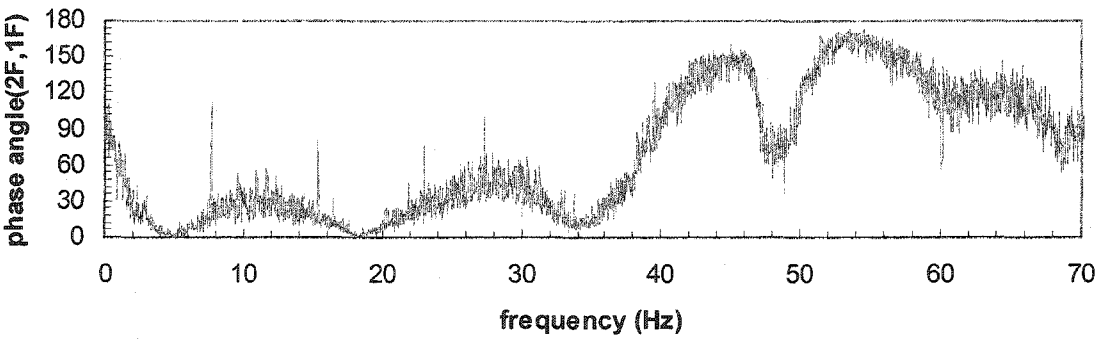

(Figure 6.3.8 continues next)

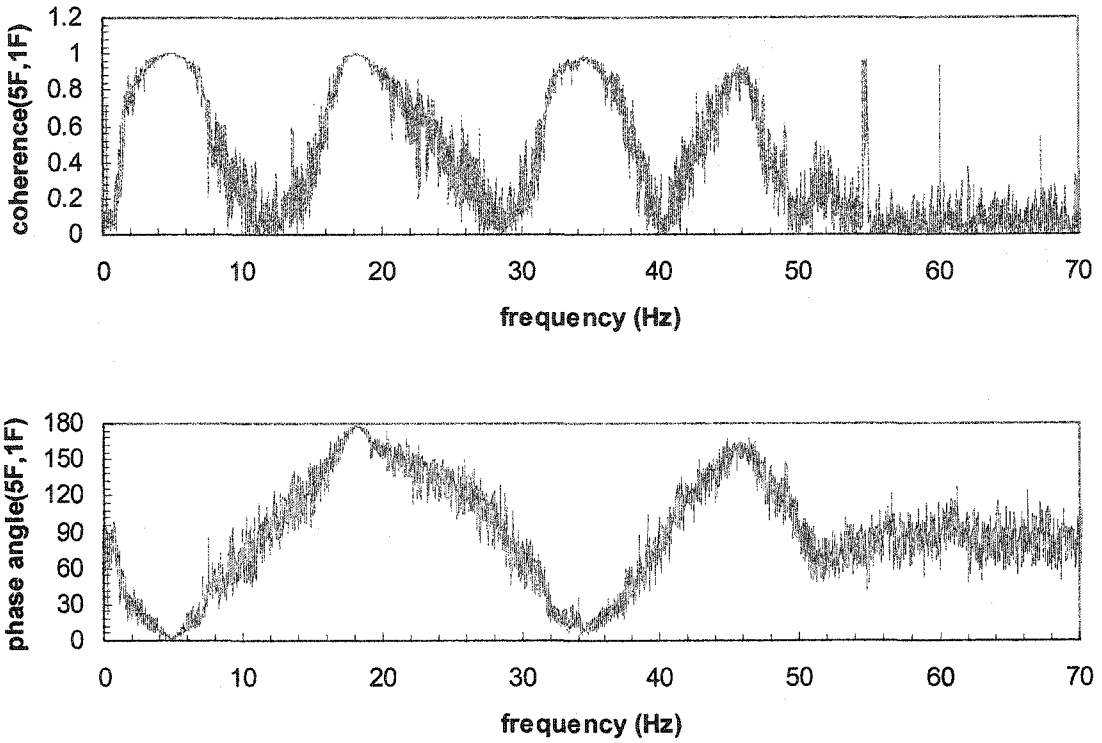

Figure 6.3.8 Coherence Functions and Phase Angles between Responses for Y direction

Comparison of the identified natural frequencies between the two sets at the same direction shows an excellent agreement. The averaged natural frequencies resulting from the two associated sets for the responses and the RD signatures are also given in Table 6.3.1. The discrepancies of the averaged natural frequencies between the responses and the RD signatures are found to be less than 1.44 %. It is remarkable that a peak around a frequency of 3.1 Hz appears in the 2X set of Figure 6.3.5. Compared with the results in Figure 6.2.10 (a), this is mainly attributed to the contribution of the vortex shedding excitation in the responses when the approaching wind is in parallel with the Y direction

of the building model. Such a frequency is therefore not considered as a dynamic mode for the building model in the development of an analytical model.

Table 6.3.1 Identified Natural Frequencies of a Building Model

Mode	Natural Frequency (Hz)						
	Data Type	1X	2X	X Average	1Y	2Y	Y Average
1	Responses	5.3427	5.2359	5.2893	5.0008	5.0008	5.0008
	RDS	5.3000	5.3000	5.3000	4.7871	5.1290	4.9581
2	Responses	17.0753	17.0967	17.0860	18.1652	18.5072	18.3362
	RDS	17.0967	16.5838	16.8403	18.1225	18.2934	18.2080
3	Responses	30.9664	30.8809	30.9237	34.4071	33.8301	34.1186
	RDS	30.7740	30.7740	30.7740	33.5095	34.0224	33.7660
4	Responses	45.9687	45.8832	45.9260	46.2252	46.4389	46.3321
	RDS	45.9901	45.9901	45.9901	45.9901	46.5030	46.2466
5	Responses	63.9416	62.3174	63.1295	52.2517	53.5767	52.9142
	RDS	63.9416	64.1126	64.0271	53.3416	52.6578	52.9997

6.3.3 Mode Shapes

If the identified natural frequencies in each set are accurate and lightly damped, the corresponding mode shapes at the measured points can be determined by Equation (6.3.4) using the amplitude and phase information in the frequency response functions.

$$\Psi_{pk} = \left|H_{pq}(f_k)\right| PH(f_k) = \frac{\phi_{pk}}{\phi_{qk}} \tag{6.3.4}$$

In Equation (6.3.4), Ψ_{pk} represents the mode shape component at a measured point p in the k^{th} mode shape, which is normalized with respect to the modal component at a reference point q. The phase function $PH(f_k)$ is based on the phase angle $\theta_{pq}(f_k)$ of a FRF $H_{pq}(f_k)$ between the responses at p and q points for the k^{th} mode. Such a phase function is expressed by:

$$PH(f_k) = \cos\left[\theta_{pq}(f_k)\right] + i\sin\left[\theta_{pq}(f_k)\right] \tag{6.3.5}$$

in which $i = \sqrt{-1}$ and $\theta_{pq}(f_k) = \arctan\left(\frac{\mathrm{Im}\{H_{pq}(f_k)\}}{\mathrm{Re}\{H_{pq}(f_k)\}}\right)$. Re{ } and Im{ } correspond to the real and imaginary components of a complex function. Experimentally, any phase angle staying in between 0 and 15° and staying in between 165° and 180° is normally regarded as 0° and 180°, respectively. Other phase angles should be treated as complex components in modes. The FRFs can be formulated in terms of the auto- and cross-spectral density functions as follows:

$$H_{pq}^{(I)}(f_k) = \frac{G_{\ddot{X}_q\ddot{X}_p}(f_k)}{G_{\ddot{X}_q\ddot{X}_q}(f_k)} = \frac{\phi_{pk}}{\phi_{qk}} \tag{6.3.6}$$

$$H_{pq}^{(II)}(f_k) = \frac{G_{\ddot{X}_p\ddot{X}_p}(f_k)}{G_{\ddot{X}_q\ddot{X}_p}(f_k)} = \frac{\phi_{pk}}{\phi_{qk}} \tag{6.3.7}$$

$$H_{pq}^{(III)}(f_k) = \sqrt{\frac{G_{\ddot{X}_p\ddot{X}_p}(f_k)}{G_{\ddot{X}_q\ddot{X}_q}(f_k)}} = \left|\frac{\phi_{pk}}{\phi_{qk}}\right| \tag{6.3.8}$$

in which ϕ_{pk} and ϕ_{qk} are the modal components of the k^{th} mode shape at the p and q points, respectively. As already known, the use of the FRFs can instantly determine the value of the coherence function.

In this study, the two groups of the mode shape components in each direction can be individually identified, as demonstrated in the following brackets:

$$\begin{Bmatrix} \Psi_{51} & \Psi_{52} & \Psi_{53} & \Psi_{54} & \Psi_{55} \\ 1 & 1 & 1 & 1 & 1 \end{Bmatrix}, \begin{Bmatrix} \Psi_{41} & \Psi_{42} & \Psi_{43} & \Psi_{44} & \Psi_{45} \\ \Psi_{31} & \Psi_{32} & \Psi_{33} & \Psi_{34} & \Psi_{35} \\ \Psi_{21} & \Psi_{22} & \Psi_{23} & \Psi_{24} & \Psi_{25} \\ 1 & 1 & 1 & 1 & 1 \end{Bmatrix}$$

The reference point in which the component is normalized to unit in the preceding two brackets is provided to assemble the complete mode shapes of the building model from the two groups, as shown in Equation (6.3.9).

$$[\varphi_1 \quad \varphi_2 \quad \varphi_3 \quad \varphi_4 \quad \varphi_5] = \begin{Bmatrix} \Psi_{51} & \Psi_{52} & \Psi_{53} & \Psi_{54} & \Psi_{55} \\ \Psi_{41} & \Psi_{42} & \Psi_{43} & \Psi_{44} & \Psi_{45} \\ \Psi_{31} & \Psi_{32} & \Psi_{33} & \Psi_{34} & \Psi_{35} \\ \Psi_{21} & \Psi_{22} & \Psi_{23} & \Psi_{24} & \Psi_{25} \\ 1 & 1 & 1 & 1 & 1 \end{Bmatrix} \tag{6.3.9}$$

in which φ_i represents a mode shape.

The results in Tables 6.3.2 and 6.3.3, which were extracted from the responses and the RD signatures, illustrate the magnitudes of the FRFs, phase angles and coherence functions with respect to the reference point at the first floor for the five modes. The number and alphabet parenthesized in the column of Tables 6.3.2 and 6.3.3 for floors denote the two measurement sets in each of the X and Y directions.

The first observation from Tables 6.3.2 and 6.3.3 is that two typical FRF relations of $|H_{p1}{}^{(I)}| \leq |H_{p1}{}^{(III)}| \leq |H_{p1}{}^{(II)}|$ for the measured responses and $|H_{p1}{}^{(I)}| = |H_{p1}{}^{(II)}| = |H_{p1}{}^{(III)}|$ for the RD signatures of the responses can be clearly seen in each mode. The former relation indicates the effect of noises, including the applied wind forces, present in the measured responses. The later relation experimentally supports the theoretical relation for the FRFs of the RD signatures derived in Equation (5.3.29). Following these evidences, it implies that the assumed lumped mass model applied to the tested building model is reasonable and the experimental reliability based on the acceleration measurements is confirmed.

The second observation from Tables 6.3.2 and 6.3.3 is that all the coherence functions for the RD signatures are equal to 1, according to the identity relation of the FRFs above. However, the authenticity of the FRFs calculated from the extracted RD

acceleration signatures is not sufficiently convincing. That is in view of the fact from the theoretical and experimental studies that the RD acceleration signatures are involved with the RD signatures of the applied forces. As demonstrated in Equations (5.3.14-16) and (5.3.25-27), the FRFs of the RD acceleration signatures are a function in terms of the RD signatures of the applied forces. To foster the applicability of the RD based method and the FRF approach when estimating the modal parameters of the building model, the emphasis is therefore placed on the assumptions required for the use of frequency domain data.

The last observation from Tables 6.3.2 and 6.3.3 is that some phase angles in the first four modes stay in a range of 15° to 165° and their mode shape components should be considered to be complex. With further inspection of these phase angles, it appears that all of their corresponding coherence functions are lower than 0.9, which reveals a higher uncertainty. The reason concerning such an uncertainty is that the measured signal of a dynamic mode at the location is quite small, when compared with those at the other locations. Such a signal is more easily contaminated by noises and interacted with adjacent dynamic modes and, consequently, leads to a problematic result for the phase angle. This problem was also experienced from the numerical investigation of the 3DOF dynamic system in Section 5.4.3. Therefore, these phase angles are presumed to be in-phase or out-of-phase to the reference response in this study. The validation of this presumption is answered by the following mode shape information.

Table 6.3.2 FRFs, Phase and Coherence of Modes in X Direction with respect to 1F

Mode	Data Type	Floors	$\|H^{(I)}\|$	$\|H^{(II)}\|$	$\|H^{(III)}\|$	Phase (°)	Coherence
1	Responses	5F(1X)	5.5542	5.5665	5.5604	3.1443	0.9978
		4F(2X)	5.1450	5.1547	5.1499	3.1238	0.9981
		3F(2X)	4.0426	4.0466	4.0446	2.7897	0.9990
		2F(2X)	2.6061	2.6078	2.6069	2.3215	0.9994
		1F(1,2X)	1	1	1	0	-
	Signatures	5F(1X)	5.6876	5.6876	5.6876	0.7814	1
		4F(2X)	5.6834	5.6834	5.6834	1.4619	1
		3F(2X)	4.3194	4.3194	4.3194	0.9913	1
		2F(2X)	2.7304	2.7304	2.7304	0.6549	1
		1F(1,2X)	1	1	1	0	-
2	Responses	5F(1X)	1.8260	1.8296	1.8278	176.93	0.9980
		4F(2X)	0.1907	0.2523	0.2193	152.89	0.7559
		3F(2X)	1.4007	1.4057	1.4032	2.7422	0.9964
		2F(2X)	1.8716	1.8731	1.8724	1.3491	0.9992
		1F(1,2X)	1	1	1	0	-
	Signatures	5F(1X)	1.7767	1.7767	1.7767	178.96	1
		4F(2X)	0.2008	0.2008	0.2008	171.50	1
		3F(2X)	1.3631	1.3631	1.3631	0.7591	1
		2F(2X)	1.8475	1.8475	1.8475	0.0874	1
		1F(1,2X)	1	1	1	0	-
3	Responses	5F(1X)	0.8494	0.8597	0.8545	5.7614	0.9880
		4F(2X)	0.8635	0.8847	0.8740	170.63	0.9760
		3F(2X)	0.7190	0.7500	0.7343	164.70	0.9587
		2F(2X)	0.7198	0.7258	0.7227	5.0155	0.9917
		1F(1,2X)	1	1	1	0	-
	Signatures	5F(1X)	1.0405	1.0405	1.0405	9.5169	1
		4F(2X)	0.8760	0.8760	0.8760	176.33	1
		3F(2X)	0.7349	0.7349	0.7349	175.87	1
		2F(2X)	0.7211	0.7211	0.7211	4.4416	1
		1F(1,2X)	1	1	1	0	-
4	Responses	5F(1X)	0.4449	0.4776	0.4610	165.91	0.9316
		4F(2X)	1.0967	1.1168	1.1067	7.4172	0.9820
		3F(2X)	0.5946	0.6145	0.6044	170.19	0.9676
		2F(2X)	0.5047	0.5475	0.5257	165.52	0.9219
		1F(1,2X)	1	1	1	0	-
	Signatures	5F(1X)	0.4908	0.4908	0.4908	164.96	1
		4F(2X)	0.7976	0.7976	0.7976	1.7452	1
		3F(2X)	0.4955	0.4955	0.4955	178.00	1
		2F(2X)	0.3018	0.3018	0.3018	166.06	1
		1F(1,2X)	1	1	1	0	-
5	Responses	5F(1X)	0.2916	0.7140	0.4563	54.248	0.4084
		4F(2X)	0.3829	0.4978	0.4366	154.48	0.7691
		3F(2X)	0.4940	0.6304	0.5581	29.743	0.7837
		2F(2X)	0.7597	0.8399	0.7988	159.05	0.9046
		1F(1,2X)	1	1	1	0	-
	Signatures	5F(1X)	0.7179	0.7179	0.7179	23.409	1
		4F(2X)	0.5527	0.5527	0.5527	125.27	1
		3F(2X)	0.3526	0.3526	0.3526	3.9320	1
		2F(2X)	0.9364	0.9364	0.9364	172.57	1
		1F(1,2X)	1	1	1	0	-

Table 6.3.3 FRFs, Phase and Coherence of the Modes in Y Direction with respect to 1F

Mode	Data Type	Floors	$\lvert H^{(I)} \rvert$	$\lvert H^{(II)} \rvert$	$\lvert H^{(III)} \rvert$	Phase (°)	Coherence
1	Responses	5F(1Y)	8.0293	8.0320	8.0307	1.0423	0.9997
		4F(2Y)	6.6740	6.6777	6.6758	2.8270	0.9994
		3F(2Y)	4.7976	4.8056	4.8016	3.8958	0.9983
		2F(2Y)	2.8674	2.8697	2.8685	2.7481	0.9992
		1F(1,2Y)	1	1	1	0	-
	Signatures	5F(1Y)	8.0586	8.0586	8.0586	0.5889	1
		4F(2Y)	6.5995	6.5995	6.5995	0.4564	1
		3F(2Y)	4.7282	4.7282	4.7282	1.3557	1
		2F(2Y)	2.8342	2.8342	2.8342	0.9501	1
		1F(1,2Y)	1	1	1	0	-
2	Responses	5F(1Y)	2.2364	2.2407	2.2385	178.14	0.9981
		4F(2Y)	0.0670	0.1657	0.1053	76.286	0.4043
		3F(2Y)	1.7757	1.7781	1.7769	1.6421	0.9987
		2F(2Y)	2.0657	2.0664	2.0660	0.8354	0.9997
		1F(1,2Y)	1	1	1	0	-
	Signatures	5F(1Y)	2.2507	2.2507	2.2507	179.29	1
		4F(2Y)	0.0341	0.0341	0.0341	29.752	1
		3F(2Y)	1.7684	1.7684	1.7684	0.7053	1
		2F(2Y)	2.0571	2.0571	2.0571	0.2418	1
		1F(1,2Y)	1	1	1	0	-
3	Responses	5F(1Y)	0.8806	0.8971	0.8888	9.8553	0.9816
		4F(2Y)	0.8484	0.8700	0.8592	170.74	0.9752
		3F(2Y)	0.5943	0.6056	0.5999	172.36	0.9813
		2F(2Y)	0.6521	0.6689	0.6604	8.1495	0.9749
		1F(1,2Y)	1	1	1	0	-
	Signatures	5F(1Y)	0.7242	0.7242	0.7242	3.4023	1
		4F(2Y)	0.9545	0.9545	0.9545	168.61	1
		3F(2Y)	0.5626	0.5626	0.5626	176.21	1
		2F(2Y)	0.7309	0.7309	0.7309	7.4938	1
		1F(1,2Y)	1	1	1	0	-
4	Responses	5F(1Y)	0.4112	0.4525	0.4314	156.10	0.9087
		4F(2Y)	1.0757	1.0795	1.0776	4.5149	0.9965
		3F(2Y)	0.6781	0.6881	0.6831	171.86	0.9855
		2F(2Y)	0.1495	0.1902	0.1686	150.74	0.7858
		1F(1,2Y)	1	1	1	0	-
	Signatures	5F(1Y)	0.5777	0.5777	0.5777	166.41	1
		4F(2Y)	1.1422	1.1422	1.1422	0.5664	1
		3F(2Y)	0.6560	0.6560	0.6560	171.42	1
		2F(2Y)	0.2004	0.2004	0.2004	115.68	1
		1F(1,2Y)	1	1	1	0	-
5	Responses	5F(1Y)	0.1294	0.5745	0.2727	72.812	0.2253
		4F(2Y)	0.2996	0.5315	0.3991	132.64	0.5638
		3F(2Y)	0.6214	0.7468	0.6812	23.429	0.8321
		2F(2Y)	0.8775	0.9336	0.9051	163.55	0.9399
		1F(1,2Y)	1	1	1	0	-
	Signatures	5F(1Y)	0.0761	0.0761	0.0761	7.6386	1
		4F(2Y)	0.4370	0.4370	0.4370	164.95	1
		3F(2Y)	0.8165	0.8165	0.8165	6.3534	1
		2F(2Y)	1.0990	1.0990	1.0990	173.64	1
		1F(1,2Y)	1	1	1	0	-

The animated mode shapes are illustrated in Figures 6.3.9 and 6.3.10, which are based on the $H^{(II)}$ estimator of the FRFs from the five modes of the original responses and the RD signatures in each direction. The fifth mode shape is still given to demonstrate its existence, although it cannot be identified with high confidence. The comparison of the mode shapes individually identified from the responses and the RD signatures exhibits an excellent degree of consistency, especially for lower modes.

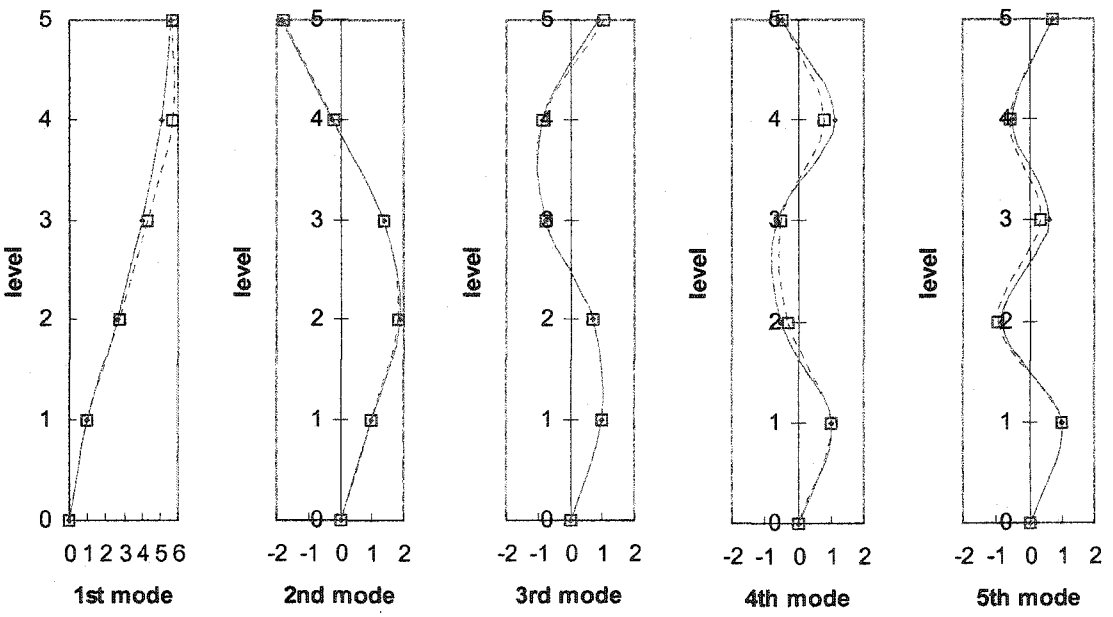

Figure 6.3.9

Comparison of Mode Shapes between RD Signatures and Responses in X Direction

—♦— Mode Shapes from Responses; --□-- Mode Shapes from RD signatures

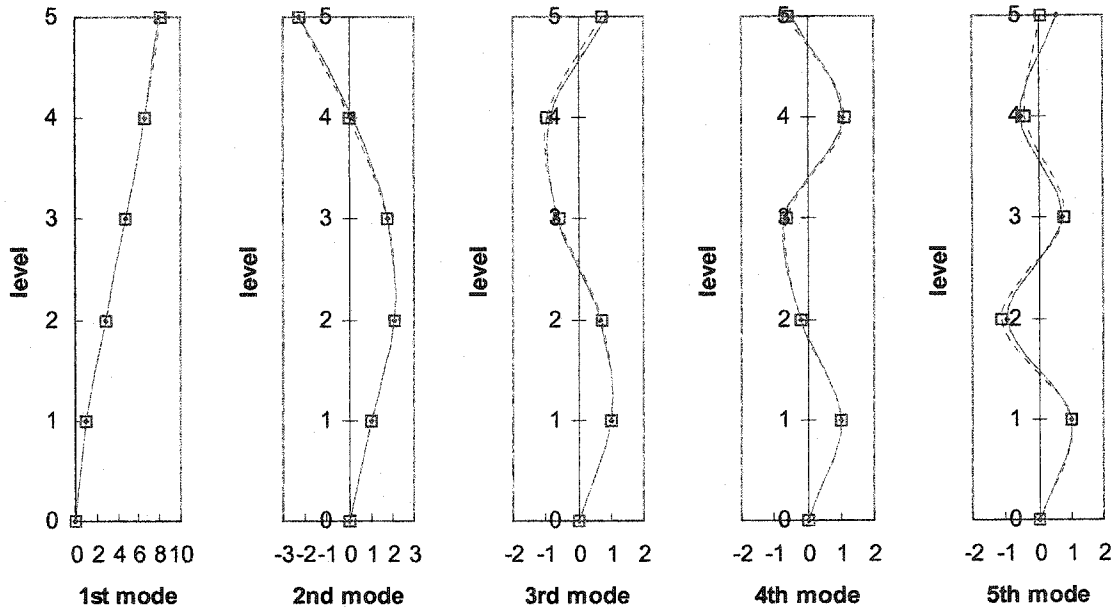

Figure 6.3.10

Comparison of Mode Shapes between RD Signatures and Responses in Y Direction

—♦— Mode Shapes from Responses; --□-- Mode Shapes from RD signatures

To quantify the correlation between two mode shapes obtained from the two different methods at a particular frequency, the mode assurance criterion (MAC) was used. The MAC is defined as [Allemang and Brown, 1983]:

$$\text{MACMAC}(\{\varphi_{iO}\},\{\varphi_{iR}\}) = \frac{\left|\{\varphi_{iO}\}^{T}\{\varphi_{iR}\}^{*}\right|^{2}}{\left[\{\varphi_{iO}\}^{T}\{\varphi_{iO}\}^{*}\right]\left[\{\varphi_{iR}\}^{T}\{\varphi_{iR}\}^{*}\right]} \tag{6.3.10}$$

in which $\{\varphi_{iO}\}$ is the i^{th} mode shape identified from the original responses, and $\{\varphi_{iR}\}$ is the corresponding mode shape obtained from the RD signatures. The superscripts * and T in Equation (6.3.10) symbolize the complex conjugate and the transpose, respectively. The basic idea of the MAC takes advantage of the orthogonality properties of the mode

shapes. Two corresponding modes are considered well correlated if the value of the MAC is closer to one. On the contrary, the value of the MAC becomes zero if two mode shapes are orthogonal with each other.

To further evaluate the correlation of all mode shapes for the two types of the signals at a common coordinate, the coordinate modal assurance criterion (COMAC) was also used. The COMAC for an individual coordinate, j, is expressed as [Ewins, 2000]:

$$\mathrm{COMAC}(j) = \frac{\left[\sum_{i=1}^{n} \varphi_{i\mathrm{O}}(j)\varphi_{i\mathrm{R}}(j)\right]^2}{\sum_{i=1}^{n}(\varphi_{i\mathrm{O}}(j))^2 \sum_{i=1}^{n}(\varphi_{i\mathrm{R}}(j))^2} \tag{6.3.11}$$

in which n represents the total number of correlated mode shape pairs, $\varphi_{i\mathrm{O}}(j)$ and $\varphi_{i\mathrm{R}}(j)$. Such mode shape pairs are the j^{th} component in the i^{th} mode shapes identified from the responses and the RD signatures. The value of the COMAC close to 1 interprets the higher level of correlation between the mode shapes for the responses and the RD signatures at location j.

The values of the MAC corresponding to the five modes for the shown mode shapes extracted from the original responses and the RD signatures for both directions are given in Table 6.3.4. As indicated by the high values of the MAC, the mode shapes identified from the response are, in general, closely correlated with respect to those identified from the RD signatures. A similar trend is obviously revealed from the values of the COMAC in Table 6.3.4 as well. It should be noted that these excellent agreements do not necessarily indicate that the correct mode shapes have been validated. However, the satisfaction of both MAC and COMAC values may lend confidence to support the

determination of the first four mode shapes, based on the various identification methods in this evaluation procedure.

Table 6.3.4 MAC and COMAC

Mode or floor	MAC		COMAC	
	X direction	Y direction	X direction	Y direction
1	0.9989	0.9999	1	1
2	0.9997	0.9987	0.9934	0.9977
3	0.9928	0.9874	0.9936	0.9997
4	0.9648	0.9945	0.9944	0.9992
5	0.9688	0.9075	0.9991	0.9958

To investigate the validity of the mode shapes, the orthogonality requirement with respect to a lumped mass matrix was usually used. In this investigation, the first four mode shapes were utilized instead of the complete mode shapes, since the fifth mode shape has been considered unreliable. The orthogonality condition in terms of the 5×5 diagonal mass matrix M is stated as follows:

$$\overline{\Psi}^{\mathrm{T}} M \overline{\Psi} = \begin{bmatrix} 1 & 0 & 0 & 0 \\ 0 & 1 & 0 & 0 \\ 0 & 0 & 1 & 0 \\ 0 & 0 & 0 & 1 \end{bmatrix} = I \tag{6.3.12}$$

in which the mass normalized modal matrix, denoted by $\overline{\Psi}$, is defined as the following 5×4 matrix [Hart and Wang, 2000]:

$$\overline{\Psi} = \begin{bmatrix} \overline{\varphi}_1 & \overline{\varphi}_2 & \overline{\varphi}_3 & \overline{\varphi}_4 \end{bmatrix} = \begin{Bmatrix} \overline{\Psi}_{51} & \overline{\Psi}_{52} & \overline{\Psi}_{53} & \overline{\Psi}_{54} \\ \overline{\Psi}_{41} & \overline{\Psi}_{42} & \overline{\Psi}_{43} & \overline{\Psi}_{44} \\ \overline{\Psi}_{31} & \overline{\Psi}_{32} & \overline{\Psi}_{33} & \overline{\Psi}_{34} \\ \overline{\Psi}_{21} & \overline{\Psi}_{22} & \overline{\Psi}_{23} & \overline{\Psi}_{24} \\ \overline{\Psi}_{11} & \overline{\Psi}_{12} & \overline{\Psi}_{13} & \overline{\Psi}_{14} \end{Bmatrix} \tag{6.3.13}$$

, and each mode shape is normalized by means of Equation (6.3.14):

$$\overline{\varphi}_i = \frac{\varphi_i}{\sqrt{\varphi_i^{\mathrm{T}} M \varphi_i}} \tag{6.3.14}$$

In Tables 6.3.5 and 6.3.6, the four mode shapes identified individually from the responses and the RD signatures in each direction satisfy the orthogonality condition, when most off-diagonal elements obtained from Equation (6.3.12) are less than 0.1. The satisfaction of the orthogonality condition implies that the presumption of the real modes for the building model seems tolerant of the uncertainty of the phase angles owing to the reason of low-amplitude responses. Certainly, an endeavor can be made by adjusting the mass matrix or modal matrix to exactly fulfill the orthogonality condition [Targoff, 1976].

Upon identifying these modal parameters, stiffness matrix was further evaluated by the following Equation (6.3.15) in order to develop the analytical model of the building model:

$$K = (\overline{\Psi}^{-1})^{\mathrm{T}} \Omega \overline{\Psi}^{-1} \tag{6.3.15}$$

in which

$$\Omega = \begin{bmatrix} \omega_1^2 & 0 & 0 & 0 \\ 0 & \omega_2^2 & 0 & 0 \\ 0 & 0 & \omega_3^2 & 0 \\ 0 & 0 & 0 & \omega_4^2 \end{bmatrix} \tag{6.3.16}$$

, and the i^{th} diagonal element in Ω is $\omega_i = 2\pi f_i$. Since $\overline{\Psi}$ is an invertible matrix in this study, Equation (6.3.15) should be solved in conjunction with Equation (6.3.12). Pre-multiplying and post-multiplying Equation (6.3.12) by $\left(\overline{\Psi}^{\mathrm{T}}\right)^{-1}$ and $\overline{\Psi}^{-1}$ give:

$$M\overline{\Psi} = \left(\overline{\Psi}^{\mathrm{T}}\right)^{-1} \tag{6.3.17}$$

$$\overline{\Psi}^{\mathrm{T}} M = \overline{\Psi}^{-1} \tag{6.3.18}$$

Substituting Equations (6.3.17) and (6.3.18) into Equation (6.3.15), it becomes that

$$K = M\overline{\Psi}\Omega\overline{\Psi}^{\mathrm{T}} M \tag{6.3.19}$$

The stiffness matrices together with the mass matrix estimated for the building model are summarized in Table 6.3.7. Similarly, the damping matrices can be obtained following the same way.

Table 6.3.5 Orthogonality of Mode Shapes in X Directions

Data type	Responses			
Mode	1	2	3	4
Normalized mode shape $\overline{\varphi}_i$	$\begin{Bmatrix} 0.1650 \\ 0.1528 \\ 0.1200 \\ 0.0773 \\ 0.0296 \end{Bmatrix}$	$\begin{Bmatrix} -0.1553 \\ -0.0214 \\ 0.1193 \\ 0.1590 \\ 0.0849 \end{Bmatrix}$	$\begin{Bmatrix} 0.1205 \\ -0.1240 \\ -0.1051 \\ 0.1017 \\ 0.1401 \end{Bmatrix}$	$\begin{Bmatrix} -0.0716 \\ 0.1675 \\ -0.0922 \\ -0.0819 \\ 0.1500 \end{Bmatrix}$
Orthogonality with respect to mass matrix $\overline{\Psi}^{\mathrm{T}} M\overline{\Psi}$	$\begin{bmatrix} 1 & 0.0108 & 0.0054 & 0.0094 \\ 0.0108 & 1 & -0.0013 & -0.0477 \\ 0.0054 & -0.0013 & 1 & -0.0796 \\ 0.0094 & -0.0477 & -0.0796 & 1 \end{bmatrix}$			
Data type	RD signatures			
Mode	1	2	3	4
Normalized mode shape $\overline{\varphi}_i$	$\begin{Bmatrix} 0.1591 \\ 0.1590 \\ 0.1208 \\ 0.0764 \\ 0.0280 \end{Bmatrix}$	$\begin{Bmatrix} -0.1541 \\ -0.0174 \\ 0.1183 \\ 0.1603 \\ 0.0868 \end{Bmatrix}$	$\begin{Bmatrix} 0.1402 \\ -0.1180 \\ -0.0990 \\ 0.0972 \\ 0.1348 \end{Bmatrix}$	$\begin{Bmatrix} -0.0875 \\ 0.1423 \\ -0.0884 \\ -0.0538 \\ 0.1784 \end{Bmatrix}$
Orthogonality with respect to mass matrix $\overline{\Psi}^{\mathrm{T}} M\overline{\Psi}$	$\begin{bmatrix} 1 & 0.0307 & 0.0389 & -0.0167 \\ 0.0307 & 1 & -0.0493 & 0.1093 \\ 0.0389 & -0.0493 & 1 & -0.0014 \\ -0.0167 & 0.1093 & -0.0014 & 1 \end{bmatrix}$			

Table 6.3.6 Orthogonality of Mode Shapes in Y Directions

Data type	Responses			
Mode	1	2	3	4
Normalized mode shape $\overline{\varphi}_i$	$\begin{Bmatrix}0.1811\\0.1506\\0.1084\\0.0647\\0.0225\end{Bmatrix}$	$\begin{Bmatrix}-0.1630\\0.0120\\0.1293\\0.1503\\0.0727\end{Bmatrix}$	$\begin{Bmatrix}0.1300\\-0.1261\\-0.0878\\0.0969\\0.1449\end{Bmatrix}$	$\begin{Bmatrix}-0.0709\\0.1692\\-0.1079\\-0.0298\\0.1567\end{Bmatrix}$
Orthogonality with respect to mass matrix $\overline{\Psi}^{\mathrm{T}} M \overline{\Psi}$	$\begin{bmatrix}1 & -0.0254 & 0.0647 & 0.0328\\-0.0254 & 1 & -0.1180 & 0.0939\\0.0647 & -0.1180 & 1 & 0.0017\\0.0328 & -0.0939 & 0.0017 & 1\end{bmatrix}$			
Data type	RD signatures			
Mode	1	2	3	4
Normalized mode shape $\overline{\varphi}_i$	$\begin{Bmatrix}0.1827\\0.1496\\0.1072\\0.0643\\0.0227\end{Bmatrix}$	$\begin{Bmatrix}-0.1640\\0.0025\\0.1289\\0.1499\\0.0729\end{Bmatrix}$	$\begin{Bmatrix}0.1063\\-0.1402\\-0.0826\\0.1073\\0.1469\end{Bmatrix}$	$\begin{Bmatrix}-0.0872\\0.1725\\-0.0990\\-0.0303\\0.1510\end{Bmatrix}$
Orthogonality with respect to mass matrix $\overline{\Psi}^{\mathrm{T}} M \overline{\Psi}$	$\begin{bmatrix}1 & -0.0555 & -0.0009 & 0.0078\\-0.0555 & 1 & -0.0164 & 0.1200\\-0.0009 & -0.0164 & 1 & -0.0694\\0.0078 & 0.1200 & -0.0694 & 1\end{bmatrix}$			

Table 7.3.7 Modal Parameter Matrices of Building Model

Mass M (Kg)	$\begin{bmatrix} 13.858 & 0 & 0 & 0 & 0 \\ 0 & 13.814 & 0 & 0 & 0 \\ 0 & 0 & 14.168 & 0 & 0 \\ 0 & 0 & 0 & 13.970 & 0 \\ 0 & 0 & 0 & 0 & 14.552 \end{bmatrix}$
Stiffness of X direction K_x ($\times 10^5$ N/m) from the responses	$\begin{bmatrix} 2.4640 & -2.8652 & -0.2352 & 1.3170 & -0.8146 \\ -2.8652 & 5.6245 & -1.5713 & -3.1721 & 2.8551 \\ -0.2352 & -1.5713 & 2.6178 & 0.8977 & -3.2706 \\ 1.3170 & -3.1721 & 0.8977 & 2.4320 & -0.6633 \\ -0.8146 & 2.8551 & -3.2706 & -0.6633 & 5.7143 \end{bmatrix}$
Stiffness of X direction K_x ($\times 10^5$ N/m) From the RD signatures	$\begin{bmatrix} 3.2052 & -3.0642 & -0.1096 & 1.2387 & -1.4970 \\ -3.0642 & 4.2793 & -1.2029 & -2.0962 & 3.0403 \\ -0.1096 & -1.2029 & 2.3919 & 0.5145 & -3.4980 \\ 1.2387 & -2.0962 & 0.5145 & 1.7354 & -0.3136 \\ -1.4970 & 3.0403 & -3.4980 & -0.3136 & 7.2442 \end{bmatrix}$
Stiffness of Y direction K_y ($\times 10^5$ N/m) from the responses	$\begin{bmatrix} 3.0502 & -3.3877 & -0.2683 & 0.8610 & -0.4628 \\ -3.3877 & 6.0710 & -1.9596 & -1.8442 & 2.8603 \\ -0.2683 & -1.9596 & 3.1587 & 0.2901 & -3.8967 \\ 0.8610 & -1.8442 & 0.2901 & 1.5833 & 0.8054 \\ -0.4628 & 2.8603 & -3.8967 & 0.8054 & 6.6032 \end{bmatrix}$
Stiffness of Y direction K_y ($\times 10^5$ N/m) from the RD signatures	$\begin{bmatrix} 2.9506 & -3.6762 & 0.1494 & 0.8252 & -1.1323 \\ -3.6762 & 6.5231 & -1.7639 & -2.1305 & 2.5688 \\ 0.1494 & -1.7639 & 2.7387 & 0.2246 & -3.4716 \\ 0.8252 & -2.1305 & 0.2246 & 1.7456 & 0.9522 \\ -1.1323 & 2.5688 & -3.4716 & 0.9522 & 6.2815 \end{bmatrix}$

6.4 Concluding Remarks

The RD based method has been proposed to identify the modal parameters of a structure from forced acceleration responses available from measurement. This method is established through the RD technique in conjunction with the FFT based algorithms. One of the potential advantages of the RD based method is that it eliminates random components and neglects the added effect of applied forces in measured acceleration responses.

To demonstrate its feasibility for practical applications, the RD based method was applied to the acceleration responses of the five-story building model measured in the wind tunnel. The FRF approach, another independent method that applies the FFT based algorithms to the measured responses, was also presented for a cross validation of the proposed methods. Because of the limited number of accelerometers, acceleration responses were measured group by group. Therefore, the mode shapes were identified group by group and, then, collected by using the result at the reference point to carry out the complete mode shapes of the building model.

Results revealed that the modal parameters of the building model for the first four modes identified by the RD based method correlated excellently with those evaluated by the FRF approach. In addition, the satisfaction of the orthogonality condition to a lumped mass model validated the identified mode shapes of the building model. In regard to the above consequences, the RD based method is capable of dealing well with the measured acceleration responses to reliably estimate the natural frequencies and corresponding mode shapes of structures. Based on the estimated natural frequencies and mode shapes, the stiffness matrices of the building model were subsequently evaluated in this study.

The exceptional experience with this experimental study is that the low amplitude response of a modal component in the build model is sensitive to noise effect and modal coupling in measurement, which adversely affects the phase angle estimate. Advanced identification techniques for extracting information from low amplitude modal responses and filtering techniques to remove noises are desirable upgrades to the RD based method.

To eliminate the added effect of the RD force signatures in the RD acceleration signatures when identifying the damping ratios, modal response may be isolated using a

band-pass digital filter for a specified frequency range. The damping ratio based on this idea may therefore be determined in the time domain through the envelope of the RD acceleration signature as if it were treated as a free vibration response. It is noted that such a method extracts the total damping, including structural damping and aeroelastic damping, because of the presence of aeroelastic interactions.

References

Allemang, R. L. and Brown, D. L. (1983), "A Correlation Coefficient For Modal Vector Analysis," Proceedings of the 1st International Modal Analysis Conference, pp. 110-116.

Cho, K. P. (1999), Passive Viscoelastic Damping Systems for Buildings, Ph.D. Dissertation, Civil Engineering Department, Colorado State University.

Ewins, D. J. (2000), Modal Testing: Theory, Practice and Application, 2nd Edition, Research Studies Press, pp. 434-437.

Felber, A. J. (1993), Development of a Hybrid Bridge Evaluation System, Ph.D. Dissertation, University of British Columbia, Canada.

Hart, G. C. and Wong, K. (2000), Structural Dynamics for Structural Engineers, 1st Edition, John Wiley & Sons, pp. 157-160.

Targoff, W. P. (1976), "Orthogonality Check And Correction Of Measured Modes", AIAA Journal, Vol. 14, No. 2, pp. 164-167.

Isyumov, N. (1981), "The Aeroelastic Modeling Of Tall Buildings", Proceedings of the International Workshop on Wind Tunnel Modeling Criteria and Techniques in Civil Engineering Applications, pp. 373-407.

Katagiri, J., Marukawa, H., Katsumura, A., and Fujii, K. (1998), "Effects Of Structural Damping And Eccentricity On Wind Responses Of High-rise Buildings", Journal of Wind Engineering and Industrial Aerodynamics, Vol. 74-76, pp. 731-740.

Templin, J. T. and Cooper, K. R. (1981), "Design And Performance Of A Multi-Degree-Of-Freedom Aeroelastic Model", Journal of Wind Engineering and Industrial Aerodynamics, Vol. 8, pp. 157-175.

Chapter 7

CLOSURE

7.1 Summary and Conclusions

Investigation of the random decrement (RD) signatures and development of the RD based method form the basis of this research objective regarding the parameter identification problem from the forced acceleration responses of a linear dynamic system. Such a problem is attributed to the added effect of the applied forcing function in the impulse acceleration response function. However, how to deal with the added effect by means of an identification procedure has not been adequately addressed in the literature, thus posing a major challenge to this study. In this regard, an intensive investigation of the identification problem has been performed using two approaches – (1) simulation of linear dynamic systems loaded by white noise excitations and practical wind forces; and (2) analysis of an aeroelastic building model tested in a wind tunnel.

The theoretical background of the RD technique has been described and further developed in this study. With the assistance of the RD technique developed, a procedure is proposed to give rise to the analytical free vibration responses of a linear dynamic system. Such a procedure adopts the concept behind the RD technique to facilitate the determination of the initial conditions through the initial points of the RD displacement and velocity signatures formed from their synchronous responses. Especially, the free vibration acceleration responses resulting from such initial conditions can therefore be compared with the RD acceleration signatures. The compared results reveal that the RD

signature of the applied force affects the RD signature of its forced acceleration response. Such a RD acceleration signature consists of two portions contributed respectively from the non-forced acceleration response and the applied force. The identity relation in the frequency response functions (FRFs) of the RD acceleration signatures for each mode obtained from numerical and experimental data corroborates such a consequence.

When the parameters of a linear dynamic system are to be extracted only from the forced acceleration responses, the RD based method has been proposed in this study to provide a solution for the identification problem. The RD based method combines the RD technique with the fast Fourier transform based algorithms to reliably and efficiently identify the modal parameters, if the dominant vibration modes are significantly excited, well separated, and lightly damped. One of the potential advantages for using the RD based method is intended to eliminate random components and neglect the added effect of the applied forces in their acceleration responses. The theoretical derivation of the RD based method has been achieved by modifying the traditional FRF approach and using the RD technique, in order to establish the theoretical basis of the FRFs defined for the RD signatures. Both numerical and experimental studies have verified the applicability of the RD based method.

The significant contribution of this study is the RD based method that can neglect the added effect of the applied forces in their acceleration responses and thus identify the modal parameters of a linear dynamic system, without knowledge of the applied forces. In addition to this, the demonstration of developing the RD based method can serve as a guideline that helps evolve and improve other identification procedures when evaluating similar problems.

7.2 Perspectives and Future Works

Some different aspects of the RD based method are pointed out here, which can be further developed and investigated in the near future.

7.2.1 Non-Gaussian Stochastic Processes

The theory of the RD based method is mainly based on the assumption of the Gaussian stochastic process for the RD technique to link the RD signatures with the correlation functions of responses. Nevertheless, there are certain problems of pressing practical concerns for which the responses of structures excited by environmental loads may have a non-Gaussian or non-stationary character. For instance, a fluid-structure interaction, related with the aeroelastic phenomena, is a sophisticated problem of this type. It would be desirable to realize how sensitive the parametric estimate using the forced acceleration responses of a structure will be if the input forces are non-Gaussian distributed or non-stationary?

7.2.2 Nonlinear Dynamic Systems

There is another interesting problem to be considered: nonlinear structures. Most civil engineering structures, when subjected to a large excitation, experience a behavior of large deflections that cannot virtually be assumed as linear. In addition, progressive damage induced in structural and non-structural components could force the response of a structure into the nonlinear regime. Non-linear properties may even play a dominant role in the internal functioning of a structure and may not be negligible in the development of a mathematical model. It would be interesting to investigate whether or not the use of the

RD based method may be possible to discern important information about the nonlinear properties.